2020

A Computational Biomechanical Model-Based Optimization of Fulcrum Support in Orthosis Enabled Closed Reduction of Developmental Dysplasia of The Hip

Christopher Rose
University of Central Florida

A COMPUTATIONAL BIOMECHANICAL MODEL-BASED OPTIMIZATION OF FULCRUM SUPPORT IN ORTHOSIS ENABLED CLOSED REDUCTION OF DEVELOPMENTAL DYSPLASIA OF THE HIP

by

CHRISTOPHER L. ROSE
B.S. Escuela Superior Politécnica del Litoral, 2012, Ecuador
M.S. University of Central Florida, 2015, United States

A dissertation submitted in partial fulfillment of the requirements
for the degree of Doctor of Philosophy
in the Department of Mechanical and Aerospace Engineering
in the College of Engineering and Computer Science
at the University of Central Florida
Orlando, Florida

Fall Term
2020

Major Professor: Alain J. Kassab

ABSTRACT

Hip abduction orthosis devices (HAOD) are used to reduce the hip joint of infants affected by developmental dysplasia of the hip (DDH). HAOD have been successful for mild cases of DDH and ineffective for severe cases. Efforts in understanding the biomechanics of lower limbs have been made to improve the success rate of current treatment methods, especially for Grade IV dislocations (G4). The aim of this dissertation is twofold: first, it proposes the use of a varying fulcrum point (FP) located below the leg to improve DDH treatment; and secondly, it defines the optimal FP (OP) location for a broad spectrum of hip joint configurations. An iterative 3D computational model of a 10-week-old infant was developed using parameters of the femur, pelvis, and lower limb muscles along with their anatomical location. The computational model provides a variety of scenarios of closed reduction and the location of the OP, which is believed to be a key parameter for a successful reduction in severe cases of DDH. The problem is posed as a maximization of an objective function whose independent parameter is the location of the FP constrained to vary over an anatomically feasible range along the femur. For each location of the FP, the model computes resultant forces and evaluates a potential energy function. The OP maximizes the projection of the resultant vector force of the femur over the least energy path to assist in achieving G4 reduction. The results of this study suggest that for the range of the parameters used in the model, G4 reduction can be achieved as the FP reaches the femoral head with the aid of additional external traction forces. Results from this study may be used to customize current orthosis design by using patient-specific parameters, which can be obtained from imaging.

DEDICATION

To my dear family, whose love and support always motivate me to be a better person and follow my dreams. To my wife, Diana, for her patience, encouragement, and support. To my children, Matthew and Megan, for their unconditional love that inspires me to conclude every new adventure in which I engage.

ACKNOWLEDGMENTS

Special thanks to:

Professor Alain Kassab for believing in my capacity and supporting me throughout the journey towards the Ph.D. degree. The opportunity and mentorship provided by Dr. Kassab have positively impacted my venture, and I am already applying what I learned in my professional career. I will endlessly be thankful for his advice.

Dr. Charles Price, together with the International Hip Dysplasia Institute, for supporting our efforts during national and international conferences. Especially our Italy research trip, which gave us a hands-on research opportunity in the area of developmental dysplasia of the hip.

Professors Faissal Moslehy, Sang-Eun Song, and Victor Huayamave for serving on my committee and being part of my professional development.

TABLE OF CONTENTS

LIST OF FIGURES

LIST OF TABLES

CHAPTER 1: INTRODUCTION

1.1 State of the Art Problem - Problem Statement

The etiology of Developmental Dysplasia of the Hip (DDH) has been associated with genetics, family history, skeletal abnormalities, gender, hormonal and environmental factors. All these factors make DDH a complex pathology [1]. The term DDH is intended to cover all the variants of the hip disorder (subluxation, dislocation, and dysplasia), no matter if they occur prenatal or postnatal [2]. Subluxation occurs when the head of the femur is simply loose in the acetabulum (the hip socket of the femoral head), dislocation occurs when it is out of the socket, and dysplasia occurs when the socket is shallow, meaning that the femur cannot firmly fit into its socket. DDH is a common condition in newborns requiring treatment in 1‰ to 3‰ of newborn infants [3][4]. The incidence per 100 live births of neonatal (pre-birth) hip instability has a significant variability between racial groups and geographic locations, ranging from 0.006 in Africans to 7.61 in Native Americans, with an average incidence of 1.075 [5]. Treatment success has shown to be inversely related to the age at which the infant receives its initial treatment [6]. DDH is a common anatomic deformity leading to hip dysfunction and osteoarthritis (OA) [7]. Dysplasia is the root for nearly 76% of all cases of osteoarthritis [8], and it has been found that subluxation even after closed reduction leads to early degenerative osteoarthritis [9].

The purposes in the treatment of DDH are to (1) attain and (2) maintain a concentric reduction of the hip, (3) avoid complications such as infections, joint stiffness, and avascular necrosis (AVN), (4) promote normal acetabular and femoral head development, and (5) avoid unnecessary patient and parental hardship [10]. Lack of guidelines regulating

different harnesses compromises assertive methods and procedures to determine treatment outcome, leaving success to mere chance. Suggestions developed in previous research have covered some conditions for a very specific configuration [11][12][13][14], limiting the fast application of previously developed information.

1.2 Motivation

This research aims to: 1) help infants affected with severe grades of DDH treated with using hip abduction orthoses device (HAOD) to effect closed reduction, 2) minimize the incidences of avascular necrosis (AVN) in the femoral head, and 3) provide a tool which generates a generic infant model that could potentially be used for other pediatric applications. The results from this study will provide insight into the optimal location of a Fulcrum Point (FP), which may be used to improve current DDH treatment using hip abduction orthoses devices (HAOD). To predict the optimal FP (OP), the present study includes 1) a wide range of biometric parameters of the femur and the lower limb muscles, 2) biometric parameter variability, 3) optimization techniques to maximize the projection of the resulting forces on the femoral head over a path of least energy and direct path to achieve reduction.

CHAPTER 2: THESIS OVERVIEW

This dissertation consists of eight chapters, beginning with the introductory chapter, which covers DDH. It is of great interest to seek an effectively closed reduction configuration, which in turn will improve the successful treatment rate. This study predicts the optimal configuration needed for closed reduction for various grades of hip dysplasia, and it will also compare it against current successful abduction braces where a fulcrum point is present. This study investigates the possibility of achieving a Graf type III or a DDH Graf type IV reduction using a support point or Fulcrum Point (FP). Specifically, a 10-week-old female in supine infant positioning with the legs flexed and abducted was used as the main configuration. In addition, a fully dislocated leg with the femoral head behind the acetabulum was included to simulate a Graf type IV dislocation. Kinetic parameters such as infant leg centroid and leg weight were also included in the model. Also, femoral biometric parameters, muscle areas, muscle origin, and insertion points were included. The proposed study aims to prove the following three hypotheses:

1. A fulcrum point exists along the thigh of the infant, and such point may assist in the reduction of a Graf type IV dislocation.
2. A fulcrum point can help reduce a grade III dislocation during direct path for Graf type IV dislocation reduction.
3. A fulcrum point can help reduce a grade III dislocation in the indirect path for Graf type IV dislocation reduction.
4. A fulcrum point can help reduce grades I and II dislocations.

For the infant model, a computer code was developed. The code iterates using different configurations that vary the fulcrum point position along the femur. The configurations were tested against current orthosis devices that attempt to reduce DDH.

Chapter three, literature review, contains an assessment of how DDH is classified, how it is diagnosed, what is the incidence of DDH with modern detection methods, the different treatment methods and the mechanisms for each treatment, and the literature needed to develop the biomechanical infant model.

Chapter four covers the theoretical framework needed to develop the lower limb model. Topics such as lower limb anatomical reconstruction, muscle structure, muscle physiology, muscle path (straight, centroid, wrapping, friction among them), cartilage, and AVN are discussed in Chapter 4.

Chapter five describes the research methodology used to develop the computational SolidWorks® model as well as the Matlab® code. In addition, it introduces the muscles that are implemented in the infant model and the variability of the biometric parameters.

Chapter six shows the results of the study. This chapter includes the OP that is needed to achieve a closed reduction in Graf Type III and Type IV dislocations. Also, a sensitivity analysis is presented to investigate the sensitivity of the FP to biometric parameters.

Chapter seven discusses all the findings, compares them with other research, and addresses current research gaps and future work needed to address these gaps.

Chapter eight, the final chapter, summarizes the contribution of this work and the conclusions. It also discusses how the research is related to the objectives and outlines the limitations.

CHAPTER 3: LITERATURE REVIEW

This literature review covers a wide range of topics which are needed for the study. Section 3.1 presents the classification of DDH, while Section 3.2 discussed its diagnosis and incidence. Section 3.3 reviews different treatment methods and reduction mechanisms.

To improve the reliability and customization of the infant computational model, significant efforts were made. For instance, the femur can be updated using a patient-specific parameter from imaging. In addition, the computational model can assess the sensitivity of the location of the muscle attachment points and is able to find equilibrium configurations which are used into muscle material parameters.

To familiarize readers with the different dislocation types, Figure 1 shows all different classification grades. Figure 1a portrays a normal hip, Figure 1b shows a subluxated hip, and Figure 1c represents a dislocated hip clearly showing the femur in the posterior aspect of the acetabulum.

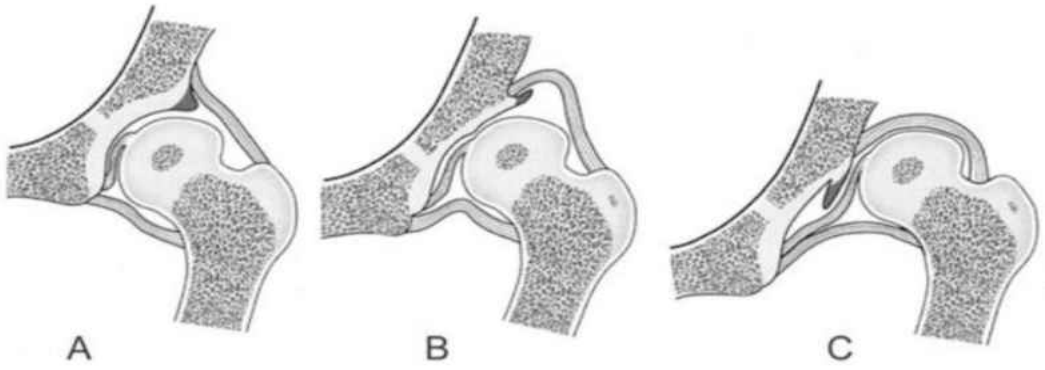

Figure 1: Anatomical Dislocation Classification (a) Normal hip, (b) Subluxated hip, and (c) Dislocated hip [15].

Figure 2 shows the hip joint configuration that will be used to describe the functionality and ranges of motion of the joints. For example, hip abduction is when opening the legs, but adduction is when closing. When referring to these angles of motion, they are with respect to the anatomical position.

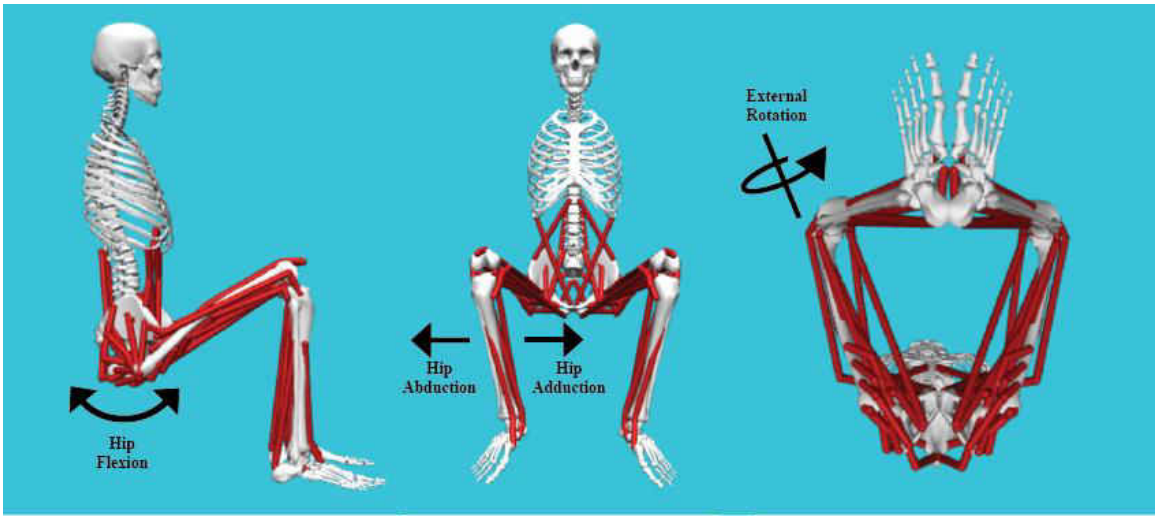

Figure 2: Anatomical hip joint motion, based on [16].

3.1 DDH Classification and severity

After examining 3500 infants using ultrasound imaging, Graf standardized the dysplasia classification, separating the neonatal hips into four categories: (a) normal; (b) delayed ossification (dysplasia); (c) partial dislocation (subluxation); and (d) dislocation (total luxation) [17]. It combines the age of the infant, and alpha and beta angles to create subgroups of the principal 4 classifications, as shown in Table 1.

Table 1: Graf classification system of DDH based on ultrasound hip angles [17].

Type	Description	Bony Roof	Bony Rim	Cartilage Roof	α-angle (deg.)	β- angle (deg.)	Subtype
I	Mature hip	Good	Angular/Blunt	Covers the femoral head	≥60	<77	Ia: β ≤ 55 degrees Ib: β > 55 degrees
IIa	Physiologically immature (< 3mo)	Deficient	Rounded	Covers the femoral head	50-59	< 55	IIa + : α = 55-59 degrees (at 6wk of age) IIa + : α = 50-54 degrees (at 6wk of age)
IIb	Delay of ossification (> 3mo)	Deficient	Rounded	Covers the femoral head	50-59	< 55	
IIc	Critical hip	Severely deficient	Rounded to flattened	Still covers the femoral head	43-49	< 77	IIc stable: under pressure β < 77 degrees IIc unstable: under pressure β > 77 degrees
IId	Decentring hip	Severely deficient	Rounded to flattened	Displaced	43-49	> 77	
III	Dislocated hip	Poor	Flattened	Pressed upward, perichondrium slopes cranially	< 43	> 77	IIIa: hypoechoic cartilage acetabular roof IIIb: hypoechoic cartilage acetabular roof
IV	Dislocated hip	Poor	Flattened	Pressed downward, perichondrium is horizontal or dips caudally	< 43		

The alpha angle is formed between the acetabular roof and the vertical cortex of the ilium. It is considered normal when the angle value is equal to or greater than 60 degrees. The beta angle is formed by the vertical cortex of the ilium and the triangular labral fibrocartilage (echogenic triangle). The beta angle is considered normal when the value is less than 77 degrees [17], Figure 3 illustrates both angles and all the different cases that

could be detrimental for proper growth and development of the hip joint. The 3 lines shown in the figure should not intersect in one point [18].

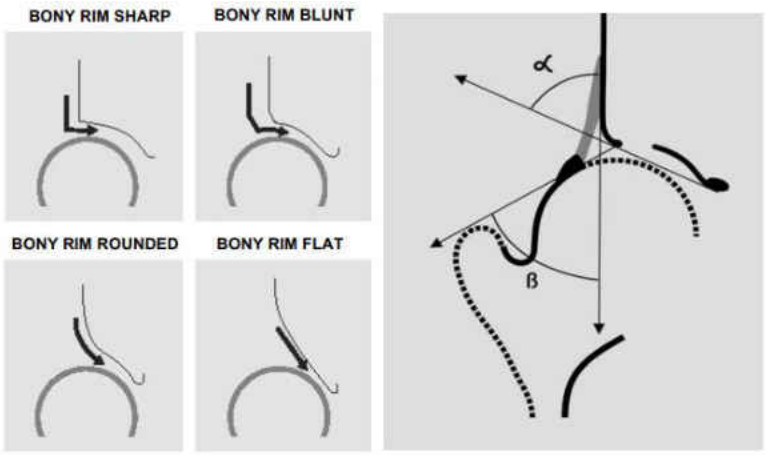

Figure 3: Illustration of different Bony Rim coverage, Alpha and Beta angles used for Graf classification, based on [18].

Most recently, the International Hip Dysplasia Institute (IHDI) [19] proposed a new grade classification system. This system does not rely on the ossification nucleus and uses the mid-point of the proximal femoral metaphysis as a reference landmark as shown in Figure 4. The IDHI approach, unlike other methods such as Tönnis classification shown in Figure 5 [20], can be used to diagnose DDH regardless of age, which makes it a more reliable and widely applicable method.

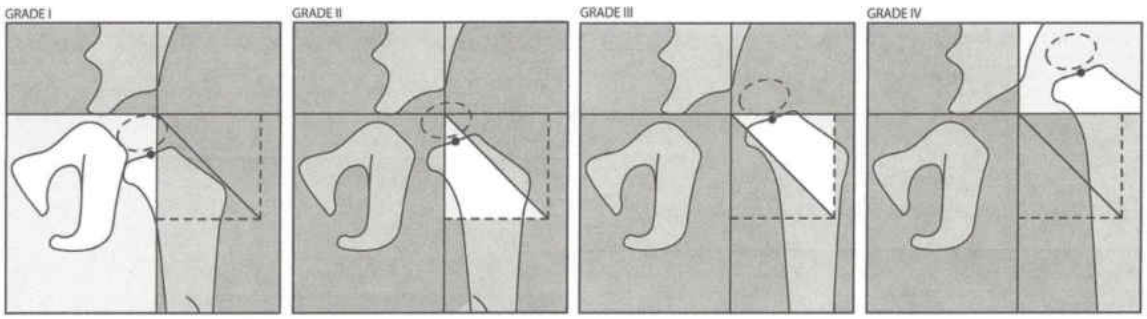

Figure 4: IHDI Classification. H-Line is Hilgenreiner's line (mostly a horizontal line) drawn through the top of the tri-radiate cartilages bilaterally. P-line is Perkin's line, drawn perpendicular to the H-Line at the superolateral margin of the acetabulum. D-Line is the diagonal at 45°. When falling in any of the white regions, the mid-point of the proximal metaphysis, defines the IHDI Grade as illustrated [20].

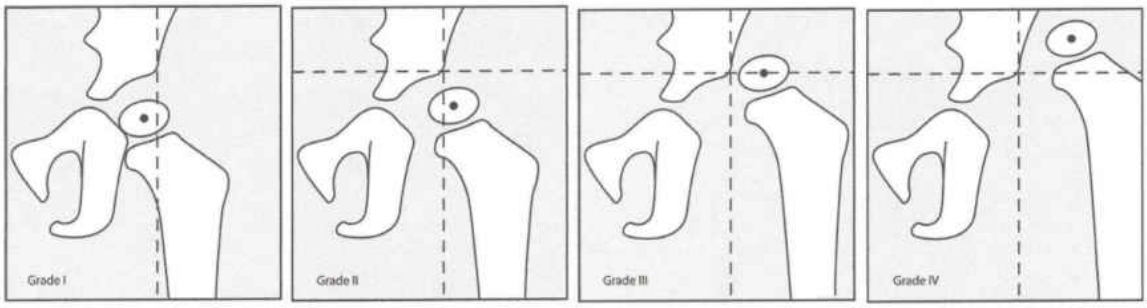

Figure 5: Tönnis Classification, the ossification center of the capital epiphysis defines the grade, uses the P-Line, and the superolateral margin of the acetabulum (SMA-Line) to divide the regions. Grade III is when the ossification center is over the SMA-Line [20].

3.2 DDH Diagnosis

Early DDH diagnoses include clinical examination that uses the Ortolani or Barlow procedures in newborns. The Ortolani procedure, currently the gold standard for clinical examination, reduces a dislocation by applying a gentle force near the greater trochanter, shown in Figure 14, with the infant supine and the hips flexed at 90 degrees as shown in Figure 6, the Ortolani procedure is usually performed at 1 and 3 months. When positive, there is a "click" in the hip joint that suggests a possible dislocation [21].

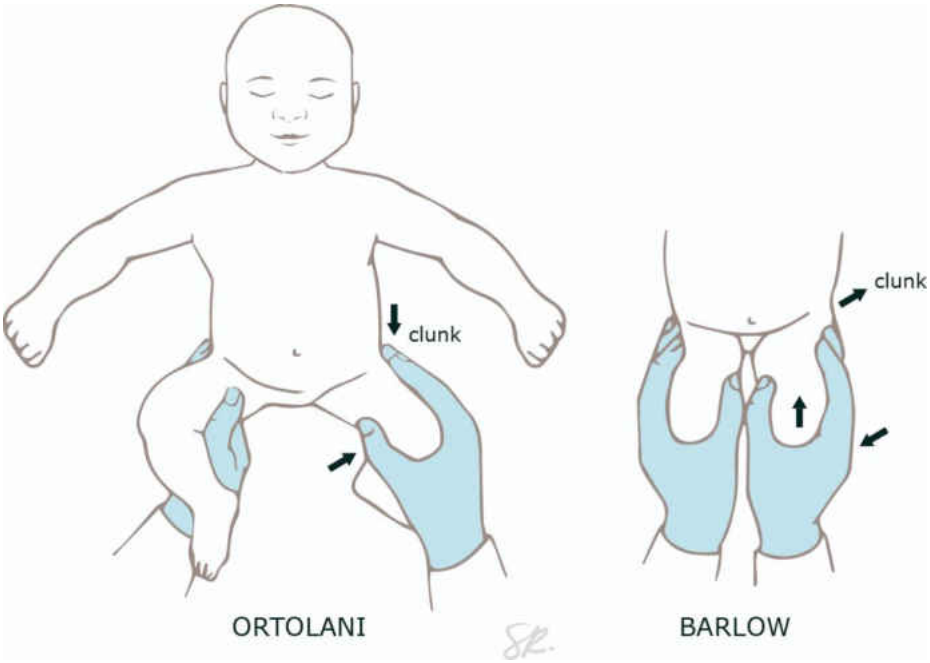

Figure 6: Ortolani and Barlow Maneuvers.

The correct application of the Ortolani maneuver consists of placing the index finger on the trochanter to toggle the femoral head into the acetabulum as illustrated in Figure 7, the index finger suggests the application of the fulcrum point for similar configurations near the trochanter.

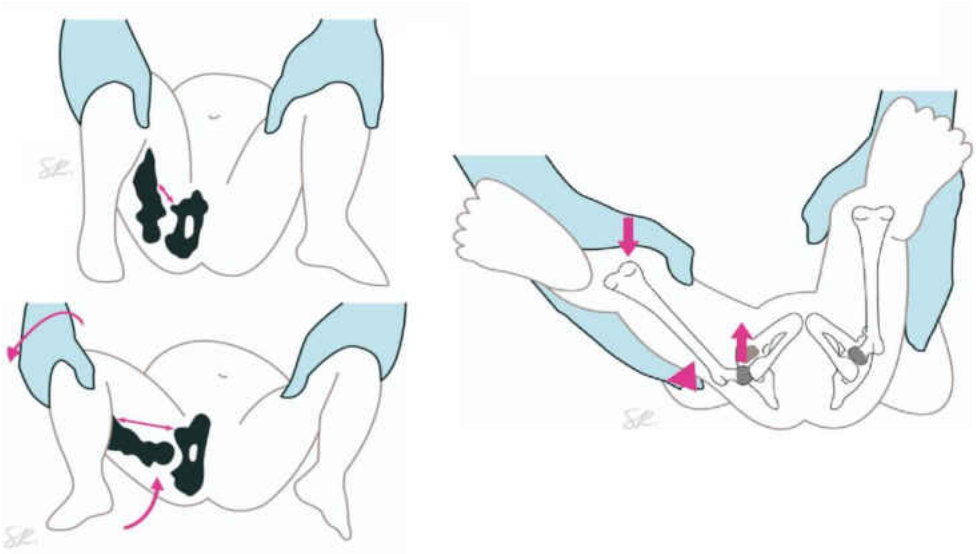

Figure 7: Ortolani Maneuver showing incorrect application (left), the correct application using the index finger over the trochanter (right).

There are other popular DDH Diagnosis tools like sonography and radiography. In a study performed by Kongsberg Hospital, Norway, from 1998 to 2006, 4245 patients received clinical examinations using the Barlow or Ortolani procedures. In addition, this study included ultrasound examination. Contrastingly, a sonography study that included 3594 patients, and followed them from 1989 to 1997, found that the number of treatments has doubled when using sonography only. The results of Ortolani and Barlow from another study showed a low incidence rate (1/1000) compared with (0.5/1000) using ultrasound [22]. This indicates ultrasound is also a valid method to assess DDH.

When comparing sonography against radiography, the classification of IHDI shows an advantage over other methods since it can be used at different ages [23].

Ultrasound has a sensitivity between 61% (44 infants) and 97% (83 infants) and specificity of 87 to 88%, which is higher than using radiography [24][25]. Radiology is not

recommended, ultrasound is the most common practice, and magnetic resonance imaging (MRI) requires sedation [24].

Ultrasound is currently the standard for early detection of DDH [26]. It can also predict the determination of correct ossification (bone formation) of the hip joint for the age of the infant, if the joint is stable, or if the joint is decentered can determine if the cartilaginous roof is blocking the pathway to a normal joint [27]. Also, the results of the measurements with ultrasound are more reproducible [27].

3.3 Closed Treatment Methods

Untreated dislocations of the hip may be detrimental to hip joint development and may affect patient-quality life. [28].

DDH treatments can be classified as an open reduction (which requires surgery) or closed reduction (no surgery). To achieve closed reduction, traction to the femur could be applied in Graf type IV dislocation, which reduces the hip by placing the femoral head back into the acetabulum. The path which the femoral head follows to achieve reduction for severe grades of DDH has been suggested [29][30][31], from which the least energy path of reduction is of interest to follow in an optimal manner. Several abduction orthoses such as the Pavlik Harness, Ilfeld bracing, Frejka Pillow, among others, have been used to improve the closed reduction success rate but have failed in achieving reduction for a Graf type IV dislocation. Many of these orthoses and their reduction capabilities will be investigated and compared in the study.

One of the key design parameters that will be covered in this study is the Fulcrum Point (FP), which is currently used by several HAOD. The FP has not been investigated, and its biomechanical effect in orthoses design remains unknown.

3.3.1 Pavlik Harness

The Pavlik harness is a device designed to position the hips of the infant aligned in the joint; to keep the hip joint secure. It is normally used to treat newborns until they reach six months of age.

While using the Pavlik Harness, both hips must be positioned in it even if there is a problem with only one hip. Aligning and stabilizing the hip joint will help the normal growth and development of the hip joint.

Figure 8 displays the mechanism of the Pavlik Harness and the abduction position of the hip. For this harness, the equivalent FP is the posterior strap close to the knee. The strap in the front is to adjust the minimum flexion angle; the one on the back is to adjust the adduction angle.

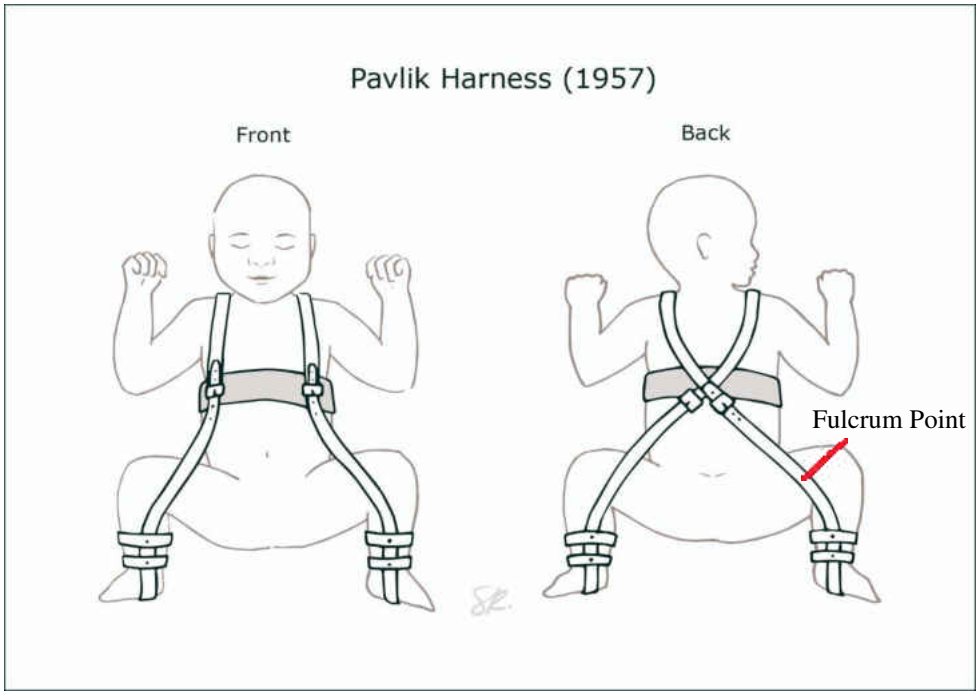

Figure 8: Illustration of the Pavlik Harness, indicating the fulcrum point location.

Early diagnosis and treatment of DDH are essential. A study of over 23 infants under the age of six months obtained a successful reduction in 88.89% of the 27 dislocated hips [32].

Another study suggests the poor application of the Pavlik harness on nine infants not only failed to achieve reduction, but they required traction, general anesthesia, reduction, and a Spica cast as post-treatment. A Spica is a type of bandage in the shape of figure eight, extending from the legs to the trunk. Bad practices included not following age recommendations, treatment follow-up, and incorrect strap placement [33].

From a study of 50 completely dislocated hips in Nagasaki, the Pavlik harness was applied to 4±3 months old infants for four to eight months; as a result, 28% developed

AVN, 26% presented avascular dysplasia one year after reduction, and 56% had anatomical healing three years after reduction [30].

From another study of nine female infants from three to seven months old with Type A and B congenital dysplasia of the hip (CDH), the spontaneous reduction occurred during the second to the fourth period of sleeping in all three type B dislocations. The reduction took place during deep sleep, without active movements in this period [31].

In a most recent study of 31 hips with DDH, treatment was successful in 58.1% using the harness from 5 to 11 weeks. However, it was noticed that in older ages, bilateral DDH have lower success rates, and Graf type IV dislocations had no success cases [26].

A study from Ramsey [32] suggested avoiding adduction less than 35 degrees, which will trigger severe dislocation, or abductions bigger than 75 degrees, which may increase the risk of AVN.

3.3.2 Other Abduction Orthoses Devices

In a study of over 49 patients, 60 hips with DDH treated with a Tübingen Hip treatment were a success in 93.3% of the cases [34].

In a study of 35 children (54 hips) in the Children's Hospital of Philadelphia during 2014, 86% of the children with DDH were treated with Ilfeld bracing, of which 25 of 29 cases achieved a reduction (86%). A comparatively stable reduction was achieved in 23 of 25 hips after applying a Spica cast (92%).

In Southern Finland between 1966 and 1975, 920 newborns with DDH treated using Frejka Pillow achieved a reduction in 94.03% of the cases, later was replaced by the Von

Rosen Splint, which from 1978 and 1981 was used in 180 newborns, it worked in 98.33 % of the cases, but reported 1 case of AVN and 19% reported temporary skin irritation [35].

In another study from 2003 through 2010, in Malmö, Sweden, from 34308 live births, there are 586 (1.7%) children of suspected neonatal instability of the hip (NIH), of which 251 did not receive treatment, and from those treated with the Von Rosen splint, they reported 2 cases of AVN, the most common cause of late diagnostic was neonatal intensive care, this study also refers to many other studies combining orthoses devices finding an incidence of AVN 0.2% to 0.9 % for the Von Rosen Orthosis [36].

From 1974 to 1986, 107 infants from one to nine-months-old with late DDH diagnosis used Frejka Pillow, followed by a Becker Device, with a 89.72% success rate, 2 out of 107 not reduced, four not achieving stabilization, four persisting dysplasia, and one case of AVN [37].

In another study, from 1988 to 1990, from 108 newborns with DDH, a 97.2% success rate was showed using Frejka Pillow, 1 case of AVN, 83% accepted the follow-up, and 17% of the patients presented an in-toeing gate (walking with the toes pointing inward) [38], indicating a better success rate than the previous Finland study.

Different types of orthoses devices with mid-thigh FP are illustrated in Figure 9.

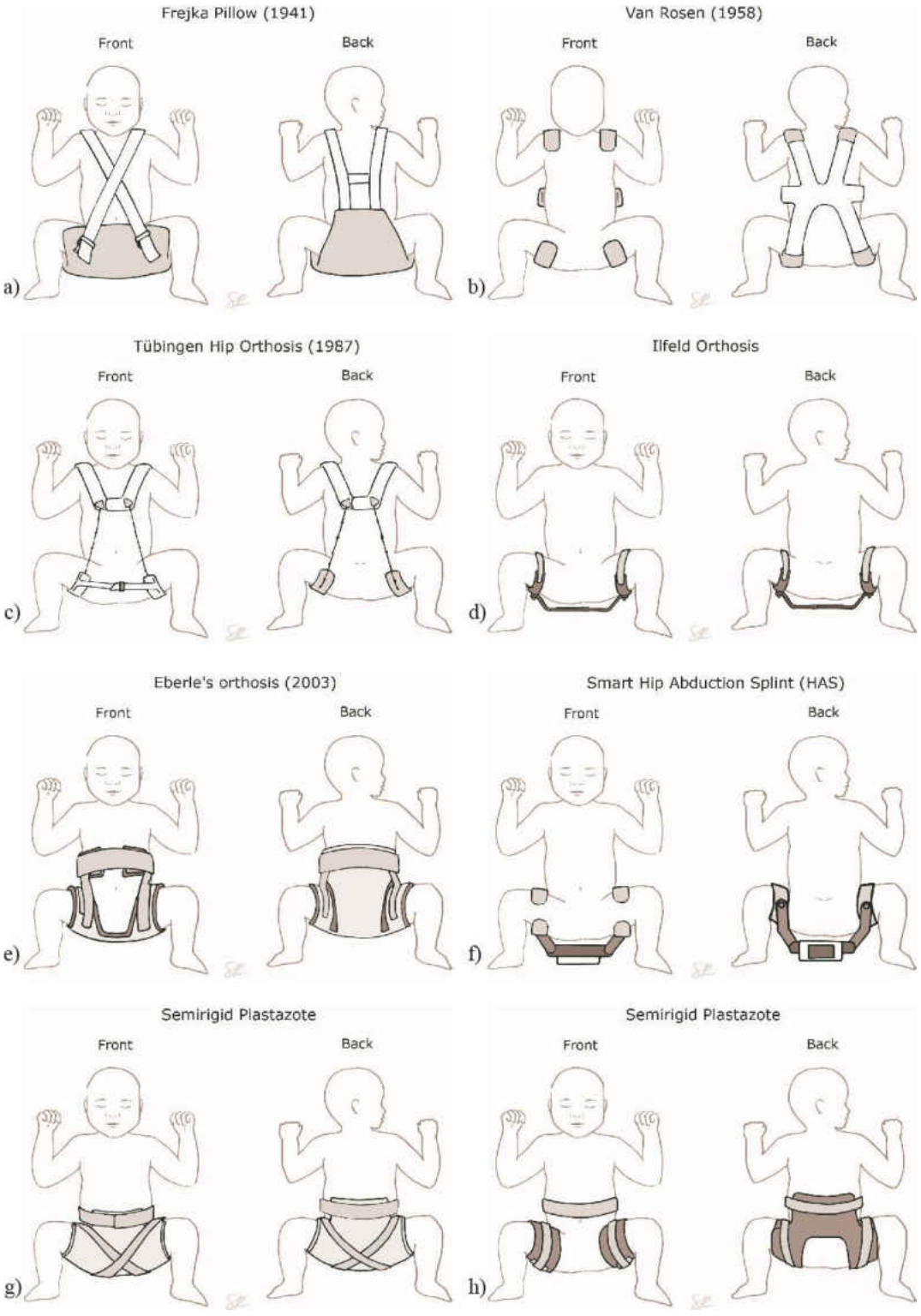

Figure 9: Illustration of different Abduction Orthoses Devices a) Frejka Pillow b) Von Rosen c) Tübingen d) Ilfeld e) Eberle f) Smart hip abduction splint g) and h) Semirigid Plastazote.

3.4 Complications of the actual treatments

Some of the risks or complications with the use of the actual harnesses are dermatitis, infections, nerve damage, flattening of the back of the femoral head, downward dislocation of the hip, subluxation of the knee, or also can cause AVN. The death of the bone tissue due to the lack of blood supply is called Avascular Necrosis (AVN) or osteonecrosis. It can be local, caused by a trauma or microtrauma, or systemic [39]. AVN can lead to a bone collapse. Fatty deposits in blood vessels or other diseases can cause AVN, including a dislocated joint, which can produce the interruption of blood flow to a section on a bone. In the early stages of AVN, it may not present symptoms, but as the condition worsens, the affected joint might hurt when weight is put on. Usually, the pain develops gradually, and when it is related to the hip, it might center on the groin, thigh, or buttock. AVN can cause the bone to lose its smooth shape, possibly leading to severe arthritis.

In studies regarding the lack of blood circulation can be found the tourniquet, which is the application of a device to stop the blood flow by compressing the limb. If the bloodstream is blocked for too long, toxins accumulate, and irreversible damage is caused. Wherein it has been shown that most of the orthopedic surgeons felt that a 15-min deflation time after a two hour tourniquet time was safe. It is concluded that the tourniquet should be inflated according to the limb occlusion pressure and should be deflated after 2 hours for the lower limb and after 1½ hours for the upper limb for at least 10 minutes. The limb occlusion pressure of 130 mmHg will require an extra safety pressure of 40 mmHg to stop blood circulation; this margin diminishes as long as the occlusion pressure decreases [40]. Figure 10 shows the blood pressure variation in the body from the aorta to the capillaries,

indicating the blood pressure in the capillaries is significantly lower. Additionally, the blood pressure of newborns is also lower, around 64 mmHg, making the occlusion pressure easier to reach. Blood pressure might also be affected by the time of the day, or in another example, infants that consume powder milk have an increase in blood pressure [41].

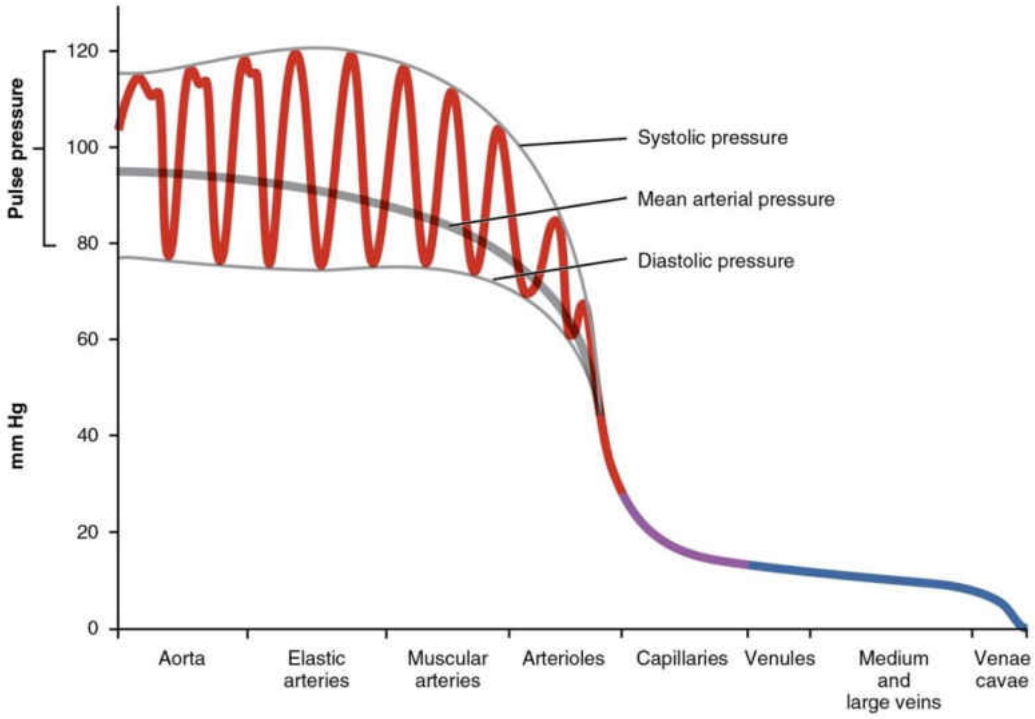

Figure 10: Systemic blood pressure throughout the blood vessels, including systolic, diastolic, mean arterial, and pulse pressures[42][43].

In contrast, cartilage does not have blood vessels; the nutrition of cells within the cartilage matrix depends on the diffusion of nutrients from blood capillaries in the perichondrium (which is the fibrous membrane that covers the cartilage surface) and/or adjacent tissues through the matrix [44]. These factors are important but challenging to correlate as an attempt to predict the effect of the HOAD over the femur to cause AVN.

CHAPTER 4: THEORETICAL FRAMEWORK

This chapter presents details of the theoretical basis and methodologies that were developed and used to investigate the moments and forces that occur in the dislocated hips while using a HAOD and a varying fulcrum point. This chapter will introduce the following sections:

4.1 Lower limb model

4.2 Reconstruction of a lower limb

4.3 Descriptive implementation of passive muscle models in the lower limb

4.4 Muscle Structure, Physiology, and behavior

4.5 Fulcrum Point

4.6 Software and numerical methods

4.1 Lower Limb Model

Research on muscle mechanics is currently governed by biological experimentation and also conducted in mechanical models. The biological approaches have significant limitations given that the analysis of human anatomy varies in each human body because no individual has identical anatomy, including twins. Dynamic locomotion depends mostly on the interaction between the muscles and the nearby bones through connective tissues.

It is of high interest to accurately define the shape, size, and anatomical landmarks of the bones and muscles. This quantitative analysis will help define the material characteristics and the muscle insertion points over the bone structure. Therefore, an accurate anatomical model will allow to precisely investigate the muscular mechanics of

the lower limb. Clinical studies have shown that DDH is more common in women than in men [5]. Therefore a ten-week-old female pelvis was chosen as a model to carry out the proposed studies. The three-dimensional mechanical model of the ten-week-old female lower limb was generated from the combination of computer tomography (CT) scans and MRI scans of a six-month-old girl and a fourteen-year-old girl, as well as data from the Visible Human Project. This model was reproduced in previous research and aided to define a procedure to find material properties, validate the model, and estimate predictions under model alterations [11].

4.2 Lower Limb Anatomical Reconstruction

The computerized anatomical model of the right lower limb was reproduced with the aid of medical segmentation packages: Mimics and 3-matic (Materialize Inc., Plymouth, MI). The lower limb was composed of the following: bones of the hip, femur, tibia, fibula, calcaneus, cuboid bone, navicular bone, talus bone, metatarsal, and phalanges. For this model, symmetry was assumed along the sagittal plane, which divided the body into equal portions, right and left.

Based solely on medical segmentation software, is a challenge the use of MRIs and CT scans when reconstructing the anatomy of a newborn, as they have large cartilaginous areas; in conjunction with the fact that retrospective CT and MRI scans of patients with dysplasia focus on the hip region and thus do not provide the needed information on the rest of the body. An infant computational model representative of a ten-week-old girl was developed using a combination of images from the Visible Human Project and CT scans

of a fourteen-year-old girl and a six-month-old baby. Moreover, anisotropic scaling was used to include important anatomical landmarks and origins/insertion points.

Furthermore, it is clinically known that bone growth is not proportional in all directions [45]. Therefore, for all bones of the lower extremities, general properties of matter were used, such as elasticity, temperature, conductivity, etc., although they vary in the direction in which they are examined.

Regarding the restoration of the hip, rough bone geometry contours were attained from a computer tomography of a six-month-old girl, later to be overlayed with a well-defined bone geometry from a tomography of a fourteen-year-old girl [46]. The overlapping of both tomographies, the six-month-old girl and the fourteen-year-old girl, were positioned in such a way that the iliac spines and acetabulum were aligned [47]. Specific programs that are available today [48][49] to simulate muscle performance, unfortunately, cannot be used to simulate dysplasia.

Five adductor muscles were recognized in previous research [11][12] as mediator muscles during closed reduction: pectineus, adductor magnus, adductor longus, adductor brevis, and gracilis. The adductor magnus is big, triangular, and has a wide femoral insertion; therefore, it is represented by three components, adductor magnus minimum, adductor magnus medius, and adductor magnus posterior. The anisotropic scale of the insertion points for the mentioned muscles was computed using the coordinate points derived from the Dostal and Andrews experiments. The resulting model is shown in Figure 11.

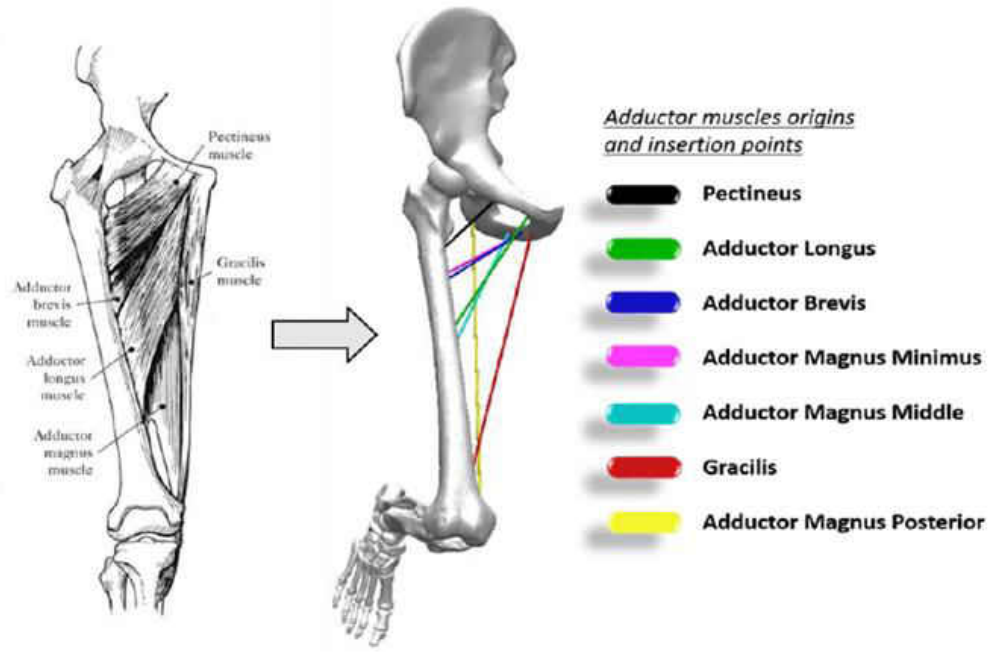

Figure 11: Anterior view of adductor muscles origin and insertion points [50].

The Global Coordinate System for the model was located at the center of the acetabulum for the hip and a local Coordinate system at the center of the femoral head for the femur. For the mentioned study, musculoskeletal tissue was modeled using a straight-line muscle path representation since lines of action do not intersect in the range of motion of interest, allowing the use of classical methods of vector analysis [68].

This model is essential because it provides a starting point to validate the forces found on the Matlab® model when simplified to only use the seven muscles mentioned.

4.3 Passive Muscle Model

In the human body, there are skeletal, smooth, and cardiac muscles [51]. These skeletal muscles link the bones, provide action and movement of the skeleton. These

muscles are composed of fascicles, which are composed of fibers as shown in Figure 12, which in turn are composed of numerous sarcomeres.

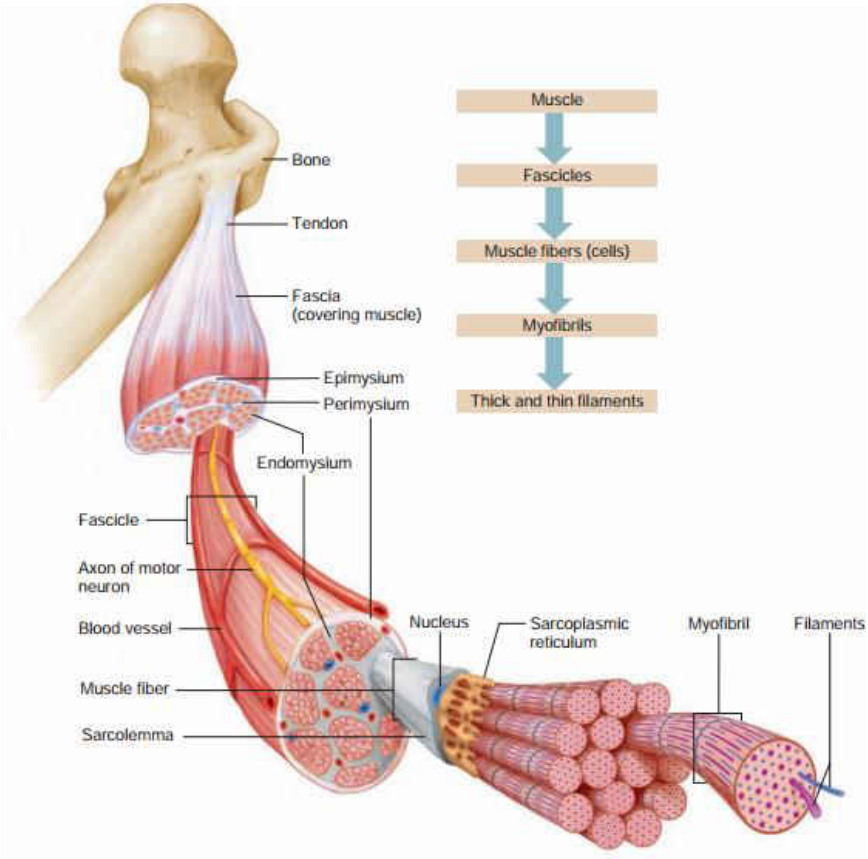

Figure 12: Skeletal muscle comprised of a variety of tissue [52].

The stiffness of a muscle increases faster than the stiffness of the individual fibers for the same strain [53], this is explained because the passive force can be distributed over or only over the epimysium, perimysium, endomysium [54][55], myofibers [53], or the fascia which is even stiffer [56].

The muscle tension is a function of the number of sarcomeres in parallel [57]. Figure 13 shows the total tension force generation, which is the summation of the active force,

provided by the muscle fibers, and a passive force, which comes from the muscle stretching [58][59]. In the case of closed reduction of DDH, only the passive component is of interest as clinical observation reveals that reduction occurs passively during sleep under the action of gravity alone [29][31].

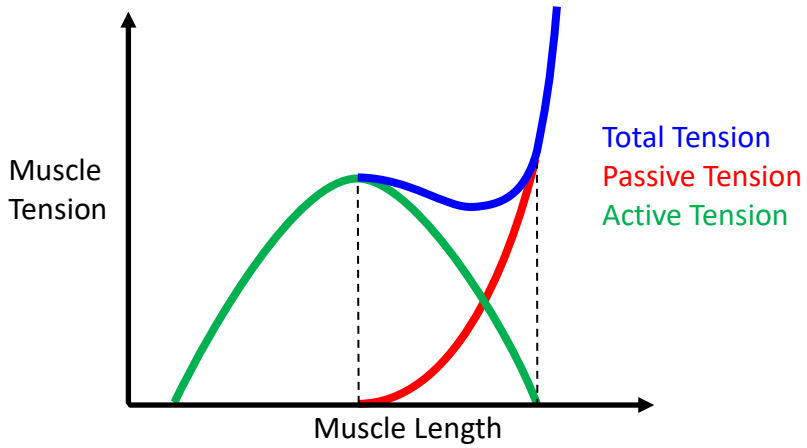

Figure 13: Tension force of a Muscle, including Passive and Active Tension [60].

The passive force of the muscles, as illustrated in Figure 13, does not obey Hooke's law. The muscle model proposed by Magid and Law [53] and developed from Fung's work [61][62] is adopted for analysis, and it is based on the expression for stress as follows:

$$\sigma = \frac{E_0}{\alpha_a}(e^{\alpha_a * \varepsilon} - 1) \tag{1}$$

Where $\boldsymbol{\sigma}$ is the unidirectional stress of the muscle, $\mathbf{E_0}$ is the initial elastic modulus (The Young modulus for biological tissue at its resting length, $\mathbf{E_0}$ has been found to increase linearly with the force), $\boldsymbol{\alpha_a}$ is an empirical constant related to the physiological cross-section area (PCSA), and the strain is defined as:

$$\varepsilon = \lambda - 1 \tag{2}$$

Where $\lambda = L/\mathrm{L}_0$ is the stretch, which is the ratio of the current muscle length L divided by $\mathbf{L_0}$ which is the length of the muscle when the fiber does not present any tension known as zero force-length.

The values for E_0 and L_0 can be found from experimental data, from which E_0 for an adult had a value of 2.6 x 103 N / m^2. Variability of α_a and E_0 are documented for adult muscles and, also based on results from animal experiments as shown [53]. Force over a Cross-sectional Area is known to be stress, forces can be calculated as:

$$F = PCSA * \sigma \tag{3}$$

In this case, the area is the physiologic cross-sectional area (PCSA) and may be calculated as:

$$PCSA = \frac{m \cos\theta}{L\, \rho_m} \tag{4}$$

Where m is the muscle mass, θ is the average pennation angle of the fibers (angle between the fiber orientation and the line of force exerted by the muscle), L is the average fiber length, and ρ_m is the muscle area density in mass/area units. However, for this research, each muscle was assigned a different PCSA area, which has been calculated scaling from an adult value by calculating a ratio of the PCSA of a single infant muscle.

Previous research measured the PCSA of an infant adductor brevis was found to have an area of 41 mm^2 [63]. This value was used relative to the provided PCSA to calculate the scaling ratio applied to all other muscles in the model. Adding this variable to the model lets each muscle have a different stiffness because of their different PCSA, as

illustrated as the red curve in Figure 13. In this way, the individual muscle parameters are adjusted to achieve static equilibrium in a reference configuration [11].

The elastic modulus of muscles E_0 is not explicitly defined for all muscles. It is modified as a group, so all muscles are re-defined in the form of constants "a" and "b". These constants are obtained by recalibrating the model to adjust to an equivalent of a 10-week-old female. These constants were used to stiffen the exponential function towards stabilizing the hip joint, modifying previous equation (1) to:

$$\sigma = a(e^{b\varepsilon} - 1) \tag{5}$$

Thelen and Delp [64][65] defined these two constants for the adult model as:

$$a = \frac{\mathrm{C}}{e^{K^{PE}} - 1} = 0.466 \frac{\mathrm{N}}{\mathrm{cm}^2} \tag{6}$$

$$b = \frac{K^{PE}}{\varepsilon_o^M} = 6.667 \tag{7}$$

Where C = 25 N.cm^2 being the specific muscle tension, the exponential form factor is $K^{PE} = 4$, and the passive muscle tension is ε_o^M.

For the 10-week-old female model, the value of “b" was assumed to be softer than an adult. So the calculation of the final equation used to describe the muscles using equations (2), (3), and (5) lead in previous research [11] to the following expression:

$$F = PCSA\left[a\left(e^{b(\lambda-1)} - 1\right)\right] \tag{8}$$

4.4 Muscle Structure, Physiology, Behavior

Much work has been done on how to model the line of action of the muscles, which affects the acting forces, therefore the behavior of biomechanical models. This can be done

using the centroid of the muscle, can be also performed using the insertion points of the muscle added as straight lines, or can include wrapping which is the most difficult to model but provides the most accurate forces [66]. For this research, the representation of the lower limb was modeled with low friction in the articulation as well as the friction between muscles.

The hip joint is completed by the femur which is the strongest bone in the whole body. It consists of 6 main areas; head, neck, greater trochanter, lesser trochanter, shaft or body, and condyle region.

The tubular part, or shaft of the femur, is the site of many insertions and muscle origins; it is comparatively rounded, and flattens out as it approaches the condyle; where, on the posterior side, has a long-running ridge called the Linea Aspera. The contact point of the femur in the region of the condyle is where the knee joins with the tibia [23][67].

Femur length measures the longest bone in the body and reflects the longitudinal growth of the fetus. Its usefulness is similar to the biparietal diameter (BPD, which is the diameter between the 2 sides of the head. Femur length increases from about 1.5 cm at 14 weeks to about 7.8 cm at term.

The head of the femur has a spherical shape, which is part of the ball and socket joint, called the hip. In shape and volume, it is ellipsoidal, non-hemispherical such as the basin, being more spherical in newborns. A cartilaginous material that covers it, the acetabulum cartilage, provides shock absorption and reduces surface friction [23][67].

A trochanter is a tubercle of the femur near its joint with the hip bone. In humans and most mammals, the trochanters serve as important muscle attachment sites. Humans

are known to have three trochanters, though the anatomic "normal", the femur includes only the greater and lesser trochanters illustrated in Figure 14.

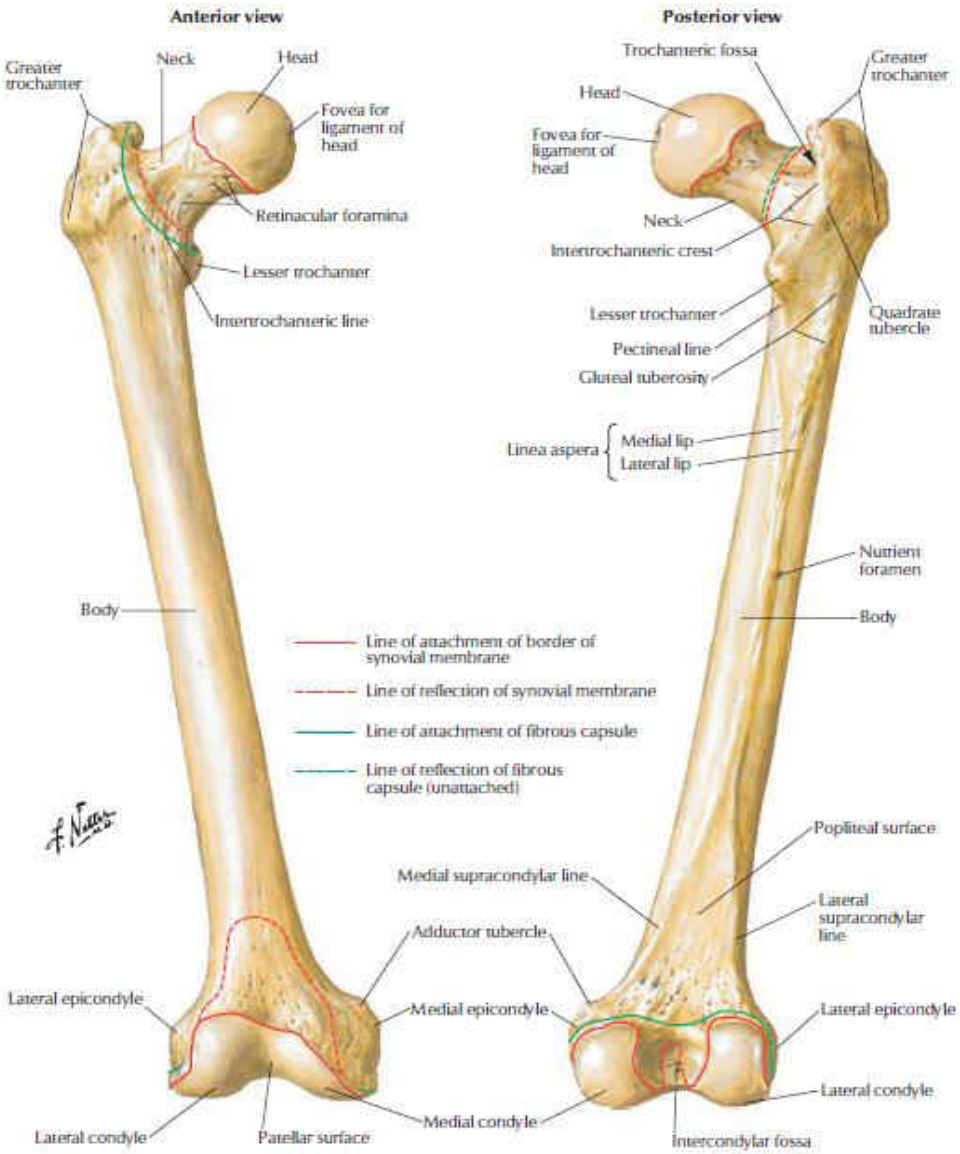

Figure 14: Femur Anatomy [68].

The average adult male femur is 48 centimeters (18.9 in) in length and 2.34 cm (0.92 in) in diameter and can support up to 30 times the weight of an adult. It forms part of the hip joint (at the acetabulum) and part of the knee joint, which is located above. The long, straight part of the femur is called the femoral shaft. When there is a break anywhere along this length of bone, it is called a femoral shaft fracture. This type of broken leg almost always requires surgery to heal. The femoral shaft runs from below the hip to where the bone begins to widen at the knee.

The line which defines the mechanical axis of the femur is extended through the distal femur to form an angle between the mechanical axis of the femur and the tibial shaft axis, this angle is known as the femur deviation angle.

Another important angle to consider is the common angle between the longitudinal axis of the proximal and distal femur, the anterior bowing angle. Those axes normally use a point 40 mm apart from the initial point to establish direction. There are other ways to define the bowing using the Mechanical Axis, or a fixed radius [69], or even defined with 3 radii [70] because each of the 3 sections of the shaft can have unique radii of curvature. Bowing should be considered instead of 2 straight lines, this parameter measurement has been illustrated in Figure 15.

To identify the sagittal femoral bowing angle (sFBA) and the coronal femoral bowing angle (cFBA), the femoral shaft is quarterly divided into the coronal and the sagittal planes. The proximal end is the lower border of the lesser trochanter and the distal end is the junction between the shaft and the condylar region. sFBA and cFBA are angles between midlines drawn in the proximal and distal quarter segments of the femoral shaft. In Figure 15**a** the points *a*, b, c, d are midpoints of the medullary cavity in the coronal plane. While

in Figure 15**b** the points *A, B, C, D* are midpoints of the medullary cavity in the sagittal plane [71].

Figure 15: The femoral shaft in a) coronal and b) sagittal planes [71].

In this dissertation, a catenary curve is employed to represent the femur curvature. A catenary is obtained in nature when a cable is constrained at its two endpoints creating an arc due to gravity, the equation of a catenary in Cartesian coordinates has the form [72].

$$y = a_c cosh\left(\frac{x}{a_c}\right) = \frac{a_c}{2}\left(e^{y/a_c} + e^{-y/a_c}\right) \tag{9}$$

The shape of the femur is not straight, to simulate the bowing for a given curvature, this shape was proposed instead of an arc of a circle or a parabola or many radii because it is shown to best fit a variety of sampled images of the femur including the Dostal and Andrews Femur used to derive the 3D muscle insertion points as shown in Figure 16.

Once the model was assembled, it was possible to computationally dislocate the hip to match physiological dislocations according to the dislocation grades under investigation.

To account for the proper weight distribution of muscles attached to the lower limb, calculations of the total body mass were based on weight for length 50^{th} percentile curve for a ten-week-old female infant (WHO Child Growth Standards, World Health Organization,2020) and shown in Table 2.

Centers of mass were also determined, thus achieving accurate load and moment distribution in the model [73]. Gravity acts as the sole external driving load in the dynamics model to be described later. Moreover, the constraints assigned to the three-dimensional model serve to restrain the motion within the envelope realized with the Pavlik harness during Grade 1-4 studies to constrain the knees in a hyper-flexed configuration for Grade 4 studies.

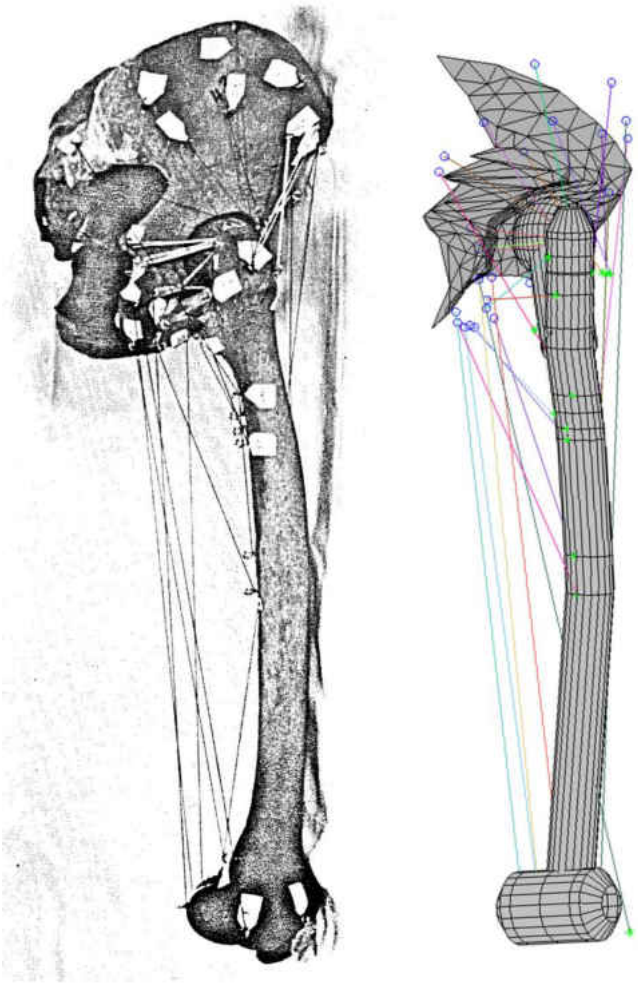

Figure 16: Comparison Dostal and Andrews femur [47] with current Matlab® model femur using a catenary equation to represent the femoral shaft path.

Table 2: Lower Extremity Mass Distribution.

	min	median	max	Description
Female Body Mass [Kg]	4.2	5.4	6.8	3 Percentile
	3.90	5.4	7.10	Range extended

4.5 Fulcrum point

The fulcrum point is considered a point where a lever turns; in particular, the pivot point. The literature does not report on the use of a fulcrum point and its effect on the treatment of DDH. However, Figure 8 and Figure 9 show that most of the HAOD present some type of support behind the leg. This force can be represented as shown in Figure 17. The leg normally will abduct further, but the fulcrum point will equilibrate the rotating moment of the femoral head with a force proportional to the moment generated by the leg and inversely proportional to the distance "d" at which the force is actuating.

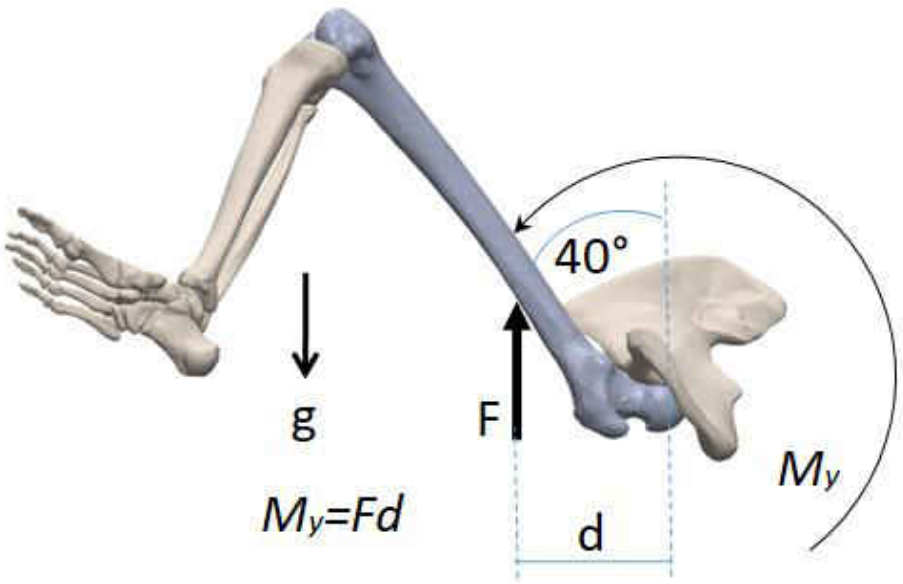

Figure 17: Example configuration of a free body diagram for the estimation of Fulcrum point force. (40° abduction, 90° flexion) Gravity vector "g" is shown for orientation, pelvis placed in supine orientation.

4.6 Software and numerical methods

From among the experimental and theoretical methods available for research, a computational model is preferred since it has the tools to repeat agilely and has the

advantage of testing broad parameter spectra, so it leaves for future research to validate the proposed FP locations. This section is divided into subsections, which will cover: 1) the software available and used for this investigation, 2) the catenary curve parameter estimation, 3) Monte Carlo methods, 4) statistical distributions, 5) Pearson and Spearman correlation matrix, 6) the Rotation matrix and Rodrigues rotation formula, 7) Singular value decomposition and scaling, and 8) collision detection.

4.6.1 Software used

The selected programming language and software was Matlab®, due to its ease of use in matrix operations and the built-in algorithms to solve some sections of the problem with the convenience of providing 3D plots for illustrations.

For the aid of information and illustrations, OpenSim version 4.1 was selected. It is an open-source software sponsored by Stanford University. This software is used in biomechanical modeling, simulation, and analysis of the musculoskeletal system. This tool has been enhanced by models, data, and scripts that the community has been developing and sharing worldwide [16].

For solid modeling, the computer-aided design tool of preference is SolidWorks®, which allows fast measurements, simulations, and 3D modeling; it runs under Windows and other operative systems being suitable for file sharing among different platforms.

To find an equation that optimizes the first guess for the catenary curve calculation parameters, the software of choice was Eureqa. This software determines from a data set

of inputs and outputs the simplest equation that best fits the data. It can also be used with many runs to define a function that behaves as the system.

For statistical analysis, Microsoft Excel® was used, as it is one of the most known software worldwide, which allows the easy management of information with multiple calculations and solvers.

4.6.2 Catenary curve parameter estimation

The a_c estimation of the catenary curves to represent the bowing of the femoral shaft in x and z-direction using the reference coordinate system shown in Figure 31 was done using Steep Descend, which is a mathematical method to find a solution to a single or multivariable problem finding the gradient of a multidimensional surface, making the next estimation in the steepest direction to converge the fastest way possible. This algorithm is extremely efficient; it only requires a large number of iterations if there are multidimensional surfaces with narrow valleys.

4.6.3 Monte Carlo methods

Monte Carlo methods or experiments encompass a broad type of algorithms based on random sampling to obtain numerical results, as shown in Figure 18. An example of random 3D points inside a sphere of radius two can be used to define the variation of the location of a point in space. It is often used in mathematical and physical problems, including biomechanics; each parameter to be randomized can have different probability distributions. Monte Carlo methods can help for strongly coupled systems as well as

kinematic models of gases, among others. Monte Carlo methods can solve any type of problem that has a probabilistic interpretation and is mostly applied when the system is too complex to define it with a simple equation or if the number of variables to cover all possibilities is impractical. If desired, Monte Carlo pseudo-random generators also allow replicating an experiment using the same seed. In this study, to understand the fulcrum point effect over multiple lower limbs, Monte Carlo methods were used to generate multiple configurations of the lower limb, changing muscle lengths and areas, muscle insertion point locations over the pelvis and femur, static equilibrium reference angles to find muscle properties, HAOD angles, among others, with the objective to consider most possible leg configurations.

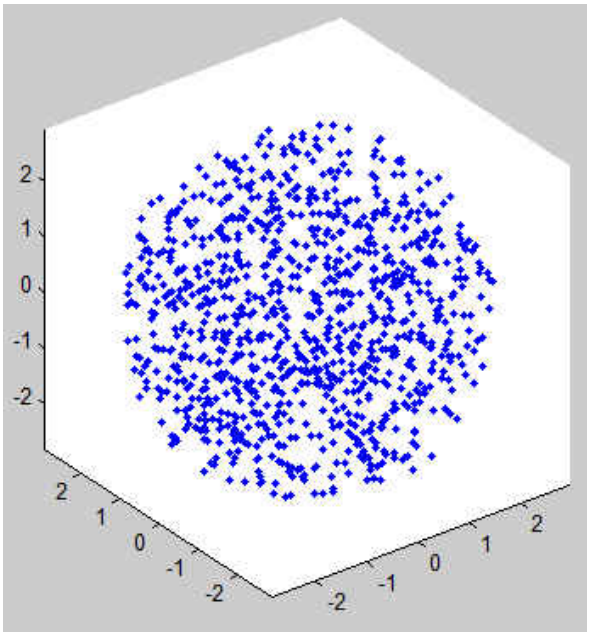

Figure 18: 3D points inside a sphere of radius 2.

4.6.4 Statistical distributions

When applying the Monte Carlo Method for this dissertation, the random selection of each of the values of the parameters for each configuration needs to be constrained in a known range; normal distribution is not a bounded distribution. One of the suitable statistical distributions is the Beta Distribution [74], which is a family of continuous probability distributions defined on the interval [0, 1] parameterized by two positive shape parameters, denoted by α and β, that appear as exponents of the random variable and control the shape of the distribution. Beta distribution has the advantage of been bounded exactly by the desired interval and can have a non-central distribution as well as other forms [75][76].

When the expected value is too close to the maximum value, a triangular distribution is the best fit; this distribution works perfectly as an alternative to the beta distribution, which suffers from difficulties involved in its maximum parameter estimation. It is possible to use a triangular distribution as a proxy to the beta distribution since the parameters of a triangular distribution line up correspondingly with a positive estimate value a_T, most likely estimate c_T. And negative estimate b_T of a quantity under consideration. Similar to the beta distribution, the triangular distribution can be positively or negatively skewed (or symmetrical) but must remain unimodal [77]. The triangular distribution is defined by:

$$f(x) = \begin{cases} 0 & x < a_T \\ \dfrac{2(x - a_T)}{(b_T - a_T)(c_T - a_T)} & a_T \leq x \leq c_T \\ \dfrac{2(b_T - x)}{(b_T - a_T)(b_T - c_T)} & c_T \leq x \leq b_T \\ 0 & x > b_T \end{cases} \tag{10}$$

Where a_T is the minimum value, $a_T \leq c_T$, c_T is the mean value, where $a_T \leq c_T \leq b_T$, and b_T is the maximum value, where $b_T \geq c_T$. If the mean is near a boundary, the triangular distribution provides a valid solution compared with the beta distribution for this research.

4.6.5 Pearson and Spearman correlation matrix

The data generated first is the Pearson correlation matrix, which compares the different parameters and finds the grade of correlation of both variables; if the correlation value is equal to one, the two chosen parameters are strongly proportionally correlated; if it is near zero, there is no linear correlation among the two parameters, if it is -1 the two parameters are strongly inversely proportional correlated, is used as a first overview for a possible linear relationship between the input and output parameters. The correlation coefficient has a range from -1 to 1 and can be calculated as:

$$r = \frac{\sum(x_i - \bar{x})(y_i - \bar{y})}{\sqrt{\sum(x_i - \bar{x})^2(y_i - \bar{y})^2}} \tag{11}$$

Where r is the correlation coefficient, x_i are the samples of one parameter with mean $\bar{x}$, y_i are the samples of the other parameter with mean $\overline{y}$.

For a second overview, it was of interest to calculate if there is a monotonic relationship between 2 parameters; for this, the Spearman rank correlation matrix is used, which summarizes the strength and direction of a relationship between pairs of parameters;

it also has the range from -1 to 1. For each parameter sorting the samples, the rank among them can be found. This correlation can be calculated using the ranks of both parameters; if it is 1 represents a perfect association of ranks; if it is -1 represents a perfect negative association of the parameters. The Spearman rank correlation coefficient ρ can be calculated as:

$$\rho = 1 - \frac{6 \sum d_i^2}{n(n^2 - 1)} \tag{12}$$

Where n is the number of observations and d_i is for each observation, the difference between the ranks of each parameter.

The interest in this dissertation in understanding the relationship among parameters is to simplify, if possible, the number of inputs needed to define the fulcrum point location, and to also analyze more in-depth parameters that show a strong correlation with the fulcrum point location to find a possible mathematical relationship. For example, if the external rotation of the femur during the measurement of the static equilibrium configuration to estimate the material parameters does not affect the fulcrum point location, then the external rotation can be removed from the analysis.

4.6.6 Rotation Matrix and Rodrigues' rotation formula

The analysis of the fulcrum point requires the model to effect numerous rotations in 3D. To rotate a point in 3D with respect to a coordinate system, it is possible to express the equation in a matricial form, in which the rotation matrices multiply an initial vector, which represents the 3D point to find the final 3D vector rotated. For example, suppose a point P_f is desired to be rotated an angle θ with respect to the z-axis, then rotated and angle

Φ with respect to a y-axis as shown in Figure 19, then the location of the point after rotation can be defined as P_2, then the mathematic representation will be the following:

$$\begin{bmatrix} x_2 \\ y_2 \\ z_2 \end{bmatrix} = \begin{bmatrix} \cos\Theta & -\sin\Theta & 0 \\ \sin\Theta & \cos\Theta & 0 \\ 0 & 0 & 1 \end{bmatrix} \begin{bmatrix} \cos\Phi & 0 & -\sin\Phi \\ 0 & 1 & 0 \\ \sin\Phi & 0 & \cos\Phi \end{bmatrix} \begin{bmatrix} x_f \\ y_f \\ z_f \end{bmatrix} \tag{13}$$

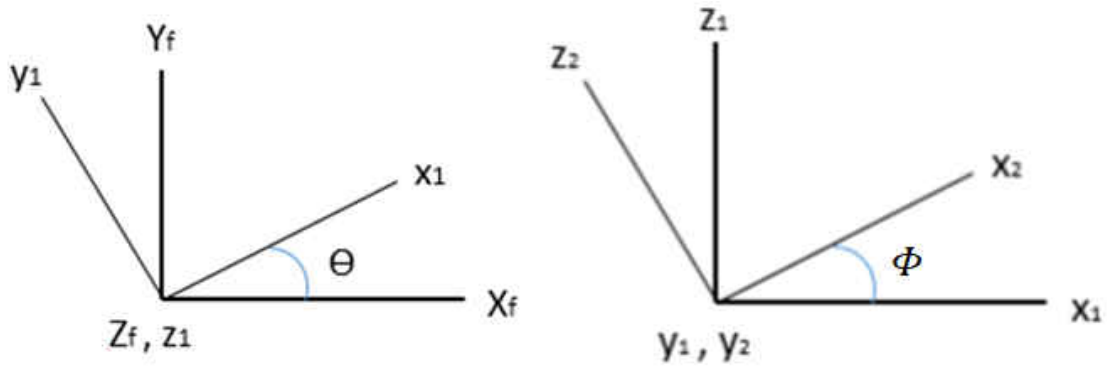

Figure 19: First (left) and second transformation (right) of P_f about two angles.

The limitation of this method is if the rotation is with respect to an axis different than in the coordinate system, the number of mathematic operations will increase significantly. Among three-dimensional rotations, the Rodrigues formula is a convenient method to rotate a point around a local axis, instead of the traditional rotation matrix, which needs a translation back and forth or a coordinate system transformation to achieve the same result. If v is a vector in $\mathbb{R}^3$ and k is a unit vector describing an axis of rotation about which v rotates by an angle φ according to the right-hand rule, the Rodrigues formula for the rotated vector V_{rot} is

$$V_{rot} = v\cos\varphi + (k \times v)\sin\varphi + k(k \cdot v)(1 - \cos\varphi) \tag{14}$$

These three angles θ, Φ, and φ respectively represent in this research the flexion, abduction, and external rotation angles illustrated before in Figure 2.

4.6.7 Singular value decomposition and scaling

Singular value decomposition (SVD) is a well-established factorization of a matrix which allows decomposing a matrix into a product of two rotation matrices and a diagonal scaling matrix. It is useful to find a rotation of a vector over a set of vectors and to align them. Umeyama [78] used SVD and included an isotropic scaling to improve the fit of the point clouds. Anisotropic scaling or non-uniform scaling (unequal along different directions) is needed for scaling down an adult model to be fitted to an infant model, which implies a modification over the Umeyama method needed to be implemented.

The entire process of scaling has been simplified using matrix representation of a set of vectors, where each vector represents a point in space, allowing fast operations between them. Umeyama uses a matrix representation for scaling, which can be modified by finding the anisotropic scales, primarily, by a deduction of a least-square best fit value.

In this dissertation, anisotropic scaling was implemented to best fit the three-dimensional points of the insertion muscles of the pelvis over the model pelvis.

4.6.8 Collision detection

In Solid Body interaction theory, collision detection is the very common tool used to find the intersection of 2 solids that are moving with respect to the others. One of the simplest methods for finding a collision is the intersection of a sphere with another. For

this dissertation, the pelvis was represented by multiple three-dimensional points, which are used to define the three-dimensional location of the center of the femoral head during its pathway from dislocation to the center of the acetabulum.

Figure 20 illustrates the path from the femoral head represented as a sphere to collide with a point Pi located over the hip; it finds the point $\overrightarrow{P_j}$, in between of the path. The solution using this method is a simple and fast collision detection algorithm, once points $\vec{P}_j$ are identified. To identify the collision point $\overrightarrow{P_j}$, calculate with all the points of the hip, the distance from those $\vec{P}_j$ nodes, to the axis vector form by $\vec{P}_c - \vec{P}_i$. If the distance "d" is lower than the radius of the femoral head r, then $\vec{P}_j$ will not collide with the sphere. If it will collide with the sphere, the shortest distance is calculated to $\vec{P}_c$, finding distance w, which allows the calculation of distance D. Therefore displacing the femoral head a distance D in the direction $\vec{P}_c$ to $\vec{P}_i$, reaches point $\vec{P}_j$.

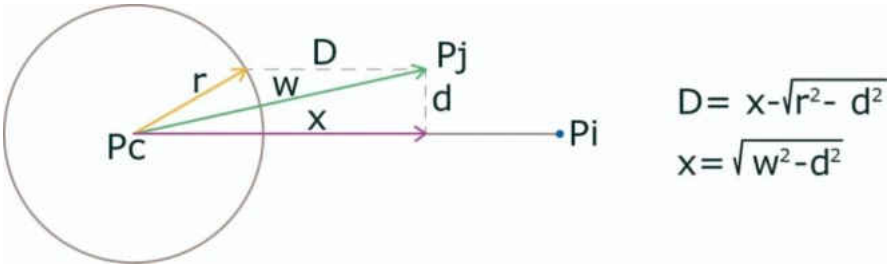

Figure 20: Path of a sphere from Pc to Pi colliding with Pj.

CHAPTER 5: RESEARCH METHODOLOGY

This chapter will cover the method used to develop the SolidWorks lower limb model, the method used to calibrate the muscle properties, and the method used to develop the Matlab model. These models are subsequently employed to investigate the question of the optimal fulcrum point for various grades of DDH. The SolidWorks® model is utilized as a verification tool for the model developed in Matlab®; the Matlab® model is utilized to generate a multitude of configurations of the lower limb anatomical parameters; these configurations subsequently are also analyzed in Matlab® for different fulcrum point locations for different brace constraints.

5.1 SolidWorks® lower limb model

Two computational models were developed, one in Matlab® and the other as shown in Figure 20 (later updated with smoother surfaces, and added Tibia/Fibula) developed in SolidWorks® for verification and calibration purposes, using the previous research developed as a starting point [11]. All this section will only refer to the SolidWorks® model [11]. This model consists of 4 different human subjects, (1) a scaled-down femur [79] with an improved spherical femoral head to more resemble infant geometry [11], (2) a scaled-down pelvis adjusted to (3) a 10-week old infant CT Scan, and (4) muscle attachment points scaled-down as well and adjusted to the geometry by projecting the points over the surface of the solid, based on muscle insertion points definitions using the expected anatomical landmarks. The orthogonal planes defined to place the geometry are similar to the ones defined in the literature [47], with the origin placed at the center of the acetabulum.

The muscles that were considered inactive during adduction were extracted from the literature [80]. When including flexion, the psoas and the iliacus muscles were found to not contribute significantly to the equilibrating forces and were discarded from this model. The muscles used for this model were the pectineus, adductor brevis, adductor longus, adductor magnus, and gracilis showed in Figure 21.

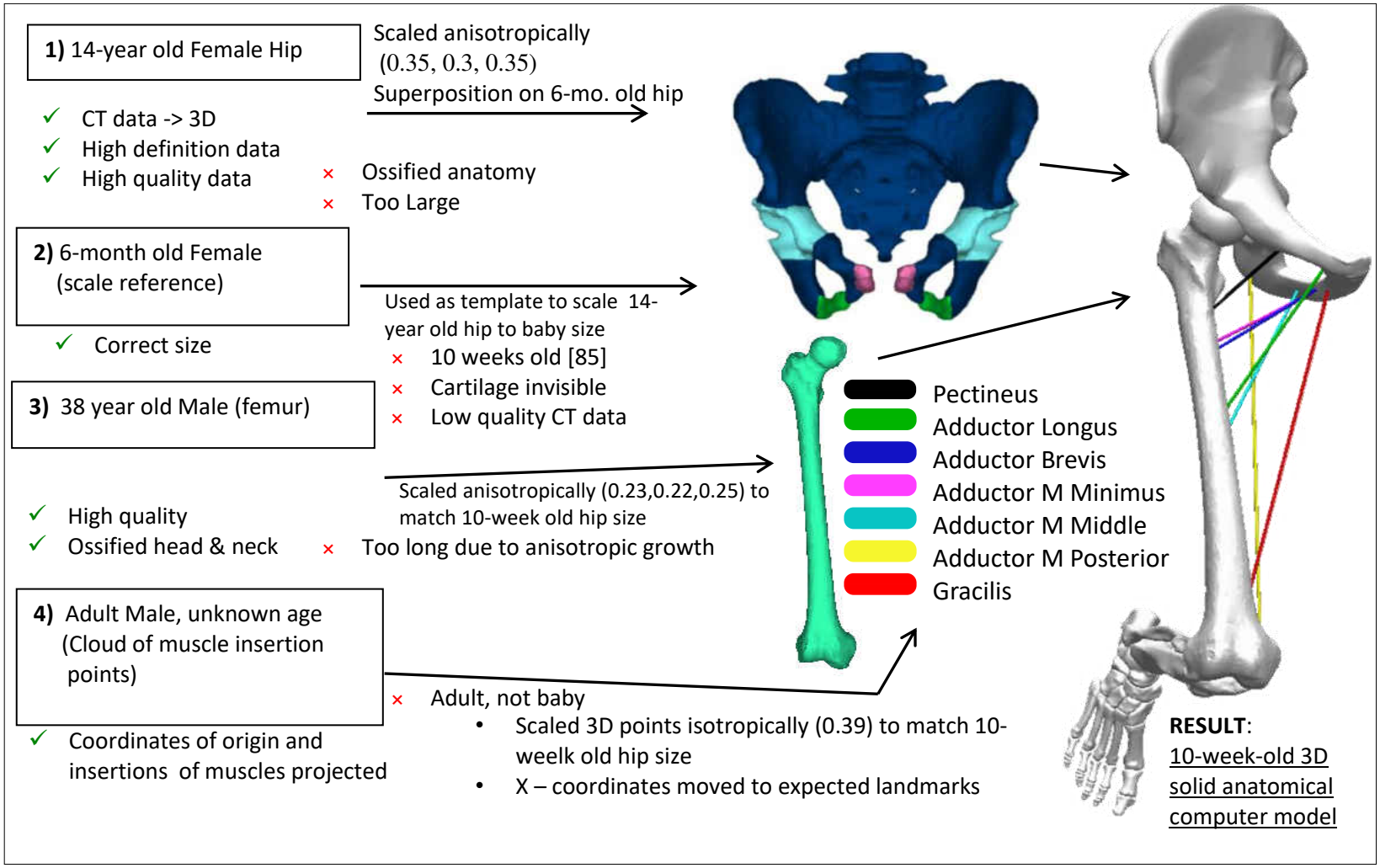

Figure 21: Three-dimensional Computational model constructed by different sources [11].

The muscles were considered as straight lines; the adductor magnus, which attaches to a line over the femur, originally shows a triangular-like shape. To model, it was divided into three linear muscles based on the literature [47]. For the scope of this model, the gluteus maximus and other wrapping muscles were not being taken into account, nor the effect of wrapping or friction.

The infant muscle mechanical properties have been calibrated from a combination of (1) the literature which indicates the proper muscle Stress-strain model to use, (2) an approximate equilibrium configuration of the leg, being at 90 degrees flexion, 80 degrees abduction, and (3) the resting muscle lengths estimated from a leg configuration being at 120 degrees flexion 20 degrees abduction, this estimation is assuming the resting length of a ten-week-old infant have not changed significantly since birth, images of several infants corroborated this assumption and was well accepted when presenting results at the 2014 Annual Meeting for Pediatric Orthopedic Society of North America (POSNA), Hollywood CA.

For this model, the adult PCSA used was based only on the first sample of an adult measured by Friederick [81] was found to be 11.52 cm^2. Therefore, it follows that the scale factor between the adult and child models was 3.56. This scale factor is used to scale the PCSA for all OpenSim muscles. Table 3 lists the OpenSim PCSA and the scale child model.

Adding this variable to the model, let each muscle have a different stiffness because of their different PCSA as illustrated in Figure 22, in which stretch is defined in equation (2).

Table 3: Scaled muscles cross-sectional area for SoliWorks® model [11].

Muscle	Adult PCSA cm^2	Scaled PCSA mm^2
Pectineus	9.03	32.14
Adductor Longus	22.73	80.9
Adductor Brevis	11.52	41
Add. Magnus Min.	25.52	90.83
Add. Magnus Med.	18.35	65.35
Add. Magnus Post.	16.95	60.33
Gracilis	3.72	13.27

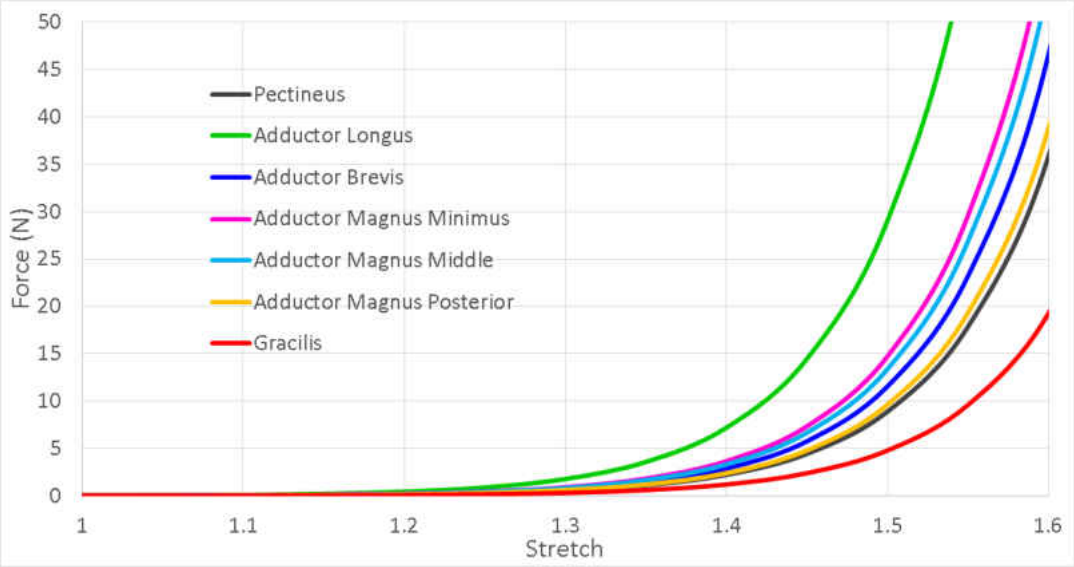

Figure 22: Passive tension force of the muscles used in the SolidWorks® model [11].

An average sarcomere resting length of 2.2 μm at max force can extend to more than 3 μm and contract to 1.6 μm, but it is important to notice the muscles in the body at resting length are at their optimal length for development of force, making this resting length dependent on the resting configuration of the muscle [57]. This resting configuration is continuously changing in time, making it difficult to compare muscle lengths, but at least provides us with an upper limit of expected muscle stretch.

When calculating the deformation energy of the muscles to be considered, it is done in the following way:

1) The collision detection algorithm is used in a computer since it uses vectors from the center point of the femoral head to points that have been selected on the pelvic surface, as illustrated in Figure 27 and Figure 28.

In this sequence, the head of the femur is located in a space away from the pelvic surface and is moved by checking contact points on its surface. Once a code has been found that defines the distance "d" that equals 7 mm, corresponding to the radius of the femoral head, the coordinates of the center of the femoral head are printed.

2) A grid of points is obtained based on the results of the collision detection, and yet another calculation is performed. For each site in the center of the sphere, the paths, or "L" distances of the muscles that had been selected, from the origin point of the femur and at the hip insertion points, are calculated; then the strain "ε" is calculated for the muscles, as represented by the equation:

$$\varepsilon = \frac{L}{L_{oi}} - 1 \tag{15}$$

L_{oi} represents the length of the referential muscle and measures 80% of the length of the same muscle in the relaxed position. When the newborn is in the fetal position, whose degree of flexion is around 120 and 20 degrees of abduction, the lengths are relaxed.

A Heaviside function is used because the muscles can only be stretched to be able to exchange the negative values of the deformations, with a zero value, as illustrated in Figure 23. Therefore, deformation effectiveness is described as

$$\varepsilon eff = \varepsilon * u(\varepsilon) \tag{16}$$

Where

$$u(\varepsilon) = \begin{cases} 0 & if \quad \varepsilon < 0 \\ 1 & if \quad \varepsilon > 0 \end{cases} \tag{17}$$

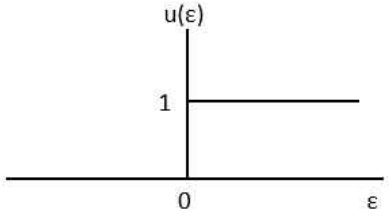

Figure 23: Heaviside function chart.

To mathematically find the strain "ε" for each muscle, the shown equation is implemented for a muscle, and then it can be used for the rest of the muscles, simply by changing the origin of the coordinates on the hip (x_h, y_h, z_h) and the insertion coordinates on the femur (x_f, y_f, z_f) towards each specific muscle. For example, in Figure 24, the pectineus muscle and the coordinates of the origin insertion are illustrated.

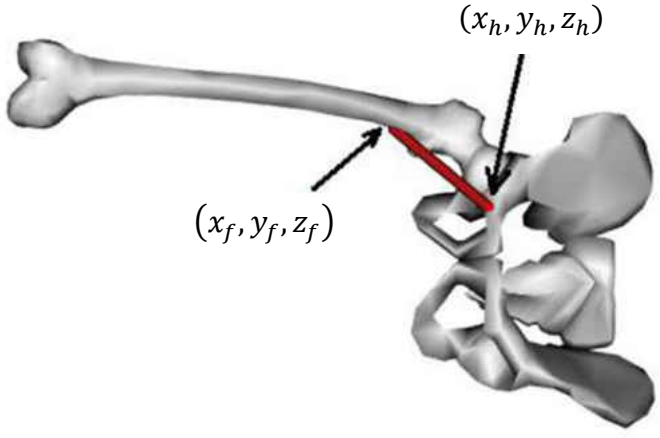

Figure 24: Insertion and origin points for the pectineus muscle.

To perform the calculations (x, y, z) are the coordinates of the center of the head of the femur, (x_1, y_1, z_1) is the first transformation of (x_f, y_f, z_f) over the flexing angle, (x_2, y_2, z_2) is the second local transformation of (x_1, y_1, z_1)over the angle of abduction, (x_3, y_3, z_3) is the third local transformation of (x_2, y_2, z_2) about the angle of rotation of the hip, θ is the flexion angle, Φ is the angle of abduction, φ is the angle of external rotation of the hip, L_{relax} is the length of the muscle in the relaxed position for the newborn baby (θ = 120° and Φ = 20°).

The first rotation is the transformation around the flexion angle from the insertion coordinate (x_f, y_f, z_f) to the coordinate (x_1, y_1, z_1), as shown on the left in Figure 19.

$$\begin{bmatrix} x_1 \\ y_1 \\ z_1 \end{bmatrix} = \begin{bmatrix} \cos\theta & -\sin\theta & 0 \\ \sin\theta & \cos\theta & 0 \\ 0 & 0 & 1 \end{bmatrix} \begin{bmatrix} X_f \\ Y_f \\ Z_f \end{bmatrix} \tag{18}$$

$$\begin{aligned} x_1 &= X_f.\cos\theta - Y_f.\sin\theta \\ y_1 &= X_f.\sin\theta + Y_f.\cos\theta \\ z_1 &= z_f \end{aligned} \tag{19}$$

The second rotation is a transformation on the angle of abduction from the coordinate (x_1, y_1, z_1) to the coordinate (x_2, y_2, z_2), as shown on the right in Figure 19.

$$\begin{aligned} x_2 &= x_1.\cos\Phi - z_1.\sin\Phi \\ y_2 &= y_1 \\ z_2 &= x_1.\sin\Phi + z_1.\cos\Phi \end{aligned} \tag{20}$$

The third rotation is from the point (x_2, y_2, z_2) on the external rotation, as illustrated in Figure 25.

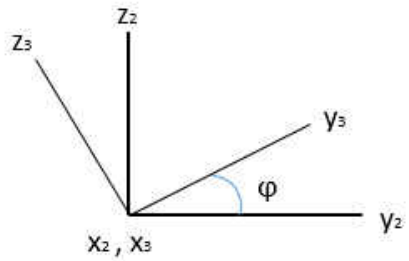

Figure 25: Third transformation on the angle of rotation of the hip.

$$\begin{bmatrix} x_3 \\ y_3 \\ z_3 \end{bmatrix} = \begin{bmatrix} 1 & 0 & 0 \\ 0 & \cos\varphi & -\sin\varphi \\ 0 & \sin\varphi & \cos\varphi \end{bmatrix} \begin{bmatrix} x_2 \\ y_2 \\ z_2 \end{bmatrix}, \text{ where } \varphi \text{ is the hip rotation angle.}$$

$$\begin{aligned} x_3 &= x_2 \\ y_3 &= y_2 \cos\varphi \ - z_2 \sin z_2 \\ z_3 &= y_2 \sin\varphi + z_2 \cos\varphi \end{aligned} \tag{21}$$

Starting from the distance equation, the length of the muscle L is calculated

$$L = \sqrt{(x_h - x_3)^2 (y_h - y_3)^2 + (z_h - z_3)^2} \tag{22}$$

The final strain equation is then derived from equation (15) as

$$\varepsilon = \frac{\sqrt{(x_h - x_3)^2 (y_h - y_3)^2 + (z_h - z_3)^2}}{L_{oi}} - 1 \tag{23}$$

Finally, from equation (2) and (16), we formulated

$$F = PCSA\left[a\left(e^{b(\varepsilon eff)} - 1\right)\right] \tag{24}$$

b it was assumed to be 13.95, and the value of "α" was recalibrated to achieve equilibrium with the infant in supine position at the 90-degree flexion angle, at the angle of rotation of the hip at 0 degrees, and an angle of abduction of 80 degrees, in which a = 0.00078 MPa.

Likewise, when integrating stress in relation to strain, the strain energy density "Uo" is established as:

$$U_o = \int_0^{\varepsilon} \sigma \, d\varepsilon \tag{25}$$

Being the final strain energy density:

$$U_o = \frac{a}{b}\left(e^{\beta.\varepsilon_{eff}} - b.\varepsilon_{eff} - 1\right) \tag{26}$$

The strain energy values "U" are derived for all distances from the center of the femoral head with varying angles of hip flexion, rotation, and abduction. The strain energy function is established as demonstrated in the equation:

$$U = Uo * \forbidden{V} = f(x,y,z,\theta,\Phi,\varphi) \tag{27}$$

Where $\forbidden{V}$ is the volume of each muscle.

5.2 Muscle Mechanics – Calibration

Because the amount of tendon, fascia, and other tissues for each muscle is unknown, the whole system was calibrated together. To calibrate the model, the total reaction force of all the muscles and the weight of the leg should be at equilibrium at least at one known configuration to verify the validity of the muscle mechanical properties as a whole. Physicians have observed equilibrium is found when the infant laying on its back has its leg flexed 90 degrees and abducted 80 degrees.

To calibrate the muscles, first, some parameters must be defined:

- The location of the femoral head
- The configuration for the resting length, which in this case for a 10-week-old infant, has been assumed to be around 120 degrees in flexion and 20 degrees in abduction.
- A pre-stretch of the muscles of 25% was assumed, meaning the initial muscle length, if increased by 25%, will reach the resting length.

$$L_r = L_0(1 + 0.25) \tag{28}$$

Notice the initial length is the length at which the muscle is not exerting any tension force, which is different from the resting length L_r at which the active force could be maximized.

The leg is placed in the anatomical position (θ=0°, Φ=0°, φ=0°) and femur head at the origin (which is the acetabulum center). The pelvis and leg insertion points, once scaled-down, and projected, and adjusted to landmarks, were the following shown in Table 4.

Current model points for the femur need to re-measure from SolidWorks® if the anteversion or femur length is changed. This model was used in this dissertation only to validate the current Matlab® model, shown in Figure 26: Free body diagram of muscles in the lower limb, text in red corresponds to muscles that generate a negative moment in y-direction and with respect to the femoral head [11].

Figure 26 shows a free body diagram for the leg adjusted to 120 degrees in flexion, 20 in degrees of abduction. In that configuration, the lengths of the muscles are measured, and this length was assumed as the straight resting length. For other configurations, if a subluxation is present, the femoral head is moved to another location, and consequently, these resting lengths should be different.

Table 4: Muscle Insertion points, having the leg in the anatomical position.

Insertion points	Pelvis			Leg		
	X	Y	Z	X	Y	Z
	mm	mm	mm	mm	mm	mm
Iliacus	11.704	2.959	-0.417	14.584	0.237	0.355
Psoas	12.224	2.421	-1.669	13.735	0.469	0.581
Pectineus	10.512	-6.518	-10.971	26.410	-6.142	-4.417
Adductor Longus	9.798	-12.167	-18.577	52.382	-0.673	-2.106
Adductor Brevis	2.000	-13.531	-17.315	34.821	-4.052	-3.837
Add. Magnus Min.	-0.213	-13.885	-16.786	31.920	-4.202	-3.000
Add. Magnus Mid.	-4.257	-13.447	-15.705	59.223	0.428	-1.756
Add. Magnus Post.	-13.832	-11.692	-10.977	103.876	4.058	7.996
Gracilis	1.105	-13.742	-17.152	110.701	-4.520	9.534
Gluteus Max Min.	-15.085	18.025	1.043	7.149	-14.109	2.103
Gluteus Max Mid.	-17.426	3.766	1.669	14.966	-15.308	-1.611
Gluteus Max Post.	-21.328	-10.492	-8.973	28.661	-11.340	0.879
Gluteus Med Min.	8.698	25.559	7.210	4.703	-12.067	-7.911
Gluteus Med Mid.	-1.454	28.394	-6.407	2.545	-12.294	-3.995
Gluteus Med Post.	-7.032	22.605	-9.542	2.586	-12.160	-3.320
Gluteus Min Min.	5.006	16.051	5.589	3.226	-10.151	-8.959
Gluteus Min Mid.	1.556	16.532	0.305	3.177	-10.574	-8.552
Gluteus Min Post.	-1.617	14.244	-0.960	2.112	-11.313	-7.071
Centroid	0.000	0.000	0.000	74.606	-10.236	0.100

After finding the resting length, the leg is adjusted to 90 degrees in flexion, 80 degrees in abduction, the initial elastic modulus E_0 is assumed to be equal in all muscles to any number, and is iterated until all the muscles precisely achieve a moment in y-direction close to zero (lower than 10^{-6} as threshold). Figure 26 shows a free body diagram illustrating how an extra abduction will generate for the pectineus and other muscles a shorter distance from the force line of action to the center of the femoral head, it will also generate a strain in the muscle increasing the force of the muscle, if the force of the muscle. If the force of the muscle increases slower than the mentioned distance, the equilibrium

point can be unstable. This can be avoided diminishing the resting length of the muscle or increasing the value of the empirical constant α_a.

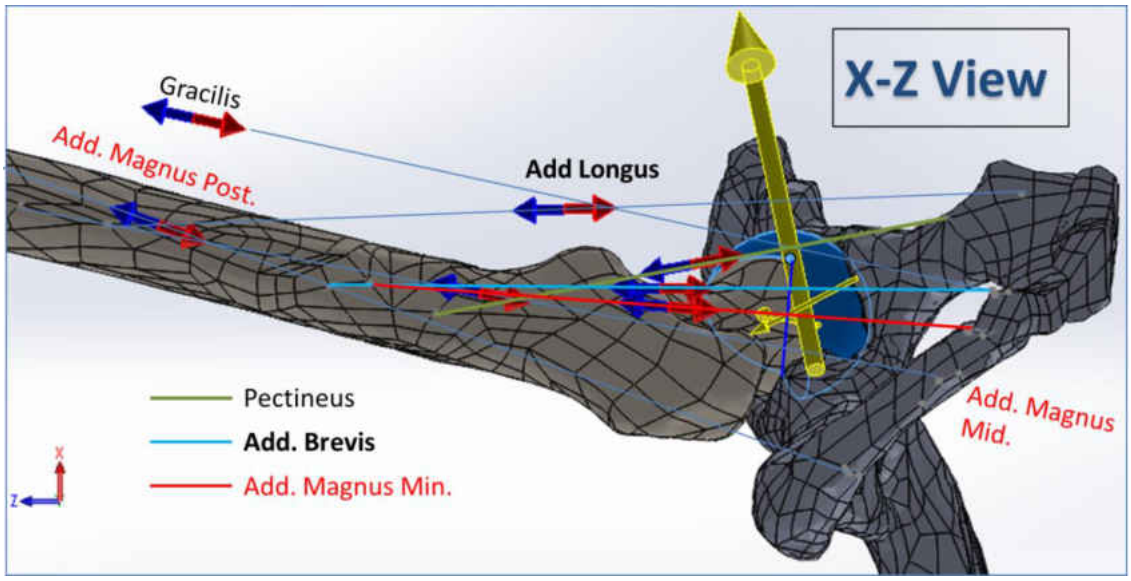

Figure 26: Free body diagram of muscles in the lower limb, text in red corresponds to muscles that generate a negative moment in y-direction and with respect to the femoral head [11].

The value of α_a can be verified by determining if the configuration is a stable system with 81 or 79 degrees of abduction verifying the moment is changing in the right direction. It has been found for the model used, that a value of α_a>10 needs to be used, based on [82] the lowest value of α_a found for a medial gastrocnemius of 13.95. α_a could be lower if the initial assumed pre-stretch is higher than 25%, or in other words, the initial muscle length can be calculated by reducing the resting length by 20%, another more realistic option is that not all the length of the muscle is deformable because of the part that are ligaments, tendons which are much stiffer than muscle tissue.

Once the stability of the configuration is verified, the initial elastic modulus can be verified by placing the equations of each muscle with this initial elastic modulus. It has been found and published that equilibrium has been achieved and the muscle force values have been reported using this method [11].

The results encompass the variation of parameters such as flexion angle, abduction angle abduction force, femur length, and acetabulum distance.

For a Graf type I infant, the initial length is the length of the muscle when the leg is at 120 degrees flexion and 20-degree abduction, then reduced in length 20%.

$$Lo_{\mathrm{I}}(1 + 0.25) = Lr_{\mathrm{I}}. \tag{29}$$

For a Graf type II, III, or IV infant, it is not clear the resting length, but will be between the resting length placing the femoral head in a Graf type I location and the resting length placing the femoral head in the Graf type II, III or IV location, therefore an average of both resting lengths has been calculated as a reasonable value to calibrate the model for the case of a Graf type II, III, or IV infant hip. If no average is calculated, the muscle forces are too low for a long resting length, and if using the muscle resting length of a healthy infant creates unrealistic high forces in the short muscles, such as the pectineus, when placing the leg in Graf type IV.

Finally, to avoid conditions of excessive force, a cutting force value was assigned to each muscle, to avoid ADAMS module of SolidWorks® failing to converge because of excessive accelerations during the collision of the femoral head with the hip.

Table 5 shows the PCSA of each muscle, the resting length at Graf type I with the muscle forces that achieve equilibrium when the leg is placed at 90 degrees flexion, 80

degrees abduction. Table 6 shows the equations in a format acceptable by SolidWorks®, for simplicity the max cutting force function is not shown.

Table 5: Muscle PCSA, resting length and muscle forces, having the leg in 90° flexion and 80° abduction for Graf type I [11].

Muscle name	PCSA [mm^2]	Resting length [mm]	Muscle Force [N]
Pectineus	32.14	30.59	45.84
Adductor Longus	80.90	61.55	15.01
Adductor Brevis	41.00	49.97	1.35
Add. Magnus Min.	90.83	48.06	1.83
Add. Magnus Mid.	65.31	75.94	0.84
Add. Magnus Post.	60.33	124.39	0.33
Gracilis	13.28	122.05	0.33

Table 6: Muscle equations for the SolidWorks® model calibrated at Graf type I [11].

Muscle name	Equation to insert in Solidworks, to check equilibrium condition
Pectineus	-0.03064*(EXP(13.95*((({CalPectineusDisp})/(0.8*30.592))-1))-1)
Adductor Longus	-0.02203*(EXP(13.95*((({CalAddLongusDisp})/(0.8*61.546))-1))-1)
Adductor Brevis	-0.02035*(EXP(13.95*((({CalAddBrevisDisp})/(0.8*49.971))-1))-1)
Add. Magnus Min.	-0.00448*(EXP(13.95*((({CalAddMagnusMinimusDisp})/(0.8*48.062))-1))-1)
Add. Magnus Mid.	-0.02426*(EXP(13.95*((({CalAddMagnusMiddleDisp})/(0.8*75.939))-1))-1)
Add. Magnus Post.	-0.02352*(EXP(13.95*((({CalAddMagnusPosteriorDisp})/(0.8*124.389))-1))-1)
Gracilis	-0.02401*(EXP(13.95*((({CalGracilisDisp})/(0.8*122.053))-1))-1)

5.3 Matlab® lower limb model

The Matlab® lower limb model was assembled using relevant points of the 3D points of the hip surface extracted from the SolidWorks® model as shown in Figure 27 for Graf type I, II and III, these points are needed for the collision detection of the femoral head with the pelvis while passively reducing the hip joint.

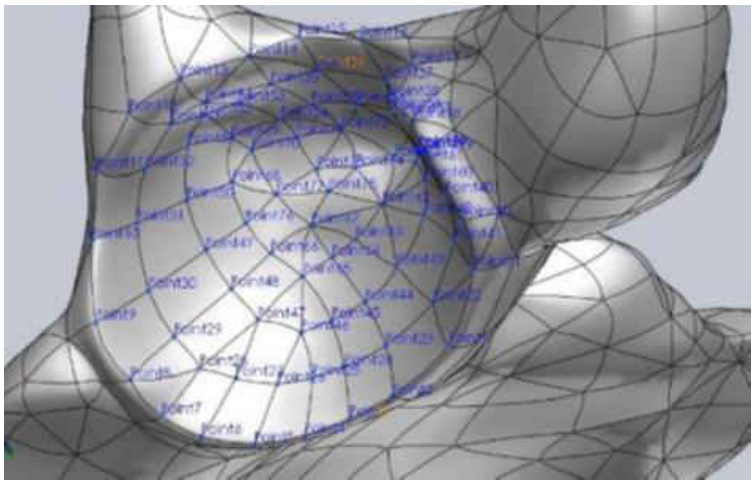

Figure 27: Wireframe Points located on the surface by using SolidWorks® for Graf type I, II, and III.

Similar approach shown in Figure 28 was done for Graf type IV. These points are needed for the collision detection of the femoral head with the pelvis while passively reducing from Graf type IV in the indirect or in the direct path. These points are also needed for finding the path of least energy which has been shown to be similar to the indirect path [14] shown in Figure 29.

For the insertion points of the muscles over the pelvis, the Points from Dostal and Andrews that were common with the SolidWorks® model were broken down into 2 subgroups based on their insertion location, because of the differences of the pelvis Geometry. The first subgroup consists of pectineus, adductor longus, adductor brevis, adductor magnus minimus, adductor magnus middle, adductor magnus posterior, and gracilis, while the second group consists of all the gluteal muscles except the gluteus maximus.

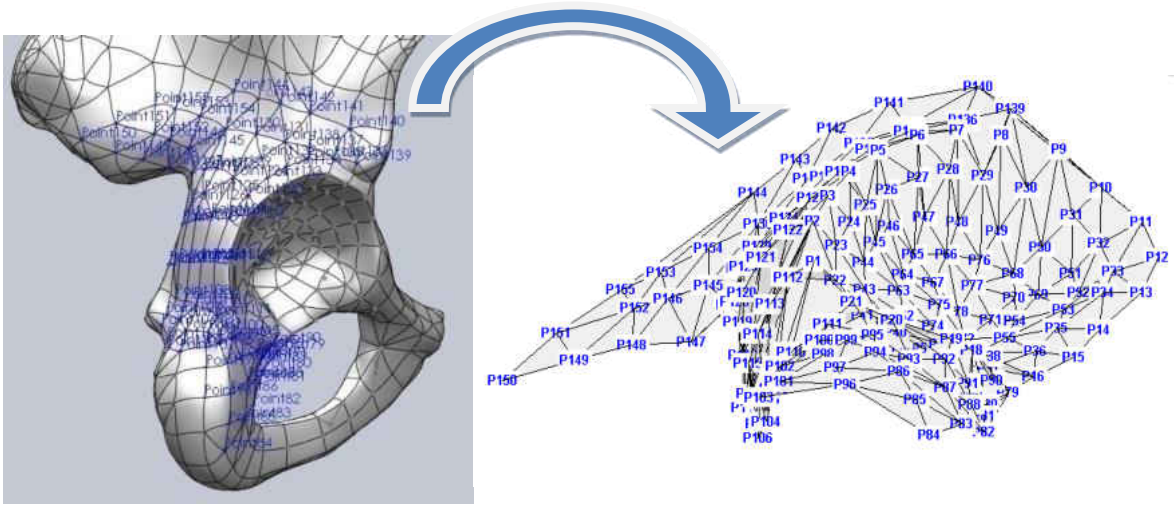

Figure 28: Point numbering in Matlab® 3Dimensional model for the relevant points of the pelvis to calculate the location of the Femoral Head.

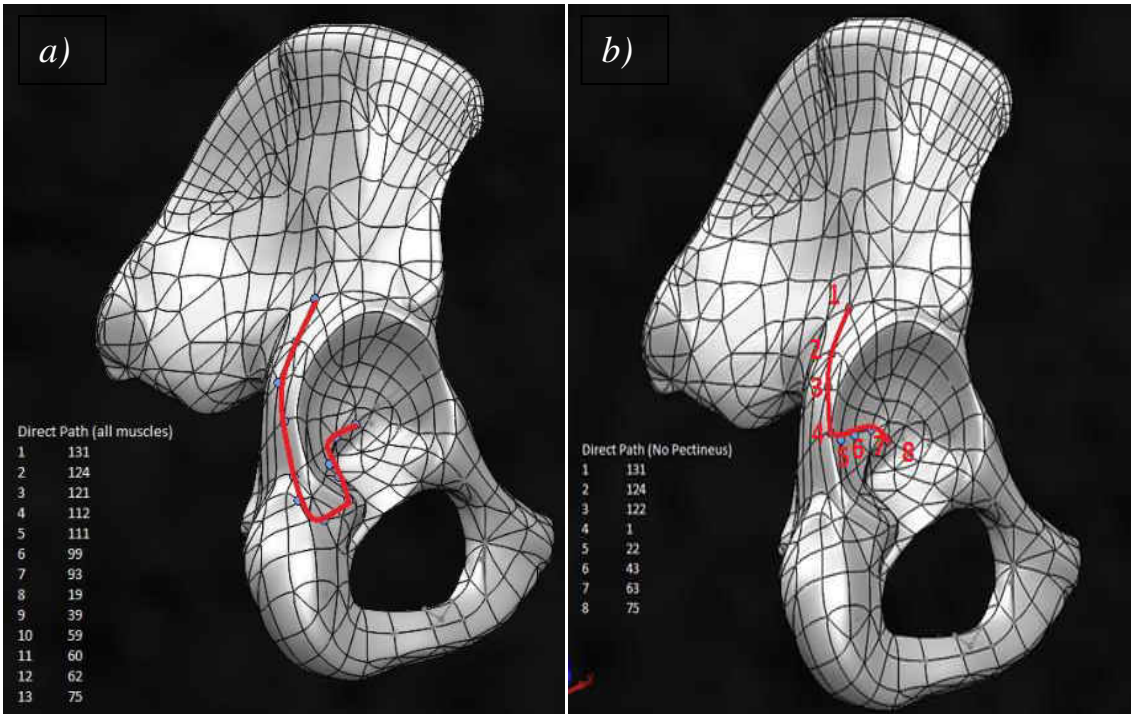

Figure 29: Grade IV: hip Dysplasia a) indirect and b) direct reduction pathways [14].

Once the groups were divided, the next step with the modified Umeyama algorithm was to find the rotations and scaling to fit all the rest of the SolidWorks model muscle insertion points, as shown in Figure 30. The first group also rotated and scaled the iliopsoas insertion point, and the second group did the same for the gluteus maximus. The Mean Squared Error of fitting the muscle pelvis muscle insertion points were 2.1853 mm and 3.0325 mm respectively for each group.

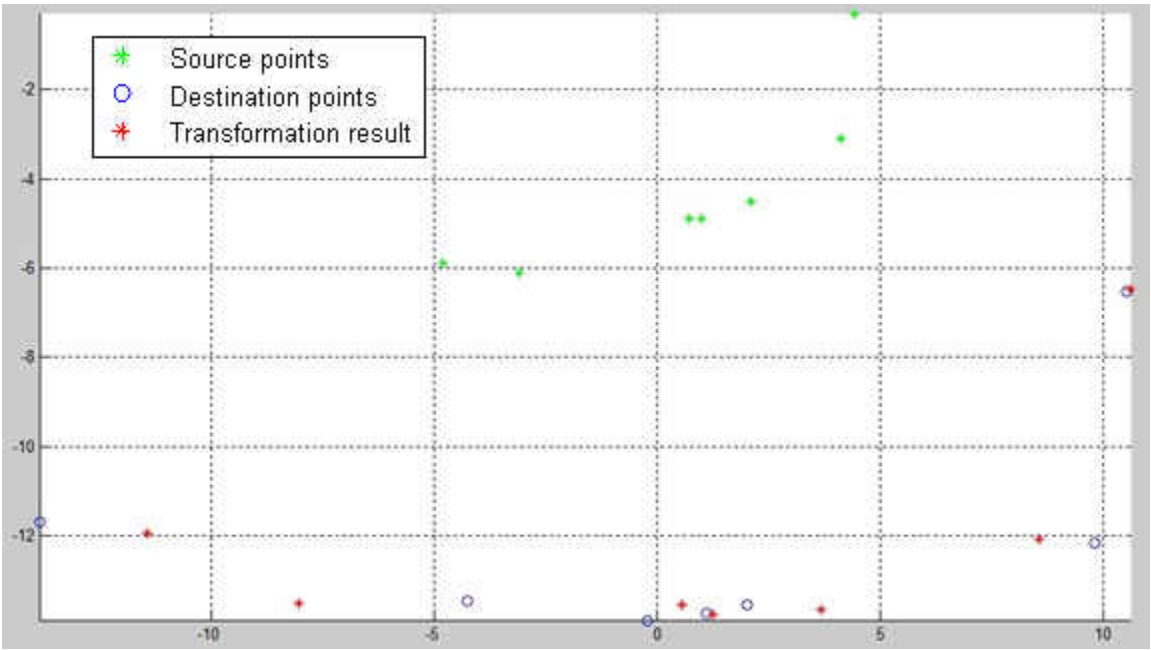

Figure 30: Rotations and scaling with the modified Umeyama algorithm of the pelvis muscle insertion points, from Dostal and Andrews [cm] to Reference points [mm] shown in Table 4.

The uncertainty of the location of the insertion points of the muscles over the hips is a sphere that possesses the diameter of the distance between the points used on the SolidWorks® model and the best-fitted points from Dostal and Andrews. For the muscles that had no reference, the maximum uncertainty of the other muscles is used.

The femur was assembled using the coordinate system as the SolidWorks® model, which is shown in Figure 31. The position is similar to the anatomical position; the differences rely on the y-direction, which should be used to define the parasagittal plane, in this model passes through the center of the line that joins the epicondyles, and passes through the center of the femoral head instead of being perfectly parallel to the medial plane. The reason is the model does not have other landmarks to define the medial plane or the mechanical axis of the limb.

The geometry of the femur is defined as breaking down into five components, the greater trochanter, the femoral head, the femoral neck, the femoral shaft, and the condyles. The greater trochanter location was defined as a distance from the center of the epicondyles to the furthermost point of the greater trochanter, the x-coordinate and z-coordinate defined by the deviation angle, The femoral head is simulated as a sphere, the condyles as a cylinder with a diameter given by measurement, the femoral neck is found with the intersection point of the femur and the greater trochanter at a point defined by the deviation angle and the incline angle, the anteversion angle and the bowing which is simulated as a catenary curve, defines the femoral shaft shown in Figure 31. This catenary curve is coincident with the scaled points of Dostal and Andrews [47], using Eureqa® software. An approximation to the initial guess of the parameters was defined to cover any range of femoral lengths, and then with the steepest descent algorithm, the exact parameters were calculated. The y-coordinate location of the points had to be calculated in a way that, after including the rotation (based on the deviation angle, and the anteversion angle) and the bowing of the femoral shaft (based on the catenary curves in the x direction and the bowing curve in the

y direction), the points are coincident with y-axis of the scale femur in the geometry of Dostal and Andrews [47] as follows.

$$Fs_y = \frac{F_l}{\sqrt{\frac{(0.1-0.2)^2}{4} + 42.3^2}} \tag{30}$$

Where, Fs_y is the femur scale in the y-direction, F_l is the femur length of the Matlab® model.

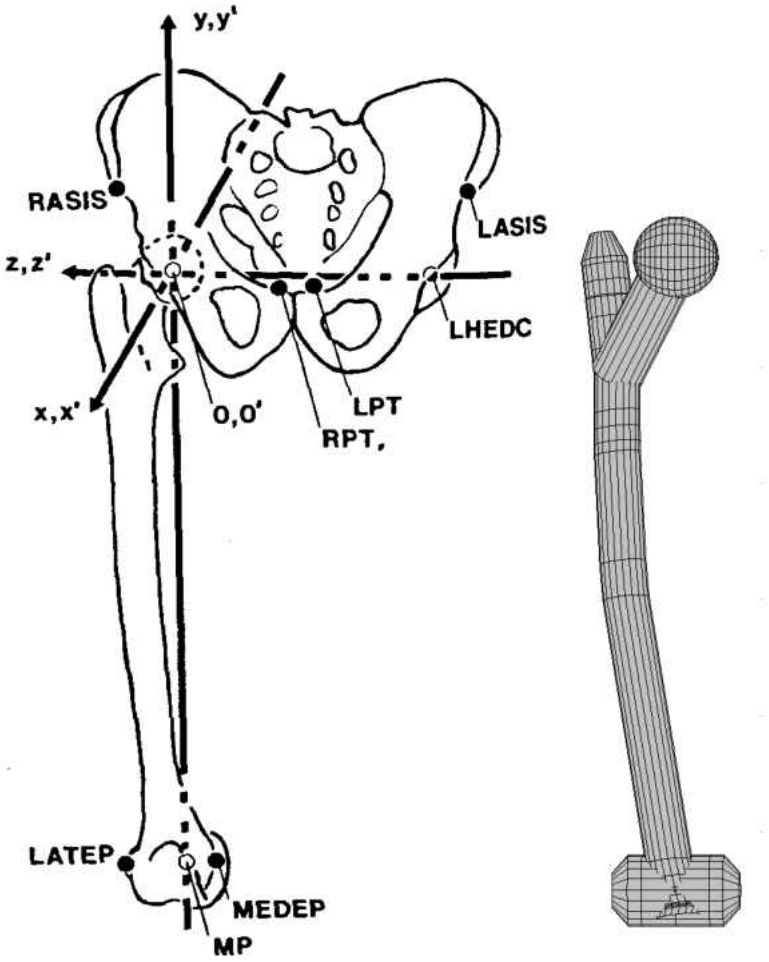

Figure 31: 3D Model comparison with Dostal and Andrews model, illustrating the coordinate system used, based on [47].

To calculate the bowing femur in the x direction, the approximation of the a_{0x} value of the catenary is found using Eureqa® to match several combinations of femur lengths and bowing angles a_{c0} for equation (9) is defined as:

$$\begin{aligned} a_{c0} = {} & \frac{sBFA}{0.000445798644809193} + \\ & \mathrm{MBdis} * \sin(1.27874632937825e-5 * sBFA) \\ & + 1.5047821181387e^{-6} \\ & * \mathrm{MBdis} * sBFA^2 + 3.01243609091884e^{-10} * \mathrm{sBFA} * \mathrm{MBdis} * \mathrm{L_{sh}^2} \\ & - 6.02306145308295e^{-5} * \mathrm{sBFA^2} \\ & - 1.96535628625619\mathrm{e}-7 * \mathrm{L_{sh}} * \mathrm{sBFA} * \mathrm{MBdis} \end{aligned} \tag{31}$$

where MBdis is the distance at which the bowing of the infant is measured, normally 40 mm [71], sFBA is the Sagittal femoral bowing angle measured in degrees, L_{sh}L is the femoral shaft length.

The location of the insertion point of the muscles over the femur consists of a polar rotation around the femoral shaft and a ratio from the epicondyles distance or the femoral shaft width. The rotation was defined with respect to the linea aspera. The positive rotation direction is defined following the right-hand rule having the thumb pointing towards the femoral head. The ratios and angles are summarized in Table 7a rotation uncertainty of ±5° and the ratio uncertainty of ±3% was assumed. The illustration of a configuration of the femur with the muscles inserted as is shown in Figure 16. This geometry is fully parameterizable, the muscle insertion points move along with the femur geometry.

Table 7: Insertion point location of the muscles over the femur using the femoral shaft and linea aspera as reference.

Lower Limb Muscle	Ratio of Femoral Shaft	Rotation Angle [deg]
Iliopsoas	1.575	-72.5
Pectineus	1	-45
Sartorius	1	-90
Rectus Femoris	1	169
Adductor Longus	1	-5
Adductor Brevis	1	-5
Adductor Magnus Minimus	1	0
Adductor Magnus (Middle)	1	0
Adductor Magnus (Posterior)	2.575	-95
Gracilis	1	-90
Gluteus Maximus	1	24
Gluteus Medius (Anterior)	1	90
Gluteus Medius (Middle)	0.6	90
Gluteus Medius (Posterior)	0.65	90
Gluteus Minimus (Anterior)	1.2	93
Gluteus Minimus (Middle)	1.2	90
Gluteus Minimus (Posterior)	1.2	87
Tensor Fascia Lata	2.075	89
Piriformis	0.13	138
Obturator Internus	0.11	118
Gemellus Superior	0.12	128
Gemellus Inferior	0.1	108
Quadratus Femoris	1	0
Obturator Externus	0.11	-24
Biceps Femoris (Long Head)	3.625	89
Semitendinosus	1	0
Semimembranosus	1	0

To define the muscle length, the value was calculated as the straight distance from the insertion points adding length that is fixed for each muscle that represents extra muscle length segments that not change length, but contribute to the calculation of stretch.

This extra length was calculated as the sum of the length of the muscles segments measured in OpenSimgait2354_simbody.osim, divided by the straight distance of the

insertion points in the anatomical position, then using the same ratio in the Matlab® model. Along with the straight lengths measured in Matlab®, the following equation was used:

$$L_x = L_s * (R_{ML} - 1) \quad (32)$$

Where L_x is the extra length, L_s is the straight distance and R_{ML} is the muscle length vs. muscle insertion point distance ratio as shown in Table 8.

Table 8: Comparison of muscle length vs. distance calculated from [83].

Muscle	Sum of arc segments	Distance between insertion points closest to the model	Ratio R_{ML}
Iliacus	0.23565	0.06880	3.425351
Psoas	0.29676	0.06626	4.478912
Iliopsoas (average)			3.952131
Pectineus	0.03723	0.03723	1
Sartorius	0.76235	0.16929	4.503277
Rectus Femoris	0.38891	0.38891	1
Adductor Magnus Middle	0.14110	0.14110	1
Gracilis	0.18316	0.11889	1.540611
Gluteus Maximus Min	0.20163	0.15078	1.337245
Gluteus Maximus Med	0.24920	0.16958	1.469539
Gluteus Maximus Post	0.26038	0.15159	1.717664
Gluteus Maximus (average)			1.508149
Gluteus Medius Anterior	0.07969	0.07969	1
Gluteus Medius Middle	0.08171	0.08171	1
Gluteus Medius Posterior	0.09331	0.09331	1
Tensor Fascia Lata	0.81239	0.43648	1.861226
Piriformis	0.16365	0.10898	1.501681
Gemellus Superior	0.12950	0.12950	1
Quadratus Femoris	0.11064	0.11064	1
Biceps Femoris (Long Head)	0.14548	0.10194	1.427137

The relaxed lengths of the muscles were assumed to start with an approximated 120 degrees of flexion 20 degrees of abduction, then measured the straight length and added the extra muscle length previously calculated.

$$L_0 = L_{s0} + L_x \tag{33}$$

Where L_0 is the relax length of the muscle, L_{s0} is the relax length of the straight segment.

When the hip is dislocated the relaxed length is calculated in both positions as a healthy infant and in the dislocated configuration, because it is not clear when the dislocation was generated, a proportion of both is used for the estimation, in previous research the proportion was 50-50 (PoD=50), for theMalab® model was calculated as:

$$L_{oi} = \frac{(\mathrm{PoD} * L_{0d} + (100 - \mathrm{PoD}) * L_{00})}{100} \tag{34}$$

Where PoD is the Percentage of Dislocation, L_{0d} is L_0 with the femoral head dislocated and L_{00} is L_0 with the femoral head in a healthy position.

The area of each muscle was calculated as the previous model, using a greater sample for normalized PCSA (PCSAn) using Friederich [81], but also added the information of Warden [84] using the following equation:

$$PCSA = PCSA_{an} * \left(\frac{PCSA_{iB}}{PCSA_{anB}}\right) \tag{35}$$

Where $PCSA_{an}$ is the normalized PCSA of the corresponding adult muscle [48] $PCSA_{iB}$ is the PCSA of the infant adductor brevis, and $PCSA_{anB}$ is the $PCSA_{an}$ of the abductor brevis.

For a more representative estimation of the PCSAn, as well as the minimum, maximum, and standard deviation of the parameters, with the PCSAn, the information was scaled by the measurement of the abductor brevis PCSA; a summary of the values used are shown in Table 9.

Table 9: Lower limb normalized PCSA and their assigned probability distribution using data from [81][84].

Parameter	Abbreviation	Mean PCSAn	StDev σ	Probability distribution[a]
Iliopsoas	ILPS	2.169	0.199	β(4.5, 3.06)
Pectineus	PEC	0.317	0.101	β(0.86, 0.53)
Sartorius	SAR	0.228	0.040	β(3.19, 4.07)
Rectus Femoris	RF	1.638	0.172	β(2.88, 2.35)
Adductor Longus	AdL	0.820	0.154	β(4.01, 4.25)
Adductor Brevis	AdB	0.604	0.089	β(2.74, 2.03)
Adductor Minimus	AdMin	1.094	0.193	β(2.96, 3.33)
Adductor Magnus (Middle)	AdMgM	0.739	0.168	β(4.02, 4.35)
Adductor Magnus (Posterior)	AdMgP	0.654	0.163	β(4.27, 4.59)
Gracilis	GR	0.252	0.042	β(3.94, 1.92)
Gluteus Maximus	Gmax	4.091	0.752	β(2.78, 2.65)
Gluteus Medius (Anterior)	GMedA	1.644	0.332	β(3.53, 3.75)
Gluteus Medius (Middle)	GMedM	1.212	0.332	β(3.57, 3.73)
Gluteus Medius (Posterior)	GMedP	1.284	0.327	β(3.67, 3.84)
Gluteus Minimus (Anterior)	GMinA	0.642	0.471	β(0.25, 0.25)
Gluteus Minimus (Middle)	GMinM	0.761	0.545	β(0.25, 0.25)
Gluteus Minimus (Posterior)	GMinP	0.795	0.350	β(0.25, 0.25)
Tensor Fascia Lata	TFL	0.344	0.031	β(0.25, 0.25)
Piriformis	PIR	1.069	0.183	β(0.25, 0.25)
Obturator Internus	ObIn	0.816	0.567	β(0.25, 0.25)
Gemellus Superior	GEMS	0.144	0.065	β(0.25, 0.25)
Gemellus Inferior	GEMI	0.198	0.000	β(0.25, 0.25)
Quadratus Femoris	QuaF	0.961	0.484	β(0.5, 0.5)
Obturator Externus	ObEx	0.381	0.364	β(0.25, 0.25)
Biceps Femoris (Long Head)	BFL	1.356	0.683	β(0.29, 0.14)
Semitendinosus	ST	0.596	0.122	β(1.15, 0.81)
Semimembranosus	SM	2.190	0.255	β(-8.4, 2.44)

[a] Beta distribution βeta(α, β) is denoted by α and β, that appear as exponents of the random variable and control the shape of the distribution. Where: α > 0 shape (real); β > 0 shape (real)

PCSAs and muscle lengths were found to define the biomechanics of skeletal muscles since muscle length is proportional to muscle excursion while PCSA is proportional to maximum muscle force as seen in Figure 32, Figure 33, and Figure 34. These figures were divided in three different plots only for illustration purposes.

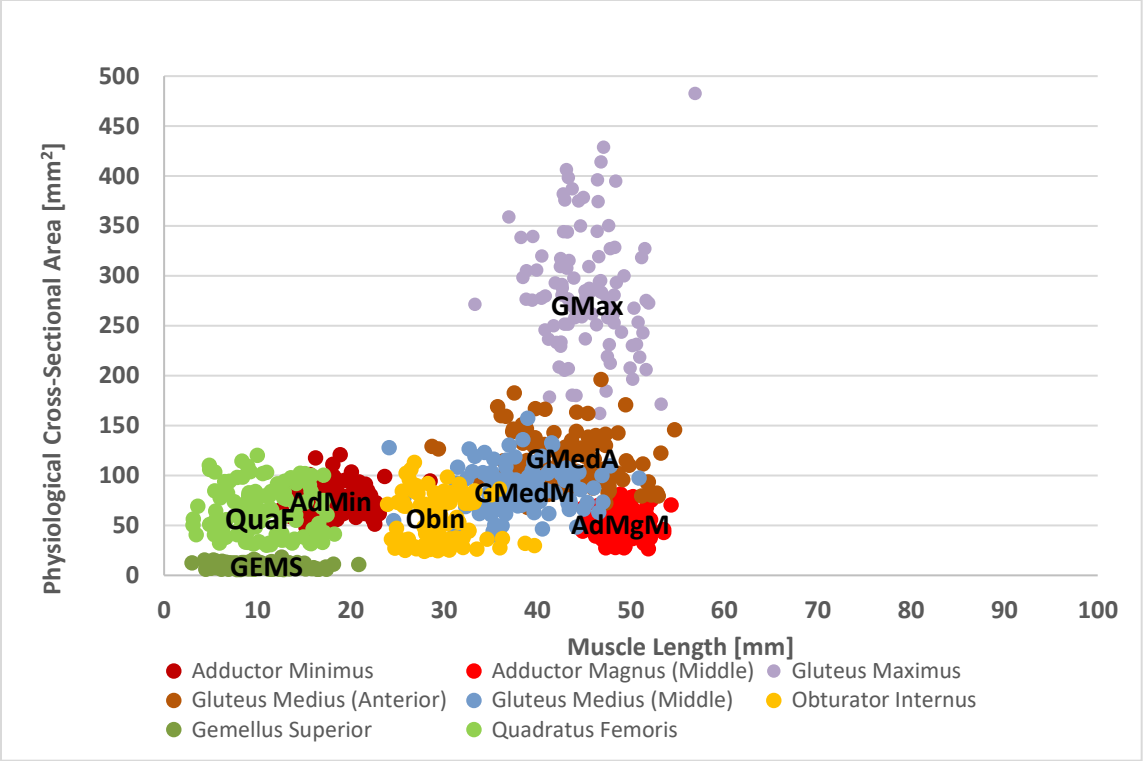

Figure 32: Lower limb muscles length and physiological cross-sectional areas.

The center of mass of the leg was estimated using SolidWorks® model using x=74.60583374, y=-10.2359 and z=0.099646807 mm. for the leg in the anatomical position with the knee bended 90 degrees. The location of the center of mass was also randomized inside a sphere of radius 5mm.

For the location of the leg when dislocation is present, a point at which the femoral head is touching the hip is estimated with the collision detection algorithm; the center of the femoral head that is in contact with the hip was found and illustrated in Figure 35 for different grades of dysplasia.

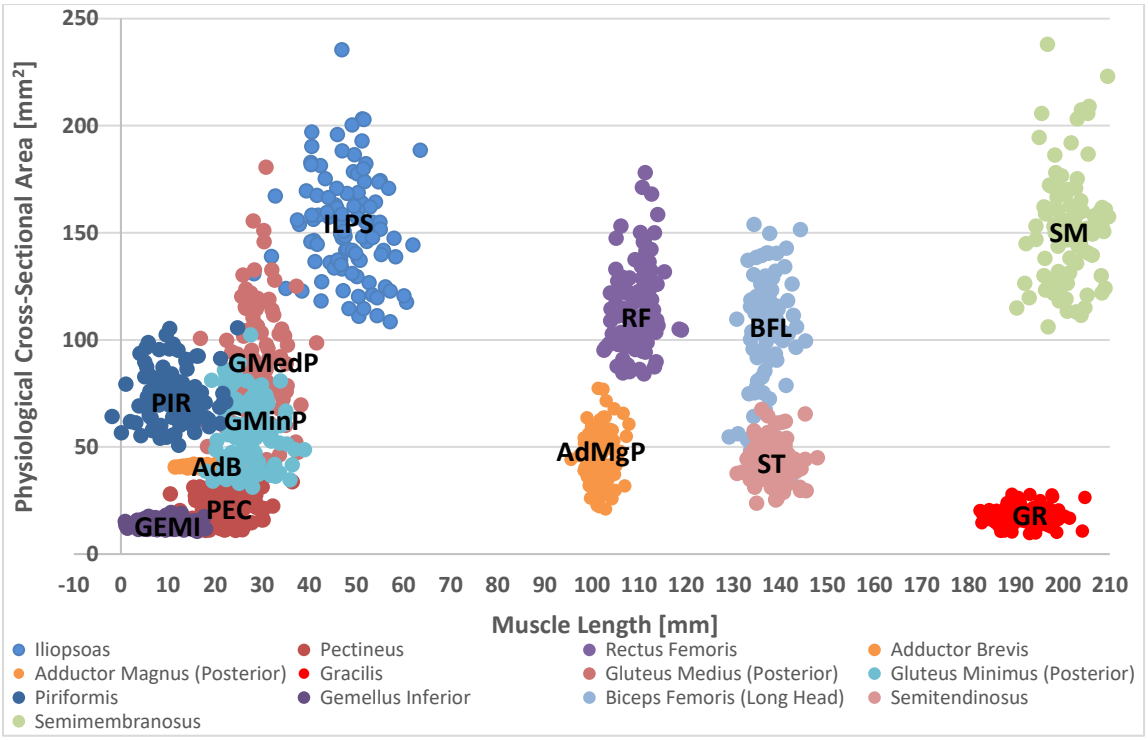

Figure 33: Lower limb muscles length and physiological cross-sectional areas.

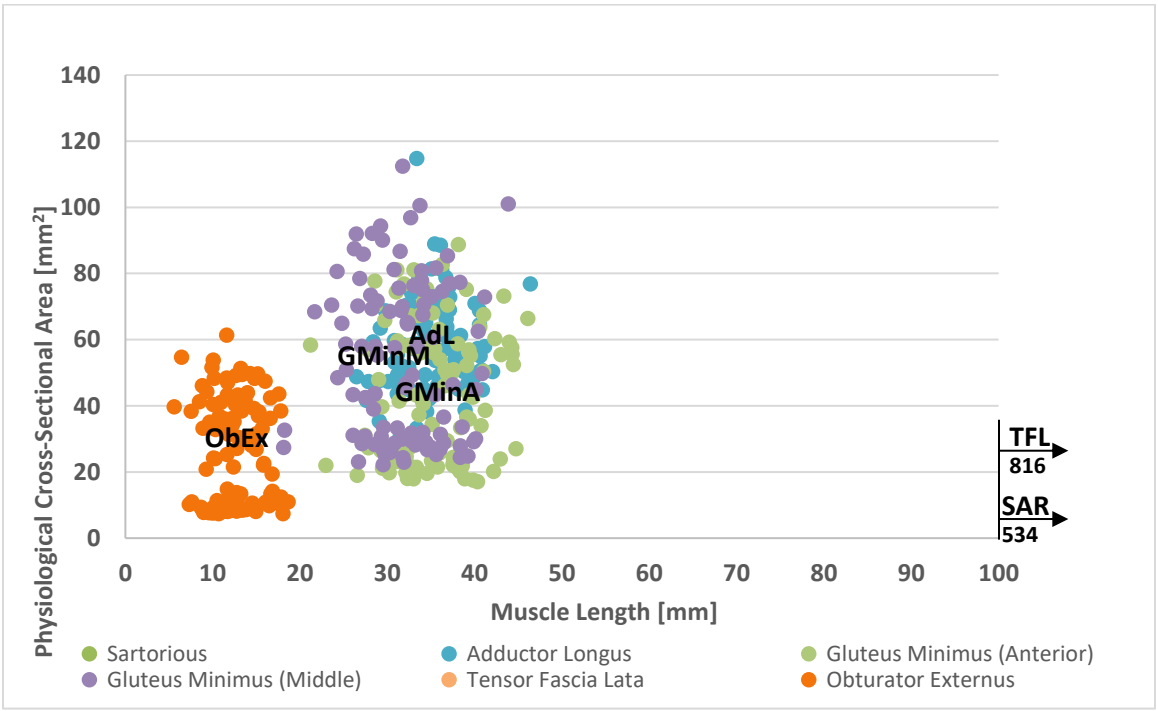

Figure 34: Lower limb muscles length and physiological cross-sectional areas.

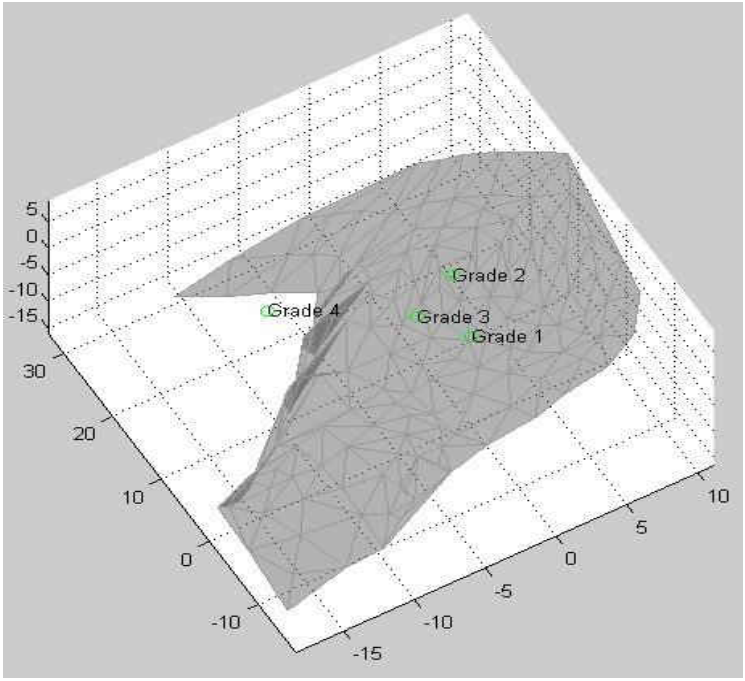

Figure 35: Illustration of a section of the mesh of the hip with the relative locations of the femoral head for different grades of dysplasia.

Once the muscle material properties are calibrated for a specific flexion, abduction, and rotation, the leg was rotated to any other typical flexion, abduction, and external rotation, then calculated the resulting forces and moments acting over the femur.

The resulting moment in y-direction denoted by M_y can be compensated with the fulcrum point to achieve static equilibrium in this example configuration as shown in Figure 17 illustrates from a proximal view with the leg flexed 90 degrees and abducted 40°, the estimation of the fulcrum point will be given by $F_{fulcrum} = M_y/d_z$ where $F_{fulcrum}$ is the force of the fulcrum point d_z is the distance in the lateral direction.

The assumed constraint of the geometric parameters in the model is illustrated in Table 10, the assumed constraints for the ranges of motion and calculating related variables are summarized in Table 11.

Table 10: Lower limb anatomic parameters and their assigned probability distribution.

Parameter	Mean	min	max	Probability distribution[ab]
Femur Length [mm]	108.95	107.95	109.95	β(4.5, 4.5)
Femur Epicondyle to Trochanter tip Length [mm] (L_T)	115.00	114.00	116.00	β(4.5, 4.5)
Femur Shaft Width [mm]	7.64	6.64	8.64	β(4.5, 4.5)
Femur Deviation Angle [deg] (Θ_d)	10.00	9.00	11.00	β(4.5, 4.5)
Femur Sagittal Bowing Angle [deg] (Θ_s)	10.00	0.00	15.00	β(5.26, 2.63)
Femur Coronal Bowing Ang [deg] (Θ_b)	0.02	0.00	5.00	X~Triangular(0, 5, 0)
Femur Head Diam [deg]	14.00	13.00	15.00	β(4.5, 4.5)
Femur Anteversion Angle [deg] (Θ_{av})	50.30	0.00	95.70	β(4.72, 4.26)
Femur Incline Angle [deg]	131.60	130.60	132.60	β(4.5, 4.5)
Femur Condyle Diameter [mm]	12.33	11.33	13.33	β(4.5, 4.5)
Femur Epicondyle Distance [mm]	21.00	20.00	22.00	β(4.5, 4.5)

[a] Beta distribution Beta(α, β) is denoted by α and β, that appear as exponents of the random variable and control the shape of the distribution. Where: α > 0 shape (real); β > 0 shape (real).

[b] For Triangular distribution X~T(a,b,μ) parameters a, b and μ, denote the minimum, maximum, and mean value.

Table 11: Lower limb configuration constraints and their assigned probability distribution.

Constraints affecting model behavior	**Mean**	**min**	**max**	**Probability distribution[ab]**
Infant body weight [Kg]	5.40	3.90	7.10	β(4.2, 4.76)
Leg percentage weight [%]	17.56	16.68	18.43	β(4.53, 4.47)
Abductor brevis PCSA measured [mm²]	41.00	40.00	42.00	β(4.5, 4.5)
Constraints affecting static equilibrium reference point	**Mean**	**min**	**max**	**Probability distribution[ab]**
Flexion [deg] (Θ_e)	90.00	85.00	105.00	β(1.63, 4.88)
Abduction [deg] (Φ_e)	80.00	75.00	85.00	β(4.5, 4.5)
External rotation [deg] (φ_e)	5.00	0.00	50.00	β(0.26, 2.34)
b	13.95	12.00	90.00	X~Triangular(12, 90, 13.95)
Constraints for iterating for a fulcrum point	**Mean**	**min**	**max**	**Probability distribution[ab]**
Flexion [deg] (Θ_i)	90.00	0.00	120.00	β(4.88, 1.63)
Abduction [deg] (Φ_i)	80.00	0.00	90.00	β(2.62, 0.33)
External rotation [deg] (φ_i)	0.00	-5.00	45.00	β(0.26, 2.34)
Constraints for calculating relaxed lengths	**Mean**	**min**	**max**	**Probability distribution[ab]**
Flexion [deg] (Θ_{rel})	120.00	119.00	121.00	β(4.5, 4.5)
Abduction [deg] (Φ_{rel})	20.00	15.00	25.00	β(4.5, 4.5)
External rotation [deg] (φ_{rel})	25.00	-5.00	50.00	β(4.86, 4.05)
Percentage Of Dislocation [%]	50.00	20.00	80.00	β(4.5, 4.5)
Muscle prestretch in relaxed length [mm]	0.80	0.60	0.80	X~Triangular(0.6, 0.8, 0.799)

[a] Beta distribution Beta(α, β) is denoted by α and β, that appear as exponents of the random variable and control the shape of the distribution. Where: α > 0 shape (real); β > 0 shape (real).

[b] For Triangular distribution X~T(a,b,μ) parameters a, b and μ, denote the minimum, maximum, and mean value.

Several different configurations were defined and grouped in the following manner along the direct and indirect path for a total of 400 configurations per path segment: Graf type I, II, and III least energy paths, Graf type IV indirect path, and Graf type IV direct path for the femoral head location. This least energy path represents the desired displacements of the femoral head's over the pelvis to achieve reduction, placing the

femoral head back to its nominal configuration inside the acetabulum; the resulting force over the femoral head contact with the pelvis is computed and projected over the desired path. It is of our interest that the fulcrum point assists the leg to maximize this projected force in the desired path direction, the projected force $Proj_{\overrightarrow{path}}\vec{F}_{tot}$ is calculated as:

$$Proj_{\overrightarrow{path}}\vec{F}_{tot} = \left(\frac{dot\left(\vec{F}_{tot}, \overrightarrow{path}\right)}{\left|\overrightarrow{path}\right|}\right)\overrightarrow{path} \tag{36}$$

Where $\vec{F}_{tot}$ is the total force acting over the femoral head as a reaction from being in contact with the hip, $\overrightarrow{path}$ is the direction vector of the desired path. This maximum force is achieved by finding the value function to maximize R_f to obtain expressed as:

$$R_f = s\frac{\left|Proj_{\overrightarrow{path}}\vec{F}_{tot}\right|}{\left|\vec{F}_{tot}\right|} \tag{37}$$

$$R_{f_{max}} = max\left(R_f\right) \tag{38}$$

Where s is the sign of R_f and is found by the cosine rule

$$s = \frac{\left(\vec{F}_{tot} \cdot \overrightarrow{path}\right)}{\left|\vec{F}_{tot}\right|\left|\overrightarrow{path}\right|} \tag{39}$$

Because the avoidance of AVN is of interest, based on the suggestions of Ramsey [32] the forces over the femoral head have been reported for angles of abduction between 75 to 90 degrees of abduction, to contrast it with the femoral head contact force over the hip during potential desirable configurations.

Once the simulations for all configurations for each femoral head locations has been obtained, the unrealistic configurations which present an unstable static equilibrium or excessive femoral head contact force (greater than 1000 N) were considered outliers and

were removed from the analysis. Following the cleaning of the data, Pearson correlation matrix and the Spearman Rank correlation matrix were used to identify initial parameter correlations between inputs and the percentage of the contact force that is in the direction of the desired path, finally all the measurable parameters for each group of configurations were placed in Eureqa® as an attempt to find a mathematical expression that can simplify the system and can be easily computed to find the OP location instead of running multiple simulations to find the best configuration.

With the results found for Graf type I and IV configurations the results were prepared and categorized to meet the constraints of each HAOD shown in Table 12. These HAODs were also reviewed.

Table 12: Summary of different constraints defining each HAOD.

Device	**Flexion** (Θ_i)	**Abduction** (Φ_i)
Pavlik harness	90° - 110°	30° - 60°
Tübingen splint	90° - 110°	45° - 55°
Spica cast	90° - 100°	45°
Von Rosen splint	90°	45°
Frejka pillow	80° - 110°	90°

CHAPTER 6: RESULTS

This chapter is divided in seven sections: 6.1 The effect of a fulcrum point using the least energy path for Graf type I; 6.2 The effect of a fulcrum point using the least energy path for Graf type II; 6.3 The effect of a fulcrum point using the least energy path for Graf type III; 6.4 The effect of a fulcrum point using the indirect reduction least energy path for Graf type IV; 6.5 The effect of a fulcrum point using the direct path for Graf type IV; and 6.6 Effectiveness of different HAOD based on the Fulcrum point.

To find the OP for each model configuration, the following parameters were used: The femoral head reaction force due to the fulcrum point was located over a straight line parallel to the femoral axis, while the fulcrum point was placed in sequential positions along the femoral axis in 5% increments.

To find the most effective fulcrum point, the goal was to maximize the magnitude of the projected resultant force over the vector that indicates the desired direction to achieve reduction ($R_{f\,max}$). This desired path for reduction was calculated with the minimum muscle potential energy, the direct and indirect path mentioned in [14].

The results suggest the location of the fulcrum point will only affect the moment in y-direction, which is defined as the vector normal to the transverse plane and tends to adduct the leg. All other moment reached equilibrium via the HAOD. The resultant projected force was compared against the magnitude of the resulting force over the femoral head to quantify the fraction of the force acting in the least potential energy direction (R_f).

Muscle resting length for all configurations, was set as mentioned to be the average between the resting length of a healthy infant and the resting length of the leg displaced, locating the femoral head in a in the corresponding configuration.

6.1 Fulcrum point effect for Graf type I configurations using the least energy path

For Graf type I configurations, the femoral head was aligned tangent to node 66 inside the acetabulum. In addition, all configurations included the anatomical average input values. Furthermore, the least energy reduction path was defined as a two-step travel path: step 1 from node 66 to node 67 and step 2 from node 67 to node 75 as shown in Figure 36. Constraints set up as mentioned in the methodology.

For the least energy reduction path, which included all input parameters from Table 7, Table 9, and Table 10, a Pearson correlation matrix was found and summarized in Appendix A Table 15 summarizes the linear relationship between all the input parameters and output parameters including the projected total force over the path of least potential energy for Graf type I configurations. Results suggest a change in the PCSA of the muscles do create a linear change in the magnitude of the projected force over the path of least energy. For the femoral anatomic parameters, only the anteversion angle showed an inverse linear relationship with respect to R_f ($r = -0.348$). All muscle insertion points over the pelvis also showed an inverse linear relationship with R_f ($r = -0.427$), the brace abduction angle shows the highest direct linear relationship with R_f ($r = 0.233$) followed by the leg centroid location in y and z ($r = 0.223$), and the centroid location in x ($r = 0.217$).

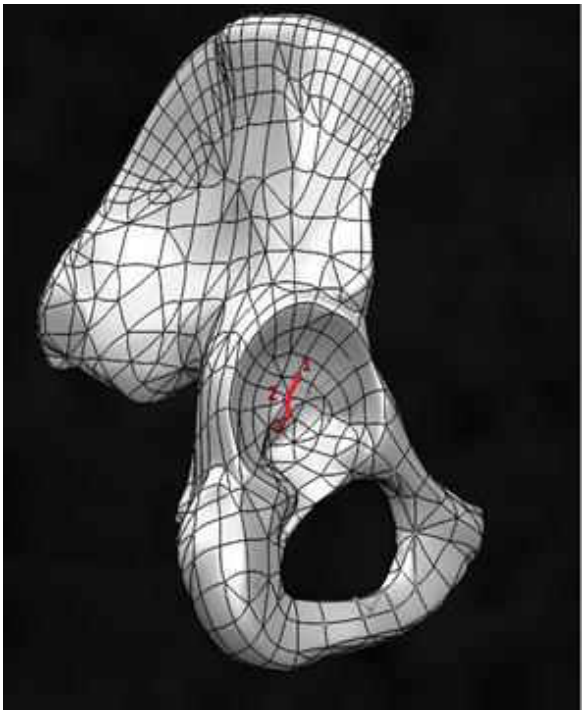

Figure 36: Graf type I least energy path, 2 step reduction [14].

With the Spearman rank correlation, it was found a significant monotonic correlations with the percentage of total force in the path of least energy, the most significant parameters with respect to R_f are, the abduction angle of the HAOD ($\rho = 0.288$), the distance of the sartorius with respect of the femoral shaft ($\rho = 0.2195$), the length of the gemellus inferior ($\rho = 0.2122$), the leg centroid along the y and z directions ($\rho = 0.2063$), the infant weight ($\rho = 0.1907$), the fascia lata' insertion point angle of rotation with respect to the femoral axis ($\rho = 0.1748$), the distance from the femoral shaft to the piriformis' insertion point ($\rho = 0.1402$), and the flexion angle of the HAOD ($\rho = 0.139$). All these parameter and others which did not show strong correlation with R_f are shown in Appendix A Table 15. The negative monotonic parameters with respect to R_f percentage amount were found to be: the insertion x coordinate of the illiopsoas ($\rho =$

-0.4087), the brace external rotation ($\rho = -0.2587$), the biceps femoris long head ($\rho = -0.2311$) and gracilis ($\rho = -0.2069$) insertion point angles of rotation with respect to the linea aspera, the femoral shaft width ($\rho = -0.1933$), Spearman correlations were added in Appendix B Table 20. $Proj_{\overrightarrow{path}} \vec{F}_{tot}$ was estimated for several fulcrum points along the femur. These values were found to decrease when the fulcrum point approached the knee as illustrated in Figure 37. The black full dots represent extreme outliers and the hollow dots represent other outliers that were not taken into consideration for the search of a mathematical relationship among the parameters. Each box in the figure represents the quartiles, in which 50% of the data was found. The vertical lines above and below the box represents the ranges for the other 50% of the values found.

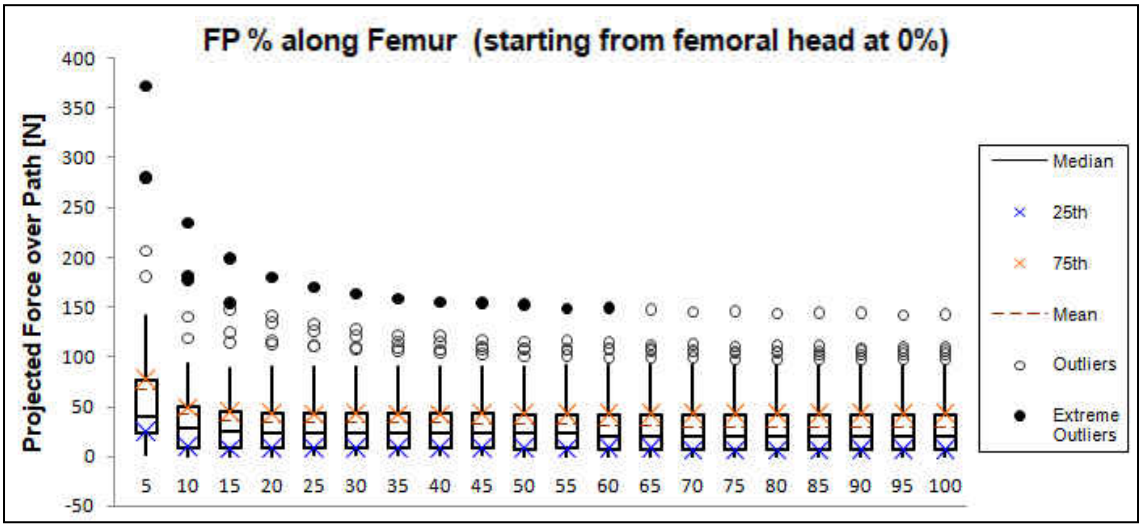

Figure 37: Graf type I projected force over the path of least energy, configurations suggest a higher $Proj_{\overrightarrow{path}} \vec{F}_{tot}$ near the femoral head.

All these configurations presented the characteristic of having around 30% of the mean $\vec{F}_{tot}$ acting over the desired path as shown in Figure 38. These results suggest that from 0% to 60% of the femoral force is acting in the desired path. In this condition, depending on each particular configuration the lowest force along the desired path can be found close to the femoral head (0%) or close to the knee (100%) for Graf type I.

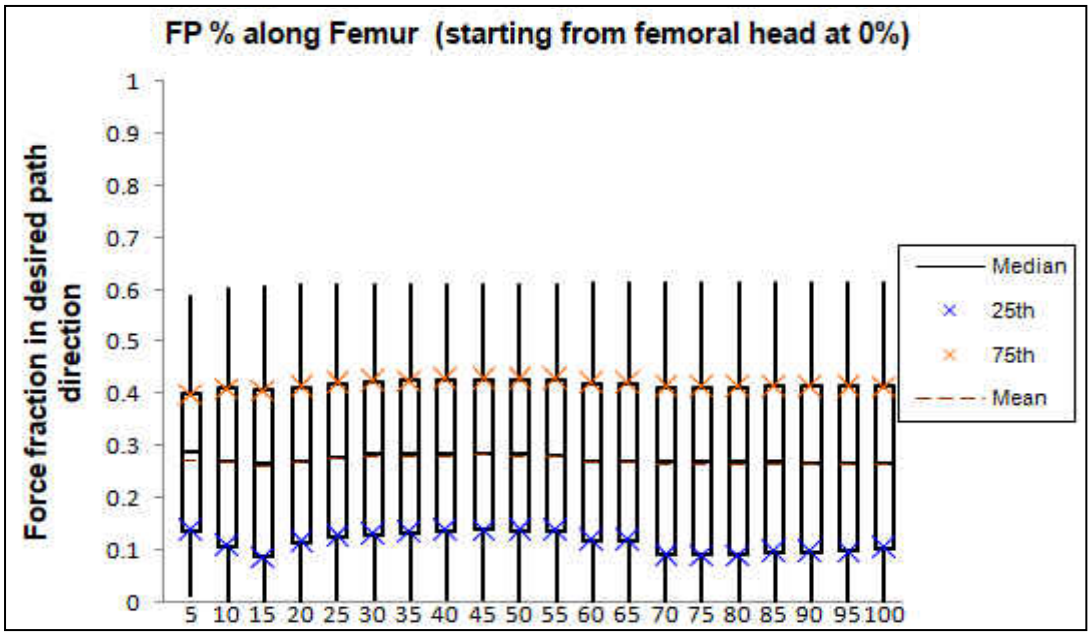

Figure 38: Graf type I projected force over the path of least energy divided by the total force acting over the femoral head.

After filtering only valid configurations, which allows static equilibrium and stable configurations, it was also found that $Proj_{\overrightarrow{path}} \vec{F}_{tot}$ can be negative (224 of 460 configurations in Graf type I). The least negative value was found near the mid tight which corresponds to 50 percent of the femoral length as shown in Figure 39.

All these Graf type I configurations presented the characteristic of having around 30% of $\vec{F}_{tot}$ acting against the desired path as shown in Figure 40. It was also found that

even when the force fraction is lower near the femoral head (0% in the figure), the projected force shown in the previous figure has a higher magnitude.

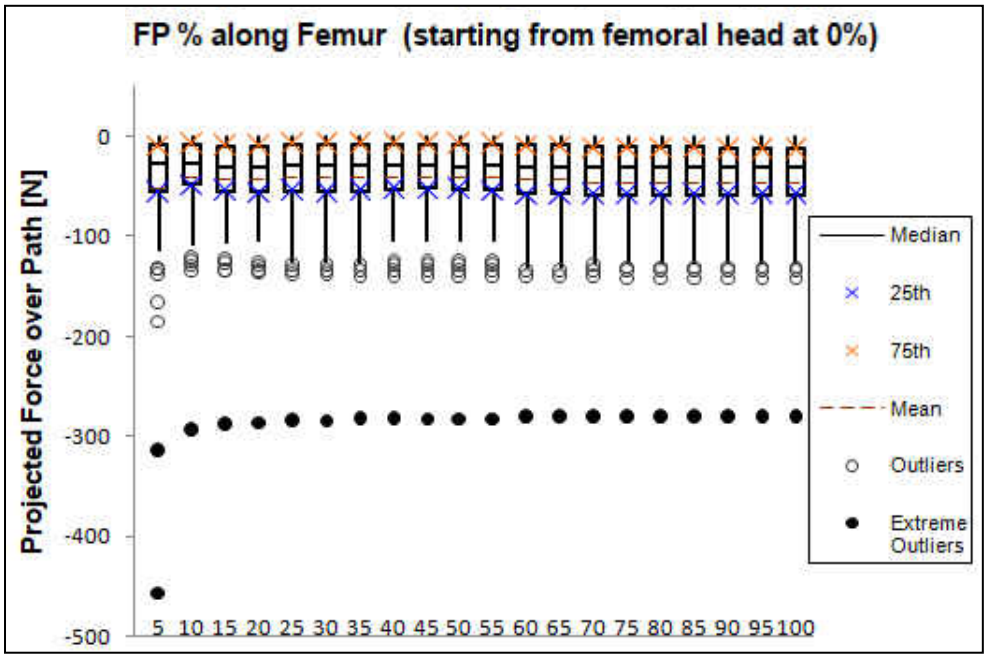

Figure 39: Graf type I projected force over the path of least energy, configurations show a similar $Proj_{\overrightarrow{path}} \vec{F}_{tot}$ along the femur once all outlier configurations were removed.

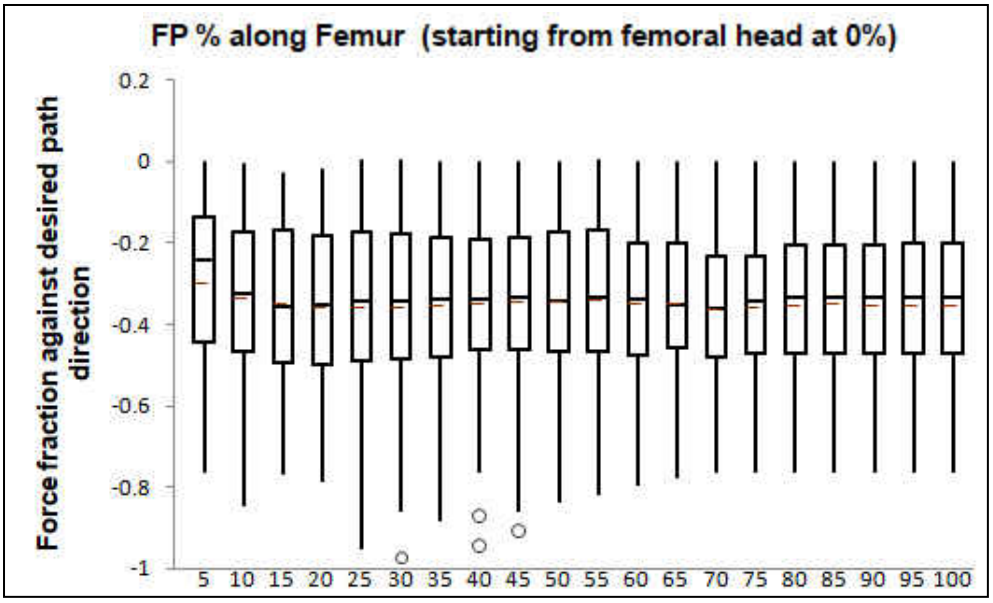

Figure 40: Graf type I projected force over the path of least energy divided by the total forces acting over the femoral head pointing against the least energy path.

Using the possible measurable input parameters of the femur there was no equation found that provided a recommended configuration that will always avoid a $Proj_{\overrightarrow{path}}\vec{F}_{tot}$ against the least energy path, the following equation was the equation that best fits the data for a Graph type I, predicting incorrectly 31.1 % of the times:

$$Best_{FP} = round\left(\frac{1452104.70607028}{1452104.70607028 + \left(\left(f_1^{f_2}\right)^{f_3}\right)^{f_4}}\right)$$

$$f_1 = 1.95716588086045 + \sin(1.87888296458386 * \Phi_i^2)$$

$$f_2 = \theta_i + \Phi_i - 172.346582882576 \quad (40)$$

$$f_3 = \theta_{av} + \frac{11.8151516647353}{\sin(-44.5302088247621 * \Phi_i)}$$

$$f_4 = 0.0740006810363588 * \theta_{av} * \Phi_i - \theta_i$$

Where Θ_{av} is the femur anteversion angle, the angles with subindex "i" indicate the angles at which the HAOD is applied, all angles in degrees. If for a specific configuration $Best_{FP}$ is found to be zero, the numerical framework will suggest placing the fulcrum point proximal to the femoral head, if is found to be one, the numerical framework will suggest placing the fulcrum point proximal to the knee. Notice this equation does not take into account any equilibrium configuration or relaxed lengths.

The incidence of configurations at which the FP is located near the knee was found in 227 of 460 configurations modeled.

6.2 Fulcrum point effect for Graf type II configurations using the least energy path

For Graf type II configurations, the femoral head was aligned tangent to node 27 inside the acetabulum. In addition, all configurations included the anatomical average input values. Furthermore, the least energy reduction path was defined as a four-step travel path: step 1 from node 27 to node 47, step 2 from node 47 to node 65 step 3 from node 65 to node 67, step 4 from 67 to 75 as shown in Figure 41. All other smaller paths from the nodes at the acetabular rim and the following node in the acetabulum are not illustrated. The Constraints set up as mentioned in the methodology.

For the least energy reduction path, which included all input parameters from Table 7, Table 9, and Table 10, a Pearson correlation Matrix was also found and summarized in Appendix A. Table 16 summarizes the linear relationship between all the input parameters and output parameters including the projected total force over the path of least potential energy for Graf type II configurations. The significant parameters which showed an inverse

linear relationship to R_f are the hip muscle insertion point location ($r = -0.429$), the semimembranosus' insertion point angle of rotation around the femoral shaft with respect to the linea aspera ($r = -0.207$), the parameters that showed linear relationship are centroid location in y and z directions ($r = 0.247$), the x coordinate of the leg centroid ($r = 0.243$).

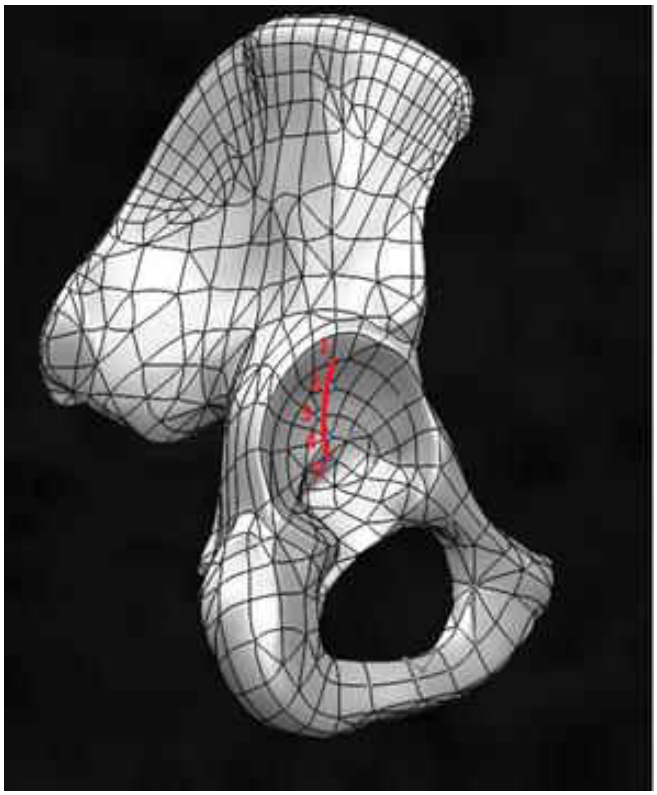

Figure 41: Graf type II least energy path 4 step reduction [14].

For Graf type II in the Spearman rank correlation matrix, the variables found to have a monotonic direct relationship with R_f were the leg centroid Y and Z coordinate ($\rho = 0.2335$) leg centroid in x ($\rho = 0.2278$), gracilis PCSA ($\rho = 0.1997$), abduction angle of the HAOD ($\rho = 0.1868$) and the PCSA of the gemellus inferior ($\rho = 0.1888$).

All these parameter and others which did not show strong correlation with R_f are shown in Appendix B Table 21.

The calculation of $Proj_{\overrightarrow{path}} \vec{F}_{tot}$ for different FP along the femur was also found as in Graf type II to decrease when de fulcrum point approaches the knee as illustrated in Figure 42 for most of the points.

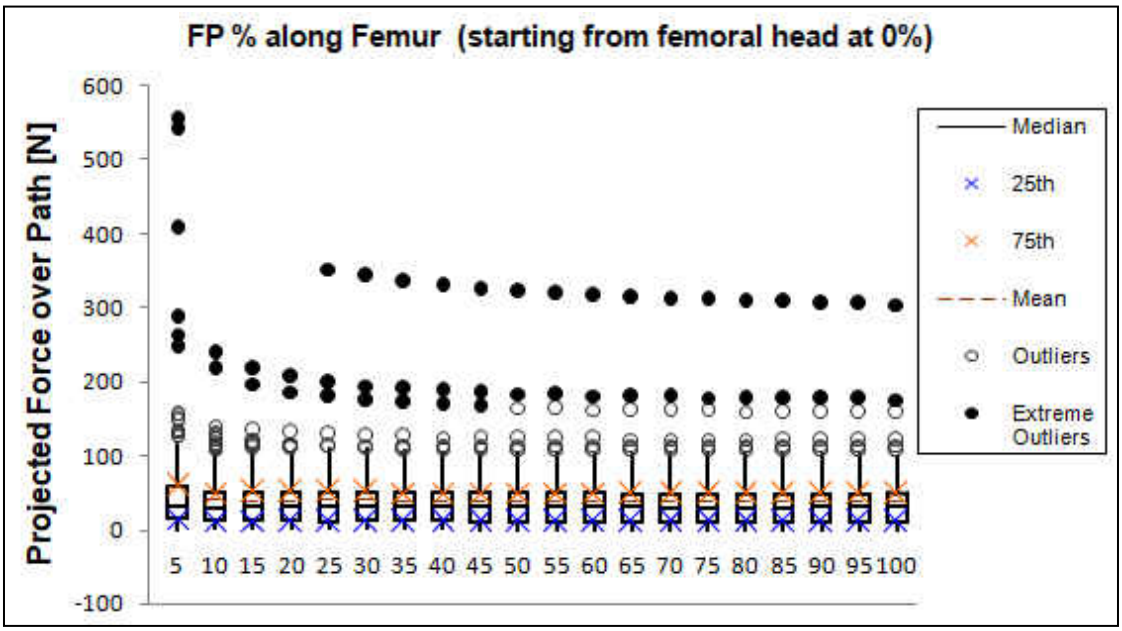

Figure 42: Graf type II projected force over the path of least energy; configurations show a higher $Proj_{\overrightarrow{path}} \vec{F}_{tot}$ near the femoral head.

All these Graf type II configurations presented the characteristic of having around 28% of $\vec{F}_{tot}$ acting in the desired path as shown in Figure 43. Even that the FP near the acetabulum (0% in the figure) presents a lower mean projected force than the other configurations for Graf type II, the projected force over the path in the above figure suggests the fulcrum point maximizes the force in the desired direction when the FP is closer to the femoral head.

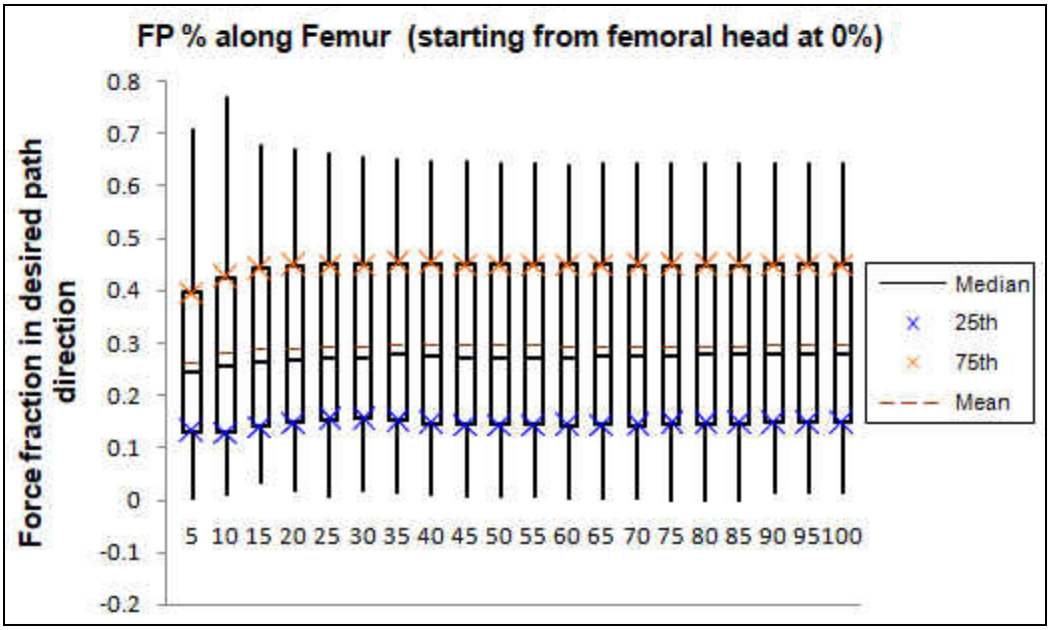

Figure 43: Graf type II $Proj_{\overrightarrow{path}}\vec{F}_{tot}$ divided by the total force acting over the femoral head.

From the configurations in Graf type II, it was also found configurations in which $Proj_{\overrightarrow{path}}\vec{F}_{tot}$ acts against the desired path of least potential energy. The incidence of Graf type II configurations acting against the desired path was 390 of 868 configurations. These configurations are represented in Figure 44. The most negative $Proj_{\overrightarrow{path}}\vec{F}_{tot}$ occurs when the FP is located near the femoral head.

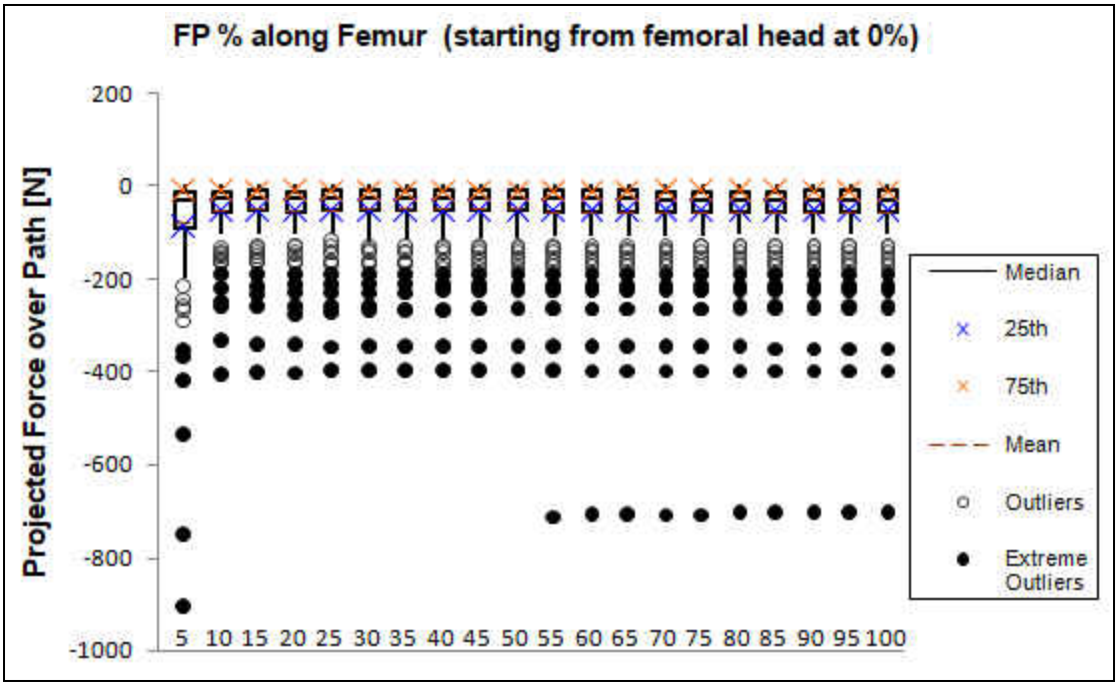

Figure 44: Graf type II projected force over the path of least energy; configurations show the most negative $Proj_{\overrightarrow{path}} \vec{F}_{tot}$ near the femoral head.

When $Proj_{\overrightarrow{path}} \vec{F}_{tot}$ is against the desired reduction direction, the maximum force found around 25% the total force over the femoral head, different configurations then the FP vary along the length of the femur is illustrated in Figure 45.

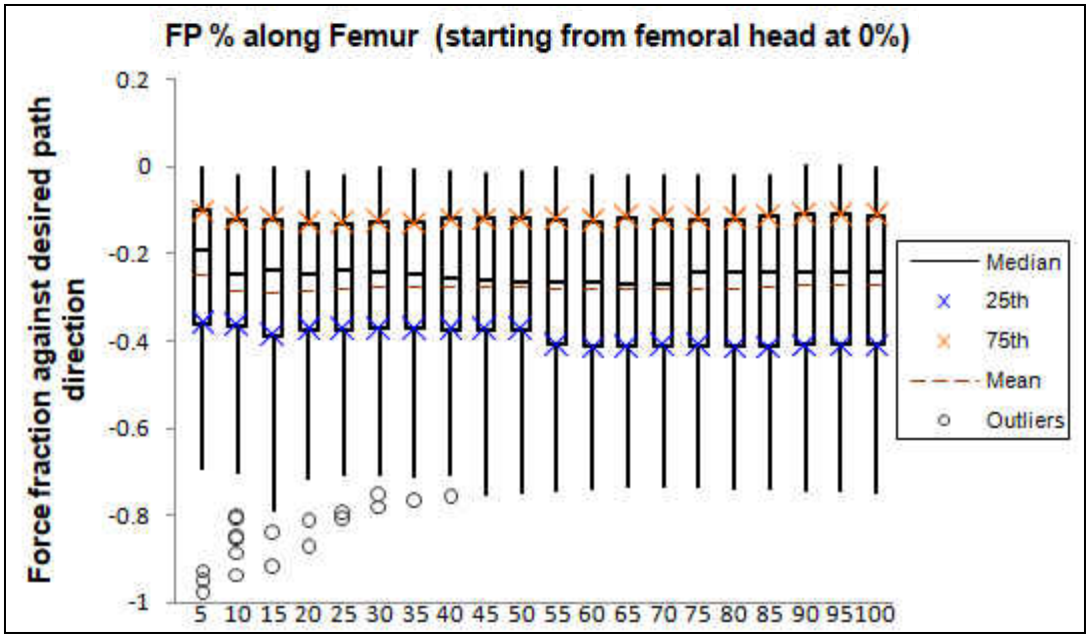

Figure 45: Graf type II projected force over the path of least energy divided by the total forces acting over the femoral head pointing against the desired path.

The incidence of configurations at which the FP is desired to be located near the knee was found in 429 of 867 configurations modeled.

The mathematical expression that best describes the location of the OP Graf type II dislocations is the following, predicting incorrectly 34.14 % of the times:

$$Best_{FP} = round\big(0.0103752367013149 * \varphi_i + (6.98066337324478e^{-5}) * \theta_i * \Phi_i + 0.0189608809687814 * \varphi_e * cos(1.2163152190702 * \Phi_i)\big) \quad (41)$$

Where φ_e represents the external rotation in degrees of the infant when equilibrated without the fulcrum point, having the leg flexed an angle near 90 degrees. θ_i, Φ_i, and φ_i

are the rotations in degrees at which the brace will be applied. Same as in Graf type I, if $Best_{FP}$ is zero, will indicate to apply the FP proximal the femoral head, if $Best_{FP}$ is one, will indicate to apply the fulcrum point proximal to the knee.

6.3 Fulcrum point effect for Graf type III configurations using the least energy path

For Graf type III configurations, the femoral head was aligned tangent to node 6 at the acetabular rim, towards node 27, which was the starting node used for the path of least energy of the previous section, forming a five-step-travel path as shown in Figure 46. In addition, all configurations included the anatomical average input values. Furthermore, the least energy reduction paths were using all nodes forming the acetabular rim to the nearest node towards the center of the acetabulum in addition to the five-step travel path starting tangent to node 6. The paths were from the following source and destination nodes: 21 to 41, 1 to 22, 2 to 23, 3 to 24, 4 to 25, 5 to 26, 6 to 27, 7 to 28, 8 to 29, 9 to 30, 10 to 31, 11 to 32, 12 to 33, 13 to 34, 14 to 35, 15 to 36, 16 to 56, 38 to 37, and from node 18 to 58. A Pearson correlation Matrix was found and summarized in Appendix A. Table 17 summarizes the linear relationship between all the input parameters and output parameters including the projected total force over the path of least potential energy for Graf type II configurations. It was found a proportional correlation of R_f with the rotation about the femoral axis of the insertion point of the adductor longus ($r = 0.419$), the PCSA of the quadratus femoris ($r = 0.2663$), the femur incline angle ($r = 0.2533$), PCSA of the obturator externus ($r = 0.2301$), and the 3D rotation around the femoral axis of the insertion point of the semimembranosus ($r = 0.2259$). Parameters which showed an

inverse linear relationship with R_f are the abduction angle of the brace ($r = -0.432$), the flexion angle of the brace ($r = -0.3803$), the obturator externus' insertion point angle of rotation around the femoral shaft with respect to the linea aspera ($r = -0.2781$), PCSA of the biceps femoris long head ($r = -0.2615$), and the Abduction angle used to equilibrate the model to find the muscle material properties ($r = -0.2455$). All these parameter and others which did not show strong correlation with $Proj_{\overrightarrow{path}} \vec{F}_{tot}$ are shown in Appendix A Table 22.

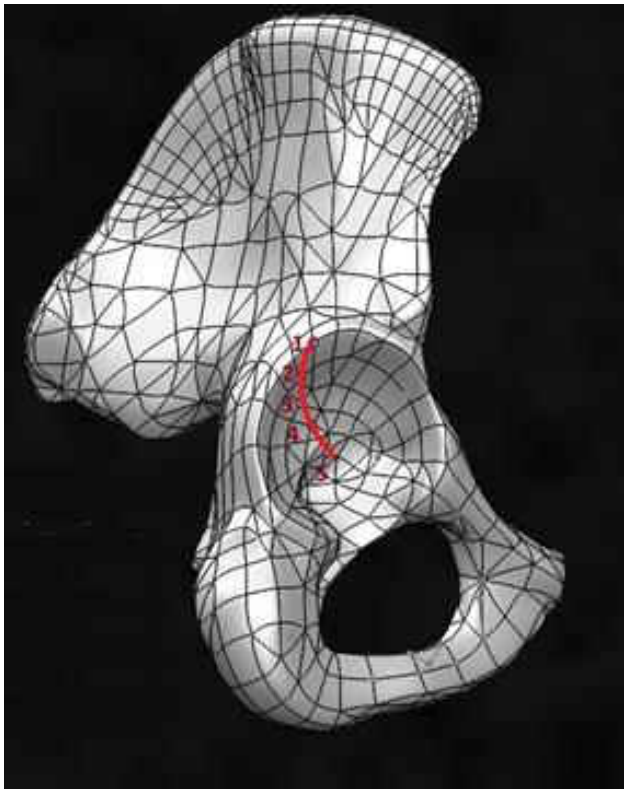

Figure 46: Graf type III least energy path shown in red, 4 step reduction [14].

With the Spearman rank correlation, it was found a significant monotonic correlations $R_f$with the percentage of total force in the path of least energy, the most

significant parameters are, the adductor longus' insertion point angle of rotation with respect to the femoral axis ($\rho = 0.2977$), the iliopsoas resting length ($\rho = 0.2734$), the PCSA of quadratus femoris ($\rho = 0.2381$), the PCSA of the obturator externus ($\rho = 0.2307$), and the the semimembranosus' insertion point angle of rotation with respect to the femoral axis ($\rho = 0.2115$). The negative monotonic parameters with respect to $R_f V$ for Graf type III were found to be: the flexion angle of the brace ($\rho = -0.3406$), the hip muscle insertion point x-coordinate on the iliopsoas ($\rho = -0.3194$), the obturator externus' insertion point angle of rotation around the femoral shaft with respect to the linea aspera ($\rho = -0.2786$), the PCSA of the gluteus minimus posterior ($\rho = -0.2417$), and the PCSA of the biceps femoris long head ($\rho = -0.2322$).

Because some generated configurations are unstable or not in static equilibrium, several outliers were removed, from the remaining configurations, $Proj_{\overrightarrow{path}} \vec{F}_{tot}$ was found to be at the highest closer to the femoral head (0%) as shown in Figure 47.

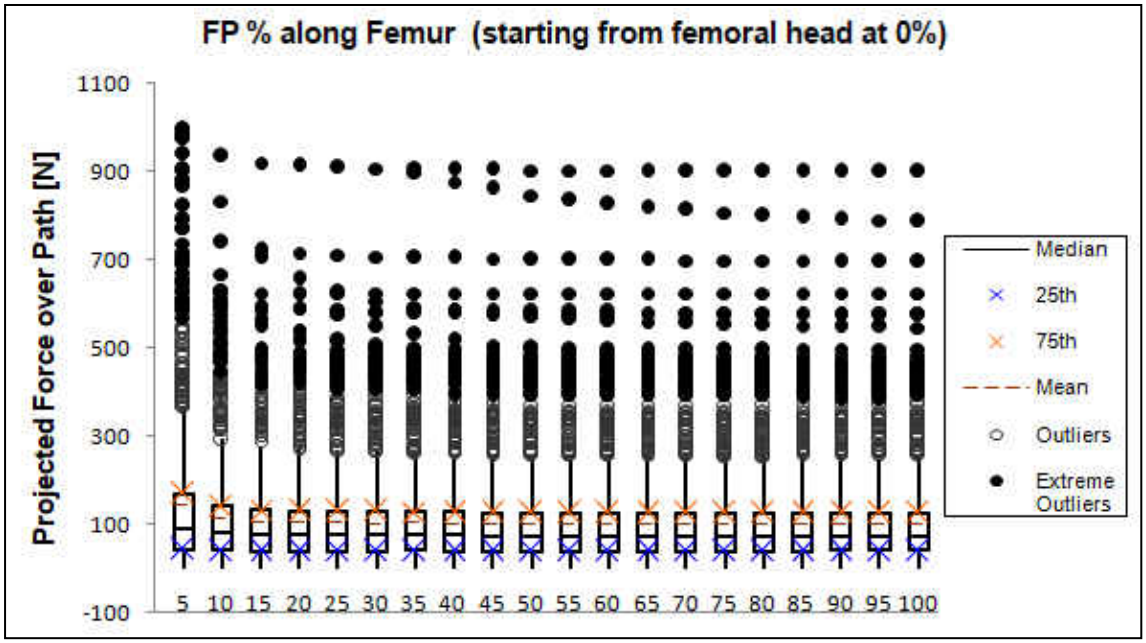

Figure 47: Graf type III projected force over the path of least energy; configurations show a higher $Proj_{\overrightarrow{path}} \vec{F}_{tot}$ near the femoral head.

All these configurations presented the characteristic of having around 62% of mean $\vec{F}_{tot}$ acting over the desired path as shown in Figure 48.

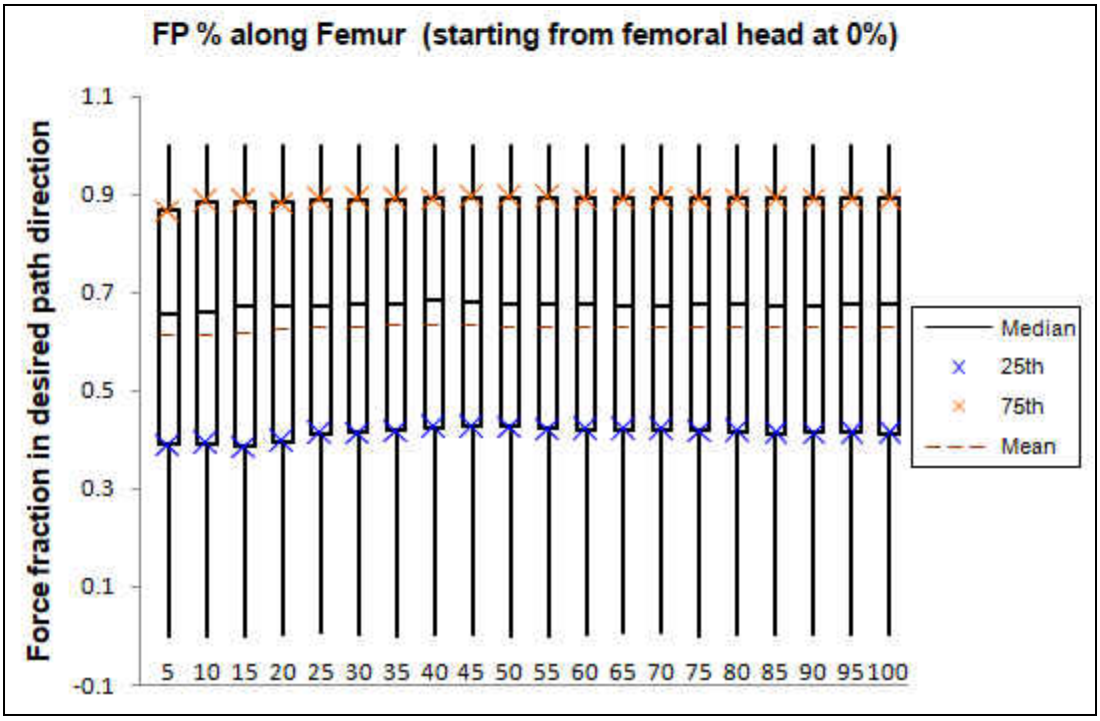

Figure 48: Graf type III $Proj_{\overrightarrow{path}} \vec{F}_{tot}$ divided by the total force acting over the femoral head.

After filtering only valid configurations, which allows static equilibrium and stable configurations, it was also found that $Proj_{\overrightarrow{path}} \vec{F}_{tot}$ can be negative (1253 of 4449 configurations in Graf type III). The most negative value was found near the femoral head shown in Figure 49.

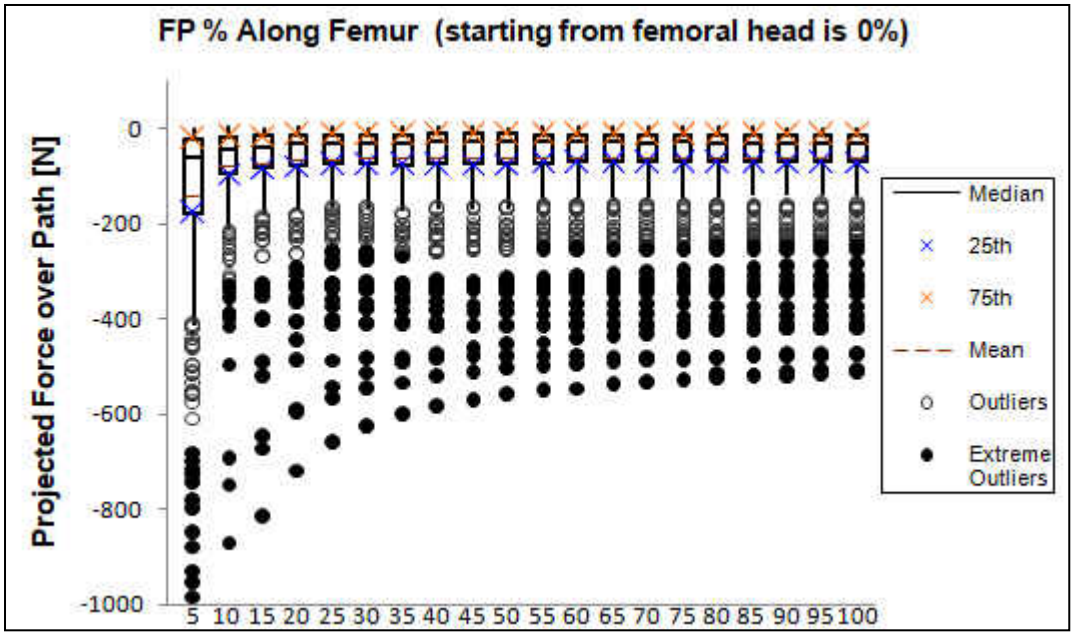

Figure 49: Graf type III projected force over the path of least energy; configurations show the most negative $Proj_{\overrightarrow{path}} \vec{F}_{tot}$ near the femoral head.

All these Graf type I configurations presented the characteristic of having around 33% of $\vec{F}_{tot}$ acting against the desired path as shown in Figure 50, with a wide range of variability from 5 to 99.98% of the force acting in the path of least potential energy.

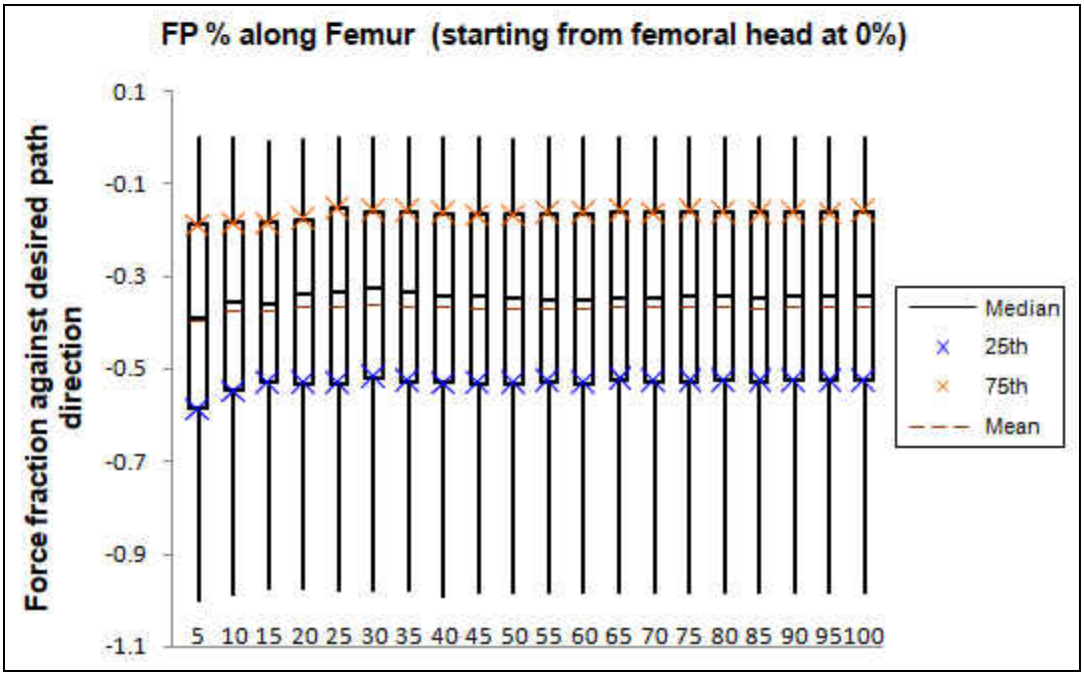

Figure 50: Graf type III projected force over the path of least energy divided by the total forces acting over the femoral head pointing against the desired path.

The incidence of configurations at which the FP is desired to be located near the knee was found in 2324 of 4449 configurations modeled.

The mathematical expression found to suggest the location of the fulcrum point for a Graf type III condition, was the following, predicting incorrectly 36.17 % of the times, with the rounding functions are to 0 decimal places:

$$
\begin{aligned}
Best_{FP} = round\big(&1.53386143131768e^{-5} * \theta_i * \Phi_i \\
&+ 0.503681322988358 \\
&* \cos(0.00236451799253333 * \theta_i) \\
&- 0.107710273111296 \\
&* \text{round}(0.118364604623652 * n - 1.40478486251699) \\
&* round(0.118364604623652 * n \\
&+ 0.00232847351093984 * \theta_i - 1.40478486251699)\big)
\end{aligned}
\tag{42}
$$

Where n denotes the node number used for the selected reduction path.

6.4 Fulcrum point effect for Graf type IV configurations using the indirect path

In this section we will cover the results of the indirect path as shown in Figure 51. The center of the femoral head moved initially to x=-11.0434, y= 13.3084, z=2.4473 mm which corresponds to a Graf type IV having contact between the hip and the femoral head. The nodes selected for this 13 step path reduction were 131, 124, 121, 112, 111, 99, 93, 19, 39, 59, 60, 62, and 75 based on [14]. All these parameter and others which did not confirm strong correlation with R_f are shown in Appendix ATable 18.

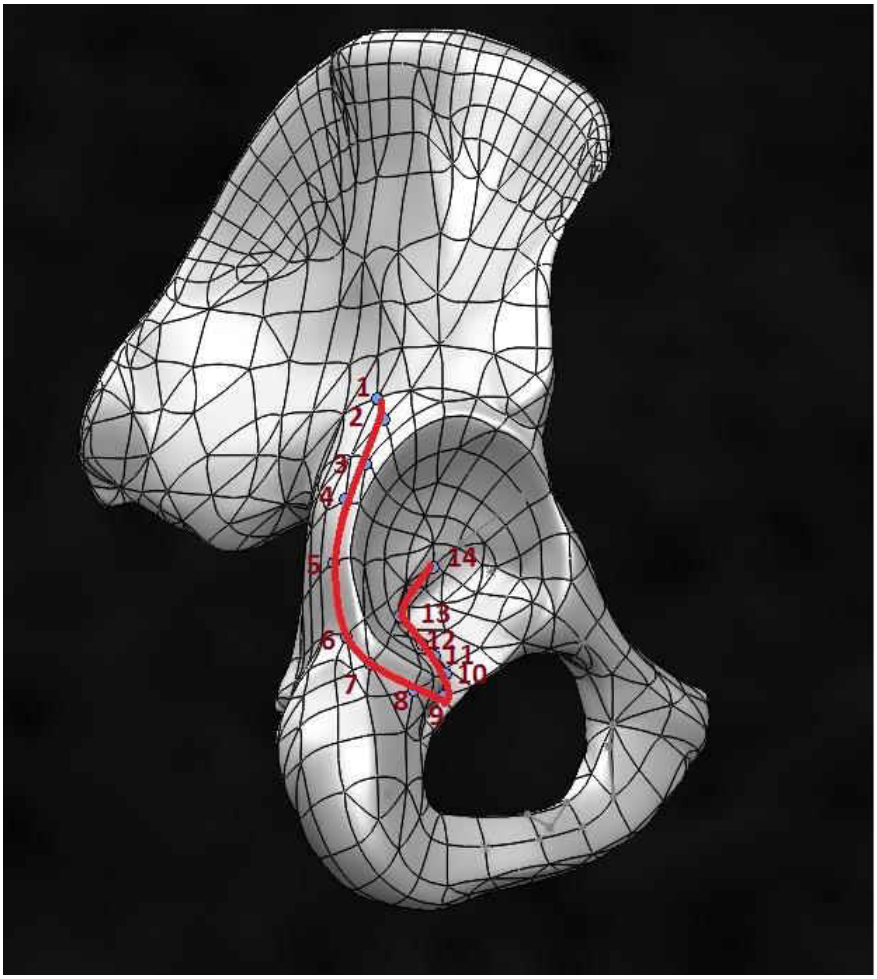

Figure 51: Graf type IV least energy (indirect path) illustrated in red, 13 step reduction [14].

Figure 52 illustrates how the projection of the resulting force over the femoral head is contributing to achieve reduction in the direct path. The figure shows the projected force is maximized when the fulcrum point is applied.

From the Pearson correlation matrix, there was no strong linear correlation found with respect to R_f , the highest values found for this Graf condition were the muscle insertion point distance from the femoral shaft of the rectus femoris ($r = 0.0852$) the

muscle relaxed length of the gluteus minimus anterior ($r = 0.0757$), the PCSA of the Gluteus minimus posterior ($r = 0.061$), the muscle insertion point rotation around the femoral shaft of the adductor magnus posterior ($r = 0.0602$), and the muscle insertion point rotation around the femoral shaft of the adductor magnus middle ($r = 0.057$) . The inversely proportional parameters also did not show strong linearity with respect to R_f, the strongest correlations were, the flexion angle at which the brace is applied ($r = -0.1207$), the muscle insertion point distance from the femoral shaft of the gemellus superior ($r = -0.0782$), the Abduction angle at which the leg finds equilibrium without the assistance of the fulcrum point, being the legs flexed near 90 degrees ($r = -0.0743$), and the 3D rotation around the femoral shaft of the insertion point of the iliopsoas ($r = -0.0683$).

for Graf type IV indirect path, in the Spearman rank correlation matrix, the variables found to have a monotonic direct relationship with R_f were the distance from the femoral shaft to the rectus femoris' insertion point ($\rho = 0.0833$), the gluteus minimus anterior resting length ($\rho = 0.0751$), the trochanter length ($\rho = 0.0689$), the PCSA gluteus minimus anterior ($\rho = 0.0628$) and the PCSA gluteus medius anterior ($\rho = 0.0588$). All these parameter and others which did not show strong correlation with $Proj_{\underrightarrow{path}} \vec{F}_{tot}$ are shown in Appendix B Table 23.

The calculation of $Proj_{\underrightarrow{path}} \vec{F}_{tot}$ for different FP along the femur was also found as in Graf type IV to decrease when de fulcrum point approaches the knee as illustrated in Figure 52 for most of the points. After removing outliers the model shows a higher value near the femoral head, suggesting the location of the FP.

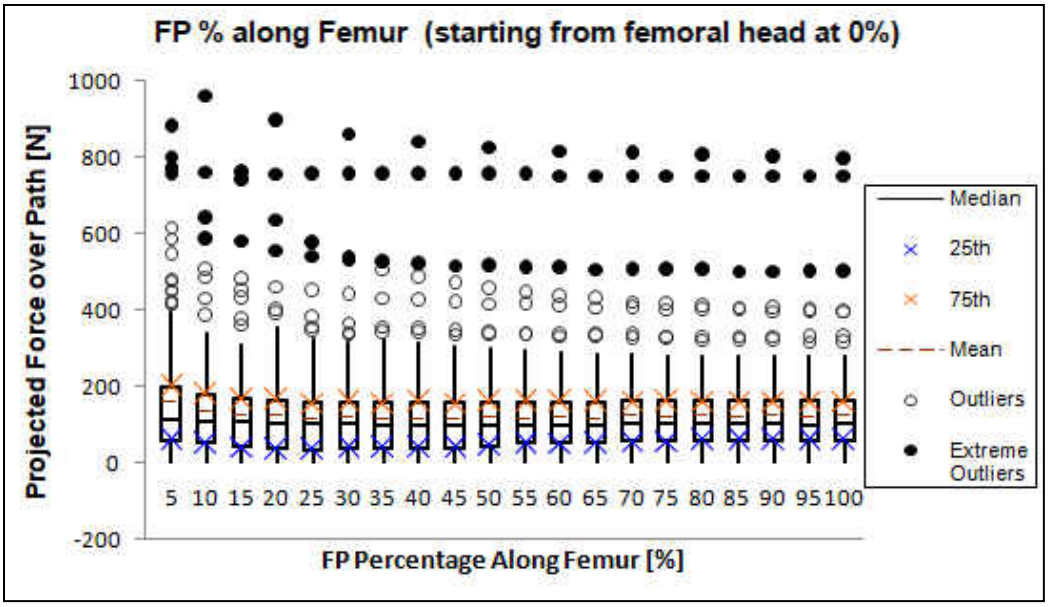

Figure 52: Graf type IV projected force over the indirect path; configurations show a higher $Proj_{\overrightarrow{path}} \vec{F}_{tot}$ near the femoral head.

It was also found $R_{f_{max}}$ is slightly increasing when the FP approaches the knee shown in Figure 53, but still the most efficient location for the FP is near the femoral head.

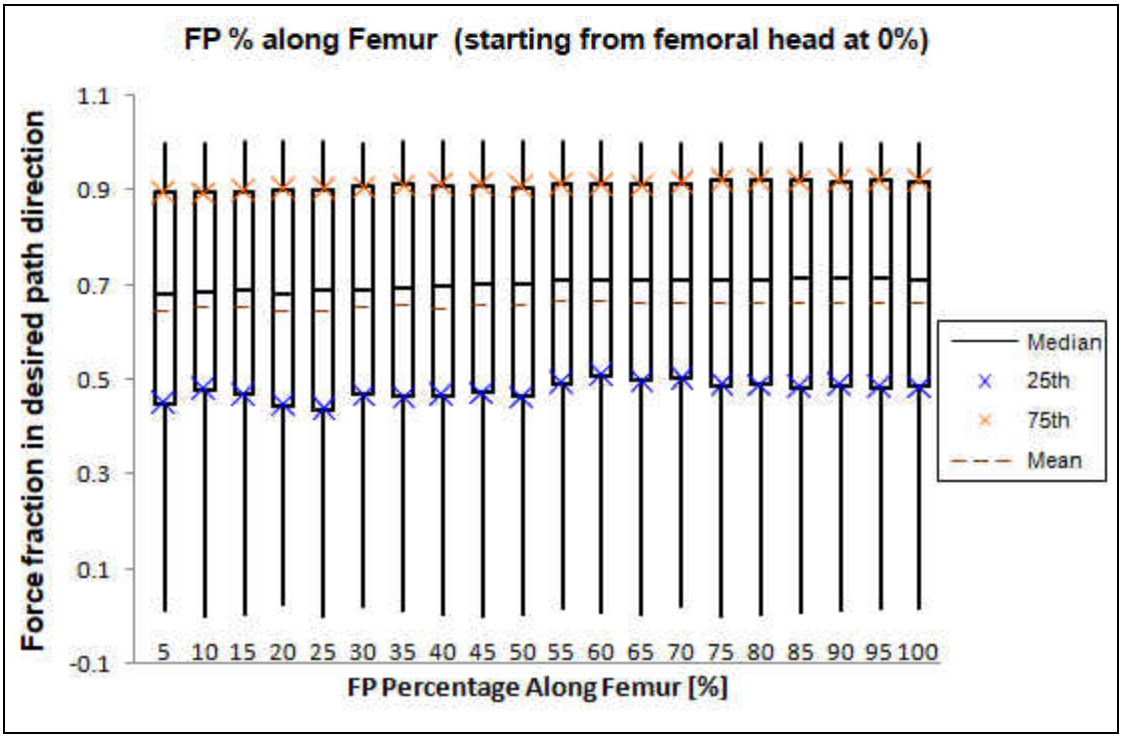

Figure 53: Graf type IV $Proj_{\overrightarrow{path}} \vec{F}_{tot}$ divided by the total force acting over the femoral head.

It was also found for Graf type IV path of least energy multiple configurations at which $R_{f\,max}$ is negative, meaning the forces are acting in opposite direction of desired path of least energy shown in Figure 54. The incidence of Graf type IV configurations acting against the desired indirect path was 614 of 2084 configurations.

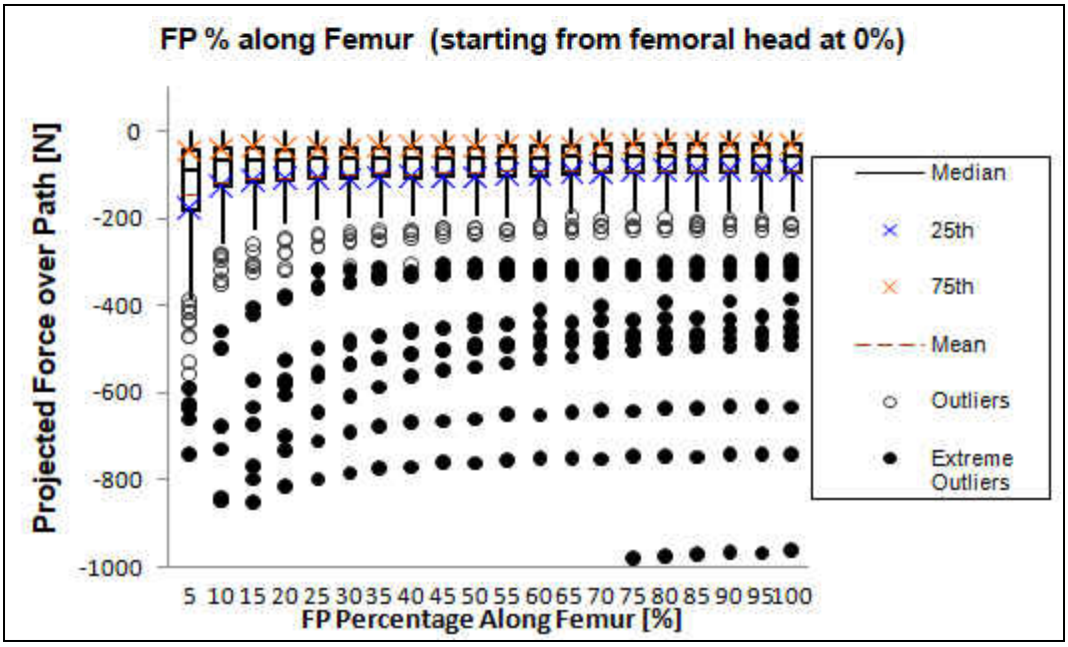

Figure 54: Graf type IV projected force over the indirect path; configurations show the most negative $Proj_{\overrightarrow{path}}\vec{F}_{tot}$ near the femoral head.

When $Proj_{\overrightarrow{path}}\vec{F}_{tot}$ is against the desired reduction direction, the maximum force found around 70% the total force over the femoral head, different configurations then the FP vary along the length of the femur is illustrated in Figure 55, also showing a wide range of variability from 0 to 99.98% of the force, is acting against the path of least potential energy.

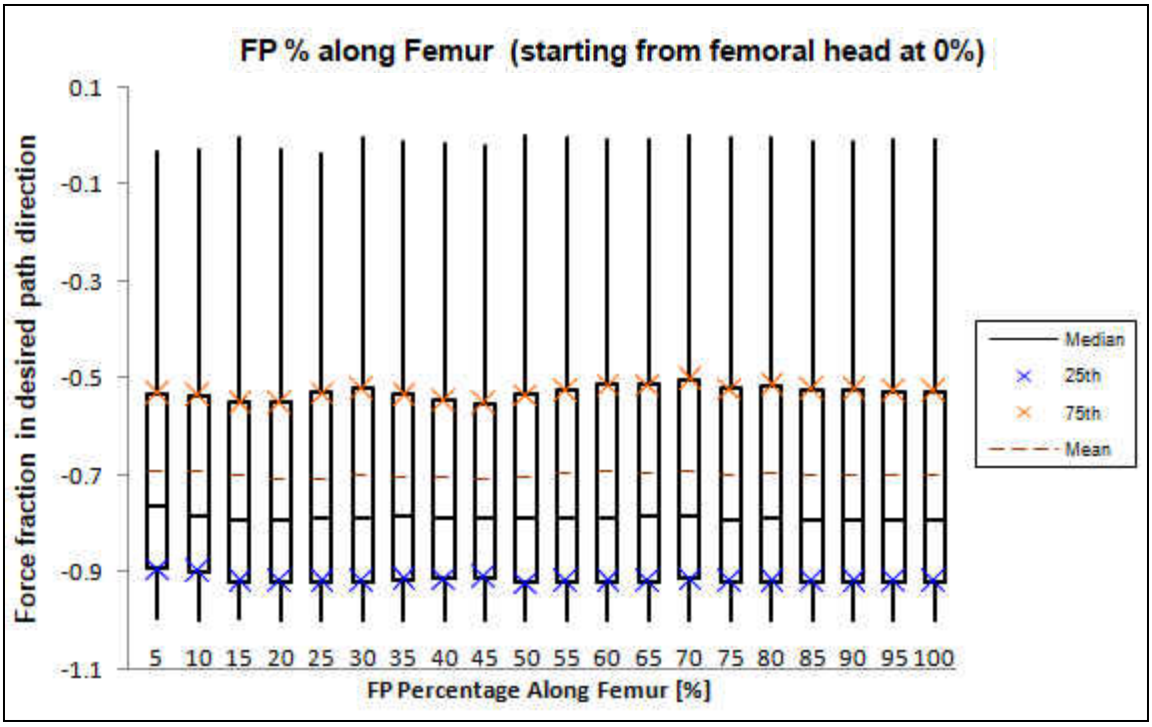

Figure 55: Graf type IV projected force over the path of least energy divided by the total forces acting over the femoral head (V_{max}) pointing against the indirect path.

The mathematical expression found to suggest the location of the fulcrum point for a Graf type IV for the indirect least energy path, was the following, predicting incorrectly 39.78 % of the times, with the rounding functions are to 0 decimal places:

$$\begin{aligned} Best_{FP} = round(&8.43642650294084e^{-7} * \theta_i * \Phi_i^2 \\ &+ 0.0014106224548619 \\ &* n * \cos(4.64484797888807 + 2.34135885958887 \\ &* n) - 0.0918389461402193 \\ &* \cos(4.64484797888807 + 2.34135885958887 * n)) \end{aligned} \quad (43)$$

6.5 Fulcrum point effect for Graf type IV configurations using the direct path

For Graf type IV, two different paths of were analyzed; in this section we will cover the results of the direct path as shown in Figure 56. The femoral head was aligned tangent to node 131 outside the acetabulum. In addition, all configurations included the anatomical average input values. Furthermore, the least energy reduction path was defined as a seven-step travel path: step 1 from node 131 to node 124, step 2 from node 124 to node 121, step 3 from node 121 to node 122, step 4 from node 122 to node 1, step 5 from node 1 to node 22, step 6 from node 22 to node 43, step 7 from node 43 to node 63, step 8 from node 63 to node 75 based on [14] shown in Figure 56. Constraints set up as mentioned in the methodology.

For the least energy reduction path, which included all input parameters from Table 7, Table 9, and Table 10, a Pearson correlation Matrix was found and summarized in Appendix A. Table 19 summarizes the linear relationship between all the input parameters and output parameters including the projected total force over the path of least potential energy for Graf type IV direct path configurations. The significant parameters which showed an inverse linear relationship $R_f V$ are the tensor fascia lata' insertion point angle of rotation with respect to the linea aspera ($r = 0.1322$), the tensor fascia lata resting length ($r = 0.129$) and the semimembranosus resting length ($r = 0.1202$), the gluteus minimus middle' insertion point angle of rotation with respect to the linea aspera ($r = 0.0931$), and the gracilis' insertion point angle of rotation with respect to the linea aspera ($r = 0.0928$). The significant parameters which showed an inverse linear relationship to V are: the PCSA of the obturator externus ($r = 0.1204$), the PCSA of the

pectineus ($r = -0.1181$), the PCSA of the obturator internus ($r = -0.1$), and the femur throcanteric length ($r = -0.0922$).

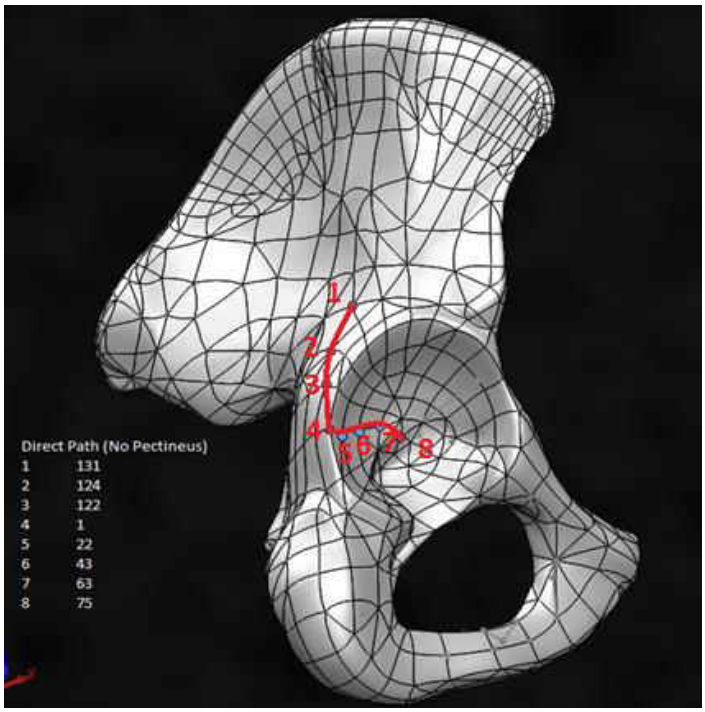

Figure 56: Graf type IV least energy direct path 7 step reduction [14].

In the Spearman rank correlation matrix, the variables found to have a monotonic direct relationship for Graf type IV direct path were the semimembranosus resting length ($\rho = 0.1322$), the tensor fascia lata resting length ($\rho = 0.1155$), the obturator internus resting length ($\rho = 0.1146$), the gluteus minimus middle' insertion point angle of rotation with respect to the linea aspera ($\rho = 0.1132$) and the tensor fascia lata' insertion point angle of rotation with respect to the linea aspera ($\rho = 0.1888$). All these parameter and others which did not show strong correlation with R_f are shown in Appendix B Table 24.

The calculation of $Proj_{\overrightarrow{path}}\vec{F}_{tot}$ for different FP along the femur was also found to decrease when de fulcrum point approaches the knee as illustrated in Figure 57 for some of the points.

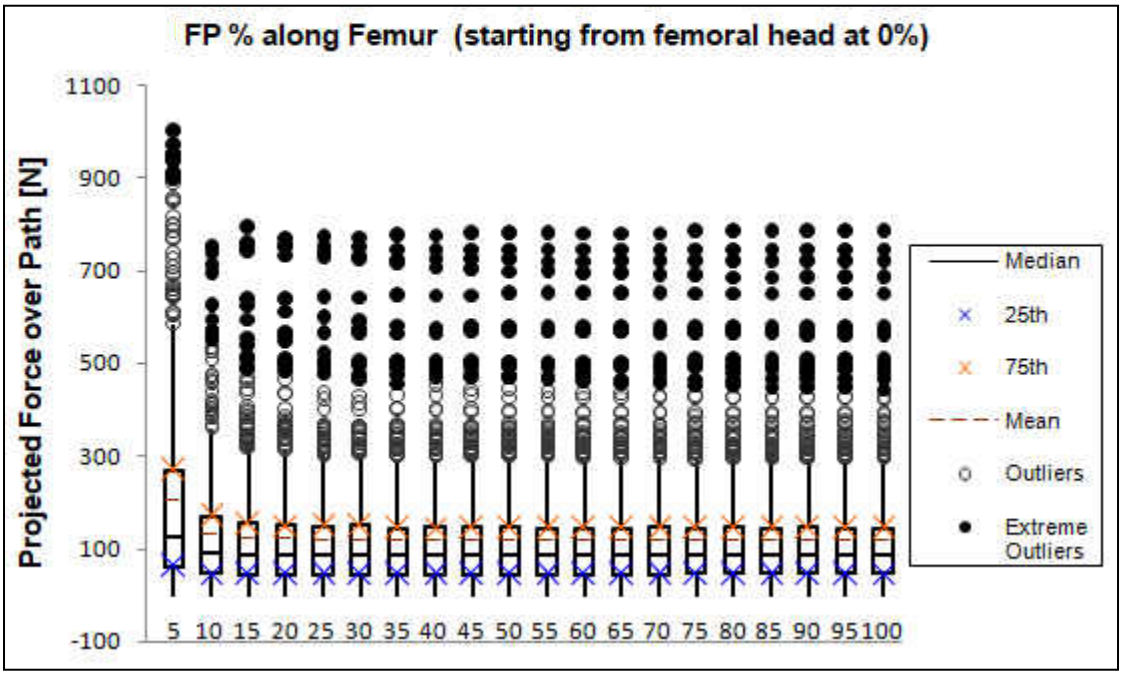

Figure 57: Graf type IV projected force over the direct path; configurations show a higher $Proj_{\overrightarrow{path}}\vec{F}_{tot}$ near the femoral head.

All these Graf type IV configurations presented the characteristic of having around 63% of $\vec{F}_{tot}$ acting in the desired path as shown in Figure 58.

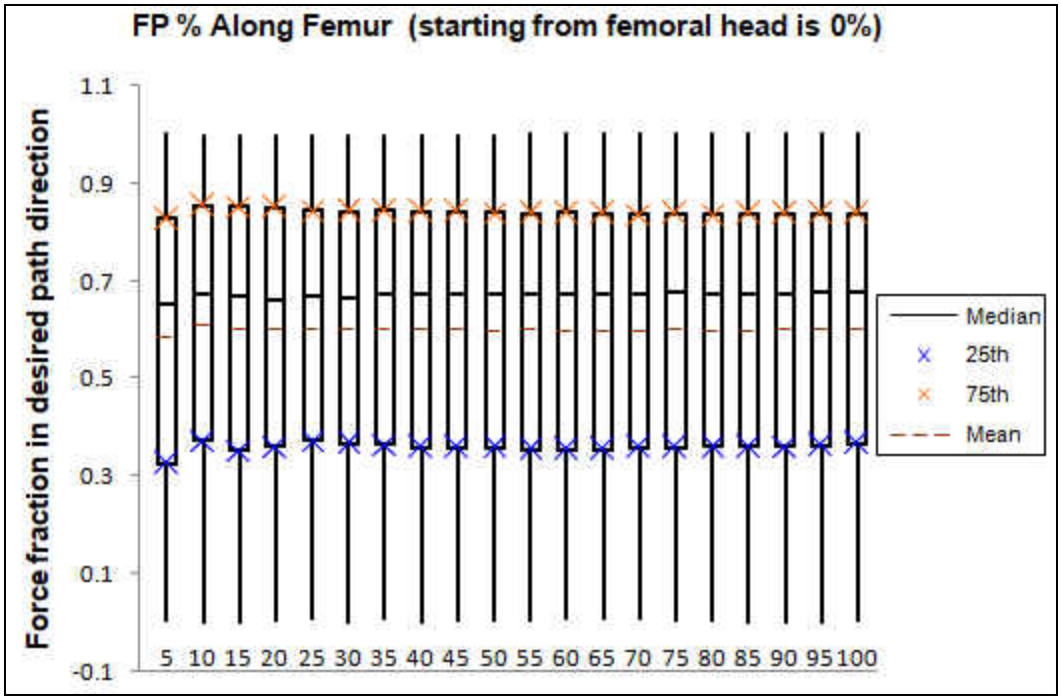

Figure 58: Graf type IV $Proj_{\overrightarrow{path}} \vec{F}_{tot}$ (direct path) divided by the total force acting over the femoral head.

From the configurations in Graf type IV (direct path), it was also found configurations in which $Proj_{\overrightarrow{path}} \vec{F}_{tot}$ acts against the desired path of least potential energy. The incidence of Graf type IV configurations acting against the desired path was 557 of 1216 valid configurations.

These configurations are represented in Figure 59. After removing outliers that had unequilibrated or unstable configurations, the most negative $Proj_{\overrightarrow{path}} \vec{F}_{tot}$ occurs when the FP is located near the femoral head.

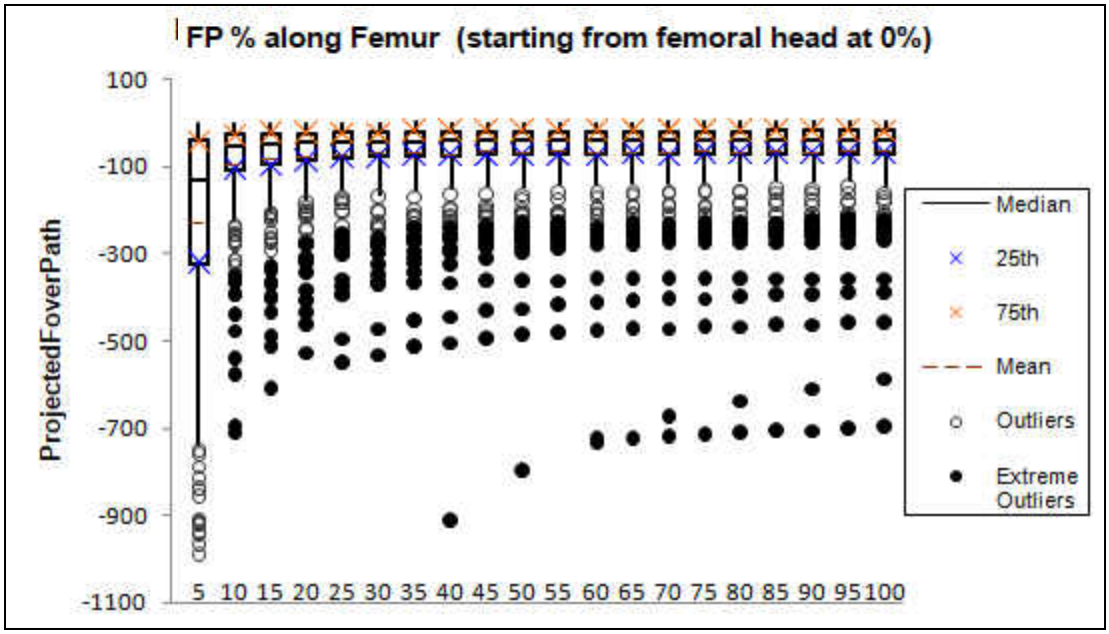

Figure 59: Graf type IV projected force over the direct path; configurations show the most negative $Proj_{\overrightarrow{path}} \vec{F}_{tot}$ near the femoral head.

When $Proj_{\overrightarrow{path}} \vec{F}_{tot}$ is against the desired reduction direction, the maximum force found around 40% the total force over the femoral head, different configurations then the FP vary along the length of the femur is illustrated in Figure 60.

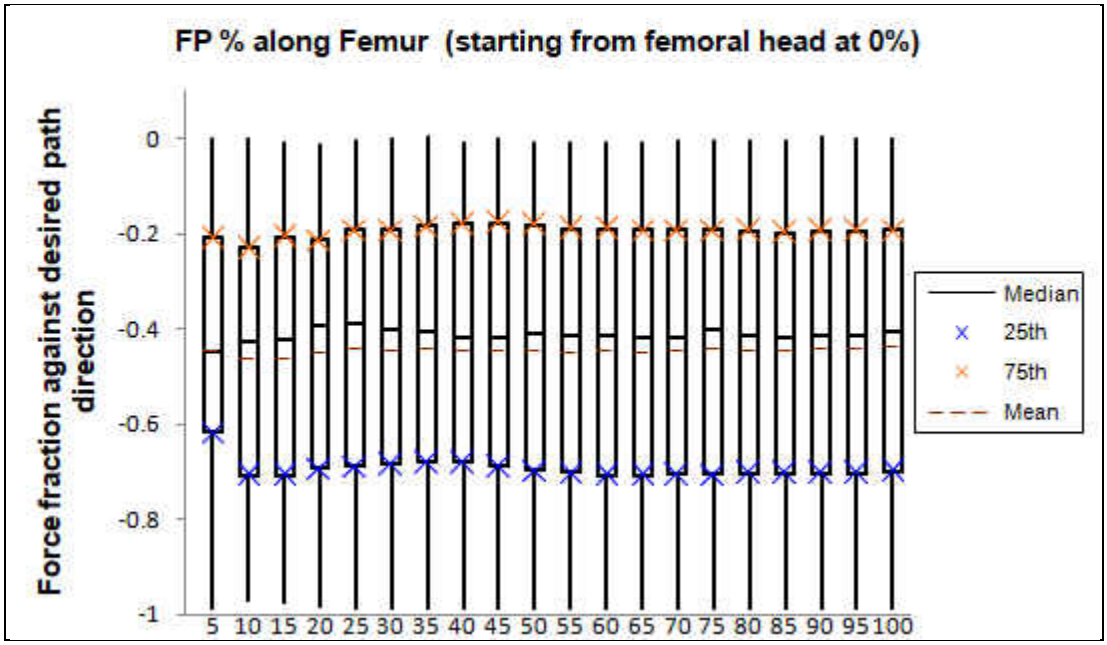

Figure 60: Graf type IV projected force over the path of least energy divided by the total forces acting over the femoral head pointing against the direct least energy path.

The incidence of configurations at which the FP is desired to be located near the knee was found in 582 of 1216 configurations modeled.

The mathematical expression found to suggest the location of the fulcrum point for a Graf type IV for the direct least energy path, was the following, predicting incorrectly 28.37 % of the times, with the rounding functions are to 0 decimal places:

$$Best_{FP} = round(\Phi_i^2(-0.277118935394169) + 0.798220592767375 * \cos(2.41537102939083 + 40.4246159324117 * \mathrm{n})) \quad (44)$$

6.6 Effectiveness of different Orthoses based on the Fulcrum point

Most of the HAOD holds the leg from the mid tight as shown in Figure 9, Frejka, Tübingen, Ilfeld, Eberle, and Semirigid Plastazote. The HAOD which holds the leg near the femoral head or at the mid tight depending of the size of the infant with respect to the HAOD size is Von Rosen, finally the Pavlik Harness, has the fulcrum point passing near the mid tight or proximal to the knee as shown in Figure 8. Individual analysis for 5 popular HAODs will be discussed, the Pavlik Harness, Tübingen splint, Spica cast, Von Rosen splint, and Frejka pillow for Graph type I and for Graf type IV direct and indirect path.

6.6.1 Pavlik harness

After the data was prepared and categorized for the Pavlik harness, 40 configurations were analyzed, results shown as a box plot in Figure 61 suggest for a Graf type I, the projected force over the path of reduction is more positive near the knee. The configuration does not take into account the force in the strap in the y-direction (perpendicular to the transverse plane).

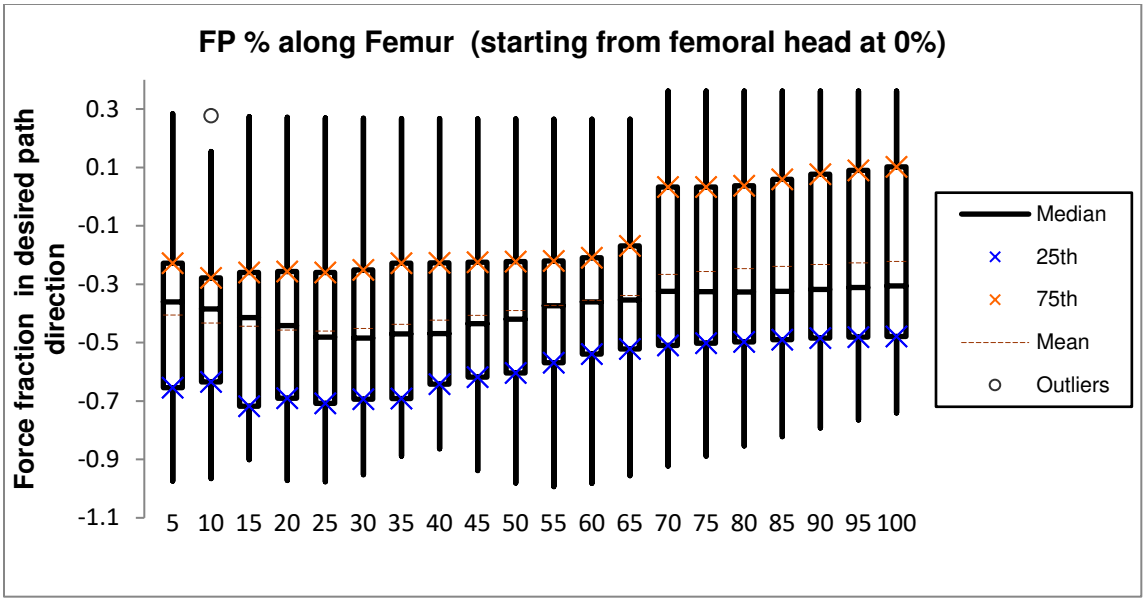

Figure 61: Graf type I projected force over the least energy path; configurations suggest the highest $Proj_{\overrightarrow{path}} \vec{F}_{tot}$ near the knee.

After the data was prepared and categorized for the Pavlik harness, 31 configurations were analyzed, results suggest for a Graf type IV in Figure 62, the projected force over the indirect path of reduction is more positive near the femoral head.

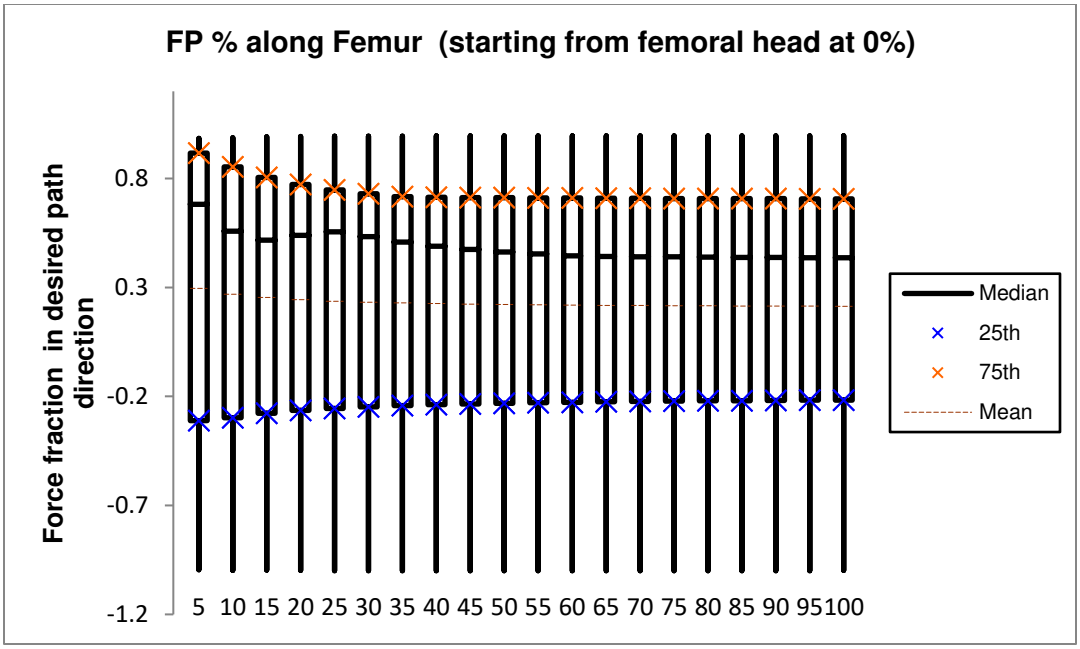

Figure 62: Graf type IV projected force over the indirect path; configurations show the most positive $Proj_{\overrightarrow{path}} \vec{F}_{tot}$ near the femoral head.

After the data was prepared and categorized for the Pavlik harness, 118 configurations were analyzed, results suggest for a Graf type IV in Figure 63, the projected force over the direct path of reduction is more positive near the femoral head.

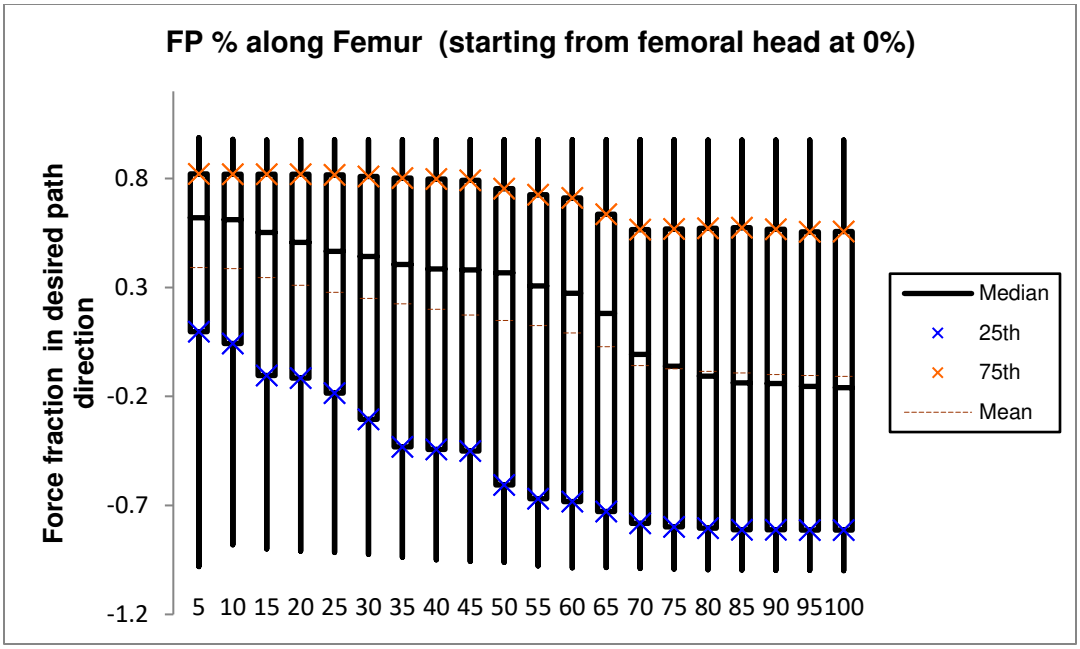

Figure 63: Graf type IV projected force over the direct path; configurations show the most positive $Proj_{\overrightarrow{path}} \vec{F}_{tot}$ near the femoral head.

6.6.2 Tübingen splint

After the data was prepared and categorized for the Tübingen splint, 23 configurations were analyzed, results shown as a box plot in Figure 64, suggest for a Graf type I, the projected force over the path of reduction is more positive near the knee. The configuration does not take into account the force of the splint in the y-direction.

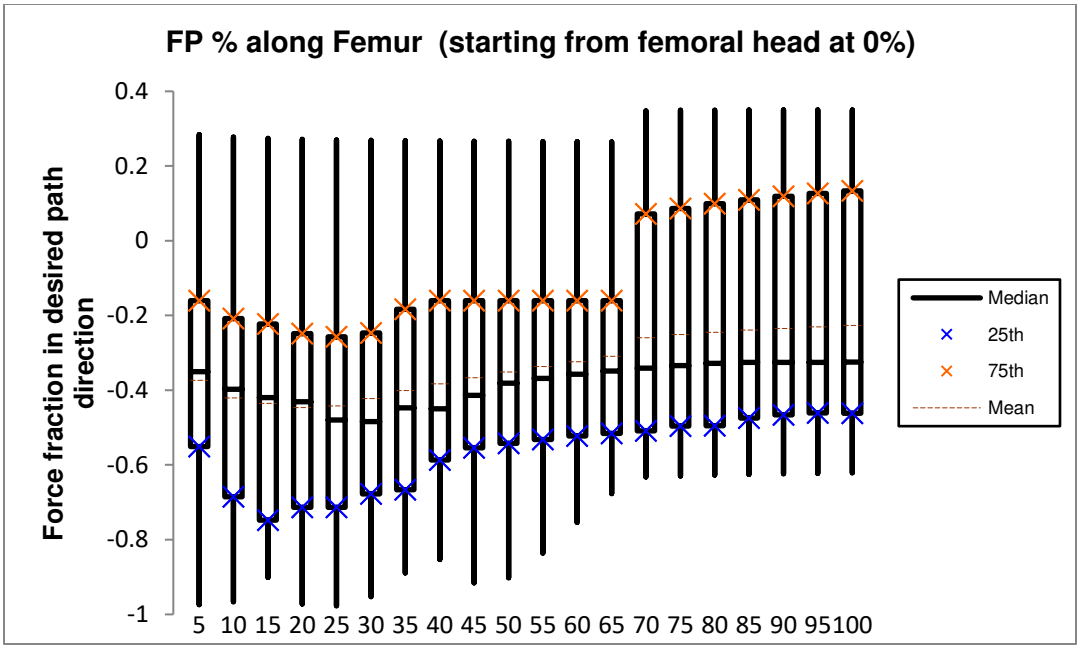

Figure 64: Graf type I projected force over the least energy path; configurations show the most positive $Proj_{\overrightarrow{path}} \vec{F}_{tot}$ near the knee.

After the data was prepared and categorized for the Tübingen splint, 20 configurations, results suggest for a Graf type IV in Figure 65, the projected force over the indirect path of reduction is more positive near the femoral head.

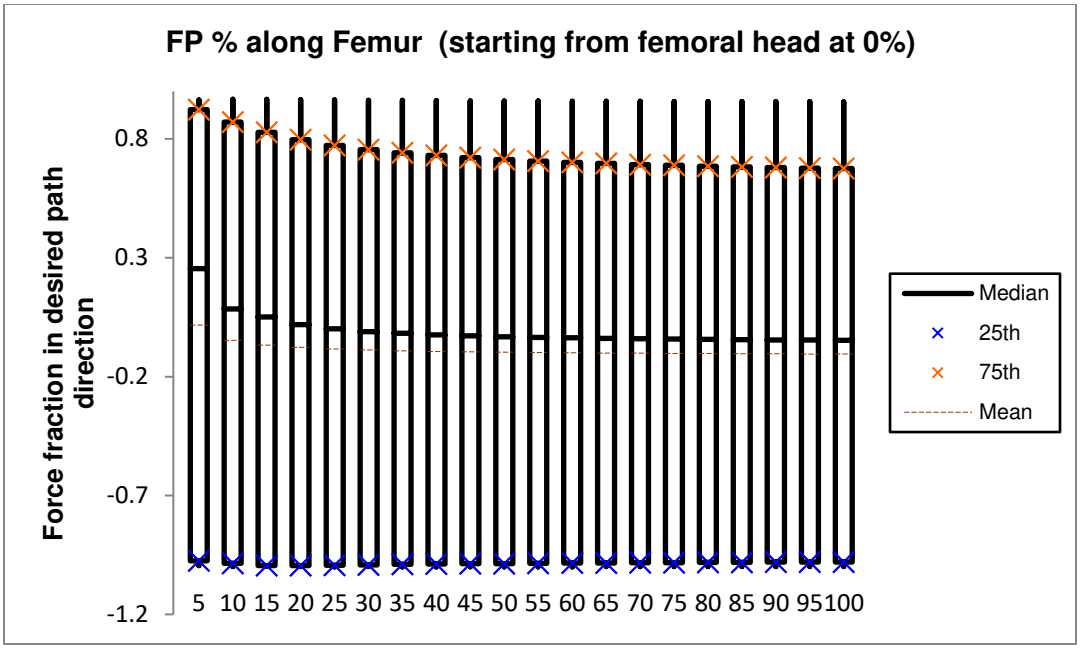

Figure 65: Graf type IV projected force over the indirect path; configurations show the most positive $Proj_{\overrightarrow{path}} \vec{F}_{tot}$ near the femoral head.

After the data was prepared and categorized for the range suggested for the Tübingen splint, 59 configurations were analyzed, results suggest for a Graf type IV in Figure 66, the projected force over the direct path of reduction is more positive near the femoral head, but presents less variability having a highest values in the range for placing the FP near the femoral head.

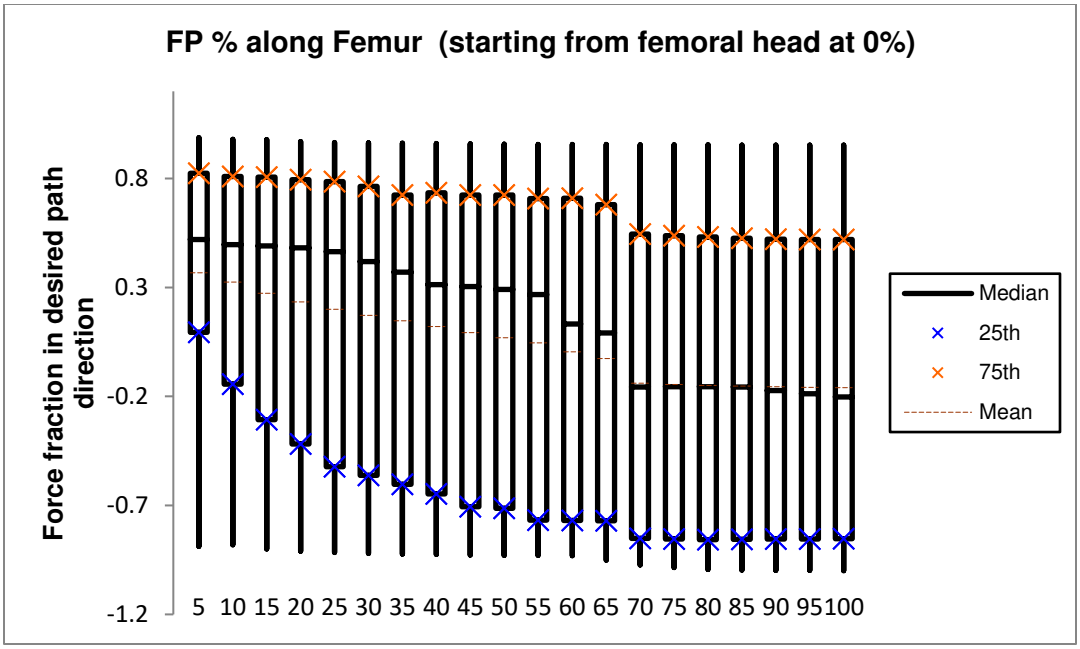

Figure 66: Graf type IV projected force over the direct path; configurations show the most positive $Proj_{\overrightarrow{path}} \vec{F}_{tot}$ near the femoral head.

6.6.3 Spica cast

After the data was prepared and categorized for the Spica cast, 17 configurations were analyzed, results shown as a box plot in Figure 67, suggests for a Graf type I, the projected force over the path of reduction is less negative at the knee. The configuration does not take into account the force of the cast in the y-direction.

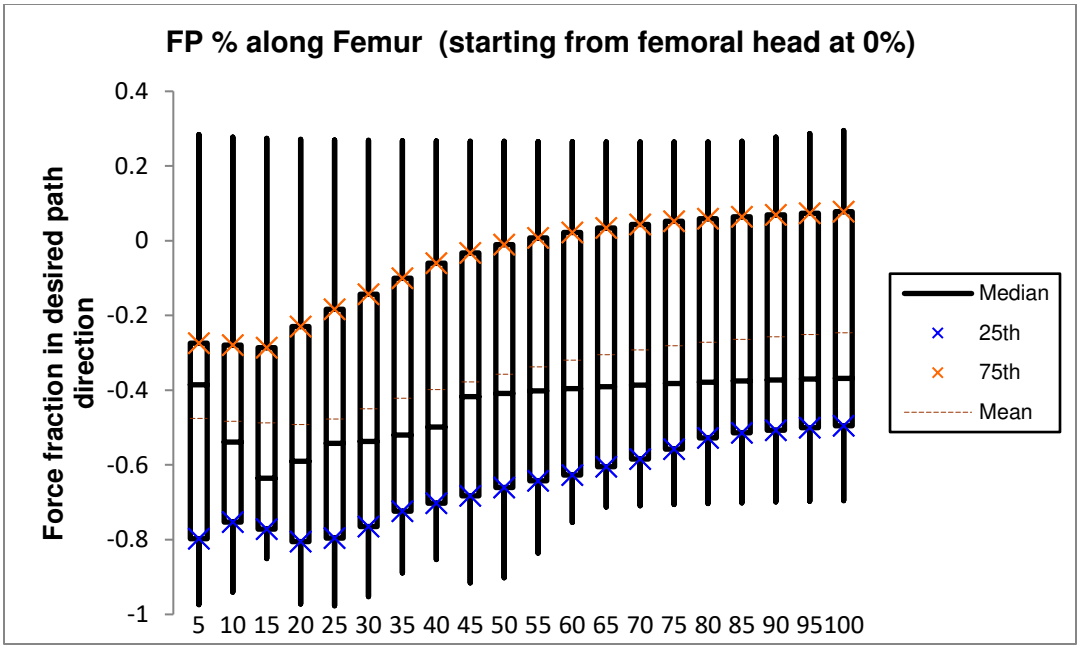

Figure 67: Graf type I projected force over the least energy path; configurations show the less negative $Proj_{\overrightarrow{path}} \vec{F}_{tot}$ near the knee.

After the data was prepared and categorized for the Spica cast, 97 configurations were analyzed, results suggest for a Graf type IV in Figure 68, $R_{f_{max}}$ is more positive near the femoral head.

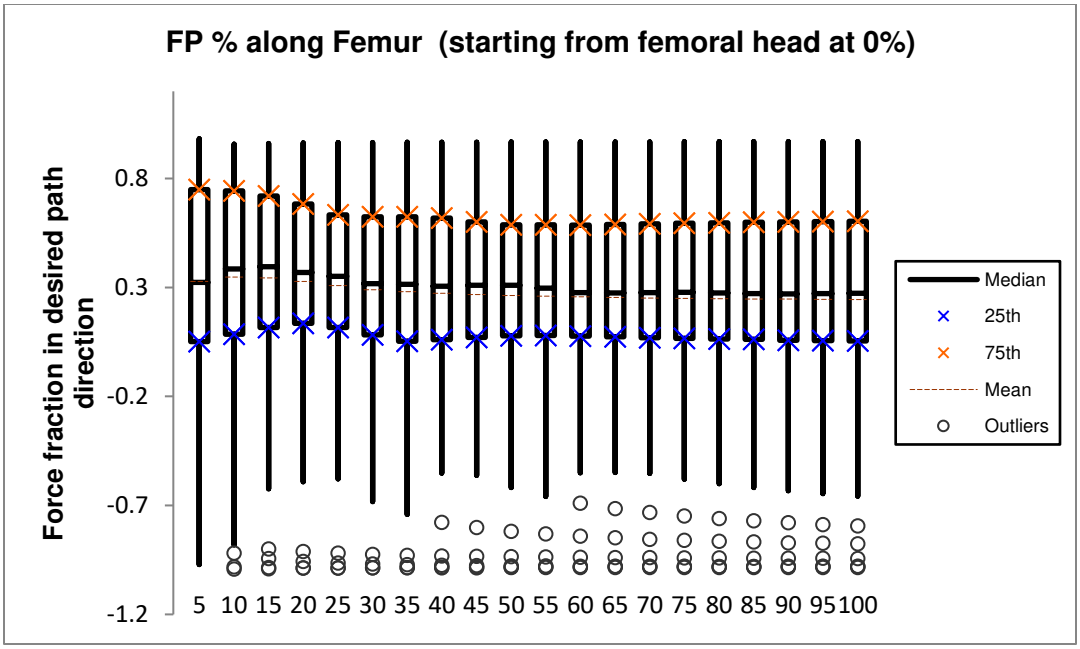

Figure 68: Graf type IV projected force over the indirect path; configurations show the most positive $Proj_{\overrightarrow{path}} \vec{F}_{tot}$ near 15% along the femoral head.

After the data was prepared and categorized for the Spica cast, 40 configurations were analyzed, results suggest for a Graf type IV direct path, the projected force over the direct path of reduction is more positive near the femoral head in Figure 72.

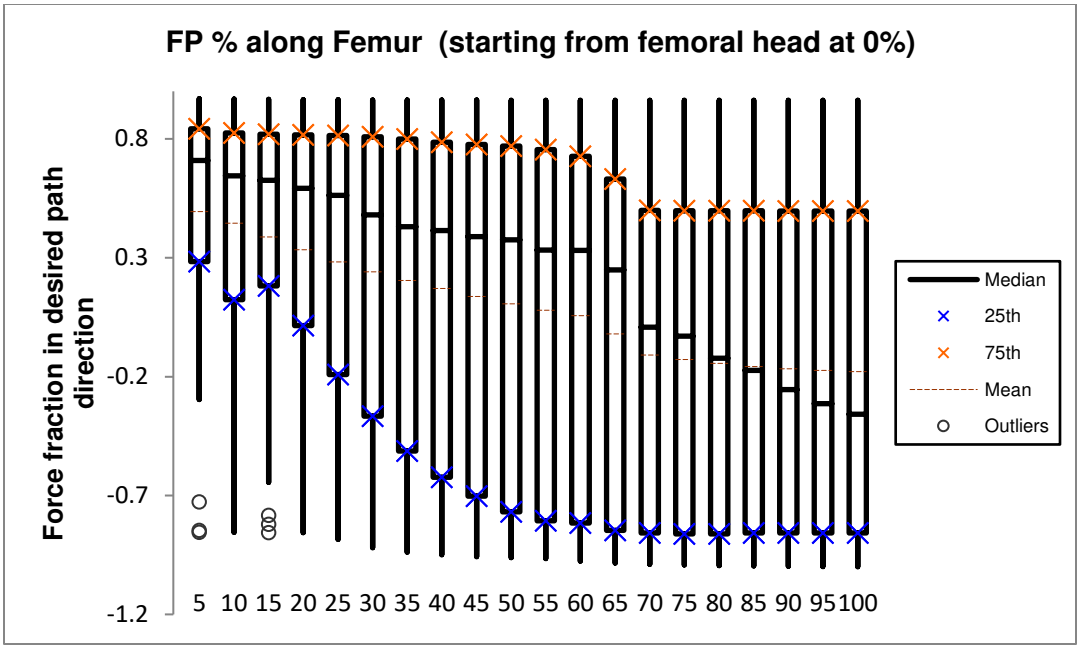

Figure 69: Graf type IV projected force over the direct path; configurations show the most negative $Proj_{\overrightarrow{path}} \vec{F}_{tot}$ near the femoral head.

6.6.4 Von Rosen splint

After the data was prepared and categorized for the Von Rosen splint, 215 configurations were analyzed, results shown as a box plot in Figure 70, suggests for a Graf type I, the projected force over the path of reduction is more positive at 10% of the femoral length. The configuration does not take into account the force of the splint in the y-direction.

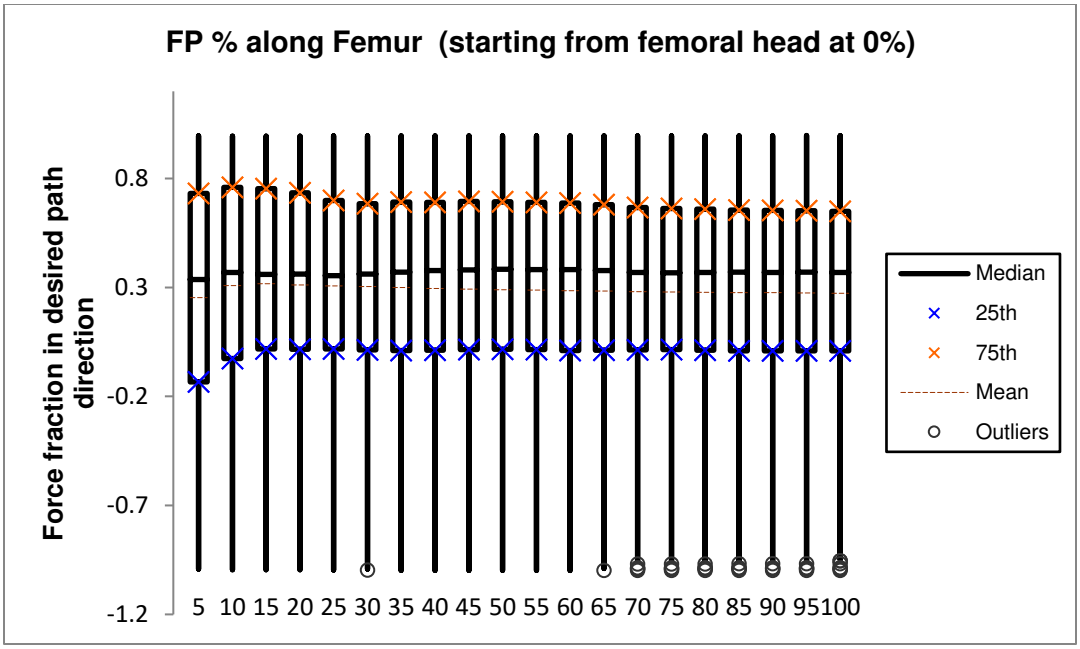

Figure 70: Graf type I projected force over the least energy path; configurations show the most negative $Proj_{\overrightarrow{path}} \vec{F}_{tot}$ near the 15% of the femoral length proximal to femoral head.

After the data was prepared and categorized for the Von Rosen splint, 110 configurations, results suggest for a Graf type IV in Figure 71, the projected force over the indirect path of reduction is more positive near the femoral head.

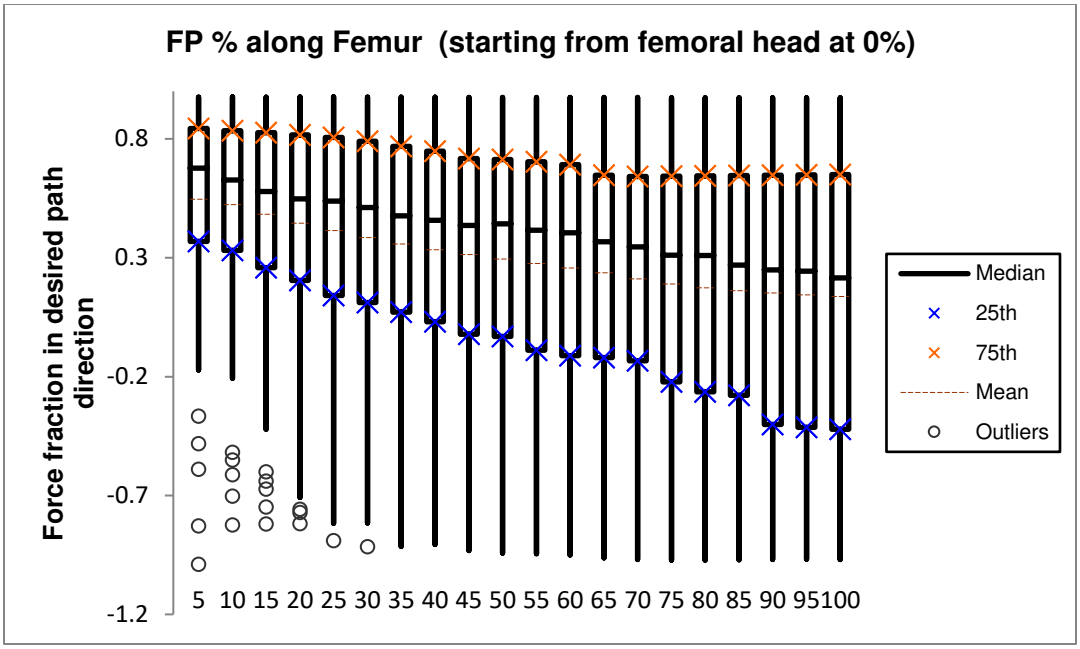

Figure 71: Graf type IV projected force over the indirect path; configurations show the most negative $Proj_{\overrightarrow{path}} \vec{F}_{tot}$ near the femoral head.

After the data was prepared and categorized for the Von Rosen splint, 40 configurations were analyzed, results suggest for a Graf type IV direct path, the projected force over the direct path of reduction is more positive near the knee as shown in Figure 72.

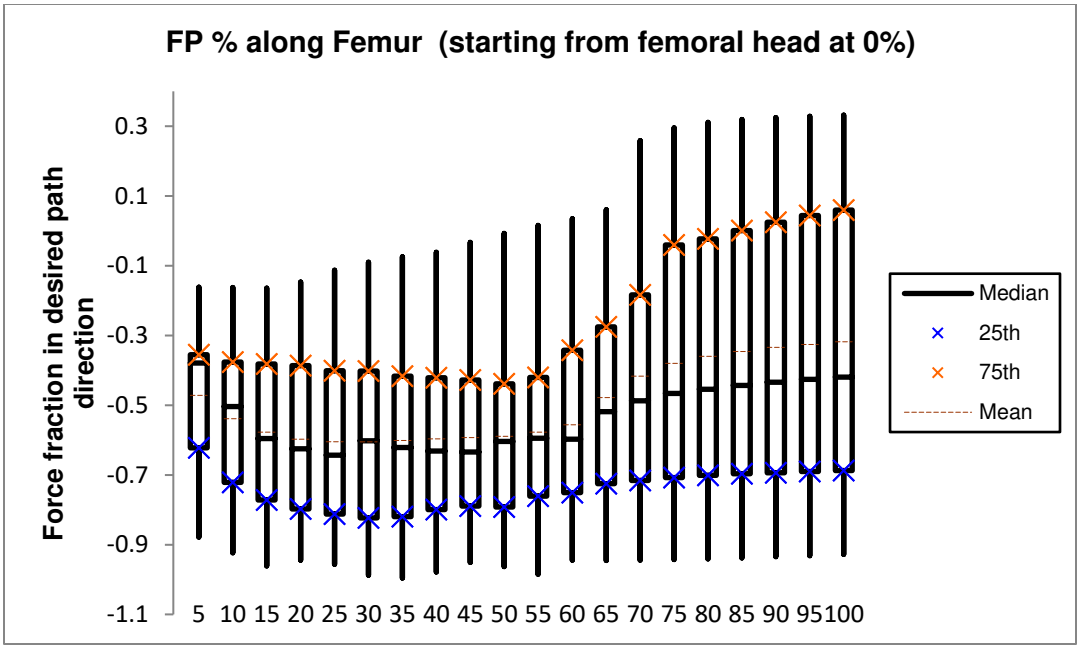

Figure 72: Graf type IV projected force over the direct path; configurations show the most negative $Proj_{\overrightarrow{path}} \vec{F}_{tot}$ near the femoral head.

6.6.5 Frejka pillow

After the data was prepared and categorized for the Frejka pillow, 36 configurations were analyzed, results shown as a box plot in Figure 64, suggests for a Graf type I, the projected force over the path of reduction shows higher values near the femoral head. The configuration does not take into account the force of the splint in the y-direction.

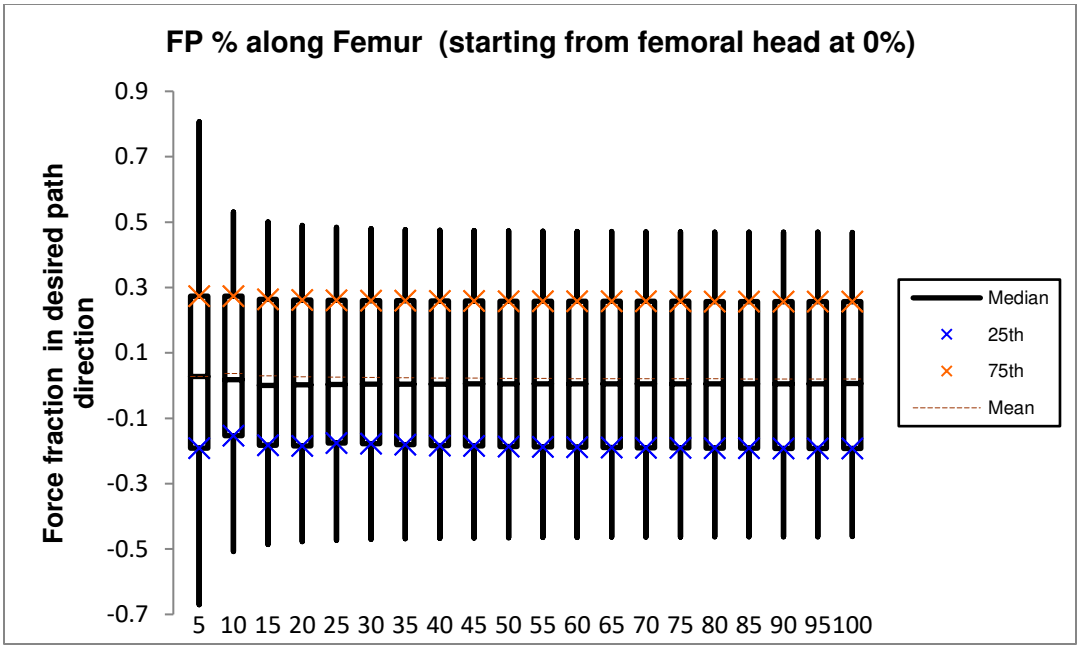

Figure 73: Graf type I projected force over the direct path; configurations show higher values of $Proj_{\overrightarrow{path}} \vec{F}_{tot}$ near the femoral head.

After the data was prepared and categorized for the Frejka pillow, 205 configurations, results suggest for a Graf type IV in Figure 65, the projected force over the indirect path of reduction is more positive near the femoral head.

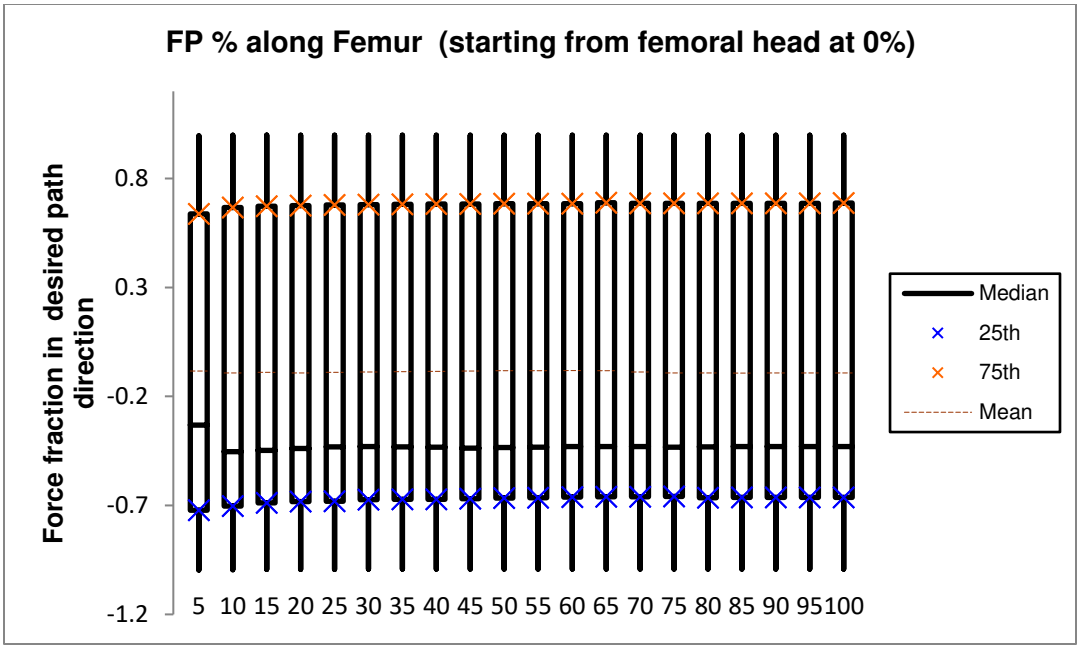

Figure 74: Graf type IV projected force over the indirect path; configurations show the most negative $Proj_{\overrightarrow{path}} \vec{F}_{tot}$ near the femoral head.

After the data was prepared and categorized for the Frejka pillow, only 20 configurations were analyzed, results suggest for a Graf type IV in Figure 75, the projected force over the direct path of reduction is more positive near the knee.

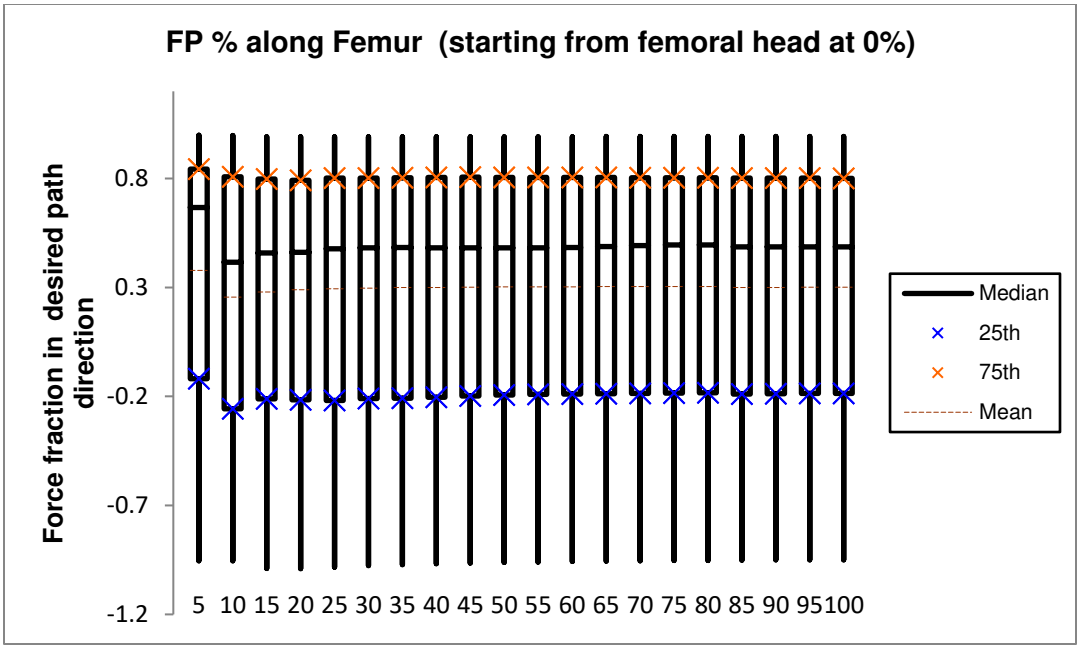

Figure 75: Graf type IV projected force over the direct path; configurations show the most negative $Proj_{\overrightarrow{path}} \vec{F}_{tot}$ near the femoral head.

CHAPTER 7: DISCUSSION

This chapter is divided in 3 sections: the Fulcrum point, the computational models, and AVN.

7.1 Fulcrum Point

While there was a large amount of parameter variability for all infant dislocation configurations, results suggest that there exist an OP that may assist reduction.

The numerical approach used in this study to predict the OP included anatomical landmarks values that can be obtained during clinical infant examinations such as the femoral length, anteversion angle, or the angles at which the HAOD will be applied. However, there are other values that may not be measurable and are important to predict the FP such as PCSA, leg centroid, exact origin and insertion points, and muscle wrapping. Nevertheless, some of these parameters can be obtained and scaled from the literature [47].

In particular, the parameters which show linear or monotonic correlation when predicting $Proj_{\overrightarrow{path}} \vec{F}_{tot}$, indicates the need to refine the model constraints. Further research is needed to decrease parameter variability to improve result accuracy.

Results suggest that for some of the Graf type I and II configurations along the least energy path, reduction is achieved when the FP is located near the femoral head as shown in Figure 37 and Figure 42 respectively. For Graf type I the OP location is strongly related with brace flexion (Θ_i), brace abduction (Φ_i), brace antversion angle (θ_{av}).

For Graf type II the OP location is strongly related with brace flexion (Θ_i), brace abduction (Φ_i), brace external rotation (φ_i), and the flexion angle at which the legs of the

infant were measured to achieve static equilibrium from which the muscle parameters were found (θ_e).

For Graf type III, results suggest there are configurations at which the OP is near the acetabulum as shown in Figure 47. The numerical framework uses the location of the femoral head to predict the OP. However, for this type of dislocation this can be improved by mapping different acetabular regions for Graf type III dislocations defining parameters such a relative angle with respect of the acetabular notch. Additionally, the results suggest the OP location is a function of brace flexion (θ_i).

Figure 52 suggests that for Graf type IV (indirect path) there are configurations at which the optimal fulcrum point is near the acetabulum. The numerical framework uses the location of the femoral head to predict the optimal fulcrum point. However, for this type of dislocation this can be improved by defining a geometrical parameter that can be measured during clinical follow ups such as the center distance from the femoral head to the acetabulum or the length of the path needed to achieve reduction. Additionally, the results suggest the OP location is a function of brace flexion (θ_i) and brace abduction (Φ_i). Contrastingly, external rotation did not have a significant contribution when predicting the OP location.

Figure 57 suggests that for Graf type IV (direct path) there are configurations at which the optimal fulcrum point is near the femoral head. The numerical framework uses the location of the femoral head to predict the optimal fulcrum point. However, for this type of dislocation this can be improved by defining a geometrical parameter that can be measured during clinical follow ups such as the center distance from the femoral head to the acetabulum or the length of the path needed to achieve reduction. Additionally, the

results suggest the OP location is a function of brace abduction (Φ_i). Contrastingly, flexion and external rotation of the brace did not have a significant contribution when predicting the OP location.

Because of the wide range of the parameters needed to reach static equilibrium and apply the FP, comparing current HAOD provide a better understanding of the effects of the fulcrum point.

For the Pavlik Harness in a Graf type I, Figure 61 corroborates the application of the fulcrum point near the knee is more convenient based on the constraints established. For Graf type IV, Figure 62 and Figure 63 suggest the application of the Pavlik harness to treat Graf type IV dislocation is suboptimal.

Comparing Pavlik harness for different severities of DDH illustrated in the numerical framework suggest for a nominal configuration (all average parameters) that for a Graf type I condition the OP is near the knee, for Graf type II and IIIi (observing only the nodes that corresponded to the indirect path of Graf type IV over the acetabular rim) the FP location does not represent a significant effect, for Graf type IIId (observing only the nodes that corresponded to the direct path of Graf type IV over the acetabular rim) the OP is recommended near the femoral head which also suggests this HAOD type of dislocation is suboptimal.

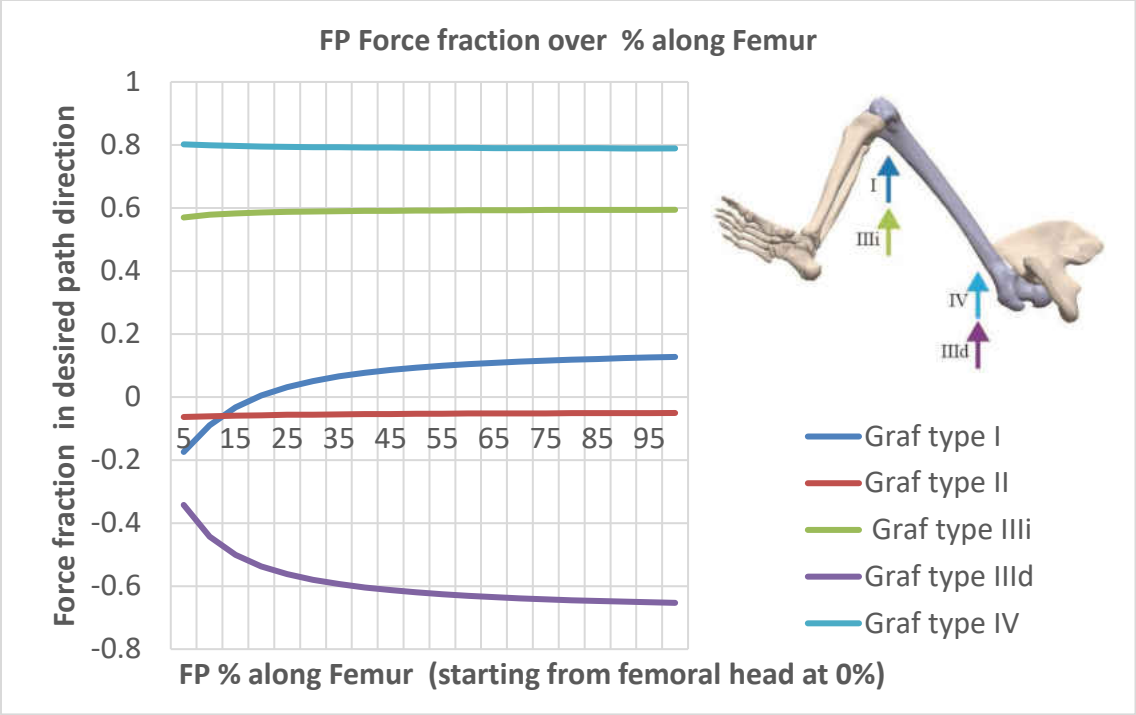

Figure 76: Graph type I, II, IIIi, IIId, and IV nominal configuration for Pavlik harness, configuration indicating $Proj_{\overrightarrow{path}} \vec{F}_{tot}$ along the femur length.

In Table 13 it is shown a comparison of the curve calculations of the equation to predict Graf I,II, and III shows to be correct for the nominal configuration parameters, but for Graf type IV there is a discrepancy in the answer for direct path, suggesting the equation needs to include parameters not easy accessible for the physician. There is no equation deduced for a particular condition of Graf type III, equation (42) is used in both direct and indirect path.

Table 13: Suggested optimal fulcrum point location comparison Matlab® calculation vs mathematic formulations for Pavlik harness nominal configuration ($\boldsymbol{\theta_i = 100°, \Phi_i = 45°, \varphi_i = 0°}$)

Severity of DDH	Equation	Predicted with equation	Calculated from Matlab® model
Graf type I	(40)	knee	knee
Graf type II	(41)	proximal	Any
Graf type IIIi	(42)	proximal	proximal
Graf type IIId	(42)	proximal	proximal
Graf type IVi	(43)	proximal	knee
Graf type IVd	(44)	knee	knee

For the Tübingen splint and Spica cast, similar results are shown in Figure 64 and Figure 66, corroborating the split works well for Graf type I. For Graf IV indirect path, Figure 65 and Figure 67 do not indicate a significant advantage of placing the fulcrum point proximal to the femoral head, although Figure 66 suggests for a Graf type IV following Papadimitriou [29] suggested indirect path, it is shown applying the fulcrum proximal to the femoral head provides a higher resulting force over the desired reduction pathway, slightly higher with Tübingen splint than with Spica cast.

For the Von Rosen splint shown in Figure 70 indicates is optimal to have the fulcrum point near 15% of the femoral length. and Figure 71 suggest an advantage of placing the fulcrum point proximal to the femoral head, although Figure 72 for a Graf type IV following Papadimitriou [29] suggested indirect path, it is shown applying the fulcrum proximal to the knee provides a higher resulting force over the desired reduction pathway. This apparent contradiction is explained when analyzing individual configurations, placing the femoral head in a single point along the pathway of reduction.

Comparing Von Rosen splint for different severities of DDH illustrated in Figure 77 the numerical framework suggest for a nominal configuration (all average parameters) that for a Graf type I and IV condition the OP is near the knee, for Graf type II the FP location does not represent a significant effect, for Graf type III (observing only the nodes that corresponded to the direct and indirect path of Graf type IV over the acetabular rim) the OP is recommended near the femoral head.

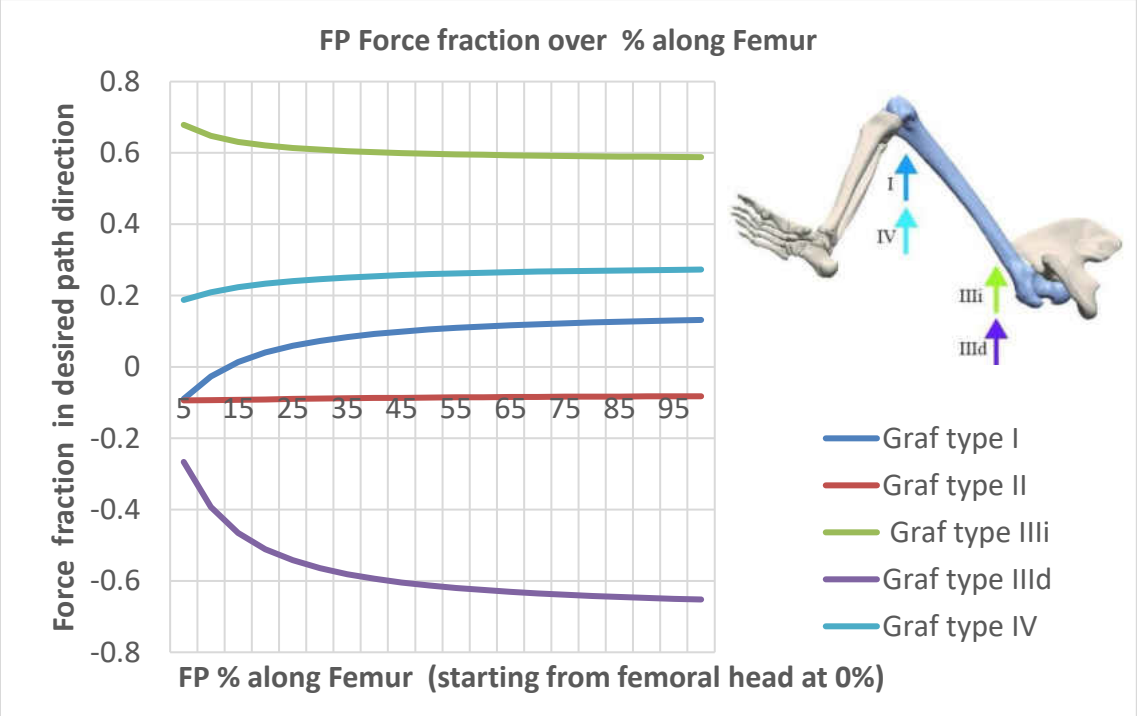

Figure 77: Graph type I, II, IIIi, IIId, and IV nominal configuration for Von Rosen splint, configuration indicating $Proj_{\underrightarrow{path}} \vec{F}_{tot}$ along the femur length.

In Table 14 it is shown a comparison of the Curve calculations of the equation to predict Graf I, II, and III shows to be correct for the nominal configuration parameters, but for Graf type IV there is a discrepancy in the answer for direct path, suggesting the equation

needs to include parameters not easy accessible, also suggesting the equation needs to include parameters not easy accessible for the physician. There is no equation deduced for a particular condition of Graf type III, equation (42) is used in both direct and indirect path.

Table 14: Suggested optimal fulcrum point location comparison Matlab calculation vs mathematic formulations for Von Rosen nominal configuration ($\boldsymbol{\theta_i = 90°, \Phi_i = 45°, \varphi_i = 0°}$)

Severity of DDH	Equation	Predicted with equation	Calculated from MatLab® model
Graf type I	(40)	knee	knee
Graf type II	(41)	proximal	any
Graf type IIIi	(42)	proximal	knee
Graf type IIId	(42)	proximal	proximal
Graf type IVi	(43)	proximal	proximal
Graf type IVd	(44)	knee	proximal

7.2 Computational Model

The SolidWorks® model, working in combination with the Matlab® model being provided key parameters, could enlighten as to why when the same HAOD was applied twice to the same infant, in the first trial reduction, it was not successful, but once applied a second-time reduction was achieved. The calculation of PCSAn can assist in further research for other lower limb configurations as well as the study of other orthoses devices for other abnormalities of the lower limb, currently was only used 2 sources, not taking into account age dependency.

The importance of the calibration of the relaxed lengths must include opposite forces to obtain more realistic muscle properties. These properties, when calculating the forces of the muscles independent of how the parameters are variated. During model

calibration, 4 muscles presented high strain, for the nominal lower limb configuration the muscles that stretched excessively were piriformis, obturator internus, gemellus superior, gemellus inferior, and quadratus femoris. They were compared with the literature found.

This showed the need for increasing a combination of the muscle elasticity, or the relaxed length, or diminish the muscle prestretch, or as well a change in the geometry of the femur by diminishing the deviation angle, to obtain realistic values.

In the Matlab® model, the rotation of the muscle insertion points concerning the Linea Aspera does not change when the anteversion angle changes, which might lead to slightly different results. Setting these constraints can be defined in future research.

For 40 degrees or more anteversion angle, the insertion of the gluteus maximus and medius over the femur is such that the force moment in y-direction flips sign. This is because of the unrealistic action angle of the muscle forces when wrapping is not included.

The Matlab® model could be further improved to simulate muscle wrapping similarly to Open Sim. The initial points can be obtained by scaling the points from Open Sim model, then finding a plane comprised of the 2 active points (the 2 points that change distance among them when there is a hip joint movement).

Skewness measures the asymmetry and the direction of the probability distribution of a random variable. With enough samples, the skewness of the probability distribution will diminish. All the probability distributions of this thesis could be refined with further data.

In terms of efficiency, the code runs around 12 seconds per configuration with set parameters, taking a total of around 14 hours for 100 configurations that run all 20 fulcrum point locations for all nodes for all paths of all Graf configurations. For each of the

configurations 65% of the configurations were invalid not reaching static equilibrium during the muscle calibration section or during the check of model stability. The muscle insertion points as well as the muscle b parameter had a mayor effect in reaching a stable configuration.

7.3 Avascular Necrosis

The pressure over the cartilage is strongly dependent on its layer thickness, which also changes depending on the location in which it is measured. It was assumed all the femoral head was in cartilage state, the properties of the acetabulum were stiffer, but the risk of AVN with the current approach was not evident, other approach which could be explored with the Matlab model is the calculation of the resulting hip joint contact force. As an example it was found in Monte Carlo simulation that for a range of not recommended abduction angles from 75 to 90 degrees, for legs flexed from 85 to 95 degrees randomly varying the PCSAs, muscle lengths, and femoral head position along the hip joint, that the maximum hip joint contact force was found to be 416.3 N which corresponded to an abduction angle (Φ_i) of 89.86 degrees, suggesting higher resultant forces for any other configuration may be of concern with regards to AVN if the force is maintained long enough without mobility of the limb.

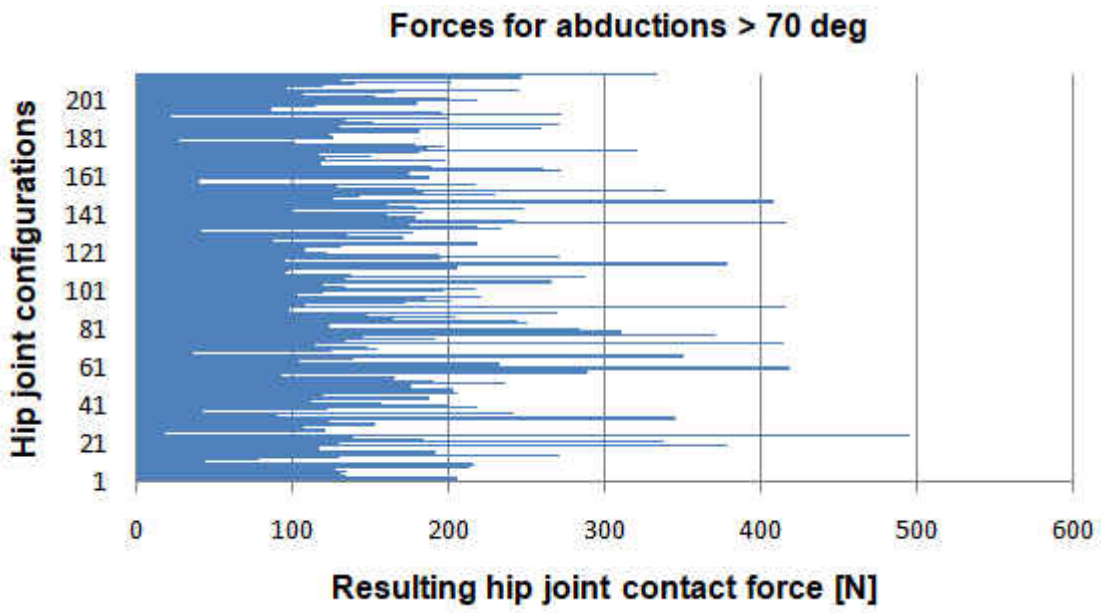

Figure 78: Resulting contact force over the hip for several configurations with a brace abduction angle (Φ_i) greater than 70 deg.

CHAPTER 8: CONCLUSION

A 3D computational model was developed to investigate the biomechanics of HAOD. The results suggest that there exists an optimal FP that may assist reduction over a range of dislocations and on different bracing methods.

Several configurations were analyzed to understand how the variability of the parameters affects the resulting contact force over the femoral head. This helps to understand the nuances of placing a strap from the Pavlik harness in a slightly different location. Results may potentially provide the information needed to design and develop a new HAOD. A new HAOD could be effective in reducing Graf type IV, which is currently treated using traction during closed reduction or open reduction for severe cases.

Future work may include additional hip parameters along with the automatic generation of models based on patient gender, height, body max index which can also include muscle wrapping effects, and the additional effect over the behavior of the lower limb caused by the inclusion of cartilage and labrum.

The present work provides a novel numerical framework to potentially treat hip dysplasia and other orthopedic abnormalities. The framework includes parameters that can be tailored to customize patient-specific anatomical configurations.

APPENDIX A: PEARSON CORRELATION MATRIX

Table 15: Pearson Correlation Matrix for Graf type I

Pearson Correlations	Percentage Of Dislocation	Sum Forces tot	FP Perc Along Femur	Sum Forces FP x	Sum Forces FP y	Sum Forces FP z	Sum Forces FP tot	Projected F over Path	% of total force in pat direction
Area Iliopsoas	-0.05	0.04	0.00	-0.04	-0.04	0.03	0.04	0.00	-0.01
Area Pectineus	0.17	-0.01	0.01	0.01	0.00	-0.01	-0.01	0.00	-0.06
Area Sartorius	0.01	0.02	0.00	-0.02	-0.03	0.02	0.02	0.00	-0.02
Area Rectus Femoris	-0.01	0.04	0.00	-0.04	-0.04	0.04	0.04	0.00	-0.06
Area Adductor Longus	0.05	0.03	0.01	-0.03	-0.03	0.03	0.03	-0.01	-0.04
Area Adductor Brevis	0.00	0.00	0.01	0.00	0.01	0.00	0.00	-0.02	-0.08
Area Adductor Magnus Minimus	0.00	0.03	0.00	-0.03	-0.04	0.03	0.03	-0.01	0.01
Area Adductor Magnus Middle	-0.05	0.04	0.01	-0.04	-0.01	0.03	0.04	0.00	0.10
Area Adductor Magnus Posterior	-0.11	0.02	0.01	-0.02	-0.05	0.02	0.02	0.00	-0.19
Area Gracilis	-0.08	0.03	0.00	-0.03	-0.04	0.03	0.03	0.00	-0.01
Area Gluteus Max	0.09	0.00	0.00	0.00	-0.02	0.00	0.00	0.01	-0.12
Area Gluteus Medius Anterior	0.00	0.01	0.00	-0.01	-0.02	0.01	0.01	-0.02	-0.02
Area Gluteus Medius Middle	0.01	0.04	0.01	-0.04	-0.04	0.03	0.04	-0.02	-0.13
Area Gluteus Medius Posterior	-0.03	0.03	0.02	-0.03	-0.05	0.03	0.03	0.00	-0.19
Area Gluteus Minimus Anterior	0.00	0.01	0.00	-0.01	0.01	0.01	0.01	-0.03	-0.03
Area Gluteus Minimus Middle	-0.01	-0.02	0.00	0.02	0.00	-0.02	-0.02	0.00	0.07
Area Gluteus Minimus Posterior	-0.14	0.04	0.01	-0.04	-0.06	0.03	0.04	0.01	0.01
Area Tensor Fascia Lata	0.01	0.06	0.00	-0.06	-0.05	0.05	0.06	-0.01	-0.06
Area Piriformis	0.01	0.01	0.00	-0.02	-0.04	0.01	0.02	0.01	0.01
Area Obturator Internus	-0.15	0.03	0.00	-0.04	-0.03	0.03	0.04	-0.02	-0.08
Area Gemellus Superior	0.02	0.05	0.00	-0.06	-0.06	0.05	0.06	-0.02	0.00
Area Gemellus Inferior	-0.04	0.05	0.00	-0.05	-0.05	0.04	0.05	0.00	-0.08
Area Quadratus Femoris	-0.10	0.01	-0.01	-0.01	0.00	0.01	0.01	-0.02	0.03
Area Obturator Externus	-0.02	0.04	0.00	-0.03	-0.02	0.03	0.04	0.00	0.04
Area Biceps Femoris (Long Head)	-0.01	0.03	0.00	-0.04	-0.06	0.03	0.03	-0.01	-0.10
Area Semitendinosus	-0.01	0.04	0.01	-0.04	-0.04	0.04	0.04	-0.01	-0.05
Area Semimembranosus	-0.07	0.04	0.01	-0.04	-0.03	0.04	0.04	-0.02	-0.11

Pearson Correlations	Percentage Of Dislocation	Sum Forces tot	FP Perc Along Femur	Sum Forces FP x	Sum Forces FP y	Sum Forces FP z	Sum Forces FP tot	Projected F over Path	% of total force in pat direction
Femur.Length	-0.02	-0.01	0.00	0.01	0.00	-0.01	-0.01	-0.02	0.08
Femur.L_Trochanteric	0.04	0.00	-0.01	0.00	-0.01	0.00	0.00	-0.01	0.04
Femur.Shaft_Width	0.34	-0.01	0.00	0.02	0.04	-0.01	-0.01	-0.02	-0.22
Femur.Deviation_Angle	0.06	0.01	0.01	-0.01	-0.04	0.01	0.01	0.01	0.12
Femur.Sagittal_Bowing_Ang	-0.12	-0.03	0.01	0.03	0.02	-0.02	-0.03	0.00	0.07
Femur.Coronal_Bowing_Ang	-0.13	0.01	0.00	-0.01	-0.03	0.01	0.01	0.02	0.04
Femur.Head_Diam	0.08	0.01	0.00	-0.01	-0.02	0.00	0.01	0.01	0.05
Femur.Anteversion_Angle	0.04	0.00	-0.01	0.00	0.01	0.00	0.00	-0.02	-0.35
Femur.Incline_Angle	-0.09	0.03	0.00	-0.03	-0.01	0.03	0.03	-0.01	-0.16
Femur.Condyle_Diameter	0.03	0.04	0.00	-0.04	-0.01	0.05	0.04	-0.05	0.03
Femur.Condyle_Spacing	0.07	0.00	-0.01	0.00	0.00	0.00	0.00	0.00	0.02
Femur.Epicondyle_Dist	-0.10	0.00	-0.01	0.01	0.06	0.00	-0.01	-0.03	0.03
Femur.Head_Module_E	-0.01	-0.01	0.00	0.01	0.00	-0.01	-0.01	0.00	0.06
Femur.Head_Module_v	0.11	0.01	0.01	-0.01	0.00	0.01	0.01	-0.01	-0.02
Hip.Acetabulum_Diam	-0.08	0.02	0.00	-0.02	-0.04	0.01	0.02	0.04	-0.05
Hip.Acetabulum_Module_E	-0.01	-0.02	0.01	0.02	0.01	-0.02	-0.02	0.04	0.21
Hip.Acetabulum_Module_v	0.15	0.02	0.00	-0.02	-0.02	0.03	0.02	-0.04	-0.04

Pearson Correlations	Percentage Of Dislocation	Sum Forces tot	FP Perc Along Femur	Sum Forces FP x	Sum Forces FP y	Sum Forces FP z	Sum Forces FP tot	Projected F over Path	% of total force in pat direction
3D_Rat Iliopsoas	-0.08	0.01	0.00	0.00	0.04	0.01	0.01	-0.02	0.01
3D_Rat Pectineus	0.15	-0.01	0.01	0.01	0.01	0.00	-0.01	-0.02	-0.08
3D_Rat Sartorius	-0.09	0.03	0.00	-0.02	0.00	0.02	0.02	-0.02	0.19
3D_Rat Rectus Femoris	-0.15	0.02	0.01	-0.02	0.00	0.02	0.02	0.00	0.09
3D_Rat Adductor Longus	0.01	0.01	0.00	-0.01	-0.03	0.01	0.01	0.00	-0.10
3D_Rat Adductor Brevis	0.08	-0.04	0.00	0.03	0.02	-0.03	-0.04	0.00	-0.10
3D_Rat Adductor Magnus Minimus	-0.05	-0.01	0.00	0.02	0.05	-0.01	-0.02	0.00	0.06
3D_Rat Adductor Magnus Middle	0.05	0.03	0.01	-0.03	-0.01	0.03	0.03	-0.02	0.05
3D_Rat Adductor Magnus Posterior	-0.20	-0.04	0.01	0.04	0.01	-0.04	-0.04	0.03	-0.10
3D_Rat Gracilis	-0.01	-0.02	0.00	0.02	0.00	-0.02	-0.02	0.01	-0.16
3D_Rat Gluteus Max	-0.08	-0.03	-0.01	0.03	0.01	-0.02	-0.03	-0.01	-0.01
3D_Rat Gluteus Medius Anterior	0.18	-0.03	-0.01	0.03	0.00	-0.03	-0.03	0.01	-0.15
3D_Rat Gluteus Medius Middle	-0.01	0.02	-0.01	-0.02	0.00	0.02	0.02	-0.01	0.05
3D_Rat Gluteus Medius Posterior	-0.07	-0.05	0.00	0.04	0.02	-0.04	-0.05	0.03	0.08
3D_Rat Gluteus Minimus Anterior	0.05	0.02	0.01	-0.02	-0.02	0.02	0.02	0.00	0.06
3D_Rat Gluteus Minimus Middle	0.10	-0.03	0.00	0.02	0.00	-0.02	-0.03	-0.03	0.03
3D_Rat Gluteus Minimus Posterior	0.06	-0.01	0.00	0.02	0.03	-0.01	-0.02	0.00	-0.02
3D_Rat Tensor Fascia Lata	-0.02	0.01	0.01	-0.01	0.01	0.01	0.01	0.01	0.12
3D_Rat Piriformis	0.05	0.00	-0.01	0.00	0.01	0.00	0.00	0.01	0.09
3D_Rat Obturator Internus	0.19	0.02	-0.01	-0.02	0.00	0.02	0.02	-0.01	-0.04
3D_Rat Gemellus Superior	-0.01	-0.04	0.02	0.05	0.04	-0.05	-0.04	0.05	0.01
3D_Rat Gemellus Inferior	0.10	0.05	0.00	-0.05	-0.05	0.05	0.05	-0.02	0.04
3D_Rat Quadratus Femoris	0.05	0.03	-0.01	-0.02	-0.01	0.03	0.03	-0.04	-0.02
3D_Rat Obturator Externus	-0.04	-0.01	0.00	0.00	-0.01	-0.01	-0.01	0.03	0.00
3D_Rat Biceps Femoris (Long Head)	-0.09	0.00	0.00	0.00	-0.01	0.00	0.00	-0.01	0.02
3D_Rat Semitendinosus	-0.10	0.01	0.00	-0.01	-0.02	0.01	0.01	0.00	-0.05
3D_Rat Semimembranosus	-0.05	-0.01	0.00	0.00	-0.06	0.00	0.00	0.01	-0.08

Pearson Correlations	Percentage Of Dislocation	Sum Forces tot	FP Perc Along Femur	Sum Forces FP x	Sum Forces FP y	Sum Forces FP z	Sum Forces FP tot	Projected F over Path	% of total force in pat direction
3D_Rot Iliopsoas	0.04	-0.01	0.01	0.01	0.00	-0.01	-0.01	0.01	-0.01
3D_Rot Pectineus	0.08	0.01	0.00	-0.01	-0.02	0.01	0.01	-0.01	0.08
3D_Rot Sartorius	0.04	-0.01	0.01	0.01	-0.01	-0.01	-0.01	0.00	-0.05
3D_Rot Rectus Femoris	-0.05	-0.01	0.00	0.01	0.01	0.00	-0.01	0.00	-0.01
3D_Rot Adductor Longus	0.03	0.01	0.01	-0.01	-0.02	0.01	0.01	0.01	-0.01
3D_Rot Adductor Brevis	0.06	-0.03	0.00	0.02	0.00	-0.03	-0.03	0.06	0.06
3D_Rot Adductor Magnus Minimus	-0.02	-0.04	0.01	0.04	0.03	-0.03	-0.04	0.01	0.01
3D_Rot Adductor Magnus Middle	0.30	0.00	-0.01	-0.01	-0.01	0.01	0.01	-0.01	0.06
3D_Rot Adductor Magnus Posterior	0.00	-0.02	-0.01	0.02	0.02	-0.01	-0.01	-0.02	0.00
3D_Rot Gracilis	-0.07	0.03	-0.01	-0.02	0.02	0.03	0.02	-0.03	-0.19
3D_Rot Gluteus Max	0.01	0.00	0.00	0.01	0.00	-0.01	-0.01	0.00	-0.06
3D_Rot Gluteus Medius Anterior	-0.05	0.01	0.01	-0.02	-0.03	0.01	0.02	0.00	0.00
3D_Rot Gluteus Medius Middle	-0.08	-0.03	0.00	0.03	0.00	-0.03	-0.03	0.00	-0.04
3D_Rot Gluteus Medius Posterior	-0.09	0.01	0.00	-0.01	0.00	0.01	0.01	-0.03	-0.02
3D_Rot Gluteus Minimus Anterior	-0.03	0.03	-0.01	-0.03	0.04	0.03	0.03	-0.03	-0.10
3D_Rot Gluteus Minimus Middle	0.09	-0.02	0.00	0.02	0.00	-0.02	-0.02	-0.01	0.05
3D_Rot Gluteus Minimus Posterior	-0.15	0.02	-0.01	-0.01	0.01	0.01	0.01	0.01	0.01
3D_Rot Tensor Fascia Lata	0.02	-0.02	0.01	0.01	-0.01	-0.01	-0.01	0.00	0.18
3D_Rot Piriformis	0.07	0.01	-0.01	-0.01	-0.01	0.01	0.01	-0.01	0.12
3D_Rot Obturator Internus	-0.06	-0.02	0.00	0.02	0.04	-0.02	-0.02	0.01	0.09
3D_Rot Gemellus Superior	-0.03	0.02	0.00	-0.02	0.00	0.03	0.02	-0.05	-0.10
3D_Rot Gemellus Inferior	0.12	-0.02	0.00	0.02	0.03	-0.02	-0.02	0.00	0.00
3D_Rot Quadratus Femoris	-0.04	0.00	0.00	0.00	0.02	0.00	0.00	0.02	0.13
3D_Rot Obturator Externus	-0.35	0.00	0.00	0.00	-0.02	0.00	0.00	0.03	0.00
3D_Rot Biceps Femoris (Long Head)	0.10	0.00	0.00	-0.01	-0.03	0.01	0.01	0.03	-0.21
3D_Rot Semitendinosus	0.14	0.00	0.01	0.00	0.03	0.00	0.00	0.00	-0.14
3D_Rot Semimembranosus	-0.11	0.01	-0.01	-0.01	0.01	0.01	0.01	0.00	-0.04

Pearson Correlations	Percentage Of Dislocation	Sum Forces tot	FP Perc Along Femur	Sum Forces FP x	Sum Forces FP y	Sum Forces FP z	Sum Forces FP tot	Projected F over Path	% of total force in pat direction
M_L_Ratio Iliopsoas	0.08	0.01	0.00	-0.01	-0.01	0.01	0.01	-0.01	-0.08
M_L_Ratio Pectineus	-0.03	-0.01	-0.01	0.00	-0.01	-0.01	-0.01	0.01	-0.04
M_L_Ratio Sartorius	0.09	0.02	0.00	-0.02	-0.05	0.02	0.02	-0.02	0.06
M_L_Ratio Rectus Femoris	-0.02	-0.01	0.00	0.00	-0.03	0.00	0.00	0.00	-0.06
M_L_Ratio Adductor Longus	0.07	-0.02	0.00	0.02	0.03	-0.01	-0.02	0.00	0.07
M_L_Ratio Adductor Brevis	-0.09	-0.01	0.00	0.01	-0.02	-0.01	-0.01	-0.02	-0.21
M_L_Ratio Adductor Magnus Minimus	0.11	-0.02	0.01	0.02	0.02	-0.01	-0.02	-0.03	-0.03
M_L_Ratio Adductor Magnus Middle	-0.01	-0.02	0.00	0.01	-0.01	-0.01	-0.01	-0.03	-0.10
M_L_Ratio Adductor Magnus Posterior	0.16	-0.02	0.01	0.02	0.04	-0.02	-0.02	-0.02	-0.04
M_L_Ratio Gracilis	-0.09	-0.05	0.00	0.05	0.03	-0.04	-0.05	0.01	0.09
M_L_Ratio Gluteus Max	0.11	-0.01	0.00	0.01	0.03	-0.02	-0.01	0.00	0.12
M_L_Ratio Gluteus Medius Anterior	-0.07	-0.03	0.00	0.03	0.04	-0.02	-0.03	0.00	0.00
M_L_Ratio Gluteus Medius Middle	-0.10	0.02	-0.01	-0.02	-0.01	0.02	0.02	0.00	-0.04
M_L_Ratio Gluteus Medius Posterior	0.01	0.00	0.00	0.00	0.00	-0.01	0.00	0.02	0.09
M_L_Ratio Gluteus Minimus Anterior	-0.04	-0.01	-0.01	0.01	0.04	0.00	-0.01	-0.03	-0.08
M_L_Ratio Gluteus Minimus Middle	0.07	-0.02	-0.01	0.02	0.01	-0.01	-0.02	0.00	-0.03
M_L_Ratio Gluteus Minimus Posterior	0.01	0.00	-0.01	0.00	0.00	0.00	0.00	0.01	0.01
M_L_Ratio Tensor Fascia Lata	-0.01	-0.02	0.01	0.02	0.03	-0.02	-0.02	0.01	0.00
M_L_Ratio Piriformis	0.09	0.01	0.00	-0.01	-0.01	0.01	0.01	-0.02	0.05
M_L_Ratio Obturator Internus	0.16	0.00	-0.01	0.00	0.00	0.00	0.00	0.02	0.09
M_L_Ratio Gemellus Superior	0.03	-0.02	0.00	0.02	0.04	-0.02	-0.02	0.03	-0.06
M_L_Ratio Gemellus Inferior	-0.07	0.03	-0.03	-0.02	0.01	0.02	0.02	-0.01	0.18
M_L_Ratio Quadratus Femoris	-0.26	0.02	0.00	-0.02	-0.04	0.02	0.02	-0.01	-0.04
M_L_Ratio Obturator Externus	0.03	0.00	0.00	0.00	-0.01	0.00	0.00	-0.01	0.00
M_L_Ratio Biceps Femoris (Long Head)	0.05	0.02	-0.01	-0.02	0.00	0.02	0.02	-0.01	0.05
M_L_Ratio Semitendinosus	0.12	0.00	0.00	0.00	0.01	0.00	0.00	-0.01	0.11
M_L_Ratio Semimembranosus	0.02	-0.01	0.01	0.00	-0.02	0.00	0.00	0.02	-0.02

Pearson Correlations	Percentage Of Dislocation	Sum Forces tot	FP Perc Along Femur	Sum Forces FP x	Sum Forces FP y	Sum Forces FP z	Sum Forces FP tot	Projected F over Path	% of total force in pat direction
Flexion_i	-0.05	0.03	0.00	-0.03	-0.02	0.03	0.03	-0.01	0.16
Abduction_i	0.05	0.02	0.01	-0.02	0.00	0.02	0.02	0.00	0.22
E_Rotation_i	-0.08	0.00	0.00	0.00	0.00	0.00	0.00	-0.01	-0.08
BWeight	-0.31	0.03	0.00	-0.03	-0.02	0.02	0.03	0.01	0.18
Leg_Perc_Weight	0.24	0.00	0.01	0.00	0.01	0.01	0.00	-0.05	-0.13
PreStretch	-0.11	0.03	-0.01	-0.03	-0.01	0.03	0.03	-0.02	0.00
Hip Muscle Insertion	0.03	0.06	-0.02	-0.05	0.04	0.05	0.05	-0.05	-0.43
Rel_Flex	0.13	0.00	0.00	0.00	0.01	0.00	0.00	0.02	-0.03
Rel_Abd	0.08	0.01	0.01	-0.01	0.00	0.01	0.01	0.01	0.10
Rel_Rot	0.11	-0.02	0.01	0.02	0.01	-0.02	-0.02	0.00	-0.04
Flexion_e	-0.05	-0.01	0.00	0.01	-0.01	-0.01	-0.01	0.01	0.04
Abduction_e	-0.08	-0.03	0.00	0.02	-0.01	-0.03	-0.02	0.01	0.01
E_Rotation_e	0.13	-0.01	0.00	0.01	-0.01	-0.01	-0.01	0.00	-0.07
Percentage_Of_Dislocation		0.00	0.00	0.00	0.00	0.00	0.00	-0.01	-0.15
Leg Centroid x		0.03	0.00	-0.03	-0.04	0.02	0.03	-0.01	0.22
Leg Centroid y		0.03	0.00	-0.03	-0.04	0.02	0.03	-0.01	0.22
Leg Centroid z		0.03	0.00	-0.03	-0.04	0.02	0.03	-0.01	0.22
Sum_Forces x		-0.98	0.04	0.99	0.69	-0.96	-0.99	0.34	0.00
Sum_Forces y		-0.56	-0.01	0.64	1.00	-0.55	-0.60	0.04	0.00
Sum_Forces z		0.98	-0.05	-0.99	-0.55	1.00	0.99	-0.55	-0.01
Sum_Forces tot		1.00	-0.05	-0.99	-0.56	0.98	1.00	-0.42	0.00
Sum_Moments x			0.04	0.96	0.62	-0.97	-0.97	0.56	0.01
Sum_Moments y			-0.05	-0.98	-0.57	0.98	0.98	-0.36	0.01
Sum_Moments z			0.02	0.88	0.85	-0.86	-0.85	0.34	-0.01
FP_Perc_Along_Femur				0.05	-0.01	-0.05	-0.05	0.02	0.05
Sum_ForcesFP x					0.64	-0.99	-1.00	0.43	0.00
Sum_ForcesFP y						-0.55	-0.60	0.04	0.00
Sum_ForcesFP z							0.99	-0.55	-0.01
Sum_ForcesFP tot								-0.44	0.00
ProjectedFoverPath									0.05

Table 16: Pearson Correlation Matrix for Graf type II

Pearson Correlations	Percentage Of Dislocation	Sum Forces tot	FP Perc Along Femur	Sum Forces FP x	Sum Forces FP y	Sum Forces FP z	Sum Forces FP tot	Projected F over Path	% of total force in pat direction
Area Iliopsoas	-0.07	0.00	0.00	0.00	0.00	0.00	0.00	0.00	0.14
Area Pectineus	-0.06	0.02	0.00	0.01	0.01	-0.01	0.02	0.01	0.04
Area Sartorius	-0.01	0.00	0.00	-0.01	0.00	0.00	0.00	-0.01	0.18
Area Rectus Femoris	-0.02	0.00	0.00	-0.01	0.00	0.00	0.00	-0.01	0.14
Area Adductor Longus	0.00	0.01	-0.01	0.00	0.01	0.00	0.01	0.00	0.10
Area Adductor Brevis	-0.05	0.01	0.01	0.01	0.00	-0.01	0.01	0.01	-0.05
Area Adductor Magnus Minimus	-0.08	0.00	0.00	0.00	0.00	0.01	0.00	0.00	0.16
Area Adductor Magnus Middle	-0.03	0.00	0.00	-0.01	0.00	0.00	0.00	-0.01	0.08
Area Adductor Magnus Posterior	-0.03	0.00	0.00	-0.01	0.00	0.01	0.00	-0.01	0.03
Area Gracilis	-0.02	-0.01	0.00	-0.02	-0.01	0.02	-0.01	-0.02	0.19
Area Gluteus Max	-0.05	0.01	-0.01	0.01	0.01	-0.01	0.01	0.01	0.17
Area Gluteus Medius Anterior	-0.12	0.00	-0.01	-0.01	0.00	0.01	0.00	-0.01	0.06
Area Gluteus Medius Middle	-0.04	0.01	0.00	0.01	0.01	-0.01	0.01	0.01	0.04
Area Gluteus Medius Posterior	-0.09	0.02	-0.01	0.01	0.02	-0.02	0.02	0.01	0.02
Area Gluteus Minimus Anterior	0.03	0.02	0.00	0.01	0.01	-0.02	0.02	0.01	0.12
Area Gluteus Minimus Middle	-0.01	-0.01	0.01	0.00	0.00	-0.01	0.00	0.00	0.03
Area Gluteus Minimus Posterior	0.08	-0.01	0.00	-0.01	-0.01	0.01	-0.01	-0.01	0.11
Area Tensor Fascia Lata	-0.04	0.01	0.00	0.00	0.01	0.00	0.01	0.00	0.15
Area Piriformis	-0.10	0.01	0.00	0.01	0.01	0.00	0.01	0.01	0.14
Area Obturator Internus	0.08	0.02	0.00	0.01	0.01	-0.01	0.02	0.01	0.09
Area Gemellus Superior	-0.03	-0.01	0.00	-0.01	-0.01	0.01	-0.01	-0.02	0.07
Area Gemellus Inferior	-0.07	0.00	0.00	0.00	0.00	0.00	0.00	0.00	0.16
Area Quadratus Femoris	-0.07	0.01	0.00	0.01	0.01	-0.01	0.01	0.02	0.07
Area Obturator Externus	-0.10	0.02	0.00	0.01	0.02	-0.02	0.02	0.01	0.07
Area Biceps Femoris (Long Head)	0.00	0.01	-0.01	0.00	0.01	0.00	0.01	0.00	0.02
Area Semitendinosus	0.01	-0.02	0.00	-0.02	-0.02	0.03	-0.02	-0.02	0.12
Area Semimembranosus	-0.07	0.01	0.00	0.01	0.01	-0.02	0.01	0.01	0.07

Pearson Correlations	Percentage Of Dislocation	Sum Forces tot	FP Perc Along Femur	Sum Forces FP x	Sum Forces FP y	Sum Forces FP z	Sum Forces FP tot	Projected F over Path	% of total force in pat direction
Femur.Length	0.02	0.00	0.00	0.00	0.00	0.00	0.00	0.00	0.00
Femur.L_Trochanteric	-0.02	0.00	0.01	0.00	0.00	0.02	0.00	0.00	-0.03
Femur.Shaft_Width	0.03	-0.04	0.00	-0.04	-0.04	0.04	-0.04	-0.04	0.02
Femur.Deviation_Angle	0.03	0.00	0.00	0.00	0.00	0.00	0.00	0.00	-0.06
Femur.Sagittal_Bowing_Ang	0.01	-0.01	0.01	-0.01	-0.01	0.01	-0.01	-0.01	0.03
Femur.Coronal_Bowing_Ang	-0.05	-0.02	0.00	-0.01	-0.02	0.01	-0.02	-0.01	0.00
Femur.Head_Diam	0.10	-0.01	0.00	-0.01	-0.01	0.01	-0.01	-0.01	0.08
Femur.Anteversion_Angle	0.07	0.00	0.00	0.00	0.00	-0.01	0.00	0.00	-0.13
Femur.Incline_Angle	-0.13	-0.03	0.00	-0.02	-0.03	0.03	-0.02	-0.02	-0.09
Femur.Condyle_Diameter	0.00	-0.01	0.00	0.00	-0.01	0.00	-0.01	0.00	-0.02
Femur.Condyle_Spacing	0.11	0.01	0.00	0.01	0.01	-0.01	0.01	0.02	0.10
Femur.Epicondyle_Dist	-0.01	-0.01	0.00	-0.02	-0.01	0.02	-0.01	-0.02	0.03
Femur.Head_Module_E	-0.03	0.00	0.00	0.00	0.00	0.00	0.00	0.00	0.05
Femur.Head_Module_v	-0.10	-0.02	0.00	-0.02	-0.02	0.02	-0.02	-0.02	0.00
Hip.Acetabulum_Diam	0.06	0.01	0.00	0.01	0.02	-0.01	0.01	0.01	-0.01
Hip.Acetabulum_Module_E	0.09	0.00	0.00	0.00	0.00	0.00	0.00	0.00	0.00
Hip.Acetabulum_Module_v	-0.01	-0.02	0.00	-0.02	-0.02	0.02	-0.02	-0.02	-0.03

Pearson Correlations	Percentage Of Dislocation	Sum Forces tot	FP Perc Along Femur	Sum Forces FP x	Sum Forces FP y	Sum Forces FP z	Sum Forces FP tot	Projected F over Path	% of total force in pat direction
3D_Rat Iliopsoas	0.01	0.00	0.01	0.00	0.00	0.00	0.00	0.00	0.07
3D_Rat Pectineus	0.12	0.02	0.00	0.01	0.02	-0.01	0.01	0.01	-0.03
3D_Rat Sartorius	0.01	0.01	0.00	0.02	0.01	-0.02	0.01	0.02	-0.01
3D_Rat Rectus Femoris	0.01	0.02	0.00	0.03	0.02	-0.02	0.02	0.03	-0.07
3D_Rat Adductor Longus	-0.02	0.00	0.00	0.00	0.00	0.00	0.00	0.00	-0.07
3D_Rat Adductor Brevis	0.02	-0.01	0.00	-0.01	-0.01	0.01	-0.01	-0.01	-0.01
3D_Rat Adductor Magnus Minimus	-0.05	-0.01	0.00	-0.01	-0.01	0.01	-0.01	-0.01	0.07
3D_Rat Adductor Magnus Middle	0.02	-0.01	0.00	-0.02	-0.02	0.01	-0.01	-0.02	-0.01
3D_Rat Adductor Magnus Posterior	0.00	0.01	0.00	0.02	0.02	-0.02	0.01	0.02	0.11
3D_Rat Gracilis	-0.08	0.00	0.00	0.00	0.00	-0.01	0.00	0.00	-0.01
3D_Rat Gluteus Max	-0.02	0.02	0.00	0.02	0.02	-0.02	0.02	0.02	0.02
3D_Rat Gluteus Medius Anterior	0.00	-0.02	0.00	-0.01	-0.02	0.01	-0.02	-0.01	0.10
3D_Rat Gluteus Medius Middle	-0.12	-0.01	0.00	-0.01	-0.01	0.02	-0.01	-0.01	-0.07
3D_Rat Gluteus Medius Posterior	0.07	-0.01	0.00	-0.01	-0.01	0.02	-0.01	-0.01	-0.05
3D_Rat Gluteus Minimus Anterior	0.07	0.00	-0.01	0.00	0.00	-0.01	0.00	0.00	0.10
3D_Rat Gluteus Minimus Middle	-0.07	0.02	0.00	0.01	0.01	-0.01	0.02	0.01	0.02
3D_Rat Gluteus Minimus Posterior	0.09	0.02	0.00	0.03	0.02	-0.02	0.02	0.03	0.00
3D_Rat Tensor Fascia Lata	-0.03	-0.01	0.00	0.00	0.00	0.00	-0.01	0.00	-0.02
3D_Rat Piriformis	-0.01	0.00	0.00	0.00	0.00	0.01	0.00	0.00	0.04
3D_Rat Obturator Internus	0.03	0.00	0.00	0.00	0.00	0.00	0.00	0.01	0.02
3D_Rat Gemellus Superior	-0.02	-0.02	0.00	-0.01	-0.01	0.01	-0.02	-0.01	0.03
3D_Rat Gemellus Inferior	0.01	0.00	0.01	0.01	0.00	-0.01	0.00	0.01	-0.05
3D_Rat Quadratus Femoris	0.00	-0.01	0.00	-0.01	-0.01	0.01	-0.01	0.00	0.03
3D_Rat Obturator Externus	0.02	-0.02	0.01	-0.01	-0.02	0.01	-0.02	-0.01	-0.02
3D_Rat Biceps Femoris (Long Head)	0.07	-0.01	0.01	-0.02	-0.01	0.01	-0.01	-0.02	-0.02
3D_Rat Semitendinosus	0.03	0.01	0.00	0.02	0.01	-0.01	0.01	0.02	0.06
3D_Rat Semimembranosus	-0.01	0.00	0.00	0.00	0.00	0.00	0.00	0.00	-0.01

Pearson Correlations	Percentage Of Dislocation	Sum Forces tot	FP Perc Along Femur	Sum Forces FP x	Sum Forces FP y	Sum Forces FP z	Sum Forces FP tot	Projected F over Path	% of total force in path direction
3D_Rot Iliopsoas	0.11	-0.02	0.01	-0.01	-0.02	0.02	-0.01	-0.01	-0.09
3D_Rot Pectineus	0.04	0.00	0.00	0.00	0.00	0.01	0.00	-0.01	0.00
3D_Rot Sartorius	-0.09	0.00	0.00	0.00	0.00	-0.01	0.00	0.00	0.00
3D_Rot Rectus Femoris	0.03	-0.03	0.01	-0.03	-0.03	0.03	-0.03	-0.02	-0.05
3D_Rot Adductor Longus	-0.07	0.00	0.00	0.00	0.00	0.00	0.00	0.00	-0.09
3D_Rot Adductor Brevis	0.02	-0.01	-0.01	-0.01	-0.01	0.01	-0.01	-0.01	0.01
3D_Rot Adductor Magnus Minimus	0.12	-0.02	0.00	-0.03	-0.02	0.03	-0.02	-0.02	0.07
3D_Rot Adductor Magnus Middle	0.02	0.01	0.00	0.01	0.01	-0.01	0.01	0.01	0.08
3D_Rot Adductor Magnus Posterior	-0.07	0.01	0.00	0.01	0.01	-0.01	0.01	0.01	0.11
3D_Rot Gracilis	0.02	0.02	0.00	0.02	0.02	-0.01	0.02	0.02	0.01
3D_Rot Gluteus Max	-0.10	-0.01	-0.01	-0.01	-0.01	0.00	-0.01	-0.01	0.04
3D_Rot Gluteus Medius Anterior	-0.05	-0.02	0.00	-0.02	-0.02	0.03	-0.02	-0.02	-0.04
3D_Rot Gluteus Medius Middle	-0.01	0.00	0.00	0.00	0.01	0.00	0.00	0.00	-0.12
3D_Rot Gluteus Medius Posterior	0.00	-0.03	0.01	-0.03	-0.03	0.03	-0.03	-0.02	-0.02
3D_Rot Gluteus Minimus Anterior	-0.05	0.02	0.00	0.02	0.02	-0.01	0.02	0.02	0.03
3D_Rot Gluteus Minimus Middle	-0.01	0.00	0.00	0.00	0.00	0.00	0.00	0.00	0.03
3D_Rot Gluteus Minimus Posterior	-0.02	0.02	-0.01	0.01	0.01	-0.01	0.02	0.01	0.08
3D_Rot Tensor Fascia Lata	-0.02	0.01	0.01	0.01	0.01	-0.01	0.01	0.01	0.02
3D_Rot Piriformis	-0.13	0.02	0.00	0.02	0.02	-0.01	0.02	0.02	0.05
3D_Rot Obturator Internus	-0.04	0.00	0.00	0.00	0.00	0.00	0.00	0.00	-0.02
3D_Rot Gemellus Superior	-0.02	0.01	0.01	0.01	0.01	-0.02	0.01	0.01	-0.01
3D_Rot Gemellus Inferior	0.12	-0.01	0.01	-0.01	-0.01	0.02	-0.01	-0.01	0.03
3D_Rot Quadratus Femoris	0.14	-0.01	0.00	-0.02	-0.02	0.03	-0.01	-0.02	0.06
3D_Rot Obturator Externus	-0.01	0.01	0.00	0.01	0.01	-0.02	0.01	0.01	-0.02
3D_Rot Biceps Femoris (Long Head)	-0.03	0.02	0.00	0.02	0.02	-0.01	0.02	0.02	-0.02
3D_Rot Semitendinosus	0.06	0.00	0.00	0.01	0.00	-0.01	0.00	0.00	-0.01
3D_Rot Semimembranosus	0.08	0.00	0.00	0.00	0.00	0.00	0.00	0.00	-0.21

Pearson Correlations	Percentage Of Dislocation	Sum Forces tot	FP Perc Along Femur	Sum Forces FP x	Sum Forces FP y	Sum Forces FP z	Sum Forces FP tot	Projected F over Path	% of total force in path direction
M_L_Ratio Iliopsoas	0.07	0.01	0.00	0.01	0.01	-0.01	0.01	0.01	0.05
M_L_Ratio Pectineus	0.07	-0.02	0.00	-0.02	-0.02	0.01	-0.02	-0.02	-0.05
M_L_Ratio Sartorius	-0.09	0.00	0.00	0.00	0.00	-0.01	0.00	0.00	0.01
M_L_Ratio Rectus Femoris	-0.04	0.03	0.00	0.03	0.03	-0.03	0.03	0.03	0.09
M_L_Ratio Adductor Longus	-0.06	0.01	0.00	0.02	0.02	-0.01	0.01	0.02	-0.10
M_L_Ratio Adductor Brevis	0.03	0.02	0.00	0.02	0.02	-0.02	0.02	0.01	-0.02
M_L_Ratio Adductor Magnus Minimus	-0.02	-0.02	0.00	-0.01	-0.02	0.01	-0.02	-0.02	-0.08
M_L_Ratio Adductor Magnus Middle	0.13	-0.02	0.00	-0.03	-0.02	0.02	-0.02	-0.03	-0.13
M_L_Ratio Adductor Magnus Posterior	0.05	0.00	0.00	0.00	0.01	0.00	0.00	0.00	0.10
M_L_Ratio Gracilis	0.15	0.00	0.00	0.00	0.00	0.00	0.00	0.00	-0.14
M_L_Ratio Gluteus Max	0.02	0.00	0.00	0.00	0.00	0.00	0.00	-0.01	-0.02
M_L_Ratio Gluteus Medius Anterior	-0.02	0.01	0.00	0.01	0.01	-0.01	0.01	0.01	0.05
M_L_Ratio Gluteus Medius Middle	0.00	-0.01	0.00	-0.01	-0.02	0.01	-0.01	-0.01	-0.11
M_L_Ratio Gluteus Medius Posterior	-0.07	-0.03	0.00	-0.02	-0.03	0.02	-0.02	-0.02	-0.04
M_L_Ratio Gluteus Minimus Anterior	0.02	0.01	0.00	0.02	0.02	-0.01	0.01	0.02	-0.07
M_L_Ratio Gluteus Minimus Middle	-0.10	-0.01	0.00	-0.01	-0.01	0.01	-0.01	-0.01	0.04
M_L_Ratio Gluteus Minimus Posterior	0.03	0.02	0.00	0.02	0.02	-0.02	0.02	0.02	0.01
M_L_Ratio Tensor Fascia Lata	0.06	-0.02	0.00	-0.02	-0.02	0.02	-0.02	-0.02	-0.01
M_L_Ratio Piriformis	0.02	0.01	0.00	0.01	0.01	0.00	0.01	0.01	-0.02
M_L_Ratio Obturator Internus	-0.05	0.03	0.00	0.03	0.03	-0.02	0.03	0.03	-0.09
M_L_Ratio Gemellus Superior	-0.03	-0.02	-0.01	-0.02	-0.02	0.02	-0.02	-0.01	0.03
M_L_Ratio Gemellus Inferior	0.06	0.00	0.00	0.00	0.00	0.00	0.00	0.00	0.10
M_L_Ratio Quadratus Femoris	0.09	-0.01	0.00	-0.01	-0.01	0.01	-0.01	-0.01	0.07
M_L_Ratio Obturator Externus	-0.02	-0.02	-0.01	-0.01	-0.01	0.02	-0.02	-0.01	0.00
M_L_Ratio Biceps Femoris (Long Head)	-0.02	0.01	0.00	0.01	0.01	-0.01	0.01	0.01	-0.06
M_L_Ratio Semitendinosus	-0.01	-0.01	0.00	-0.01	-0.01	0.00	-0.01	-0.01	-0.10
M_L_Ratio Semimembranosus	0.03	-0.01	0.00	-0.01	-0.01	0.01	-0.01	0.00	0.03

Pearson Correlations	Percentage Of Dislocation	Sum Forces tot	FP Perc Along Femur	Sum Forces FP x	Sum Forces FP y	Sum Forces FP z	Sum Forces FP tot	Projected F over Path	% of total force in pat direction
Flexion_i	0.09	-0.03	0.01	-0.03	-0.03	0.04	-0.03	-0.03	-0.03
Abduction_i	-0.01	-0.01	0.00	-0.02	-0.01	0.04	-0.01	-0.01	0.16
E_Rotation_i	0.04	-0.01	0.00	-0.01	-0.01	0.01	-0.01	-0.01	-0.06
BWeight	0.02	-0.02	0.00	-0.02	-0.02	0.02	-0.02	-0.01	0.01
Leg_Perc_Weight	-0.11	-0.01	0.00	-0.01	-0.01	0.02	-0.01	-0.01	0.07
PreStretch	0.00	0.02	0.00	0.02	0.02	-0.02	0.02	0.02	0.11
Hip Muscle Insertion	0.01	0.02	-0.01	0.01	0.02	-0.02	0.02	0.01	-0.43
Rel_Flex	-0.05	0.02	0.00	0.02	0.02	-0.02	0.02	0.02	-0.01
Rel_Abd	-0.04	0.02	-0.01	0.01	0.02	-0.01	0.02	0.01	-0.02
Rel_Rot	-0.02	-0.01	0.01	-0.01	-0.01	0.01	-0.01	-0.01	-0.07
Flexion_e	-0.01	-0.01	0.00	-0.01	-0.01	0.00	-0.01	-0.01	-0.03
Abduction_e	0.08	0.01	0.00	0.01	0.01	0.00	0.01	0.01	-0.04
E_Rotation_e	0.01	-0.01	-0.01	-0.01	-0.01	0.01	-0.01	-0.01	0.06
Percentage_Of_Dislocation	1.00	0.02	0.00	0.02	0.02	-0.03	0.02	0.02	-0.01
Leg Centroid x		-0.02	0.01	-0.02	-0.02	0.02	-0.02	-0.02	0.24
Leg Centroid y		-0.02	0.01	-0.02	-0.02	0.02	-0.02	-0.02	0.25
Leg Centroid z		-0.02	0.01	-0.02	-0.02	0.02	-0.02	-0.02	0.25
Sum_Forces x		0.97	-0.02	1.00	0.98	-0.93	0.97	0.99	0.00
Sum_Forces y		1.00	-0.03	0.98	1.00	-0.91	0.99	0.96	0.00
Sum_Forces z		-0.90	0.03	-0.92	-0.91	1.00	-0.89	-0.88	0.00
Sum_Forces tot		1.00	-0.03	0.97	1.00	-0.90	1.00	0.95	0.00
Sum_Moments x			-0.03	0.98	1.00	-0.93	0.99	0.96	0.00
Sum_Moments y			0.02	-1.00	-0.99	0.92	-0.98	-0.99	0.00
Sum_Moments z			-0.03	0.98	1.00	-0.91	1.00	0.97	0.00
FP_Perc_Along_Femur				-0.02	-0.03	0.03	-0.03	-0.02	0.01
Sum_ForcesFP x					0.98	-0.92	0.97	0.99	0.00
Sum_ForcesFP y						-0.91	0.99	0.96	0.00
Sum_ForcesFP z							-0.89	-0.88	0.00
Sum_ForcesFP tot								0.96	0.00
ProjectedFoverPath									0.01
Sum_MomentsFP x									0.00
Sum_MomentsFP y									0.00
Sum_MomentsFP z									0.00

Table 17: Pearson Correlation Matrix for Graf type III.

Pearson Correlations	Percentage Of Dislocation	Sum Forces tot	FP Perc Along Femur	Sum Forces FP x	Sum Forces FP y	Sum Forces FP z	Sum Forces FP tot	Projected F over Path	% of total force in pat direction
Area Iliopsoas	-0.20	0.00	0.00	0.02	0.01	-0.03	0.00	0.02	-0.11
Area Pectineus	-0.17	0.03	0.00	0.03	0.03	-0.03	0.03	0.03	-0.05
Area Sartorius	-0.24	0.04	0.00	0.04	0.04	-0.03	0.04	0.04	0.04
Area Rectus Femoris	-0.20	-0.02	0.01	-0.01	-0.01	0.01	-0.02	-0.01	-0.06
Area Adductor Longus	-0.15	0.00	0.01	0.00	0.00	0.00	0.00	0.00	-0.06
Area Adductor Brevis	-0.10	-0.05	0.01	-0.03	-0.03	0.02	-0.05	-0.03	-0.18
Area Adductor Magnus Minimus	-0.28	0.00	0.00	0.00	0.00	0.00	0.00	0.00	0.09
Area Adductor Magnus Middle	0.07	0.03	0.01	0.05	0.05	-0.06	0.04	0.05	0.03
Area Adductor Magnus Posterior	-0.14	-0.03	0.00	-0.02	-0.02	0.01	-0.03	-0.02	0.07
Area Gracilis	-0.11	-0.02	0.02	-0.01	-0.01	0.00	-0.02	0.00	-0.07
Area Gluteus Max	-0.24	0.01	0.00	0.02	0.01	-0.02	0.01	0.02	-0.02
Area Gluteus Medius Anterior	-0.10	0.02	0.00	0.02	0.02	-0.02	0.02	0.02	-0.03
Area Gluteus Medius Middle	-0.17	-0.03	0.01	-0.03	-0.03	0.02	-0.03	-0.03	-0.04
Area Gluteus Medius Posterior	-0.03	0.03	-0.01	0.03	0.03	-0.03	0.03	0.03	-0.05
Area Gluteus Minimus Anterior	0.15	-0.01	0.01	-0.01	-0.01	0.01	-0.01	-0.01	-0.07
Area Gluteus Minimus Middle	-0.10	0.01	0.01	0.01	0.01	-0.01	0.02	0.01	0.14
Area Gluteus Minimus Posterior	-0.01	0.02	0.01	0.04	0.04	-0.04	0.02	0.04	-0.21
Area Tensor Fascia Lata	-0.17	-0.01	0.01	0.00	-0.01	0.00	-0.01	0.00	-0.03
Area Piriformis	-0.08	0.01	0.01	0.02	0.02	-0.02	0.01	0.02	-0.04
Area Obturator Internus	0.03	-0.05	0.01	-0.03	-0.03	0.02	-0.04	-0.03	-0.09
Area Gemellus Superior	-0.25	0.02	0.01	0.02	0.02	-0.02	0.03	0.02	0.20
Area Gemellus Inferior	-0.19	-0.01	0.01	0.01	0.01	-0.02	0.00	0.01	-0.07
Area Quadratus Femoris	-0.11	-0.04	0.02	-0.03	-0.03	0.02	-0.04	-0.03	0.27
Area Obturator Externus	-0.15	0.00	0.00	-0.01	-0.01	0.01	0.00	-0.01	0.23
Area Biceps Femoris (Long Head)	0.12	-0.05	0.00	-0.03	-0.03	0.02	-0.05	-0.03	-0.26
Area Semitendinosus	-0.23	0.00	0.01	0.01	0.00	-0.01	0.00	0.01	0.05
Area Semimembranosus	-0.17	0.02	0.01	0.01	0.01	-0.01	0.02	0.01	-0.03

Pearson Correlations	Percentage Of Dislocation	Sum Forces tot	FP Perc Along Femur	Sum Forces FP x	Sum Forces FP y	Sum Forces FP z	Sum Forces FP tot	Projected F over Path	% of total force in pat direction
Femur.Length	0.07	-0.02	0.00	-0.02	-0.03	0.02	-0.02	-0.02	-0.04
Femur.L_Trochanteric	0.03	0.04	0.01	0.04	0.04	-0.03	0.04	0.04	-0.11
Femur.Shaft_Width	-0.05	-0.05	0.00	-0.04	-0.04	0.04	-0.05	-0.04	0.19
Femur.Deviation_Angle	0.06	-0.04	0.00	-0.04	-0.04	0.04	-0.04	-0.04	-0.08
Femur.Sagittal_Bowing_Ang	-0.10	0.02	0.00	0.02	0.02	-0.02	0.02	0.02	0.04
Femur.Coronal_Bowing_Ang	0.16	-0.03	0.00	-0.04	-0.04	0.04	-0.03	-0.04	-0.06
Femur.Head_Diam	0.10	0.00	0.00	0.02	0.02	-0.03	0.00	0.02	-0.07
Femur.Anteversion_Angle	-0.16	0.04	0.00	0.02	0.02	0.00	0.04	0.01	0.11
Femur.Incline_Angle	0.16	-0.01	0.00	0.01	0.00	-0.02	-0.01	0.01	0.25
Femur.Condyle_Diameter	-0.13	-0.04	0.01	-0.03	-0.03	0.02	-0.04	-0.02	0.02
Femur.Condyle_Spacing	0.14	0.00	0.00	0.00	0.00	0.01	0.00	0.00	0.05
Femur.Epicondyle_Dist	0.14	-0.04	0.01	-0.05	-0.05	0.06	-0.04	-0.05	-0.04
Femur.Head_Module_E	0.07	0.00	0.00	0.02	0.02	-0.02	0.01	0.02	-0.04
Femur.Head_Module_v	0.05	-0.01	0.01	-0.01	-0.01	0.01	-0.01	-0.01	-0.12
Hip.Acetabulum_Diam	-0.06	0.04	0.00	0.05	0.05	-0.05	0.04	0.05	0.16
Hip.Acetabulum_Module_E	0.17	0.07	-0.02	0.06	0.06	-0.05	0.07	0.05	0.00
Hip.Acetabulum_Module_v	0.05	0.00	0.00	0.01	0.01	-0.01	0.00	0.01	-0.18

Pearson Correlations	Percentage Of Dislocation	Sum Forces tot	FP Perc Along Femur	Sum Forces FP x	Sum Forces FP y	Sum Forces FP z	Sum Forces FP tot	Projected F over Path	% of total force in pat direction
3D_Rat Iliopsoas	0.01	0.01	0.01	0.02	0.02	-0.02	0.01	0.02	-0.02
3D_Rat Pectineus	-0.18	0.00	0.01	-0.01	-0.01	0.01	0.00	-0.01	-0.08
3D_Rat Sartorius	0.21	0.01	0.00	0.01	0.01	-0.01	0.01	0.01	-0.18
3D_Rat Rectus Femoris	-0.03	-0.01	0.00	-0.01	-0.01	0.01	-0.01	-0.01	-0.16
3D_Rat Adductor Longus	0.03	-0.03	0.00	-0.01	-0.01	0.00	-0.03	-0.01	0.42
3D_Rat Adductor Brevis	0.01	0.02	0.00	0.03	0.03	-0.03	0.02	0.03	-0.08
3D_Rat Adductor Magnus Minimus	0.04	-0.05	0.00	-0.01	-0.02	0.00	-0.05	-0.01	0.01
3D_Rat Adductor Magnus Middle	0.01	0.01	0.00	0.01	0.01	-0.01	0.01	0.01	-0.05
3D_Rat Adductor Magnus Posterior	0.13	0.03	0.00	0.02	0.02	-0.02	0.03	0.02	0.09
3D_Rat Gracilis	-0.27	0.04	0.00	0.03	0.03	-0.02	0.04	0.03	0.18
3D_Rat Gluteus Max	-0.15	0.01	-0.01	0.00	0.00	0.01	0.01	-0.01	0.03
3D_Rat Gluteus Medius Anterior	0.01	0.01	0.00	0.00	0.00	0.01	0.01	0.00	0.14
3D_Rat Gluteus Medius Middle	-0.19	0.00	0.00	0.00	0.00	0.01	0.00	-0.01	-0.03
3D_Rat Gluteus Medius Posterior	0.23	-0.01	0.00	-0.01	-0.01	0.01	-0.01	-0.01	0.07
3D_Rat Gluteus Minimus Anterior	-0.15	-0.05	0.00	-0.05	-0.06	0.05	-0.05	-0.05	-0.12
3D_Rat Gluteus Minimus Middle	-0.13	0.02	0.00	0.02	0.02	-0.03	0.02	0.02	0.05
3D_Rat Gluteus Minimus Posterior	-0.12	0.00	-0.01	0.00	0.00	0.01	0.00	0.00	-0.07
3D_Rat Tensor Fascia Lata	0.02	-0.02	0.00	-0.02	-0.02	0.02	-0.02	-0.02	0.07
3D_Rat Piriformis	0.10	0.00	0.00	0.00	0.00	0.01	0.00	0.00	0.01
3D_Rat Obturator Internus	-0.07	-0.03	0.01	-0.02	-0.02	0.02	-0.03	-0.02	-0.12
3D_Rat Gemellus Superior	0.14	-0.06	0.00	-0.06	-0.06	0.06	-0.06	-0.06	-0.02
3D_Rat Gemellus Inferior	-0.12	0.05	-0.01	0.05	0.05	-0.05	0.05	0.05	0.05
3D_Rat Quadratus Femoris	-0.34	0.02	0.00	0.01	0.01	0.00	0.02	0.01	-0.03
3D_Rat Obturator Externus	-0.03	-0.03	0.01	-0.01	-0.01	-0.01	-0.03	0.00	-0.28
3D_Rat Biceps Femoris (Long Head)	0.22	-0.02	0.01	0.00	0.00	-0.01	-0.02	0.00	0.01
3D_Rat Semitendinosus	0.37	-0.03	0.01	-0.05	-0.05	0.05	-0.03	-0.05	-0.07
3D_Rat Semimembranosus	0.06	0.02	0.00	0.01	0.01	0.00	0.02	0.00	-0.01

Pearson Correlations	Percentage Of Dislocation	Sum Forces tot	FP Perc Along Femur	Sum Forces FP x	Sum Forces FP y	Sum Forces FP z	Sum Forces FP tot	Projected F over Path	% of total force in pat direction
3D_Rot Iliopsoas	0.19	-0.02	0.00	0.01	0.01	-0.02	-0.02	0.01	0.13
3D_Rot Pectineus	-0.16	0.06	0.00	0.04	0.04	-0.03	0.06	0.04	0.05
3D_Rot Sartorius	-0.02	-0.05	-0.01	-0.05	-0.05	0.05	-0.05	-0.05	-0.07
3D_Rot Rectus Femoris	-0.14	-0.03	0.01	-0.02	-0.02	0.01	-0.03	-0.02	-0.12
3D_Rot Adductor Longus	0.25	-0.04	0.00	-0.03	-0.03	0.03	-0.04	-0.03	0.00
3D_Rot Adductor Brevis	0.25	0.01	0.00	0.00	0.00	0.01	0.01	0.00	0.02
3D_Rot Adductor Magnus Minimus	0.07	-0.01	0.00	0.02	0.02	-0.03	-0.01	0.02	0.04
3D_Rot Adductor Magnus Middle	-0.26	-0.05	0.01	-0.06	-0.06	0.07	-0.05	-0.06	0.07
3D_Rot Adductor Magnus Posterior	0.17	0.03	-0.01	0.04	0.04	-0.04	0.03	0.04	-0.04
3D_Rot Gracilis	-0.01	0.02	-0.01	0.02	0.02	-0.02	0.02	0.02	0.02
3D_Rot Gluteus Max	0.04	-0.05	0.01	-0.06	-0.06	0.06	-0.05	-0.06	0.17
3D_Rot Gluteus Medius Anterior	-0.08	0.02	-0.01	-0.01	0.00	0.02	0.02	-0.01	0.05
3D_Rot Gluteus Medius Middle	0.07	-0.02	-0.01	-0.03	-0.03	0.03	-0.02	-0.03	-0.12
3D_Rot Gluteus Medius Posterior	-0.05	-0.03	0.00	-0.04	-0.04	0.04	-0.03	-0.04	-0.07
3D_Rot Gluteus Minimus Anterior	0.19	0.02	0.00	0.03	0.03	-0.04	0.02	0.04	0.02
3D_Rot Gluteus Minimus Middle	-0.02	-0.04	0.01	-0.05	-0.05	0.06	-0.04	-0.05	0.05
3D_Rot Gluteus Minimus Posterior	0.13	0.02	0.00	0.02	0.03	-0.02	0.02	0.02	-0.07
3D_Rot Tensor Fascia Lata	0.17	-0.01	0.00	-0.02	-0.02	0.02	-0.01	-0.02	0.01
3D_Rot Piriformis	0.01	0.02	0.00	0.03	0.03	-0.04	0.02	0.03	-0.05
3D_Rot Obturator Internus	-0.03	0.02	0.00	0.01	0.01	0.00	0.02	0.01	0.00
3D_Rot Gemellus Superior	0.09	0.01	0.01	0.01	0.01	-0.01	0.01	0.01	0.11
3D_Rot Gemellus Inferior	0.09	-0.02	0.00	0.01	0.01	-0.02	-0.02	0.01	-0.03
3D_Rot Quadratus Femoris	-0.13	0.03	0.00	0.04	0.04	-0.04	0.03	0.04	-0.13
3D_Rot Obturator Externus	-0.04	-0.01	-0.01	-0.04	-0.04	0.05	-0.01	-0.04	0.03
3D_Rot Biceps Femoris (Long Head)	-0.21	-0.05	0.00	-0.04	-0.04	0.04	-0.05	-0.04	0.13
3D_Rot Semitendinosus	-0.10	-0.01	0.00	-0.01	-0.01	0.01	-0.01	-0.01	-0.07
3D_Rot Semimembranosus	0.05	0.03	0.00	0.03	0.03	-0.02	0.03	0.03	0.23

Pearson Correlations	Percentage Of Dislocation	Sum Forces tot	FP Perc Along Femur	Sum Forces FP x	Sum Forces FP y	Sum Forces FP z	Sum Forces FP tot	Projected F over Path	% of total force in pat direction
M_L_Ratio Iliopsoas	-0.23	-0.05	0.00	-0.04	-0.04	0.03	-0.05	-0.04	0.18
M_L_Ratio Pectineus	0.00	0.02	0.00	0.03	0.03	-0.03	0.02	0.03	-0.03
M_L_Ratio Sartorius	-0.01	-0.02	0.00	-0.02	-0.02	0.02	-0.02	-0.02	0.15
M_L_Ratio Rectus Femoris	-0.12	0.05	0.00	0.04	0.04	-0.02	0.05	0.03	-0.13
M_L_Ratio Adductor Longus	0.04	-0.01	0.00	-0.01	-0.01	0.01	-0.01	-0.01	0.02
M_L_Ratio Adductor Brevis	0.09	0.02	-0.01	0.01	0.01	0.00	0.02	0.01	0.16
M_L_Ratio Adductor Magnus Minimus	-0.16	0.00	0.02	0.02	0.01	-0.03	0.00	0.02	-0.22
M_L_Ratio Adductor Magnus Middle	0.04	0.00	0.00	0.01	0.01	-0.02	0.00	0.01	-0.20
M_L_Ratio Adductor Magnus Posterior	0.02	-0.01	-0.01	-0.02	-0.02	0.02	-0.01	-0.02	-0.01
M_L_Ratio Gracilis	-0.10	0.04	-0.01	0.05	0.05	-0.06	0.04	0.05	0.17
M_L_Ratio Gluteus Max	-0.10	0.01	0.00	0.03	0.02	-0.03	0.01	0.03	0.04
M_L_Ratio Gluteus Medius Anterior	-0.05	-0.03	0.00	-0.03	-0.03	0.03	-0.03	-0.03	-0.01
M_L_Ratio Gluteus Medius Middle	-0.04	-0.01	0.01	0.01	0.00	-0.01	-0.01	0.01	0.00
M_L_Ratio Gluteus Medius Posterior	0.08	-0.03	0.00	-0.01	-0.01	0.00	-0.03	-0.01	-0.11
M_L_Ratio Gluteus Minimus Anterior	-0.08	0.01	0.01	0.02	0.02	-0.02	0.02	0.02	-0.24
M_L_Ratio Gluteus Minimus Middle	0.19	0.01	0.00	0.00	0.00	0.01	0.01	0.00	-0.15
M_L_Ratio Gluteus Minimus Posterior	-0.02	0.00	0.00	-0.02	-0.02	0.03	0.00	-0.02	-0.04
M_L_Ratio Tensor Fascia Lata	0.02	0.02	0.01	0.03	0.03	-0.03	0.02	0.03	-0.16
M_L_Ratio Piriformis	0.04	0.05	0.00	0.05	0.05	-0.05	0.05	0.05	-0.22
M_L_Ratio Obturator Internus	0.23	0.01	0.00	0.00	0.00	0.00	0.01	0.00	-0.02
M_L_Ratio Gemellus Superior	-0.21	-0.05	0.01	-0.04	-0.04	0.03	-0.05	-0.04	0.13
M_L_Ratio Gemellus Inferior	-0.20	-0.01	0.00	-0.02	-0.02	0.02	-0.01	-0.02	-0.09
M_L_Ratio Quadratus Femoris	0.09	0.01	-0.01	0.00	0.00	0.01	0.01	0.00	0.08
M_L_Ratio Obturator Externus	-0.07	0.03	0.01	0.03	0.02	-0.02	0.03	0.03	0.13
M_L_Ratio Biceps Femoris (Long Head)	-0.05	0.03	0.00	0.02	0.02	-0.01	0.03	0.02	0.05
M_L_Ratio Semitendinosus	0.00	-0.02	0.01	-0.03	-0.03	0.02	-0.02	-0.02	0.01
M_L_Ratio Semimembranosus	0.13	0.05	0.00	0.04	0.04	-0.03	0.05	0.04	-0.02

Pearson Correlations	Percentage Of Dislocation	Sum Forces tot	FP Perc Along Femur	Sum Forces FP x	Sum Forces FP y	Sum Forces FP z	Sum Forces FP tot	Projected F over Path	% of total force in pat direction
Flexion_i	-0.06	-0.06	0.01	-0.07	-0.07	0.07	-0.06	-0.07	-0.38
Abduction_i	-0.17	0.02	0.00	0.02	0.02	-0.01	0.02	0.02	-0.43
E_Rotation_i	0.09	-0.02	0.00	-0.02	-0.02	0.01	-0.02	-0.01	-0.12
BWeight	0.05	0.01	0.01	0.01	0.00	0.00	0.01	0.00	0.13
Leg_Perc_Weight	0.04	-0.05	0.01	-0.04	-0.04	0.02	-0.05	-0.03	0.05
PreStretch	-0.14	-0.01	0.00	-0.02	-0.02	0.02	-0.01	-0.02	0.04
Hip Muscle Ins X Iliopsoas	-0.05	0.02	-0.01	0.02	0.02	-0.01	0.02	0.02	-0.29
Rel_Flex	-0.04	0.00	0.01	0.00	0.00	0.01	0.00	0.00	0.17
Rel_Abd	-0.07	0.01	-0.01	0.02	0.02	-0.02	0.01	0.02	0.02
Rel_Rot	-0.14	-0.02	0.01	-0.02	-0.02	0.02	-0.02	-0.02	-0.03
Flexion_e	-0.06	0.08	-0.01	0.06	0.06	-0.04	0.08	0.05	0.07
Abduction_e	-0.05	0.01	0.01	0.02	0.02	-0.02	0.02	0.02	-0.25
E_Rotation_e	0.19	-0.02	0.00	-0.01	-0.02	0.01	-0.02	-0.01	-0.04
Percentage_Of_Dislocation		-0.02	0.00	-0.01	-0.02	0.01	-0.02	-0.01	0.06
Leg Centroid x		0.00	0.00	0.00	0.00	0.01	0.00	-0.01	-0.09
Leg Centroid y		0.00	0.00	-0.01	0.00	0.01	0.00	-0.01	-0.10
Leg Centroid z		0.00	0.00	-0.01	0.00	0.01	0.00	-0.01	-0.10
Sum_Forces x		0.92	-0.04	1.00	1.00	-0.97	0.92	1.00	0.05
Sum_Forces y		0.93	-0.04	1.00	1.00	-0.96	0.93	0.99	0.05
Sum_Forces z		-0.81	0.03	-0.97	-0.96	1.00	-0.81	-0.98	-0.05
Sum_Forces tot			-0.06	0.92	0.93	-0.81	1.00	0.90	0.04
a			0.00	0.00	0.00	0.00	0.00	0.00	-0.14
Sum_Moments x			-0.04	1.00	1.00	-0.97	0.93	1.00	0.05
Sum_Moments y			0.04	-1.00	-1.00	0.98	-0.92	-1.00	-0.05
Sum_Moments z			-0.05	0.99	1.00	-0.94	0.96	0.98	0.05
FP_Perc_Along_Femur				-0.04	-0.04	0.03	-0.06	-0.03	-0.09
Sum_ForcesFP x					1.00	-0.97	0.92	1.00	0.05
Sum_ForcesFP y						-0.96	0.93	0.99	0.05
Sum_ForcesFP z							-0.81	-0.98	-0.05
Sum_ForcesFP tot								0.90	0.04
ProjectedFoverPath									0.05
Sum_MomentsFP x									0.05
Sum_MomentsFP y									0.04
Sum_MomentsFP z									0.05

Table 18: Pearson Correlation Matrix for Graf type IV indirect path

Pearson Correlations	Percentage Of Dislocation	Sum Forces tot	FP Perc Along Femur	Sum Forces FP x	Sum Forces FP y	Sum Forces FP z	Sum Forces FP tot	Projected F over Path	% of total force in pat direction
Area Iliopsoas	-0.06	0.00	0.00	-0.01	-0.01	0.02	0.01	-0.01	0.05
Area Pectineus	0.03	-0.01	0.00	-0.01	0.00	-0.01	0.01	-0.01	0.03
Area Sartorius	0.02	0.00	0.00	0.00	0.01	0.01	0.00	0.00	0.04
Area Rectus Femoris	-0.02	0.01	0.00	-0.01	0.00	0.02	0.01	-0.01	0.04
Area Adductor Longus	-0.03	-0.01	0.00	0.00	0.00	0.00	-0.01	0.00	0.03
Area Adductor Brevis	0.06	0.01	0.00	-0.01	0.03	0.01	0.01	-0.01	-0.05
Area Adductor Magnus Minimus	0.00	-0.01	0.00	-0.01	-0.01	-0.01	0.01	-0.01	0.02
Area Adductor Magnus Middle	0.01	0.01	0.00	-0.01	0.02	0.04	0.01	0.00	0.04
Area Adductor Magnus Posterior	-0.01	-0.01	0.00	0.01	0.01	0.01	-0.01	0.01	0.01
Area Gracilis	-0.04	0.01	0.00	-0.01	0.00	0.02	0.01	-0.01	0.01
Area Gluteus Max	-0.02	0.01	0.00	-0.01	-0.02	0.02	0.01	-0.01	0.05
Area Gluteus Medius Anterior	-0.04	-0.01	0.00	-0.01	0.00	0.00	0.01	-0.01	0.04
Area Gluteus Medius Middle	-0.05	-0.01	0.00	0.00	0.00	-0.01	0.00	0.00	0.02
Area Gluteus Medius Posterior	-0.07	0.00	0.00	0.00	-0.01	0.01	0.00	0.00	0.00
Area Gluteus Minimus Anterior	0.04	-0.01	0.00	-0.01	0.02	0.01	0.01	-0.01	0.05
Area Gluteus Minimus Middle	-0.08	-0.01	0.00	-0.01	0.00	0.01	0.01	-0.01	0.00
Area Gluteus Minimus Posterior	0.00	-0.01	0.00	0.00	0.00	0.02	-0.01	0.00	0.06
Area Tensor Fascia Lata	-0.07	-0.01	0.00	0.00	-0.01	0.01	0.00	0.00	0.01
Area Piriformis	0.01	-0.01	0.00	0.01	-0.01	0.01	-0.01	0.01	0.01
Area Obturator Internus	-0.04	0.00	0.00	0.01	-0.01	0.01	-0.01	0.01	0.01
Area Gemellus Superior	-0.04	0.02	0.00	0.01	-0.03	0.02	-0.01	0.01	0.04
Area Gemellus Inferior	-0.05	0.00	0.00	0.00	-0.01	0.02	0.00	0.00	0.05
Area Quadratus Femoris	-0.09	0.00	0.00	0.01	0.00	0.04	-0.01	0.01	0.06
Area Obturator Externus	0.03	-0.02	0.00	-0.01	-0.03	0.00	0.01	-0.01	0.03
Area Biceps Femoris (Long Head)	-0.09	0.01	0.00	-0.01	0.01	0.03	0.01	-0.01	0.03
Area Semitendinosus	-0.05	-0.01	0.00	0.00	0.01	0.01	0.00	0.00	0.01
Area Semimembranosus	-0.02	0.01	0.00	0.00	-0.02	0.02	0.00	0.00	0.04

Pearson Correlations	Percentage Of Dislocation	Sum Forces tot	FP Perc Along Femur	Sum Forces FP x	Sum Forces FP y	Sum Forces FP z	Sum Forces FP tot	Projected F over Path	% of total force in pat direction
Femur.Length	-0.03	-0.02	0.00	0.00	0.01	0.00	-0.01	0.00	0.01
Femur.L_Trochanteric	-0.01	0.01	0.00	0.00	-0.01	-0.02	0.00	0.00	0.06
Femur.Deviation_Angle	0.00	-0.02	0.00	0.00	-0.01	0.01	0.00	0.00	0.03
Femur.Shaft_Width	0.03	0.00	0.00	-0.02	0.01	0.00	0.02	-0.02	-0.03
Femur.Sagittal_Bowing_Ang	-0.02	-0.01	0.00	0.00	0.03	0.00	0.00	0.00	-0.01
Femur.Coronal_Bowing_Ang	-0.03	0.01	0.00	0.01	0.02	0.02	-0.01	0.01	0.00
Femur.Head_Diam	-0.02	0.01	0.00	0.01	0.02	0.02	-0.01	0.01	0.01
Femur.Anteversion_Angle	-0.02	0.02	0.01	0.01	-0.05	0.10	-0.01	0.01	-0.04
Femur.Incline_Angle	0.05	0.01	0.00	-0.01	-0.01	-0.01	0.01	-0.01	0.02
Femur.Condyle_Diameter	-0.04	0.04	0.00	0.01	0.00	0.01	-0.01	0.01	0.04
Femur.Condyle_Spacing	-0.04	0.01	0.00	-0.01	0.04	0.02	0.01	-0.01	0.00
Femur.Epicondyle_Dist	0.06	0.00	0.00	0.00	0.01	0.00	0.00	0.00	0.01
Femur.Head_Module_E	0.03	-0.04	0.00	0.01	-0.04	-0.01	-0.01	0.01	0.01
Femur.Head_Module_v	-0.01	-0.03	0.00	0.01	-0.01	-0.02	-0.01	0.01	-0.07
Hip.Acetabulum_Diam	0.01	0.00	0.00	-0.01	-0.01	-0.01	0.01	-0.01	-0.03
Hip.Acetabulum_Module_E	0.04	-0.02	0.00	0.00	0.00	-0.01	0.00	0.00	-0.02
Hip.Acetabulum_Module_v	-0.02	0.00	0.00	0.00	0.00	0.00	0.00	0.00	0.01

Pearson Correlations	Percentage Of Dislocation	Sum Forces tot	FP Perc Along Femur	Sum Forces FP x	Sum Forces FP y	Sum Forces FP z	Sum Forces FP tot	Projected F over Path	% of total force in pat direction
3D_Rat Iliopsoas	-0.02	-0.02	0.00	0.01	-0.01	-0.01	-0.01	0.01	-0.07
3D_Rat Pectineus	-0.04	-0.01	0.00	0.00	-0.01	-0.02	0.00	0.00	0.04
3D_Rat Sartorius	0.03	-0.02	0.00	0.01	-0.01	0.00	-0.01	0.01	0.01
3D_Rat Rectus Femoris	0.00	0.01	0.00	-0.01	-0.03	0.00	0.01	-0.01	0.09
3D_Rat Adductor Longus	-0.01	0.00	0.00	0.02	-0.01	0.02	-0.02	0.02	0.00
3D_Rat Adductor Brevis	-0.05	0.01	0.00	0.00	-0.03	0.01	0.00	0.00	0.04
3D_Rat Adductor Magnus Minimus	0.05	0.01	0.00	0.00	-0.02	-0.01	0.00	0.00	0.01
3D_Rat Adductor Magnus Middle	0.02	0.00	0.00	0.00	-0.03	-0.02	0.00	0.00	-0.01
3D_Rat Adductor Magnus Posterior	-0.01	-0.01	0.00	0.00	0.00	0.00	0.00	0.00	0.01
3D_Rat Gracilis	0.05	-0.01	0.00	0.00	0.01	-0.02	0.00	0.00	0.02
3D_Rat Gluteus Max	0.02	-0.01	0.00	0.01	-0.01	0.00	-0.01	0.01	-0.01
3D_Rat Gluteus Medius Anterior	-0.02	0.01	0.00	0.00	-0.02	-0.01	0.00	0.00	0.01
3D_Rat Gluteus Medius Middle	0.04	0.01	0.00	0.01	0.01	0.02	-0.01	0.01	0.02
3D_Rat Gluteus Medius Posterior	0.03	-0.02	0.00	0.00	0.01	0.02	0.00	0.00	0.05
3D_Rat Gluteus Minimus Anterior	0.07	0.00	0.00	0.01	0.01	-0.01	-0.01	0.01	-0.01
3D_Rat Gluteus Minimus Middle	0.03	0.01	0.00	-0.01	0.01	-0.01	0.01	-0.01	-0.05
3D_Rat Gluteus Minimus Posterior	-0.02	-0.02	0.00	0.01	0.01	0.00	-0.01	0.01	0.03
3D_Rat Tensor Fascia Lata	0.01	-0.01	0.00	0.01	-0.03	-0.02	-0.01	0.01	0.01
3D_Rat Piriformis	0.03	0.00	0.00	0.00	-0.02	0.01	0.00	0.00	0.05
3D_Rat Obturator Internus	-0.01	-0.01	0.00	0.01	0.00	-0.01	-0.01	0.01	0.05
3D_Rat Gemellus Superior	0.00	0.00	0.00	0.00	0.00	-0.01	-0.01	0.00	-0.08
3D_Rat Gemellus Inferior	-0.01	0.00	0.00	0.00	-0.01	0.00	0.00	0.00	-0.05
3D_Rat Quadratus Femoris	-0.06	-0.01	0.00	0.00	0.00	-0.02	0.00	0.00	-0.03
3D_Rat Obturator Externus	0.04	-0.01	0.00	-0.01	0.00	0.00	0.01	-0.01	0.05
3D_Rat Biceps Femoris (Long Head)	0.01	-0.03	0.00	0.00	0.01	0.00	0.00	0.00	-0.07
3D_Rat Semitendinosus	-0.04	0.01	0.00	0.00	0.00	0.01	0.00	0.00	-0.03
3D_Rat Semimembranosus	0.00	-0.02	0.00	0.01	0.01	0.01	-0.01	0.00	-0.03

Pearson Correlations	Percentage Of Dislocation	Sum Forces tot	FP Perc Along Femur	Sum Forces FP x	Sum Forces FP y	Sum Forces FP z	Sum Forces FP tot	Projected F over Path	% of total force in pat direction
3D_Rot Iliopsoas	0.02	0.04	0.00	-0.01	0.02	0.03	0.01	-0.01	-0.07
3D_Rot Pectineus	-0.09	-0.01	0.00	0.02	-0.01	0.01	-0.02	0.01	0.00
3D_Rot Sartorius	0.05	-0.01	0.00	0.00	0.01	-0.01	0.00	0.00	0.00
3D_Rot Rectus Femoris	0.00	-0.01	0.00	0.00	-0.01	0.01	0.00	0.00	0.01
3D_Rot Adductor Longus	0.00	0.02	0.00	-0.02	0.01	-0.01	0.02	-0.02	-0.04
3D_Rot Adductor Brevis	0.06	-0.01	0.00	0.00	0.01	-0.02	0.00	0.00	0.03
3D_Rot Adductor Magnus Minimus	0.00	-0.02	0.00	0.00	0.00	-0.01	0.00	0.00	-0.07
3D_Rot Adductor Magnus Middle	-0.09	0.00	0.00	-0.01	-0.03	-0.02	0.01	-0.01	0.06
3D_Rot Adductor Magnus Posterior	-0.03	0.01	0.00	-0.02	-0.03	-0.03	0.02	-0.02	0.06
3D_Rot Gracilis	0.00	-0.01	0.00	-0.01	0.01	-0.01	0.01	-0.01	0.01
3D_Rot Gluteus Max	-0.01	-0.02	0.00	0.01	-0.03	0.00	-0.01	0.01	0.00
3D_Rot Gluteus Medius Anterior	0.03	0.00	0.00	0.00	0.03	0.00	0.00	0.00	0.02
3D_Rot Gluteus Medius Middle	0.01	-0.03	0.00	-0.01	0.02	0.00	0.01	-0.01	0.00
3D_Rot Gluteus Medius Posterior	0.01	0.00	0.00	0.01	-0.02	-0.01	-0.01	0.01	-0.04
3D_Rot Gluteus Minimus Anterior	0.02	-0.01	0.00	0.00	-0.01	-0.02	0.01	0.00	-0.04
3D_Rot Gluteus Minimus Middle	-0.03	0.03	0.00	0.00	0.01	0.03	0.00	0.00	0.03
3D_Rot Gluteus Minimus Posterior	-0.01	0.00	0.00	0.00	0.01	-0.03	0.00	0.00	-0.02
3D_Rot Tensor Fascia Lata	-0.03	-0.01	0.00	0.00	0.01	-0.02	0.00	0.00	-0.02
3D_Rot Piriformis	0.03	0.00	0.00	0.01	-0.01	0.01	-0.01	0.01	-0.01
3D_Rot Obturator Internus	0.06	0.00	0.00	0.00	0.00	-0.01	0.00	0.00	0.02
3D_Rot Gemellus Superior	-0.01	0.00	0.00	-0.01	-0.03	0.02	0.01	-0.01	0.02
3D_Rot Gemellus Inferior	-0.05	0.01	0.00	-0.01	-0.01	0.01	0.01	-0.01	-0.01
3D_Rot Quadratus Femoris	-0.01	0.01	0.00	-0.01	0.01	0.01	0.01	-0.01	-0.01
3D_Rot Obturator Externus	0.03	0.00	0.00	0.01	0.00	0.01	-0.01	0.01	-0.01
3D_Rot Biceps Femoris (Long Head)	-0.11	-0.01	0.00	0.01	0.00	0.00	-0.01	0.01	0.00
3D_Rot Semitendinosus	0.03	0.02	0.00	-0.01	0.03	-0.02	0.01	-0.01	0.01
3D_Rot Semimembranosus	-0.06	0.00	0.00	0.01	0.00	0.00	-0.01	0.01	-0.03

Pearson Correlations	Percentage Of Dislocation	Sum Forces tot	FP Perc Along Femur	Sum Forces FP x	Sum Forces FP y	Sum Forces FP z	Sum Forces FP tot	Projected F over Path	% of total force in pat direction
M_L_Ratio Iliopsoas	0.04	-0.03	0.00	0.00	0.02	0.00	0.00	0.00	0.00
M_L_Ratio Pectineus	0.01	0.01	0.00	0.01	0.00	-0.01	-0.01	0.01	0.04
M_L_Ratio Sartorius	0.00	-0.01	0.00	-0.01	0.02	0.01	0.01	-0.01	0.04
M_L_Ratio Rectus Femoris	0.01	0.02	0.00	0.01	0.01	0.01	-0.01	0.01	0.00
M_L_Ratio Adductor Longus	-0.05	0.03	0.00	0.00	0.02	0.03	0.01	0.00	-0.01
M_L_Ratio Adductor Brevis	-0.12	-0.01	0.00	0.00	-0.02	0.01	0.00	0.00	-0.02
M_L_Ratio Adductor Magnus Minimus	-0.03	-0.01	0.00	-0.01	0.01	0.01	0.00	0.00	-0.03
M_L_Ratio Adductor Magnus Middle	0.01	0.01	0.00	0.02	-0.02	0.00	-0.02	0.02	0.01
M_L_Ratio Adductor Magnus Posterior	-0.01	-0.02	0.00	0.00	0.00	-0.01	0.00	0.00	-0.02
M_L_Ratio Gracilis	0.03	0.02	0.00	0.00	0.00	-0.01	0.00	0.00	0.00
M_L_Ratio Gluteus Max	-0.01	-0.01	0.00	-0.01	0.02	0.01	0.01	-0.01	-0.03
M_L_Ratio Gluteus Medius Anterior	0.04	-0.01	0.00	0.01	-0.01	0.01	-0.01	0.01	-0.03
M_L_Ratio Gluteus Medius Middle	-0.02	0.00	0.00	0.01	0.01	0.00	0.00	0.00	0.02
M_L_Ratio Gluteus Medius Posterior	0.01	-0.01	0.00	0.00	-0.01	0.02	0.00	0.00	0.01
M_L_Ratio Gluteus Minimus Anterior	-0.06	-0.02	0.00	0.00	0.01	0.02	0.00	0.00	0.08
M_L_Ratio Gluteus Minimus Middle	-0.03	0.02	0.00	0.00	-0.02	0.01	0.00	0.00	0.03
M_L_Ratio Gluteus Minimus Posterior	-0.01	0.00	0.00	0.00	-0.01	-0.01	0.01	0.00	0.03
M_L_Ratio Tensor Fascia Lata	0.10	-0.03	0.00	0.00	0.01	-0.02	-0.01	0.00	-0.02
M_L_Ratio Piriformis	0.00	-0.01	0.00	-0.01	0.01	-0.01	0.01	-0.01	-0.03
M_L_Ratio Obturator Internus	0.01	0.00	0.00	-0.01	0.00	-0.02	0.01	-0.01	-0.01
M_L_Ratio Gemellus Superior	-0.01	-0.01	0.00	0.00	0.01	0.00	0.00	0.00	0.01
M_L_Ratio Gemellus Inferior	0.02	0.00	0.00	-0.01	0.00	0.01	0.01	-0.01	-0.04
M_L_Ratio Quadratus Femoris	-0.06	0.00	0.00	0.00	-0.03	-0.01	0.00	0.00	-0.03
M_L_Ratio Obturator Externus	-0.03	0.02	0.00	0.01	0.00	0.01	-0.01	0.01	-0.01
M_L_Ratio Biceps Femoris (Long Head)	-0.03	-0.01	0.00	-0.01	0.00	0.02	0.01	-0.01	0.01
M_L_Ratio Semitendinosus	-0.05	0.00	0.00	0.00	0.02	0.01	0.00	0.00	-0.03
M_L_Ratio Semimembranosus	0.03	0.02	0.00	0.01	-0.01	0.00	-0.01	0.01	0.04

Pearson Correlations	Percentage Of Dislocation	Sum Forces tot	FP Perc Along Femur	Sum Forces FP x	Sum Forces FP y	Sum Forces FP z	Sum Forces FP tot	Projected F over Path	% of total force in pat direction
Flexion_i	-0.03	-0.06	0.00	0.02	-0.04	0.03	-0.02	0.02	-0.12
Abduction_i	0.00	0.01	0.00	-0.01	0.00	0.01	0.01	-0.01	-0.02
E_Rotation_i	-0.03	0.00	0.00	0.01	-0.05	-0.01	0.00	0.01	-0.06
BWeight	0.04	0.03	0.00	0.01	-0.02	0.01	-0.01	0.01	-0.01
Leg_Perc_Weight	-0.02	0.02	0.00	0.00	-0.03	0.03	0.00	0.00	0.00
PreStretch	0.02	-0.02	0.00	0.00	-0.04	0.01	-0.01	0.00	-0.04
Hip Muscle Ins X Iliopsoas	0.01	0.11	-0.01	0.01	0.09	0.10	-0.01	0.01	0.02
Rel_Flex	0.02	0.02	0.00	0.00	0.01	0.01	0.00	0.00	-0.03
Rel_Abd	0.06	-0.01	0.00	-0.01	0.00	0.00	0.01	-0.01	-0.03
Rel_Rot	-0.02	0.02	0.00	0.00	0.06	-0.01	0.00	0.00	-0.06
Flexion_e	0.01	0.02	0.00	0.01	-0.03	-0.02	-0.01	0.01	0.01
Abduction_e	0.05	0.01	0.00	0.00	-0.01	0.02	0.00	0.00	-0.07
E_Rotation_e	0.02	0.02	0.00	0.00	0.01	0.02	0.00	0.00	-0.04
Percentage_Of_Dislocation		0.00	0.00	0.00	0.02	-0.01	0.00	0.00	0.01
Leg Centroid x		0.02	0.00	0.00	-0.02	-0.04	0.00	0.00	0.07
Leg Centroid y		0.02	0.00	0.00	-0.02	-0.05	0.00	0.00	0.07
Leg Centroid z		0.02	0.00	0.00	-0.02	-0.05	0.00	0.00	0.07
Sum_Forces x		0.47	-0.02	-0.48	0.41	0.71	0.49	-0.48	-0.02
Sum_Forces y		0.68	-0.03	-0.37	0.83	0.00	0.39	-0.38	-0.02
Sum_Forces z		0.37	-0.02	0.03	0.00	0.98	-0.01	0.03	0.01
Sum_Forces tot			-0.04	-0.37	0.49	0.47	0.39	-0.37	0.01
Sum_Moments x			-0.03	-0.32	0.66	-0.06	0.33	-0.32	-0.03
Sum_Moments y			0.01	0.67	-0.70	-0.02	-0.69	0.68	0.04
Sum_Moments z			-0.02	0.03	0.53	0.25	-0.01	0.03	0.02
FP_Perc_Along_Femur				0.01	-0.03	-0.02	-0.02	0.01	0.01
Sum_ForcesFP x					-0.45	0.03	-1.00	1.00	0.02
Sum_ForcesFP y						0.00	0.47	-0.45	-0.02
Sum_ForcesFP z							-0.01	0.03	0.01
Sum_ForcesFP tot								-1.00	-0.02
ProjectedFoverPath									0.02
Sum_MomentsFP x									-0.03
Sum_MomentsFP y									0.00
Sum_MomentsFP z									0.01
% of total force in pat direction									

Table 19: Pearson Correlation Matrix for Graf type IV direct path

Pearson Correlations	Percentage Of Dislocation	Sum Forces tot	FP Perc Along Femur	Sum Forces FP x	Sum Forces FP y	Sum Forces FP z	Sum Forces FP tot	Projected F over Path	% of total force in pat direction
Area Iliopsoas	-0.05	0.01	0.00	0.01	0.01	-0.02	0.01	0.01	-0.02
Area Pectineus	-0.05	0.02	0.00	0.02	0.02	-0.02	0.02	0.02	-0.12
Area Sartorius	-0.05	0.02	0.00	0.01	0.01	0.00	0.02	0.01	0.03
Area Rectus Femoris	-0.08	0.02	0.00	0.02	0.02	-0.01	0.02	0.02	0.01
Area Adductor Longus	-0.03	0.01	0.00	0.01	0.01	-0.01	0.01	0.01	0.09
Area Adductor Brevis	-0.05	-0.01	0.00	-0.01	-0.01	0.00	-0.01	-0.01	-0.07
Area Adductor Magnus Minimus	0.04	0.00	0.00	0.00	0.00	0.00	0.00	0.00	0.03
Area Adductor Magnus Middle	-0.02	0.00	0.00	0.01	0.01	-0.02	0.00	0.01	0.06
Area Adductor Magnus Posterior	0.00	0.02	0.00	0.02	0.02	-0.02	0.02	0.02	-0.02
Area Gracilis	-0.07	0.02	0.00	0.02	0.02	-0.02	0.02	0.02	0.01
Area Gluteus Max	-0.01	-0.01	0.00	0.00	-0.01	0.00	-0.01	0.00	-0.01
Area Gluteus Medius Anterior	-0.01	0.02	0.00	0.02	0.02	-0.02	0.02	0.02	-0.03
Area Gluteus Medius Middle	-0.15	0.01	0.00	0.01	0.01	-0.01	0.01	0.01	-0.01
Area Gluteus Medius Posterior	0.00	0.02	0.00	0.02	0.02	-0.01	0.02	0.02	-0.05
Area Gluteus Minimus Anterior	-0.01	0.02	0.00	0.02	0.02	-0.01	0.02	0.02	0.02
Area Gluteus Minimus Middle	-0.02	-0.01	0.00	-0.01	-0.01	0.00	-0.01	-0.01	-0.02
Area Gluteus Minimus Posterior	-0.05	-0.01	0.00	0.00	0.00	0.00	-0.01	0.00	-0.04
Area Tensor Fascia Lata	-0.09	0.01	0.00	0.01	0.01	-0.01	0.01	0.01	-0.01
Area Piriformis	-0.05	0.00	0.00	0.00	0.00	0.01	0.00	0.00	-0.01
Area Obturator Internus	0.09	0.02	0.00	0.02	0.02	-0.01	0.02	0.02	-0.10
Area Gemellus Superior	0.00	0.02	0.00	0.02	0.02	-0.01	0.02	0.02	0.00
Area Gemellus Inferior	-0.06	0.01	0.00	0.01	0.01	-0.01	0.01	0.01	-0.02
Area Quadratus Femoris	0.05	0.00	0.00	0.00	0.00	0.01	0.00	0.00	-0.05
Area Obturator Externus	0.06	0.01	0.00	0.01	0.01	-0.01	0.01	0.01	-0.12
Area Biceps Femoris (Long Head)	-0.05	0.01	0.00	0.02	0.02	-0.03	0.01	0.02	-0.03
Area Semitendinosus	0.01	-0.01	0.00	-0.01	-0.01	0.02	-0.01	-0.01	0.01
Area Semimembranosus	-0.02	0.00	0.00	0.00	0.00	0.00	0.00	0.00	0.02

Pearson Correlations	Percentage Of Dislocation	Sum Forces tot	FP Perc Along Femur	Sum Forces FP x	Sum Forces FP y	Sum Forces FP z	Sum Forces FP tot	Projected F over Path	% of total force in pat direction
Femur.Length	0.03	0.02	0.00	0.02	0.02	-0.02	0.02	0.02	0.00
Femur.L_Trochanteric	-0.01	0.01	0.00	0.01	0.01	-0.01	0.01	0.01	-0.09
Femur.Shaft_Width	-0.01	0.01	0.00	0.01	0.01	-0.01	0.01	0.01	0.07
Femur.Deviation_Angle	-0.02	-0.01	-0.01	-0.01	-0.01	0.01	-0.01	-0.01	0.04
Femur.Sagittal_Bowing_Ang	-0.08	0.01	0.00	0.01	0.01	-0.01	0.01	0.01	0.06
Femur.Coronal_Bowing_Ang	-0.09	0.00	0.00	0.00	0.00	0.00	0.00	0.00	-0.05
Femur.Head_Diam	-0.09	0.00	0.00	0.00	0.00	0.00	0.00	0.00	0.01
Femur.Anteversion_Angle	0.05	-0.01	0.00	-0.01	-0.01	0.01	-0.01	-0.01	0.04
Femur.Incline_Angle	-0.02	0.03	0.00	0.03	0.03	-0.03	0.03	0.03	0.06
Femur.Condyle_Diameter	-0.06	-0.01	0.00	-0.02	-0.02	0.02	-0.01	-0.02	-0.05
Femur.Condyle_Spacing	-0.01	0.01	0.00	0.01	0.01	0.00	0.01	0.01	0.03
Femur.Epicondyle_Dist	-0.02	0.01	0.00	0.01	0.01	-0.02	0.01	0.01	0.00
Femur.Head_Module_E	0.07	0.00	0.00	-0.01	0.00	0.02	0.00	-0.01	-0.04
Femur.Head_Module_v	0.05	-0.02	0.00	-0.02	-0.02	0.02	-0.02	-0.02	0.04
Hip.Acetabulum_Diam	-0.04	-0.01	0.00	-0.01	-0.01	0.00	-0.01	-0.01	-0.01
Hip.Acetabulum_Module_E	-0.02	0.00	0.00	0.00	0.00	0.00	0.00	0.00	-0.02
Hip.Acetabulum_Module_v	-0.05	0.00	0.00	0.00	0.00	0.00	0.00	0.00	-0.02

Pearson Correlations	Percentage Of Dislocation	Sum Forces tot	FP Perc Along Femur	Sum Forces FP x	Sum Forces FP y	Sum Forces FP z	Sum Forces FP tot	Projected F over Path	% of total force in pat direction
3D_Rat Iliopsoas	0.02	0.01	0.00	0.01	0.01	0.00	0.01	0.01	0.04
3D_Rat Pectineus	0.10	-0.01	0.00	-0.01	-0.01	0.01	-0.01	-0.01	-0.06
3D_Rat Sartorius	0.02	-0.01	0.00	-0.01	-0.01	0.01	-0.01	-0.01	-0.09
3D_Rat Rectus Femoris	-0.08	0.01	0.00	0.02	0.01	-0.02	0.01	0.02	0.08
3D_Rat Adductor Longus	-0.08	0.01	0.00	0.01	0.01	-0.01	0.01	0.01	-0.08
3D_Rat Adductor Brevis	-0.06	0.01	0.00	0.01	0.01	-0.01	0.01	0.01	-0.08
3D_Rat Adductor Magnus Minimus	0.06	0.01	0.00	0.01	0.01	0.00	0.01	0.01	-0.07
3D_Rat Adductor Magnus Middle	-0.04	-0.01	0.00	-0.01	-0.01	0.01	-0.01	-0.01	-0.04
3D_Rat Adductor Magnus Posterior	0.11	0.00	0.00	0.00	0.00	-0.01	0.00	0.00	-0.03
3D_Rat Gracilis	0.05	0.01	0.00	0.01	0.01	-0.01	0.01	0.01	-0.02
3D_Rat Gluteus Max	-0.01	0.00	0.00	0.00	0.00	0.01	0.00	0.00	0.06
3D_Rat Gluteus Medius Anterior	0.08	0.00	0.00	0.00	0.00	0.01	0.01	0.00	-0.04
3D_Rat Gluteus Medius Middle	0.01	0.02	0.00	0.02	0.02	-0.03	0.02	0.02	-0.07
3D_Rat Gluteus Medius Posterior	-0.04	0.01	-0.01	0.01	0.01	-0.01	0.01	0.01	0.00
3D_Rat Gluteus Minimus Anterior	0.04	-0.02	0.00	-0.02	-0.02	0.02	-0.02	-0.02	-0.03
3D_Rat Gluteus Minimus Middle	-0.06	0.02	0.00	0.02	0.02	-0.02	0.02	0.02	0.07
3D_Rat Gluteus Minimus Posterior	-0.03	-0.01	0.00	-0.01	-0.01	0.01	-0.01	-0.01	0.06
3D_Rat Tensor Fascia Lata	-0.04	0.01	0.00	0.01	0.01	-0.01	0.01	0.01	0.00
3D_Rat Piriformis	-0.06	-0.01	0.00	-0.01	-0.01	0.02	-0.01	-0.02	0.02
3D_Rat Obturator Internus	-0.03	0.01	0.00	0.00	0.01	0.01	0.01	0.00	-0.07
3D_Rat Gemellus Superior	-0.02	0.02	0.00	0.01	0.01	-0.01	0.02	0.01	-0.01
3D_Rat Gemellus Inferior	-0.08	0.01	0.00	0.01	0.01	-0.02	0.01	0.01	-0.09
3D_Rat Quadratus Femoris	0.05	0.00	0.00	0.00	0.00	-0.01	0.00	0.00	0.05
3D_Rat Obturator Externus	-0.13	-0.01	0.00	-0.01	-0.01	0.01	-0.01	-0.01	-0.01
3D_Rat Biceps Femoris (Long Head)	-0.02	0.01	0.00	0.00	0.00	0.00	0.01	0.00	0.00
3D_Rat Semitendinosus	0.03	0.01	0.00	0.01	0.01	-0.01	0.01	0.01	-0.03
3D_Rat Semimembranosus	-0.01	0.00	0.00	0.00	0.00	-0.01	0.00	0.00	0.01

Pearson Correlations	Percentage Of Dislocation	Sum Forces tot	FP Perc Along Femur	Sum Forces FP x	Sum Forces FP y	Sum Forces FP z	Sum Forces FP tot	Projected F over Path	% of total force in pat direction
3D_Rot Iliopsoas	0.01	0.01	0.00	0.01	0.01	-0.02	0.01	0.01	-0.03
3D_Rot Pectineus	-0.02	-0.01	0.00	-0.01	-0.01	0.01	-0.01	-0.01	-0.03
3D_Rot Sartorius	0.11	0.00	0.00	0.00	0.00	0.01	0.00	0.00	0.02
3D_Rot Rectus Femoris	0.00	0.01	0.00	0.01	0.01	-0.02	0.00	0.01	-0.02
3D_Rot Adductor Longus	-0.03	0.03	0.00	0.03	0.03	-0.03	0.03	0.03	0.00
3D_Rot Adductor Brevis	-0.03	0.00	0.00	0.00	0.00	0.01	0.00	0.00	0.00
3D_Rot Adductor Magnus Minimus	-0.06	0.00	0.00	0.00	0.00	0.01	0.00	0.00	0.00
3D_Rot Adductor Magnus Middle	0.03	0.01	0.00	0.00	0.00	0.01	0.01	0.00	-0.05
3D_Rot Adductor Magnus Posterior	0.07	0.01	0.00	0.01	0.01	-0.02	0.01	0.01	-0.04
3D_Rot Gracilis	0.02	0.00	0.00	0.00	0.00	0.00	0.00	0.00	0.09
3D_Rot Gluteus Max	-0.04	0.02	0.00	0.02	0.02	-0.01	0.02	0.02	-0.03
3D_Rot Gluteus Medius Anterior	0.00	0.01	0.00	0.01	0.01	-0.02	0.01	0.01	0.00
3D_Rot Gluteus Medius Middle	-0.02	0.00	0.00	0.00	0.00	0.00	0.00	0.00	-0.02
3D_Rot Gluteus Medius Posterior	0.08	0.00	0.00	-0.01	0.00	0.01	0.00	-0.01	0.00
3D_Rot Gluteus Minimus Anterior	0.04	0.00	0.00	0.00	0.00	0.00	0.00	0.00	0.02
3D_Rot Gluteus Minimus Middle	0.04	-0.02	0.00	-0.02	-0.02	0.01	-0.02	-0.02	0.09
3D_Rot Gluteus Minimus Posterior	0.14	-0.01	0.00	-0.01	-0.01	0.01	-0.01	-0.01	-0.03
3D_Rot Tensor Fascia Lata	-0.04	-0.01	0.00	-0.02	-0.02	0.02	-0.01	-0.02	0.13
3D_Rot Piriformis	-0.06	0.01	0.00	0.01	0.01	0.00	0.01	0.01	0.00
3D_Rot Obturator Internus	-0.02	-0.02	0.00	-0.02	-0.02	0.01	-0.02	-0.02	0.07
3D_Rot Gemellus Superior	0.07	0.00	0.00	0.00	0.00	0.00	0.00	0.00	0.01
3D_Rot Gemellus Inferior	-0.02	-0.01	0.00	-0.01	-0.01	0.01	-0.01	-0.01	0.02
3D_Rot Quadratus Femoris	-0.07	0.02	0.00	0.02	0.02	-0.01	0.02	0.02	-0.06
3D_Rot Obturator Externus	0.00	-0.03	0.00	-0.02	-0.03	0.02	-0.03	-0.02	0.06
3D_Rot Biceps Femoris (Long Head)	0.01	0.01	0.00	0.01	0.01	-0.01	0.00	0.01	0.08
3D_Rot Semitendinosus	-0.01	-0.01	0.00	-0.01	-0.01	0.01	-0.01	-0.01	-0.05
3D_Rot Semimembranosus	-0.03	0.00	0.00	0.00	0.00	0.00	0.00	0.00	0.02

Pearson Correlations	Percentage Of Dislocation	Sum Forces tot	FP Perc Along Femur	Sum Forces FP x	Sum Forces FP y	Sum Forces FP z	Sum Forces FP tot	Projected F over Path	% of total force in pat direction
M_L_Ratio Iliopsoas	0.00	0.00	0.00	0.00	0.00	0.00	0.00	0.00	-0.01
M_L_Ratio Pectineus	0.03	0.01	0.00	0.01	0.01	-0.02	0.01	0.01	-0.03
M_L_Ratio Sartorius	-0.05	-0.01	0.00	-0.01	-0.01	0.00	-0.01	-0.01	0.07
M_L_Ratio Rectus Femoris	0.01	0.00	0.00	0.00	0.00	0.00	0.00	0.00	0.00
M_L_Ratio Adductor Longus	-0.04	-0.01	0.00	-0.01	-0.01	0.01	-0.01	-0.01	0.01
M_L_Ratio Adductor Brevis	0.03	-0.02	0.00	-0.01	-0.02	0.00	-0.02	-0.01	0.03
M_L_Ratio Adductor Magnus Minimus	-0.10	0.00	0.00	0.00	0.00	0.01	0.00	0.00	0.05
M_L_Ratio Adductor Magnus Middle	-0.10	0.01	0.00	0.01	0.01	-0.01	0.01	0.01	-0.05
M_L_Ratio Adductor Magnus Posterior	0.04	-0.01	0.00	-0.01	-0.01	0.01	-0.01	-0.01	0.02
M_L_Ratio Gracilis	0.04	-0.02	0.00	-0.02	-0.02	0.02	-0.02	-0.02	0.03
M_L_Ratio Gluteus Max	0.05	0.01	0.00	0.01	0.01	0.00	0.01	0.01	-0.06
M_L_Ratio Gluteus Medius Anterior	0.00	-0.01	0.00	-0.01	-0.01	0.01	-0.01	-0.01	-0.09
M_L_Ratio Gluteus Medius Middle	0.10	0.01	0.00	0.01	0.01	-0.01	0.01	0.01	0.03
M_L_Ratio Gluteus Medius Posterior	0.07	0.00	0.00	0.00	0.00	0.00	0.00	0.00	-0.05
M_L_Ratio Gluteus Minimus Anterior	0.04	-0.01	0.00	-0.01	-0.01	0.00	-0.01	-0.01	0.03
M_L_Ratio Gluteus Minimus Middle	-0.08	0.01	0.00	0.01	0.01	-0.01	0.01	0.01	0.05
M_L_Ratio Gluteus Minimus Posterior	-0.03	0.01	0.00	0.01	0.01	-0.01	0.01	0.01	0.02
M_L_Ratio Tensor Fascia Lata	0.04	0.00	0.00	0.00	0.00	0.02	0.00	-0.01	0.13
M_L_Ratio Piriformis	-0.05	-0.01	0.00	-0.01	-0.01	0.01	-0.01	-0.01	0.00
M_L_Ratio Obturator Internus	0.05	0.01	0.00	0.00	0.00	0.00	0.01	0.00	0.09
M_L_Ratio Gemellus Superior	-0.09	-0.01	0.00	-0.01	-0.01	0.01	-0.01	-0.01	0.09
M_L_Ratio Gemellus Inferior	0.00	0.02	0.00	0.03	0.03	-0.03	0.02	0.03	-0.02
M_L_Ratio Quadratus Femoris	-0.14	0.00	0.00	-0.01	0.00	0.01	0.00	-0.01	0.05
M_L_Ratio Obturator Externus	-0.09	0.00	0.00	0.00	0.00	-0.01	0.00	0.00	0.01
M_L_Ratio Biceps Femoris (Long Head)	0.06	0.00	0.00	0.00	0.00	-0.01	0.00	0.00	-0.06
M_L_Ratio Semitendinosus	0.03	0.01	0.00	0.01	0.01	0.00	0.01	0.01	0.04
M_L_Ratio Semimembranosus	-0.02	-0.02	0.00	-0.02	-0.02	0.02	-0.02	-0.02	0.12

Pearson Correlations	Percentage Of Dislocation	Sum Forces tot	FP Perc Along Femur	Sum Forces FP x	Sum Forces FP y	Sum Forces FP z	Sum Forces FP tot	Projected F over Path	% of total force in pat direction
Flexion_i	0.04	-0.01	0.00	-0.01	-0.01	0.02	-0.01	-0.01	-0.17
Abduction_i	-0.03	0.01	0.00	0.01	0.01	0.00	0.01	0.01	-0.18
E_Rotation_i	0.00	0.00	0.00	0.00	0.00	0.00	0.00	0.00	-0.08
BWeight	-0.03	-0.01	0.00	-0.01	-0.01	0.01	-0.01	-0.01	0.07
Leg_Perc_Weight	0.12	0.02	0.00	0.02	0.02	-0.03	0.02	0.02	-0.07
PreStretch	0.09	0.01	-0.01	0.01	0.01	-0.01	0.01	0.01	0.08
Hip Muscle Ins X Iliopsoas	0.03	0.00	-0.01	0.00	0.00	0.00	0.00	0.00	-0.12
Rel_Flex	-0.03	0.02	0.00	0.02	0.02	-0.02	0.02	0.02	-0.06
Rel_Abd	-0.03	0.01	0.00	0.01	0.01	-0.01	0.01	0.01	-0.05
Rel_Rot	-0.08	-0.01	0.00	-0.01	-0.01	0.00	-0.01	-0.01	-0.01
Flexion_e	0.03	0.02	-0.01	0.02	0.02	-0.01	0.02	0.02	0.01
Abduction_e	0.04	0.01	0.00	0.01	0.01	0.00	0.01	0.01	0.03
E_Rotation_e	0.00	-0.01	0.00	-0.01	-0.01	0.00	-0.01	-0.01	0.03
Percentage_Of_Dislocation	1.00	0.01	0.00	0.01	0.01	-0.01	0.01	0.01	0.00
Leg Centroid x		-0.02	0.00	-0.02	-0.02	0.01	-0.02	-0.02	-0.02
Leg Centroid y		-0.02	0.00	-0.02	-0.02	0.01	-0.02	-0.02	-0.02
Leg Centroid z		-0.02	0.00	-0.02	-0.02	0.01	-0.02	-0.02	-0.02
Sum_Forces x		0.99	-0.02	1.00	1.00	-0.87	0.99	1.00	0.02
Sum_Forces y		1.00	-0.02	1.00	1.00	-0.84	1.00	1.00	0.01
Sum_Forces z		-0.80	0.00	-0.88	-0.84	1.00	-0.79	-0.89	-0.02
Sum_Forces tot		1.00	-0.02	0.99	1.00	-0.80	1.00	0.99	0.01
Sum_Moments x			-0.02	1.00	1.00	-0.86	0.99	1.00	0.01
Sum_Moments y			0.02	-1.00	-1.00	0.88	-0.99	-1.00	-0.02
Sum_Moments z			-0.02	1.00	1.00	-0.85	0.99	1.00	0.01
FP_Perc_Along_Femur			1.00	-0.02	-0.02	0.00	-0.02	-0.02	-0.05
Sum_ForcesFP x				1.00	1.00	-0.88	0.99	1.00	0.02
Sum_ForcesFP y					1.00	-0.84	1.00	1.00	0.01
Sum_ForcesFP z						1.00	-0.79	-0.89	-0.02
Sum_ForcesFP tot							1.00	0.98	0.01
ProjectedFoverPath								1.00	0.02
Sum_MomentsFP x									0.01
Sum_MomentsFP y									0.00
Sum_MomentsFP z									0.02
% of total force in pat direction									1.00

APPENDIX B: SPEARMAN RANK CORRELATION MATRIX

Table 20: Spearman Rank Correlation Matrix for Graf type I

Spearman Rank Correlations	Percentage Of Dislocation	Sum Forces tot	FP Perc Along Femur	Sum Forces FP x	Sum Forces FP y	Sum Forces FP z	Sum Forces FP tot	Projected F over Path	% of total force in pat direction
Area Iliopsoas	-0.08	0.06	0.00	0.03	0.06	0.04	0.06	-0.03	-0.03
Area Pectineus	0.15	0.14	0.01	-0.03	0.14	0.11	0.14	-0.11	-0.09
Area Sartorius	0.02	0.02	0.00	-0.01	-0.07	-0.01	0.03	0.02	-0.02
Area Rectus Femoris	0.01	0.04	0.00	0.06	0.05	0.02	0.04	-0.03	-0.08
Area Adductor Longus	0.04	0.13	0.01	-0.11	0.06	0.04	0.14	-0.05	-0.03
Area Adductor Brevis	0.02	0.03	0.01	-0.12	-0.04	0.11	0.03	-0.07	-0.10
Area Adductor Magnus Minimus	-0.02	0.16	0.00	-0.13	0.01	0.05	0.15	0.03	0.02
Area Adductor Magnus Middle	-0.05	0.06	0.01	-0.04	0.10	-0.11	0.10	0.08	0.07
Area Adductor Magnus Posterior	-0.17	-0.07	0.01	0.11	-0.05	0.13	-0.06	-0.12	-0.17
Area Gracilis	-0.12	0.02	0.00	0.07	0.02	-0.05	0.03	-0.01	-0.03
Area Gluteus Max	0.08	-0.03	0.00	0.04	0.01	0.12	-0.03	-0.13	-0.13
Area Gluteus Medius Anterior	-0.04	0.18	0.00	-0.10	0.13	0.05	0.16	0.03	0.01
Area Gluteus Medius Middle	0.00	0.01	0.01	0.14	0.14	0.06	0.02	-0.14	-0.14
Area Gluteus Medius Posterior	-0.03	0.09	0.02	0.03	0.03	0.18	0.11	-0.20	-0.18
Area Gluteus Minimus Anterior	0.04	0.17	0.00	-0.24	-0.03	0.19	0.18	-0.11	-0.09
Area Gluteus Minimus Middle	-0.03	0.05	0.01	0.09	0.09	0.02	0.05	0.07	0.04
Area Gluteus Minimus Posterior	-0.15	0.09	0.01	0.01	0.06	-0.01	0.09	-0.01	0.02
Area Tensor Fascia Lata	-0.01	0.12	0.01	-0.04	0.05	0.08	0.13	-0.04	-0.07
Area Piriformis	-0.01	0.10	0.00	-0.05	0.03	0.07	0.10	0.00	-0.01
Area Obturator Internus	-0.16	0.10	0.01	-0.06	0.01	0.03	0.12	-0.06	-0.10
Area Gemellus Superior	0.00	-0.05	0.00	0.06	0.10	-0.05	-0.04	0.00	-0.01
Area Gemellus Inferior	-0.06	0.09	0.01	0.02	0.06	0.08	0.09	-0.06	-0.08
Area Quadratus Femoris	-0.14	-0.13	-0.01	0.09	-0.31	-0.01	-0.12	0.03	0.01
Area Obturator Externus	-0.04	-0.05	0.00	0.14	-0.03	-0.10	-0.05	0.00	0.06
Area Biceps Femoris (Long Head)	-0.02	0.13	0.00	-0.05	0.05	0.00	0.14	-0.07	-0.11
Area Semitendinosus	-0.02	-0.04	0.01	0.10	-0.07	0.00	-0.02	-0.02	-0.06
Area Semimembranosus	-0.08	-0.01	0.01	0.07	0.04	0.04	0.01	-0.08	-0.09

Spearman Rank Correlations	Percentage Of Dislocation	Sum Forces tot	FP Perc Along Femur	Sum Forces FP x	Sum Forces FP y	Sum Forces FP z	Sum Forces FP tot	Projected F over Path	% of total force in pat direction
Femur.Length	-0.01	0.12	0.00	-0.03	0.08	0.02	0.12	0.05	0.05
Femur.L_Trochanteric	0.02	0.09	-0.01	0.05	-0.01	-0.05	0.08	0.03	0.05
Femur.Shaft_Width	0.34	0.01	0.00	0.10	0.10	0.13	0.00	-0.22	-0.19
Femur.Deviation_Angle	0.08	-0.09	0.01	-0.13	-0.08	-0.16	-0.07	0.13	0.13
Femur.Sagittal_Bowing_Ang	-0.12	-0.06	0.00	0.06	0.07	-0.12	-0.07	0.04	0.07
Femur.Coronal_Bowing_Ang	-0.15	-0.01	0.00	0.00	0.00	-0.10	-0.01	0.07	0.06
Femur.Head_Diam	0.09	-0.01	-0.01	0.00	-0.01	-0.15	0.00	0.00	0.03
Femur.Anteversion_Angle	0.08	-0.09	-0.01	0.15	-0.02	0.31	-0.08	-0.30	-0.36
Femur.Incline_Angle	-0.09	0.12	0.00	-0.06	0.04	0.08	0.13	-0.06	-0.15
Femur.Condyle_Diameter	0.03	0.05	0.00	-0.07	0.07	0.02	0.03	0.04	0.02
Femur.Condyle_Spacing	0.07	0.09	-0.01	0.00	0.09	0.00	0.08	0.00	0.02
Femur.Epicondyle_Dist	-0.10	-0.05	-0.01	0.04	0.03	-0.03	-0.07	0.05	0.04
Femur.Head_Module_E	-0.01	0.01	0.00	0.05	0.00	-0.12	0.01	0.02	0.04
Femur.Head_Module_v	0.13	0.09	0.01	-0.16	0.06	0.01	0.11	0.03	-0.02
Hip.Acetabulum_Diam	-0.08	0.05	0.00	-0.03	0.04	0.03	0.05	0.01	-0.03
Hip.Acetabulum_Module_E	-0.02	0.04	0.01	-0.16	0.10	-0.09	0.04	0.26	0.22
Hip.Acetabulum_Module_v	0.10	-0.07	0.00	0.12	-0.06	0.09	-0.07	-0.09	-0.09

Spearman Rank Correlations	Percentage Of Dislocation	Sum Forces tot	FP Perc Along Femur	Sum Forces FP x	Sum Forces FP y	Sum Forces FP z	Sum Forces FP tot	Projected F over Path	% of total force in pat direction
3D_Rat Iliopsoas	-0.11	-0.06	0.00	0.06	0.05	0.00	-0.07	0.07	0.01
3D_Rat Pectineus	0.15	-0.01	0.01	0.04	-0.09	0.03	0.00	-0.07	-0.08
3D_Rat Sartorius	-0.09	-0.02	0.00	-0.03	-0.04	-0.22	-0.01	0.21	0.22
3D_Rat Rectus Femoris	-0.12	0.02	0.01	-0.11	0.10	-0.18	0.06	0.19	0.11
3D_Rat Adductor Longus	-0.02	-0.24	0.00	0.13	-0.19	-0.05	-0.22	-0.08	-0.09
3D_Rat Adductor Brevis	0.07	-0.16	0.00	0.23	-0.08	0.05	-0.16	-0.16	-0.11
3D_Rat Adductor Magnus Minimus	-0.05	0.03	0.00	-0.05	0.05	-0.01	0.03	0.01	0.06
3D_Rat Adductor Magnus Middle	0.03	-0.25	0.01	0.07	-0.12	-0.13	-0.21	0.05	0.04
3D_Rat Adductor Magnus Posterior	-0.21	-0.03	0.01	0.01	-0.16	0.10	-0.02	-0.06	-0.07
3D_Rat Gracilis	0.01	-0.01	0.00	0.00	-0.07	0.14	-0.01	-0.20	-0.18
3D_Rat Gluteus Max	-0.08	-0.07	-0.01	0.12	0.01	0.00	-0.08	-0.09	-0.02
3D_Rat Gluteus Medius Anterior	0.20	0.05	-0.01	0.04	0.03	0.16	0.03	-0.13	-0.15
3D_Rat Gluteus Medius Middle	-0.02	0.03	-0.01	0.02	0.10	-0.05	0.03	0.10	0.06
3D_Rat Gluteus Medius Posterior	-0.08	0.02	0.00	-0.01	-0.01	-0.05	0.03	0.13	0.07
3D_Rat Gluteus Minimus Anterior	0.04	0.21	0.00	-0.20	0.03	-0.01	0.21	0.08	0.08
3D_Rat Gluteus Minimus Middle	0.13	-0.06	0.01	-0.07	-0.02	-0.01	-0.06	-0.04	0.02
3D_Rat Gluteus Minimus Posterior	0.10	-0.04	0.00	0.12	0.09	-0.05	-0.03	-0.08	-0.07
3D_Rat Tensor Fascia Lata	-0.01	0.00	0.01	-0.03	-0.01	-0.22	0.00	0.15	0.11
3D_Rat Piriformis	0.05	0.04	-0.01	0.08	0.12	-0.17	0.02	0.10	0.14
3D_Rat Obturator Internus	0.15	-0.09	-0.01	0.04	-0.14	-0.02	-0.10	0.03	-0.02
3D_Rat Gemellus Superior	0.00	-0.11	0.02	0.10	0.03	-0.02	-0.09	0.03	0.02
3D_Rat Gemellus Inferior	0.09	0.01	0.00	-0.03	-0.07	-0.01	0.02	0.01	0.03
3D_Rat Quadratus Femoris	0.06	-0.08	-0.01	0.14	0.01	-0.08	-0.10	-0.06	-0.01
3D_Rat Obturator Externus	-0.06	0.01	0.01	0.04	-0.01	0.07	0.01	-0.05	-0.02
3D_Rat Biceps Femoris (Long Head)	-0.07	0.01	0.00	-0.17	-0.05	-0.03	0.02	-0.03	0.02
3D_Rat Semitendinosus	-0.12	0.01	0.01	-0.03	-0.05	0.10	0.01	-0.06	-0.06
3D_Rat Semimembranosus	-0.07	0.02	0.01	-0.03	-0.06	0.05	0.01	-0.01	-0.07

Spearman Rank Correlations	Percentage Of Dislocation	Sum Forces tot	FP Perc Along Femur	Sum Forces FP x	Sum Forces FP y	Sum Forces FP z	Sum Forces FP tot	Projected F over Path	% of total force in pat direction
3D_Rot Iliopsoas	0.01	0.00	0.01	-0.05	-0.14	0.08	0.01	-0.02	-0.01
3D_Rot Pectineus	0.07	-0.12	0.00	0.06	-0.08	-0.11	-0.11	0.04	0.08
3D_Rot Sartorius	0.06	-0.02	0.01	-0.01	-0.04	0.05	-0.02	-0.10	-0.04
3D_Rot Rectus Femoris	-0.07	0.08	0.00	-0.07	0.06	0.00	0.08	-0.01	0.01
3D_Rot Adductor Longus	0.03	0.07	0.01	-0.09	0.08	0.00	0.07	0.04	0.00
3D_Rot Adductor Brevis	0.07	-0.07	0.00	0.02	-0.01	-0.02	-0.05	0.02	0.05
3D_Rot Adductor Magnus Minimus	-0.02	-0.12	0.01	0.13	-0.07	-0.18	-0.11	0.03	0.02
3D_Rot Adductor Magnus Middle	0.30	0.01	-0.01	-0.02	0.07	-0.01	-0.01	0.03	0.03
3D_Rot Adductor Magnus Posterior	-0.04	-0.02	-0.01	0.03	-0.04	-0.01	-0.01	0.00	-0.01
3D_Rot Gracilis	-0.05	0.11	-0.01	0.00	0.05	0.22	0.11	-0.13	-0.21
3D_Rot Gluteus Max	-0.01	-0.01	0.00	0.17	0.03	0.04	-0.02	-0.06	-0.05
3D_Rot Gluteus Medius Anterior	-0.06	-0.09	0.01	0.07	-0.06	-0.15	-0.07	0.00	0.02
3D_Rot Gluteus Medius Middle	-0.08	-0.09	0.00	0.09	-0.02	0.04	-0.09	-0.04	-0.04
3D_Rot Gluteus Medius Posterior	-0.11	-0.07	0.00	0.16	0.09	-0.05	-0.07	-0.01	-0.01
3D_Rot Gluteus Minimus Anterior	-0.02	-0.07	-0.01	0.09	-0.06	0.08	-0.08	-0.03	-0.09
3D_Rot Gluteus Minimus Middle	0.08	-0.08	0.00	0.06	-0.05	-0.10	-0.09	0.04	0.05
3D_Rot Gluteus Minimus Posterior	-0.13	-0.12	0.00	0.02	-0.12	0.00	-0.12	0.01	0.01
3D_Rot Tensor Fascia Lata	0.00	0.01	0.01	-0.08	-0.02	-0.19	0.03	0.07	0.17
3D_Rot Piriformis	0.04	0.04	0.00	0.07	0.12	-0.16	0.04	0.15	0.13
3D_Rot Obturator Internus	-0.04	-0.09	0.00	0.01	0.01	-0.10	-0.08	0.14	0.09
3D_Rot Gemellus Superior	-0.05	-0.15	0.00	-0.02	-0.10	-0.01	-0.14	-0.13	-0.05
3D_Rot Gemellus Inferior	0.15	-0.08	0.00	0.05	-0.09	-0.03	-0.09	-0.03	0.02
3D_Rot Quadratus Femoris	-0.06	0.04	-0.01	0.01	0.23	-0.11	0.03	0.12	0.13
3D_Rot Obturator Externus	-0.31	-0.14	0.00	0.02	-0.18	0.03	-0.13	0.01	0.01
3D_Rot Biceps Femoris (Long Head)	0.10	-0.13	0.00	0.17	-0.06	0.17	-0.11	-0.22	-0.23
3D_Rot Semitendinosus	0.17	0.05	0.00	0.06	0.12	0.27	0.04	-0.16	-0.13
3D_Rot Semimembranosus	-0.07	0.12	0.00	-0.06	0.07	0.02	0.13	-0.01	-0.07

Spearman Rank Correlations	Percentage Of Dislocation	Sum Forces tot	FP Perc Along Femur	Sum Forces FP x	Sum Forces FP y	Sum Forces FP z	Sum Forces FP tot	Projected F over Path	% of total force in pat direction
M_L_Ratio Iliopsoas	0.10	0.10	0.00	-0.09	0.00	0.06	0.10	-0.06	-0.06
M_L_Ratio Pectineus	0.01	-0.10	-0.01	0.15	0.04	-0.04	-0.10	-0.05	-0.04
M_L_Ratio Sartorius	0.08	-0.17	0.00	0.13	-0.08	-0.05	-0.16	0.00	0.07
M_L_Ratio Rectus Femoris	0.02	0.01	0.00	0.06	-0.08	0.05	0.02	-0.13	-0.08
M_L_Ratio Adductor Longus	0.07	0.04	0.00	-0.06	0.08	0.01	0.02	0.05	0.05
M_L_Ratio Adductor Brevis	-0.06	-0.11	0.00	0.14	-0.11	0.11	-0.09	-0.20	-0.18
M_L_Ratio Adductor Magnus Minimus	0.09	-0.25	0.01	0.11	-0.24	-0.09	-0.21	-0.03	-0.01
M_L_Ratio Adductor Magnus Middle	-0.02	-0.07	0.00	0.08	-0.02	0.02	-0.07	-0.08	-0.09
M_L_Ratio Adductor Magnus Posterior	0.16	0.11	0.01	-0.08	0.18	0.04	0.12	0.00	-0.05
M_L_Ratio Gracilis	-0.12	0.09	0.00	-0.07	0.00	-0.03	0.07	0.08	0.10
M_L_Ratio Gluteus Max	0.11	0.10	0.00	-0.03	0.03	0.06	0.09	0.09	0.11
M_L_Ratio Gluteus Medius Anterior	-0.07	0.11	0.00	0.03	0.03	0.03	0.11	0.05	0.00
M_L_Ratio Gluteus Medius Middle	-0.06	0.02	-0.01	-0.08	-0.07	0.02	0.02	-0.02	-0.06
M_L_Ratio Gluteus Medius Posterior	0.01	-0.02	0.00	0.03	-0.01	-0.11	-0.03	0.02	0.08
M_L_Ratio Gluteus Minimus Anterior	-0.05	-0.05	-0.01	0.08	-0.05	0.01	-0.06	-0.10	-0.05
M_L_Ratio Gluteus Minimus Middle	0.07	-0.11	-0.01	0.09	-0.13	-0.09	-0.11	-0.01	-0.02
M_L_Ratio Gluteus Minimus Posterior	0.00	-0.02	-0.01	-0.02	-0.04	-0.04	-0.05	0.02	0.04
M_L_Ratio Tensor Fascia Lata	-0.02	0.09	0.01	-0.09	0.13	0.07	0.08	-0.01	-0.01
M_L_Ratio Piriformis	0.07	-0.02	0.00	0.07	-0.10	-0.03	-0.02	0.03	0.03
M_L_Ratio Obturator Internus	0.14	0.00	-0.01	-0.02	-0.04	-0.04	-0.01	0.09	0.09
M_L_Ratio Gemellus Superior	0.04	-0.16	0.00	0.03	-0.10	0.02	-0.16	0.00	-0.03
M_L_Ratio Gemellus Inferior	-0.04	-0.07	-0.02	0.05	-0.11	-0.22	-0.09	0.17	0.21
M_L_Ratio Quadratus Femoris	-0.27	-0.07	0.00	0.00	-0.26	-0.01	-0.06	0.00	-0.03
M_L_Ratio Obturator Externus	0.07	-0.04	0.01	-0.01	-0.02	0.07	-0.05	0.02	0.02
M_L_Ratio Biceps Femoris (Long Head)	0.06	0.06	-0.01	-0.08	-0.01	-0.11	0.07	0.12	0.07
M_L_Ratio Semitendinosus	0.11	0.03	0.00	-0.06	0.08	-0.07	0.03	0.10	0.11
M_L_Ratio Semimembranosus	0.01	-0.04	0.01	-0.03	-0.07	0.03	-0.03	0.01	-0.03

Spearman Rank Correlations	Percentage Of Dislocation	Sum Forces tot	FP Perc Along Femur	Sum Forces FP x	Sum Forces FP y	Sum Forces FP z	Sum Forces FP tot	Projected F over Path	% of total force in pat direction
Flexion_i	-0.03	0.22	0.00	-0.47	-0.18	-0.02	0.21	0.17	0.14
Abduction_i	0.04	0.32	0.01	-0.48	0.22	-0.15	0.33	0.29	0.29
E_Rotation_i	-0.05	0.15	0.01	-0.19	0.01	0.22	0.12	-0.13	-0.12
BWeight	-0.29	0.24	0.00	-0.18	0.12	-0.11	0.24	0.19	0.19
Leg_Perc_Weight	0.19	0.05	0.01	0.06	0.13	0.13	0.04	-0.14	-0.11
PreStretch	-0.10	-0.14	-0.01	-0.07	-0.43	-0.11	-0.12	0.03	0.00
Hip Muscle Ins x Iliopsoas	0.04	0.50	-0.02	-0.07	0.29	0.45	0.44	-0.36	-0.41
Rel_Flex	0.13	0.14	0.00	-0.14	0.17	0.10	0.13	-0.01	-0.01
Rel_Abd	0.04	0.16	0.01	-0.29	0.00	-0.09	0.16	0.12	0.14
Rel_Rot	0.08	0.03	0.00	0.10	0.20	-0.03	0.03	-0.04	0.01
Flexion_e	-0.01	-0.13	-0.01	0.05	-0.04	-0.01	-0.14	0.00	0.03
Abduction_e	-0.07	-0.16	0.00	0.06	-0.15	-0.11	-0.14	-0.02	0.00
E_Rotation_e	0.11	-0.06	0.01	0.15	0.06	0.30	-0.08	-0.27	-0.26
Percentage_Of_Dislocation	1.00	0.02	0.00	0.04	0.14	0.17	0.02	-0.15	-0.18
Leg Centroid x		0.05	0.00	-0.07	-0.02	-0.29	0.01	0.14	0.20
Leg Centroid y		0.04	0.00	-0.07	-0.03	-0.30	0.01	0.14	0.21
Leg Centroid z		0.04	0.00	-0.07	-0.03	-0.30	0.01	0.14	0.21
Sum_Forces x		-0.69	-0.01	0.95	-0.21	-0.03	-0.65	-0.33	-0.30
Sum_Forces y		0.65	0.00	-0.18	0.97	0.06	0.60	0.05	0.03
Sum_Forces z		0.24	-0.03	-0.01	0.05	0.97	0.18	-0.71	-0.75
Sum_Forces tot		1.00	0.00	-0.63	0.63	0.23	0.93	0.06	0.03
Sum_Moments x			0.01	-0.15	0.64	-0.43	0.35	0.32	0.34
Sum_Moments y			0.01	-0.86	0.08	-0.03	0.48	0.32	0.28
Sum_Moments z			0.00	0.43	0.42	0.15	0.03	-0.21	-0.21
FP_Perc_Along_Femur			1.00	-0.08	0.05	0.02	0.01	0.03	0.05
Sum_ForcesFP x				1.00	-0.21	-0.04	-0.67	-0.34	-0.31
Sum_ForcesFP y					1.00	0.07	0.64	0.06	0.03
Sum_ForcesFP z						1.00	0.22	-0.72	-0.75
Sum_ForcesFP tot							1.00	0.07	0.03
ProjectedFoverPath								1.00	0.91
Sum_MomentsFP x									0.34
Sum_MomentsFP y									-0.03
Sum_MomentsFP z									-0.25

Table 21: Spearman Rank Correlation Matrix for Graf type II

Spearman Rank Correlations	Percentage Of Dislocation	Sum Forces tot	FP Perc Along Femur	Sum Forces FP x	Sum Forces FP y	Sum Forces FP z	Sum Forces FP tot	Projected F over Path	% of total force in pat direction
Area Iliopsoas	-0.05	0.03	0.00	0.04	0.07	-0.13	0.03	0.15	0.14
Area Pectineus	-0.08	0.06	0.00	-0.03	0.05	-0.02	0.06	0.07	0.05
Area Sartorius	0.00	0.08	0.00	0.00	0.12	-0.17	0.09	0.17	0.17
Area Rectus Femoris	-0.02	-0.06	-0.01	0.08	0.06	-0.14	-0.06	0.19	0.16
Area Adductor Longus	-0.01	0.04	-0.01	0.03	0.03	-0.09	0.03	0.10	0.09
Area Adductor Brevis	-0.03	-0.01	0.01	0.02	0.03	0.03	-0.02	-0.06	-0.05
Area Adductor Magnus Minimus	-0.11	0.05	-0.01	-0.01	0.04	-0.15	0.05	0.18	0.15
Area Adductor Magnus Middle	-0.05	-0.04	0.00	0.08	-0.02	-0.04	-0.02	0.06	0.07
Area Adductor Magnus Posterior	-0.04	0.11	0.00	0.04	0.21	-0.15	0.12	0.04	0.04
Area Gracilis	-0.02	0.05	0.00	-0.05	0.05	-0.11	0.04	0.22	0.20
Area Gluteus Max	-0.06	0.02	-0.01	0.00	0.04	-0.14	0.02	0.19	0.16
Area Gluteus Medius Anterior	-0.09	0.05	-0.01	0.00	0.02	-0.02	0.05	0.03	0.04
Area Gluteus Medius Middle	-0.03	0.05	0.00	-0.06	-0.01	-0.08	0.05	0.05	0.05
Area Gluteus Medius Posterior	-0.08	-0.02	-0.01	0.05	0.00	0.05	-0.02	0.08	0.03
Area Gluteus Minimus Anterior	0.03	0.09	0.00	-0.08	-0.05	-0.13	0.09	0.13	0.13
Area Gluteus Minimus Middle	0.00	0.07	0.01	0.04	0.09	-0.10	0.07	0.03	0.04
Area Gluteus Minimus Posterior	0.09	0.04	0.00	0.01	0.12	-0.18	0.04	0.11	0.11
Area Tensor Fascia Lata	-0.05	0.02	-0.01	0.03	0.07	-0.14	0.03	0.18	0.16
Area Piriformis	-0.11	0.09	0.00	-0.04	0.07	-0.07	0.07	0.14	0.12
Area Obturator Internus	0.05	0.03	0.00	-0.06	0.01	-0.10	0.03	0.11	0.09
Area Gemellus Superior	-0.02	0.05	0.00	-0.01	0.10	-0.05	0.05	0.11	0.08
Area Gemellus Inferior	-0.08	0.03	0.00	0.03	0.07	-0.14	0.03	0.19	0.17
Area Quadratus Femoris	-0.07	0.09	0.00	-0.14	0.00	-0.11	0.07	0.12	0.06
Area Obturator Externus	-0.09	0.12	0.00	-0.05	0.03	-0.11	0.13	0.07	0.09
Area Biceps Femoris (Long Head)	-0.02	-0.09	-0.01	0.08	-0.10	0.06	-0.09	0.05	0.02
Area Semitendinosus	0.03	0.09	0.00	-0.02	0.07	-0.20	0.09	0.12	0.11
Area Semimembranosus	-0.08	0.04	0.00	0.01	0.11	-0.05	0.05	0.07	0.06

Spearman Rank Correlations	Percentage Of Dislocation	Sum Forces tot	FP Perc Along Femur	Sum Forces FP x	Sum Forces FP y	Sum Forces FP z	Sum Forces FP tot	Projected F over Path	% of total force in pat direction
Femur.Length	0.01	-0.07	0.00	0.06	-0.01	0.06	-0.07	0.00	0.01
Femur.L_Trochanteric	-0.03	0.12	0.01	-0.11	-0.02	0.01	0.13	0.02	-0.03
Femur.Shaft_Width	0.01	0.11	0.00	-0.21	-0.05	0.02	0.12	0.03	0.02
Femur.Deviation_Angle	0.00	-0.07	0.00	0.11	0.02	0.03	-0.06	-0.04	-0.05
Femur.Sagittal_Bowing_Ang	0.02	0.01	0.01	-0.01	-0.11	0.01	0.03	0.03	0.04
Femur.Coronal_Bowing_Ang	-0.07	0.00	0.00	0.03	0.02	0.00	0.00	0.03	0.00
Femur.Head_Diam	0.09	0.03	0.00	-0.06	0.03	-0.11	0.02	0.11	0.08
Femur.Anteversion_Angle	0.06	-0.07	0.00	0.08	-0.09	0.18	-0.05	-0.15	-0.13
Femur.Incline_Angle	-0.12	-0.06	0.00	0.00	-0.01	0.09	-0.07	-0.10	-0.10
Femur.Condyle_Diameter	0.00	0.09	0.00	-0.10	-0.04	0.04	0.09	-0.01	-0.03
Femur.Condyle_Spacing	0.13	-0.01	0.00	0.06	-0.02	-0.04	-0.01	0.09	0.10
Femur.Epicondyle_Dist	0.00	0.02	0.00	0.00	0.01	-0.01	0.01	0.02	0.02
Femur.Head_Module_E	-0.06	-0.05	0.00	0.04	-0.08	-0.09	-0.05	0.09	0.07
Femur.Head_Module_v	-0.12	0.00	0.00	0.01	0.03	0.06	0.00	-0.03	0.01
Hip.Acetabulum_Diam	0.08	-0.01	0.00	-0.01	-0.05	-0.04	-0.01	0.00	-0.01
Hip.Acetabulum_Module_E	0.08	-0.01	0.00	-0.01	0.02	0.01	-0.01	-0.02	-0.01
Hip.Acetabulum_Module_v	-0.01	0.04	0.00	-0.03	0.04	-0.08	0.03	0.07	0.03

Spearman Rank Correlations	Percentage Of Dislocation	Sum Forces tot	FP Perc Along Femur	Sum Forces FP x	Sum Forces FP y	Sum Forces FP z	Sum Forces FP tot	Projected F over Path	% of total force in pat direction
3D_Rat Iliopsoas	0.01	0.06	0.01	-0.08	0.02	-0.02	0.05	0.07	0.10
3D_Rat Pectineus	0.14	-0.11	0.00	0.08	-0.09	0.04	-0.10	0.01	0.00
3D_Rat Sartorius	0.00	-0.02	0.00	0.03	-0.03	-0.03	0.00	0.03	0.01
3D_Rat Rectus Femoris	0.00	-0.09	0.00	0.10	0.04	0.06	-0.09	0.00	-0.06
3D_Rat Adductor Longus	-0.02	0.02	0.00	-0.03	0.00	0.05	0.03	0.00	-0.06
3D_Rat Adductor Brevis	0.00	-0.05	0.00	0.04	-0.13	0.04	-0.04	0.03	0.01
3D_Rat Adductor Magnus Minimus	-0.06	-0.06	0.00	0.05	0.00	-0.11	-0.07	0.05	0.07
3D_Rat Adductor Magnus Middle	0.02	0.12	0.00	-0.08	0.05	-0.06	0.11	-0.01	-0.01
3D_Rat Adductor Magnus Posterior	-0.01	0.00	0.00	-0.02	0.01	0.00	-0.02	0.10	0.11
3D_Rat Gracilis	-0.07	0.00	0.00	0.03	-0.05	0.06	0.00	-0.04	-0.03
3D_Rat Gluteus Max	0.00	-0.16	0.00	0.12	-0.09	0.02	-0.14	0.00	0.00
3D_Rat Gluteus Medius Anterior	-0.01	0.04	0.01	-0.04	-0.03	-0.11	0.04	0.06	0.12
3D_Rat Gluteus Medius Middle	-0.12	0.01	0.00	0.02	-0.01	0.06	0.03	-0.03	-0.06
3D_Rat Gluteus Medius Posterior	0.09	0.06	0.00	-0.03	-0.01	-0.01	0.06	-0.04	-0.03
3D_Rat Gluteus Minimus Anterior	0.08	0.01	-0.01	0.02	0.07	-0.08	0.00	0.13	0.11
3D_Rat Gluteus Minimus Middle	-0.09	-0.02	0.00	-0.09	-0.08	0.02	-0.02	0.05	0.02
3D_Rat Gluteus Minimus Posterior	0.07	-0.21	-0.01	0.16	-0.16	0.04	-0.21	-0.02	0.00
3D_Rat Tensor Fascia Lata	-0.02	-0.02	0.00	0.05	-0.03	0.03	-0.01	0.02	-0.03
3D_Rat Piriformis	0.02	0.11	0.00	-0.07	0.11	-0.06	0.12	0.07	0.05
3D_Rat Obturator Internus	0.02	0.04	0.00	-0.02	0.02	-0.06	0.04	0.04	0.04
3D_Rat Gemellus Superior	-0.03	-0.10	0.00	0.11	0.01	-0.08	-0.09	0.04	0.03
3D_Rat Gemellus Inferior	0.00	0.00	0.01	-0.04	-0.06	-0.02	0.00	0.01	-0.03
3D_Rat Quadratus Femoris	0.02	-0.01	0.00	0.00	0.00	-0.03	-0.02	-0.01	0.01
3D_Rat Obturator Externus	0.02	-0.01	0.01	0.04	-0.03	0.01	-0.01	-0.01	-0.03
3D_Rat Biceps Femoris (Long Head)	0.05	-0.14	0.01	0.05	-0.15	0.03	-0.13	-0.06	-0.01
3D_Rat Semitendinosus	0.00	-0.08	0.01	-0.06	-0.15	0.08	-0.08	0.13	0.09
3D_Rat Semimembranosus	-0.02	-0.05	0.00	0.05	-0.10	0.00	-0.05	-0.05	-0.02

Spearman Rank Correlations	Percentage Of Dislocation	Sum Forces tot	FP Perc Along Femur	Sum Forces FP x	Sum Forces FP y	Sum Forces FP z	Sum Forces FP tot	Projected F over Path	% of total force in pat direction
3D_Rot Iliopsoas	0.13	-0.01	0.01	0.02	0.06	0.06	0.00	-0.07	-0.07
3D_Rot Pectineus	0.04	-0.04	0.00	0.07	0.00	0.02	-0.03	0.03	0.00
3D_Rot Sartorius	-0.10	0.03	0.00	0.01	0.02	0.01	0.04	-0.02	0.00
3D_Rot Rectus Femoris	0.00	-0.05	0.01	0.06	-0.06	0.09	-0.06	-0.05	-0.06
3D_Rot Adductor Longus	-0.09	0.09	0.00	-0.04	0.12	0.02	0.08	-0.04	-0.06
3D_Rot Adductor Brevis	0.05	0.07	-0.01	-0.08	0.01	-0.08	0.06	0.01	0.03
3D_Rot Adductor Magnus Minimus	0.12	0.01	0.00	0.00	0.03	-0.05	0.00	0.08	0.09
3D_Rot Adductor Magnus Middle	0.01	0.10	0.00	-0.05	0.13	-0.10	0.09	0.01	0.06
3D_Rot Adductor Magnus Posterior	-0.06	-0.07	0.00	0.01	-0.01	-0.10	-0.07	0.07	0.10
3D_Rot Gracilis	0.01	-0.07	0.00	-0.01	-0.06	-0.02	-0.07	0.02	0.01
3D_Rot Gluteus Max	-0.12	0.10	-0.01	-0.08	0.04	-0.06	0.10	-0.01	0.04
3D_Rot Gluteus Medius Anterior	-0.06	-0.13	0.00	0.08	-0.06	0.05	-0.14	-0.06	-0.03
3D_Rot Gluteus Medius Middle	0.01	-0.03	0.00	0.02	-0.06	0.03	-0.04	-0.08	-0.10
3D_Rot Gluteus Medius Posterior	-0.05	0.02	0.01	-0.02	0.08	0.07	0.04	-0.01	-0.01
3D_Rot Gluteus Minimus Anterior	-0.02	-0.10	0.00	0.06	-0.05	-0.03	-0.08	0.02	0.02
3D_Rot Gluteus Minimus Middle	0.00	-0.04	0.00	0.08	0.00	-0.11	-0.06	0.06	0.05
3D_Rot Gluteus Minimus Posterior	0.01	0.06	-0.01	-0.13	-0.02	-0.02	0.05	0.07	0.07
3D_Rot Tensor Fascia Lata	-0.02	0.02	0.01	-0.03	-0.01	-0.02	0.02	0.09	0.02
3D_Rot Piriformis	-0.13	-0.08	0.00	0.00	-0.10	0.04	-0.09	0.03	0.05
3D_Rot Obturator Internus	-0.04	-0.01	0.00	0.00	0.06	0.05	-0.02	-0.06	0.00
3D_Rot Gemellus Superior	-0.01	0.05	0.01	-0.10	0.02	-0.01	0.06	0.03	-0.01
3D_Rot Gemellus Inferior	0.11	0.01	0.01	0.02	0.10	0.01	0.01	0.01	0.02
3D_Rot Quadratus Femoris	0.14	-0.08	0.00	-0.03	-0.17	0.01	-0.08	0.09	0.06
3D_Rot Obturator Externus	-0.01	-0.11	0.00	0.11	-0.03	0.08	-0.12	-0.05	-0.01
3D_Rot Biceps Femoris (Long Head)	-0.03	0.02	0.00	-0.06	-0.04	0.05	0.02	0.05	0.02
3D_Rot Semitendinosus	0.09	-0.07	0.00	0.07	-0.05	0.05	-0.07	-0.05	-0.01
3D_Rot Semimembranosus	0.08	0.10	0.00	0.00	0.03	0.15	0.11	-0.22	-0.20

Spearman Rank Correlations	Percentage Of Dislocation	Sum Forces tot	FP Perc Along Femur	Sum Forces FP x	Sum Forces FP y	Sum Forces FP z	Sum Forces FP tot	Projected F over Path	% of total force in pat direction
M_L_Ratio Iliopsoas	0.05	0.01	0.00	-0.13	-0.02	-0.10	0.02	0.01	0.04
M_L_Ratio Pectineus	0.08	-0.10	0.00	0.09	-0.03	0.00	-0.08	-0.03	-0.05
M_L_Ratio Sartorius	-0.07	0.06	0.00	-0.17	-0.03	0.07	0.05	0.00	0.01
M_L_Ratio Rectus Femoris	-0.03	-0.03	0.00	-0.01	-0.02	-0.05	-0.03	0.08	0.09
M_L_Ratio Adductor Longus	-0.06	-0.06	0.00	0.07	-0.06	0.06	-0.08	-0.14	-0.12
M_L_Ratio Adductor Brevis	0.04	0.05	0.00	-0.05	0.01	0.01	0.04	0.01	-0.01
M_L_Ratio Adductor Magnus Minimus	-0.06	-0.02	0.00	0.10	-0.05	-0.02	-0.02	-0.04	-0.09
M_L_Ratio Adductor Magnus Middle	0.11	0.03	0.00	0.12	0.14	0.06	0.04	-0.09	-0.12
M_L_Ratio Adductor Magnus Posterior	0.06	0.01	0.00	0.08	0.11	-0.11	0.01	0.09	0.09
M_L_Ratio Gracilis	0.13	0.01	0.00	0.07	0.05	0.13	0.00	-0.18	-0.15
M_L_Ratio Gluteus Max	0.03	0.04	0.00	-0.11	0.04	0.05	0.04	0.04	-0.03
M_L_Ratio Gluteus Medius Anterior	-0.02	0.05	0.00	-0.06	0.02	-0.03	0.05	0.02	0.05
M_L_Ratio Gluteus Medius Middle	-0.02	-0.02	0.00	0.00	-0.08	0.00	-0.02	-0.06	-0.12
M_L_Ratio Gluteus Medius Posterior	-0.08	0.00	0.00	-0.03	-0.02	-0.02	0.00	0.00	-0.04
M_L_Ratio Gluteus Minimus Anterior	0.03	0.04	0.00	0.02	0.06	0.10	0.04	-0.09	-0.08
M_L_Ratio Gluteus Minimus Middle	-0.09	0.00	0.00	-0.10	-0.06	-0.04	0.02	0.06	0.03
M_L_Ratio Gluteus Minimus Posterior	0.00	0.10	0.00	-0.01	0.03	-0.05	0.09	0.03	0.03
M_L_Ratio Tensor Fascia Lata	0.03	0.08	0.00	-0.13	0.04	-0.07	0.08	0.02	-0.01
M_L_Ratio Piriformis	0.03	-0.08	0.00	0.11	-0.07	0.01	-0.08	0.02	0.00
M_L_Ratio Obturator Internus	-0.05	0.04	0.00	0.03	0.12	-0.01	0.03	-0.11	-0.11
M_L_Ratio Gemellus Superior	0.00	-0.04	-0.01	0.05	-0.08	-0.01	-0.04	0.04	0.05
M_L_Ratio Gemellus Inferior	0.05	0.13	0.00	-0.12	0.07	-0.11	0.12	0.13	0.10
M_L_Ratio Quadratus Femoris	0.08	0.01	0.00	-0.08	-0.08	0.00	0.02	0.07	0.06
M_L_Ratio Obturator Externus	0.00	0.03	-0.01	-0.01	0.01	-0.02	0.02	0.00	0.00
M_L_Ratio Biceps Femoris (Long Head)	0.00	0.03	0.00	0.02	0.05	0.05	0.03	-0.03	-0.05
M_L_Ratio Semitendinosus	-0.02	-0.17	0.00	0.04	-0.16	0.08	-0.17	-0.08	-0.09
M_L_Ratio Semimembranosus	0.01	-0.01	0.00	-0.09	-0.01	0.10	-0.02	0.04	0.02

Spearman Rank Correlations	Percentage Of Dislocation	Sum Forces tot	FP Perc Along Femur	Sum Forces FP x	Sum Forces FP y	Sum Forces FP z	Sum Forces FP tot	Projected F over Path	% of total force in pat direction
Flexion_i	0.05	0.15	0.01	-0.38	-0.14	0.02	0.14	0.04	0.00
Abduction_i	-0.03	0.44	0.00	-0.51	0.22	-0.19	0.41	0.22	0.19
E_Rotation_i	0.05	0.09	0.00	-0.23	-0.20	0.17	0.09	-0.11	-0.13
BWeight	0.02	0.15	0.00	-0.13	-0.01	0.02	0.14	0.09	0.03
Leg_Perc_Weight	-0.11	-0.06	0.00	-0.03	-0.10	0.04	-0.05	0.09	0.07
PreStretch	-0.02	-0.09	0.00	-0.03	-0.26	-0.07	-0.09	0.10	0.11
Hip Muscle Ins X Iliopsoas	0.01	0.47	-0.01	-0.08	0.38	0.31	0.43	-0.40	-0.48
Rel_Flex	-0.01	-0.04	0.00	0.00	-0.14	-0.05	-0.04	0.02	-0.01
Rel_Abd	-0.05	0.13	-0.01	-0.04	0.11	0.06	0.10	-0.01	0.00
Rel_Rot	0.04	0.06	0.01	0.01	0.18	-0.05	0.07	-0.03	-0.02
Flexion_e	0.00	-0.15	0.00	0.05	-0.11	0.05	-0.14	0.03	-0.02
Abduction_e	0.07	0.00	0.00	-0.06	-0.02	0.03	0.00	-0.01	-0.03
E_Rotation_e	0.01	-0.06	-0.01	-0.06	-0.08	0.04	-0.07	0.03	0.06
Percentage_Of_Dislocation	1.00	0.01	0.00	0.02	0.00	-0.07	0.01	-0.01	0.01
Leg Centroid x		0.05	0.01	-0.04	0.07	-0.21	0.03	0.17	0.23
Leg Centroid y		0.05	0.00	-0.04	0.07	-0.22	0.03	0.17	0.23
Leg Centroid z		0.05	0.00	-0.04	0.07	-0.22	0.03	0.17	0.23
Sum_Forces x		-0.69	-0.01	0.97	-0.14	0.11	-0.65	-0.26	-0.16
Sum_Forces y		0.60	-0.01	-0.11	0.98	-0.18	0.56	-0.07	-0.08
Sum_Forces z		-0.15	-0.01	0.11	-0.19	0.99	-0.15	-0.64	-0.67
Sum_Forces tot		1.00	-0.01	-0.65	0.58	-0.15	0.95	0.02	-0.05
Sum_Moments x			0.00	-0.10	0.66	-0.52	0.31	0.28	0.29
Sum_Moments y			0.00	-0.86	-0.01	-0.08	0.50	0.25	0.17
Sum_Moments z			-0.01	0.47	0.42	0.06	-0.03	-0.29	-0.22
FP_Perc_Along_Femur			1.00	-0.03	0.02	0.00	-0.01	0.01	0.01
Sum_ForcesFP x				1.00	-0.13	0.10	-0.67	-0.26	-0.16
Sum_ForcesFP y					1.00	-0.19	0.58	-0.07	-0.08
Sum_ForcesFP z						1.00	-0.14	-0.64	-0.67
Sum_ForcesFP tot							1.00	0.02	-0.06
ProjectedFoverPath								1.00	0.90
Sum_MomentsFP x									0.29
Sum_MomentsFP y									-0.02
Sum_MomentsFP z									-0.23
% of total force in pat direction									1.00

Table 22: Spearman Rank Correlation Matrix for Graf type III

Spearman Rank Correlations	Percentage Of Dislocation	Sum Forces tot	FP Perc Along Femur	Sum Forces FP x	Sum Forces FP y	Sum Forces FP z	Sum Forces FP tot	Projected F over Path	% of total force in pat direction
Area Iliopsoas	-0.18	0.18	0.00	-0.07	0.14	0.01	0.17	-0.13	-0.11
Area Pectineus	-0.13	-0.02	0.00	-0.13	-0.07	-0.01	-0.02	-0.05	-0.12
Area Sartorius	-0.30	0.07	0.00	0.05	-0.01	0.04	0.08	0.00	-0.02
Area Rectus Femoris	-0.19	0.17	0.01	-0.15	-0.03	-0.09	0.18	-0.09	-0.04
Area Adductor Longus	-0.19	0.12	0.01	-0.05	-0.01	0.11	0.14	-0.08	-0.06
Area Adductor Brevis	-0.03	0.28	0.01	-0.32	0.06	-0.14	0.28	-0.28	-0.14
Area Adductor Magnus Minimus	-0.28	0.15	0.00	0.14	0.15	-0.07	0.18	0.02	0.08
Area Adductor Magnus Middle	0.03	0.15	0.01	-0.02	0.08	0.06	0.16	-0.06	-0.04
Area Adductor Magnus Posterior	-0.17	-0.01	0.01	0.24	0.07	-0.02	0.01	0.18	0.09
Area Gracilis	-0.13	0.22	0.01	-0.12	0.02	-0.03	0.22	-0.17	-0.04
Area Gluteus Max	-0.29	0.14	0.00	0.00	0.16	-0.19	0.14	-0.05	-0.03
Area Gluteus Medius Anterior	-0.04	0.09	0.00	-0.06	0.04	-0.11	0.12	0.04	0.01
Area Gluteus Medius Middle	-0.15	0.01	0.01	-0.01	0.14	-0.07	0.03	-0.09	-0.06
Area Gluteus Medius Posterior	-0.10	-0.02	-0.01	0.00	0.10	0.02	-0.03	0.01	-0.04
Area Gluteus Minimus Anterior	0.15	0.08	0.01	-0.22	-0.09	0.05	0.09	-0.12	-0.08
Area Gluteus Minimus Middle	-0.09	-0.01	0.01	0.09	-0.01	-0.14	0.01	0.10	0.06
Area Gluteus Minimus Posterior	-0.05	-0.21	0.01	-0.03	0.07	0.12	-0.21	-0.04	-0.24
Area Tensor Fascia Lata	-0.19	0.14	0.01	-0.02	0.04	0.01	0.16	-0.04	-0.01
Area Piriformis	-0.08	0.07	0.01	-0.09	0.04	-0.11	0.09	-0.01	0.02
Area Obturator Internus	0.02	0.23	0.02	-0.15	-0.02	0.29	0.21	-0.19	-0.11
Area Gemellus Superior	-0.27	-0.03	0.01	0.13	-0.07	0.09	0.01	0.17	0.10
Area Gemellus Inferior	-0.21	0.09	0.01	-0.08	0.02	-0.01	0.10	-0.04	-0.03
Area Quadratus Femoris	-0.11	0.03	0.01	0.15	-0.04	-0.22	0.04	0.20	0.24
Area Obturator Externus	-0.14	-0.14	0.00	0.16	-0.11	-0.08	-0.12	0.26	0.23
Area Biceps Femoris (Long Head)	0.05	0.07	0.00	-0.33	0.02	0.00	0.06	-0.22	-0.23
Area Semitendinosus	-0.21	0.07	0.01	-0.14	-0.05	-0.13	0.08	-0.03	-0.01
Area Semimembranosus	-0.18	0.18	0.01	-0.09	0.00	0.00	0.19	-0.08	-0.01

Spearman Rank Correlations	Percentage Of Dislocation	Sum Forces tot	FP Perc Along Femur	Sum Forces FP x	Sum Forces FP y	Sum Forces FP z	Sum Forces FP tot	Projected F over Path	% of total force in pat direction
Femur.Length	0.07	0.06	0.00	-0.10	-0.06	-0.10	0.04	0.04	0.03
Femur.L_Trochanteric	0.00	0.18	0.01	0.08	0.23	0.01	0.15	-0.16	-0.07
Femur.Shaft_Width	-0.01	0.06	0.00	0.11	-0.06	-0.21	0.08	0.14	0.16
Femur.Deviation_Angle	-0.01	-0.25	0.00	0.04	-0.01	0.22	-0.24	0.00	-0.09
Femur.Sagittal_Bowing_Ang	-0.07	0.02	0.00	0.11	0.14	0.05	0.01	0.05	0.01
Femur.Coronal_Bowing_Ang	0.12	-0.09	0.00	-0.12	-0.16	0.12	-0.11	0.03	-0.07
Femur.Head_Diam	0.12	0.01	0.00	0.20	0.15	0.00	0.01	0.03	-0.04
Femur.Anteversion_Angle	-0.15	-0.02	0.00	0.12	-0.17	0.29	-0.01	0.07	0.00
Femur.Incline_Angle	0.10	0.04	0.00	0.21	-0.05	-0.08	0.07	0.15	0.20
Femur.Condyle_Diameter	-0.11	-0.27	0.01	0.06	-0.01	0.07	-0.26	0.08	-0.09
Femur.Condyle_Spacing	0.16	-0.10	0.00	-0.05	-0.05	-0.05	-0.06	-0.02	-0.04
Femur.Epicondyle_Dist	0.16	0.20	0.01	-0.10	-0.04	-0.04	0.17	-0.12	-0.01
Femur.Head_Module_E	0.04	0.03	0.01	-0.09	0.17	-0.12	0.03	-0.19	-0.16
Femur.Head_Module_v	0.02	0.12	0.01	0.04	0.10	0.06	0.10	-0.10	-0.07
Hip.Acetabulum_Diam	-0.04	-0.09	0.00	0.03	-0.17	0.18	-0.07	0.18	0.12
Hip.Acetabulum_Module_E	0.17	-0.06	-0.02	0.04	0.05	0.20	-0.03	0.06	0.00
Hip.Acetabulum_Module_v	0.08	0.02	0.00	0.01	0.05	0.03	0.02	-0.03	-0.11

Spearman Rank Correlations	Percentage Of Dislocation	Sum Forces tot	FP Perc Along Femur	Sum Forces FP x	Sum Forces FP y	Sum Forces FP z	Sum Forces FP tot	Projected F over Path	% of total force in pat direction
3D_Rat Iliopsoas	-0.01	-0.10	0.01	0.12	0.18	-0.08	-0.13	-0.02	-0.05
3D_Rat Pectineus	-0.18	-0.24	0.01	0.15	0.02	0.11	-0.23	0.07	-0.06
3D_Rat Sartorius	0.13	-0.14	0.00	-0.12	0.08	0.14	-0.16	-0.05	-0.18
3D_Rat Rectus Femoris	-0.04	-0.04	0.00	-0.07	0.18	0.09	-0.04	-0.16	-0.16
3D_Rat Adductor Longus	0.05	0.11	0.00	0.21	0.05	-0.30	0.16	0.23	0.30
3D_Rat Adductor Brevis	0.04	-0.09	0.00	0.15	0.09	0.15	-0.08	-0.05	-0.12
3D_Rat Adductor Magnus Minimus	0.03	-0.21	0.00	0.22	0.02	-0.02	-0.21	0.28	0.14
3D_Rat Adductor Magnus Middle	-0.01	0.17	0.00	-0.32	-0.20	-0.03	0.18	-0.13	-0.03
3D_Rat Adductor Magnus Posterior	0.08	0.02	0.00	0.08	0.00	-0.19	0.04	0.09	0.14
3D_Rat Gracilis	-0.21	0.11	0.00	0.13	-0.02	-0.27	0.13	0.20	0.20
3D_Rat Gluteus Max	-0.18	0.01	-0.01	-0.14	-0.14	-0.02	-0.01	0.00	-0.02
3D_Rat Gluteus Medius Anterior	-0.04	-0.05	0.00	0.14	-0.13	0.13	-0.04	0.18	0.11
3D_Rat Gluteus Medius Middle	-0.19	0.08	0.00	-0.02	0.02	0.05	0.09	-0.14	-0.13
3D_Rat Gluteus Medius Posterior	0.14	0.03	0.00	0.01	-0.01	0.16	0.07	0.00	0.01
3D_Rat Gluteus Minimus Anterior	-0.06	-0.13	0.00	0.05	-0.05	0.34	-0.12	-0.04	-0.14
3D_Rat Gluteus Minimus Middle	-0.14	-0.11	0.00	0.02	-0.14	0.07	-0.13	0.13	0.01
3D_Rat Gluteus Minimus Posterior	-0.13	0.24	-0.01	-0.02	0.04	0.02	0.20	-0.11	-0.03
3D_Rat Tensor Fascia Lata	-0.02	0.09	0.00	0.04	-0.04	0.00	0.09	0.08	0.08
3D_Rat Piriformis	0.10	0.02	0.00	-0.15	-0.02	-0.19	0.03	-0.03	0.03
3D_Rat Obturator Internus	-0.06	0.19	0.01	-0.20	0.02	-0.02	0.18	-0.24	-0.09
3D_Rat Gemellus Superior	0.10	-0.03	0.00	0.15	0.06	0.07	-0.03	-0.04	-0.01
3D_Rat Gemellus Inferior	-0.09	-0.03	-0.01	0.02	-0.04	0.05	-0.01	-0.02	0.07
3D_Rat Quadratus Femoris	-0.30	-0.11	0.00	-0.14	-0.18	0.09	-0.12	-0.08	-0.01
3D_Rat Obturator Externus	0.01	0.14	0.01	-0.22	0.25	-0.04	0.12	-0.30	-0.28
3D_Rat Biceps Femoris (Long Head)	0.17	0.03	0.01	0.10	-0.05	0.18	0.01	0.05	0.06
3D_Rat Semitendinosus	0.36	-0.17	0.01	0.02	0.13	0.08	-0.17	-0.07	-0.14
3D_Rat Semimembranosus	0.14	0.04	0.00	0.09	0.06	-0.03	0.02	0.02	-0.05

Spearman Rank Correlations	Percentage Of Dislocation	Sum Forces tot	FP Perc Along Femur	Sum Forces FP x	Sum Forces FP y	Sum Forces FP z	Sum Forces FP tot	Projected F over Path	% of total force in pat direction
3D_Rot Iliopsoas	0.20	0.08	0.00	-0.15	-0.18	-0.08	0.07	0.03	0.11
3D_Rot Pectineus	-0.16	0.01	-0.01	0.13	-0.08	0.10	-0.03	0.14	0.14
3D_Rot Sartorius	0.03	0.15	-0.01	0.08	0.20	-0.23	0.16	-0.05	-0.06
3D_Rot Rectus Femoris	-0.15	-0.02	0.01	-0.08	-0.02	0.06	-0.02	-0.10	-0.10
3D_Rot Adductor Longus	0.28	-0.17	0.00	-0.03	-0.18	0.12	-0.16	0.08	-0.04
3D_Rot Adductor Brevis	0.16	-0.08	0.00	0.01	-0.23	0.30	-0.10	0.04	0.00
3D_Rot Adductor Magnus Minimus	0.12	-0.15	0.00	-0.15	-0.26	-0.05	-0.16	0.08	0.06
3D_Rot Adductor Magnus Middle	-0.26	0.12	0.01	-0.01	-0.04	-0.15	0.14	0.03	0.10
3D_Rot Adductor Magnus Posterior	0.16	0.13	-0.01	0.11	0.21	-0.02	0.15	0.00	-0.03
3D_Rot Gracilis	0.02	-0.15	-0.01	0.17	-0.01	0.15	-0.16	0.07	-0.06
3D_Rot Gluteus Max	-0.02	-0.10	0.01	0.25	0.00	0.10	-0.07	0.17	0.10
3D_Rot Gluteus Medius Anterior	-0.09	-0.13	-0.01	-0.07	-0.07	-0.17	-0.12	0.09	0.06
3D_Rot Gluteus Medius Middle	0.06	-0.09	-0.02	0.23	0.24	0.31	-0.09	0.01	-0.16
3D_Rot Gluteus Medius Posterior	-0.12	0.06	0.00	-0.05	0.08	-0.19	0.01	-0.02	-0.05
3D_Rot Gluteus Minimus Anterior	0.23	0.07	0.00	0.02	0.07	0.07	0.07	-0.10	0.00
3D_Rot Gluteus Minimus Middle	-0.09	-0.11	0.00	-0.10	-0.19	0.26	-0.11	0.03	0.05
3D_Rot Gluteus Minimus Posterior	0.16	-0.09	0.00	-0.06	-0.15	0.15	-0.10	0.09	-0.04
3D_Rot Tensor Fascia Lata	0.15	-0.01	0.00	-0.07	-0.04	-0.18	0.01	-0.01	0.03
3D_Rot Piriformis	0.05	0.04	0.00	0.15	0.10	-0.07	0.02	0.08	0.10
3D_Rot Obturator Internus	-0.01	0.00	0.00	0.06	0.04	-0.03	0.03	-0.06	-0.14
3D_Rot Gemellus Superior	0.06	0.15	0.01	-0.06	0.10	-0.18	0.17	0.07	0.09
3D_Rot Gemellus Inferior	0.11	0.04	0.00	-0.05	0.05	-0.07	0.06	-0.01	0.07
3D_Rot Quadratus Femoris	-0.13	0.02	-0.01	-0.03	0.06	0.12	0.02	-0.05	-0.16
3D_Rot Obturator Externus	0.04	0.07	-0.01	-0.07	-0.01	-0.21	0.09	-0.07	0.12
3D_Rot Biceps Femoris (Long Head)	-0.21	-0.10	0.00	0.31	0.03	0.12	-0.12	0.16	0.12
3D_Rot Semitendinosus	-0.05	-0.13	0.00	0.11	0.07	0.20	-0.11	-0.04	-0.13
3D_Rot Semimembranosus	0.09	-0.08	0.00	0.06	-0.18	-0.12	-0.06	0.24	0.21

Spearman Rank Correlations	Percentage Of Dislocation	Sum Forces tot	FP Perc Along Femur	Sum Forces FP x	Sum Forces FP y	Sum Forces FP z	Sum Forces FP tot	Projected F over Path	% of total force in pat direction
M_L_Ratio Iliopsoas	-0.21	-0.04	0.00	-0.08	-0.27	-0.13	-0.03	0.23	0.27
M_L_Ratio Pectineus	0.01	-0.01	0.00	-0.03	-0.10	0.15	-0.02	-0.06	-0.03
M_L_Ratio Sartorius	0.08	0.08	0.01	-0.01	-0.11	-0.09	0.10	0.09	0.19
M_L_Ratio Rectus Femoris	-0.05	0.14	0.00	0.10	0.21	0.02	0.13	-0.12	-0.21
M_L_Ratio Adductor Longus	0.00	0.11	0.00	-0.08	0.06	-0.04	0.13	-0.14	-0.09
M_L_Ratio Adductor Brevis	0.00	0.08	-0.01	0.28	0.12	-0.07	0.09	0.06	0.15
M_L_Ratio Adductor Magnus Minimus	-0.13	-0.03	0.02	-0.21	-0.01	0.12	-0.05	-0.29	-0.23
M_L_Ratio Adductor Magnus Middle	-0.01	0.08	0.00	0.01	0.09	0.05	0.04	-0.07	-0.14
M_L_Ratio Adductor Magnus Posterior	0.03	-0.10	-0.01	0.07	0.10	0.03	-0.12	-0.03	-0.07
M_L_Ratio Gracilis	-0.11	0.00	-0.01	-0.12	-0.21	-0.11	0.01	0.10	0.10
M_L_Ratio Gluteus Max	-0.17	-0.10	0.00	-0.01	-0.02	0.04	-0.09	-0.01	-0.03
M_L_Ratio Gluteus Medius Anterior	-0.05	-0.09	0.00	0.11	0.05	0.22	-0.10	0.00	-0.02
M_L_Ratio Gluteus Medius Middle	0.02	-0.18	0.01	0.23	0.06	0.13	-0.20	0.15	0.02
M_L_Ratio Gluteus Medius Posterior	0.10	0.25	0.00	-0.40	-0.15	-0.10	0.23	-0.23	-0.06
M_L_Ratio Gluteus Minimus Anterior	-0.03	0.03	0.01	-0.07	0.02	-0.03	0.02	-0.10	-0.14
M_L_Ratio Gluteus Minimus Middle	0.19	0.04	0.00	-0.04	0.16	0.09	0.01	-0.16	-0.15
M_L_Ratio Gluteus Minimus Posterior	-0.04	-0.07	0.00	0.18	0.09	0.25	-0.06	-0.05	-0.19
M_L_Ratio Tensor Fascia Lata	0.10	-0.01	0.01	-0.22	0.07	-0.09	-0.02	-0.18	-0.17
M_L_Ratio Piriformis	0.04	0.11	0.01	-0.01	0.10	0.19	0.09	-0.21	-0.18
M_L_Ratio Obturator Internus	0.17	0.04	0.00	-0.02	0.04	0.07	0.04	0.01	-0.02
M_L_Ratio Gemellus Superior	-0.17	-0.08	0.01	-0.08	-0.29	0.06	-0.06	0.11	0.10
M_L_Ratio Gemellus Inferior	-0.24	-0.07	0.00	-0.11	-0.01	-0.08	-0.08	-0.01	-0.04
M_L_Ratio Quadratus Femoris	0.13	-0.09	-0.01	0.28	0.07	0.07	-0.07	0.09	0.08
M_L_Ratio Obturator Externus	-0.11	-0.03	0.01	0.02	-0.05	-0.20	-0.02	0.07	0.15
M_L_Ratio Biceps Femoris (Long Head)	0.02	0.14	0.00	-0.02	-0.05	0.06	0.14	-0.04	0.05
M_L_Ratio Semitendinosus	0.01	0.01	0.00	0.09	0.16	0.00	0.00	-0.12	-0.06
M_L_Ratio Semimembranosus	0.17	0.24	0.00	-0.18	0.01	-0.18	0.22	-0.09	0.05

Spearman Rank Correlations	Percentage Of Dislocation	Sum Forces tot	FP Perc Along Femur	Sum Forces FP x	Sum Forces FP y	Sum Forces FP z	Sum Forces FP tot	Projected F over Path	% of total force in pat direction
Flexion_i	-0.02	0.02	0.00	-0.42	-0.09	0.20	-0.02	-0.30	-0.34
Abduction_i	-0.11	0.24	0.00	-0.66	-0.11	-0.27	0.21	-0.37	-0.22
E_Rotation_i	0.05	0.13	0.01	-0.11	0.04	0.29	0.12	-0.27	-0.20
BWeight	0.07	-0.01	0.01	0.18	-0.02	-0.09	-0.01	0.20	0.14
Leg_Perc_Weight	0.02	-0.11	0.01	0.08	0.06	-0.01	-0.11	0.10	0.01
PreStretch	-0.08	0.19	0.00	-0.17	-0.22	-0.09	0.21	0.04	0.15
Hip Muscle Ins X Iliopsoas	-0.02	0.34	-0.01	0.02	0.35	0.15	0.29	-0.36	-0.32
Rel_Flex	0.02	0.00	0.01	0.00	-0.06	-0.08	0.04	0.10	0.07
Rel_Abd	-0.10	-0.03	-0.01	0.06	-0.06	0.08	-0.05	0.11	0.03
Rel_Rot	-0.10	0.07	0.01	0.02	0.09	-0.42	0.07	0.05	0.08
Flexion_e	-0.02	0.00	-0.01	0.15	0.12	0.00	0.03	0.08	0.01
Abduction_e	-0.05	0.05	0.01	-0.24	-0.01	0.01	0.01	-0.15	-0.10
E_Rotation_e	0.05	0.09	0.01	-0.19	-0.16	-0.27	0.10	0.09	0.14
Percentage_Of_Dislocation	1.00	-0.07	0.00	0.00	-0.06	0.04	-0.06	0.08	0.06
Leg Centroid x		0.30	0.00	-0.25	0.04	-0.30	0.26	-0.18	0.01
Leg Centroid y		0.29	0.00	-0.24	0.05	-0.31	0.26	-0.17	0.01
Leg Centroid z		0.29	0.00	-0.24	0.05	-0.31	0.26	-0.17	0.01
Sum_Forces x		-0.36	-0.01	0.98	0.24	0.15	-0.33	0.56	0.35
Sum_Forces y		0.19	-0.02	0.28	1.00	-0.07	0.16	-0.46	-0.48
Sum_Forces z		-0.40	0.02	0.17	-0.07	1.00	-0.42	-0.06	-0.36
Sum_Forces tot		1.00	-0.02	-0.34	0.19	-0.40	0.98	-0.48	-0.08
a			0.00	-0.03	0.23	0.11	0.23	-0.28	-0.29
Sum_Moments x			-0.01	0.24	0.42	-0.54	-0.18	0.14	0.10
Sum_Moments y			0.01	-0.84	-0.41	-0.21	0.17	-0.37	-0.20
Sum_Moments z			-0.01	0.55	0.60	0.01	0.18	-0.03	-0.02
FP_Perc_Along_Femur			1.00	-0.05	-0.02	0.02	-0.06	-0.04	-0.10
Sum_ForcesFP x				1.00	0.28	0.17	-0.31	0.54	0.35
Sum_ForcesFP y					1.00	-0.07	0.16	-0.46	-0.48
Sum_ForcesFP z						1.00	-0.42	-0.06	-0.36
Sum_ForcesFP tot							1.00	-0.43	-0.02
ProjectedFoverPath								1.00	0.80
Sum_MomentsFP x									0.10
Sum_MomentsFP y									0.02
Sum_MomentsFP z									0.02
% of total force in pat direction									1.00

Table 23: Spearman Rank Correlation Matrix for Graf type IV indirect path

Spearman Rank Correlations	Percentage Of Dislocation	Sum Forces tot	FP Perc Along Femur	Sum Forces FP x	Sum Forces FP y	Sum Forces FP z	Sum Forces FP tot	Projected F over Path	% of total force in pat direction
Area Iliopsoas	-0.05	-0.01	0.00	0.02	-0.04	0.05	-0.02	0.04	0.06
Area Pectineus	0.05	-0.02	0.00	-0.01	0.05	-0.03	-0.02	0.03	0.03
Area Sartorius	0.02	0.00	0.00	-0.03	0.02	0.04	0.00	0.03	0.02
Area Rectus Femoris	-0.01	0.01	0.00	0.04	0.00	0.06	0.01	0.05	0.04
Area Adductor Longus	-0.01	0.02	0.00	0.01	0.00	0.05	0.01	0.04	0.05
Area Adductor Brevis	0.06	0.05	0.00	-0.06	0.02	0.07	0.05	-0.01	-0.04
Area Adductor Magnus Minimus	0.01	0.03	0.00	-0.01	-0.04	0.00	0.03	0.04	0.02
Area Adductor Magnus Middle	0.01	-0.01	0.00	0.01	-0.01	0.06	-0.01	0.03	0.02
Area Adductor Magnus Posterior	0.01	0.04	0.00	-0.01	0.03	0.06	0.04	0.03	0.02
Area Gracilis	-0.03	-0.01	0.00	0.02	-0.01	0.07	-0.01	0.01	0.01
Area Gluteus Max	0.00	-0.01	0.00	-0.07	-0.05	0.03	-0.01	0.01	0.02
Area Gluteus Medius Anterior	-0.04	0.01	0.00	0.04	-0.02	0.01	0.01	0.07	0.06
Area Gluteus Medius Middle	-0.04	-0.03	0.00	-0.01	0.00	0.02	-0.03	-0.01	0.04
Area Gluteus Medius Posterior	-0.07	0.02	0.00	0.00	-0.05	0.06	0.01	0.01	0.00
Area Gluteus Minimus Anterior	0.04	0.03	0.00	0.04	0.02	0.07	0.03	0.06	0.06
Area Gluteus Minimus Middle	-0.08	-0.01	0.00	-0.01	-0.02	0.05	-0.01	0.00	0.00
Area Gluteus Minimus Posterior	0.00	-0.02	0.00	0.02	0.00	0.08	-0.02	0.07	0.04
Area Tensor Fascia Lata	-0.05	-0.01	0.00	0.03	-0.02	0.07	-0.01	0.02	0.02
Area Piriformis	0.02	0.00	0.00	0.03	-0.03	0.04	-0.01	0.01	0.01
Area Obturator Internus	-0.04	-0.03	0.00	0.03	-0.02	0.09	-0.03	0.02	0.01
Area Gemellus Superior	-0.03	0.02	0.00	0.02	-0.05	0.08	0.02	0.04	0.03
Area Gemellus Inferior	-0.04	0.03	0.00	0.02	-0.01	0.09	0.02	0.05	0.04
Area Quadratus Femoris	-0.08	0.01	0.00	0.03	0.01	0.08	0.01	0.05	0.05
Area Obturator Externus	0.02	0.05	0.00	-0.04	-0.10	0.04	0.04	0.06	0.03
Area Biceps Femoris (Long Head)	-0.07	0.01	0.00	0.06	0.04	0.09	0.01	0.04	0.04
Area Semitendinosus	-0.06	-0.02	0.00	0.03	0.03	0.08	-0.02	0.01	0.01
Area Semimembranosus	-0.02	0.02	0.00	0.03	-0.05	0.08	0.01	0.05	0.04

Spearman Rank Correlations	Percentage Of Dislocation	Sum Forces tot	FP Perc Along Femur	Sum Forces FP x	Sum Forces FP y	Sum Forces FP z	Sum Forces FP tot	Projected F over Path	% of total force in pat direction
Femur.Length	-0.03	-0.01	0.00	0.01	0.04	0.02	-0.02	-0.02	0.01
Femur.L_Trochanteric	-0.03	-0.01	0.00	0.02	0.06	-0.03	-0.01	0.02	0.07
Femur.Deviation_Angle	0.00	-0.01	0.00	-0.01	-0.05	0.04	-0.01	0.00	0.02
Femur.Shaft_Width	0.04	0.00	0.00	0.00	0.00	-0.01	0.00	-0.01	-0.02
Femur.Sagittal_Bowing_Ang	-0.01	0.01	0.00	-0.01	0.06	-0.01	0.00	0.01	-0.01
Femur.Coronal_Bowing_Ang	-0.02	0.07	0.00	-0.03	0.04	0.06	0.06	0.01	0.01
Femur.Head_Diam	-0.02	0.08	0.00	0.06	0.07	0.04	0.07	0.04	0.01
Femur.Anteversion_Angle	-0.01	0.13	0.01	0.14	-0.08	0.42	0.13	0.03	-0.06
Femur.Incline_Angle	0.06	0.05	0.00	0.02	-0.01	0.01	0.04	0.01	0.00
Femur.Condyle_Diameter	-0.05	0.01	0.00	0.03	-0.02	0.02	0.01	0.00	0.02
Femur.Condyle_Spacing	-0.03	0.02	0.00	0.00	0.07	0.01	0.02	0.00	-0.02
Femur.Epicondyle_Dist	0.06	0.07	0.00	0.03	0.01	0.07	0.07	0.01	0.03
Femur.Head_Module_E	0.03	-0.04	0.00	-0.01	-0.03	0.00	-0.04	0.00	0.03
Femur.Head_Module_v	-0.02	-0.03	0.00	-0.01	0.02	-0.05	-0.02	-0.05	-0.08
Hip.Acetabulum_Diam	0.02	-0.01	0.00	-0.02	-0.05	-0.02	0.00	-0.06	-0.03
Hip.Acetabulum_Module_E	0.04	0.01	0.00	-0.03	-0.01	0.01	0.01	-0.01	-0.02
Hip.Acetabulum_Module_v	-0.02	-0.03	0.00	0.06	0.00	-0.06	-0.02	-0.02	0.01

Spearman Rank Correlations	Percentage Of Dislocation	Sum Forces tot	FP Perc Along Femur	Sum Forces FP x	Sum Forces FP y	Sum Forces FP z	Sum Forces FP tot	Projected F over Path	% of total force in pat direction
3D_Rat Iliopsoas	-0.02	-0.13	0.00	0.05	-0.05	-0.04	-0.12	-0.10	-0.06
3D_Rat Pectineus	-0.03	-0.01	0.00	-0.02	-0.01	0.00	-0.02	0.02	0.02
3D_Rat Sartorius	0.03	0.00	0.00	0.00	0.01	-0.02	0.00	0.00	0.00
3D_Rat Rectus Femoris	0.00	-0.03	0.00	-0.01	-0.06	-0.02	-0.02	0.08	0.08
3D_Rat Adductor Longus	-0.01	0.07	0.00	-0.04	0.01	0.05	0.06	0.02	-0.01
3D_Rat Adductor Brevis	-0.04	-0.03	0.00	0.05	-0.04	0.05	-0.03	0.02	0.03
3D_Rat Adductor Magnus Minimus	0.06	0.00	0.00	-0.01	-0.04	-0.05	0.00	0.00	0.03
3D_Rat Adductor Magnus Middle	0.02	-0.08	0.00	-0.05	-0.11	-0.08	-0.09	-0.04	0.00
3D_Rat Adductor Magnus Posterior	0.00	0.04	0.00	0.05	0.02	0.05	0.04	0.02	0.02
3D_Rat Gracilis	0.04	-0.04	0.00	-0.04	-0.02	-0.07	-0.04	0.01	0.03
3D_Rat Gluteus Max	0.02	-0.07	0.00	0.06	0.01	-0.05	-0.06	-0.03	-0.01
3D_Rat Gluteus Medius Anterior	-0.01	-0.02	0.00	-0.01	-0.02	-0.04	-0.02	0.03	0.03
3D_Rat Gluteus Medius Middle	0.04	-0.02	0.00	-0.04	0.06	0.03	-0.02	0.03	0.00
3D_Rat Gluteus Medius Posterior	0.01	0.03	0.00	0.03	-0.01	0.05	0.02	0.03	0.04
3D_Rat Gluteus Minimus Anterior	0.06	-0.02	0.00	-0.02	0.05	0.02	-0.02	-0.05	-0.02
3D_Rat Gluteus Minimus Middle	0.04	-0.03	0.00	0.02	0.03	0.00	-0.03	-0.04	-0.05
3D_Rat Gluteus Minimus Posterior	-0.02	0.00	0.00	0.01	0.03	-0.02	0.01	0.02	0.03
3D_Rat Tensor Fascia Lata	0.01	-0.04	0.00	0.05	-0.02	-0.03	-0.04	-0.01	0.02
3D_Rat Piriformis	0.06	-0.03	0.00	-0.06	-0.06	0.00	-0.04	0.02	0.05
3D_Rat Obturator Internus	-0.02	-0.04	0.00	-0.09	-0.02	-0.07	-0.04	0.00	0.03
3D_Rat Gemellus Superior	0.00	-0.05	0.00	0.03	0.01	-0.04	-0.04	-0.08	-0.08
3D_Rat Gemellus Inferior	0.00	0.04	0.00	0.04	-0.02	0.01	0.05	-0.05	-0.06
3D_Rat Quadratus Femoris	-0.05	-0.02	0.00	-0.01	0.00	-0.06	-0.01	-0.04	-0.03
3D_Rat Obturator Externus	0.04	0.01	0.00	-0.01	0.00	0.02	0.00	0.04	0.04
3D_Rat Biceps Femoris (Long Head)	0.01	-0.04	0.00	-0.05	0.02	-0.02	-0.03	-0.06	-0.05
3D_Rat Semitendinosus	-0.04	0.02	0.00	0.02	-0.02	0.03	0.02	-0.02	-0.03
3D_Rat Semimembranosus	0.00	-0.07	0.00	0.00	0.01	0.00	-0.07	-0.03	-0.02

Spearman Rank Correlations	Percentage Of Dislocation	Sum Forces tot	FP Perc Along Femur	Sum Forces FP x	Sum Forces FP y	Sum Forces FP z	Sum Forces FP tot	Projected F over Path	% of total force in pat direction
3D_Rot Iliopsoas	0.03	0.08	0.00	0.06	0.03	0.08	0.08	-0.04	-0.07
3D_Rot Pectineus	-0.08	0.02	0.00	0.00	-0.04	0.08	0.02	-0.01	0.00
3D_Rot Sartorius	0.05	-0.04	0.00	-0.03	0.01	0.00	-0.04	-0.04	0.00
3D_Rot Rectus Femoris	0.00	-0.06	0.00	0.05	-0.02	0.01	-0.06	-0.03	0.00
3D_Rot Adductor Longus	0.00	-0.02	0.00	-0.02	0.02	-0.03	-0.02	-0.01	-0.03
3D_Rot Adductor Brevis	0.07	-0.06	0.00	0.02	-0.01	-0.06	-0.06	0.02	0.03
3D_Rot Adductor Magnus Minimus	0.00	0.02	0.00	0.01	-0.01	0.03	0.02	-0.04	-0.06
3D_Rot Adductor Magnus Middle	-0.08	-0.04	0.00	0.01	-0.05	0.00	-0.05	0.02	0.05
3D_Rot Adductor Magnus Posterior	-0.04	0.01	0.00	0.03	-0.07	0.00	0.01	0.04	0.05
3D_Rot Gracilis	0.00	-0.01	0.00	-0.02	0.03	0.01	-0.02	0.00	0.00
3D_Rot Gluteus Max	0.00	-0.04	0.00	0.00	-0.08	-0.01	-0.03	-0.04	-0.01
3D_Rot Gluteus Medius Anterior	0.04	-0.01	0.00	0.04	0.06	0.01	-0.02	0.02	0.01
3D_Rot Gluteus Medius Middle	-0.01	0.01	0.00	0.05	0.04	0.01	0.03	0.01	0.01
3D_Rot Gluteus Medius Posterior	0.01	0.03	0.00	-0.04	-0.07	-0.03	0.03	-0.04	-0.04
3D_Rot Gluteus Minimus Anterior	0.00	-0.06	0.00	-0.01	0.00	-0.04	-0.07	-0.03	-0.03
3D_Rot Gluteus Minimus Middle	-0.03	0.04	0.00	0.00	0.08	0.08	0.04	0.02	0.03
3D_Rot Gluteus Minimus Posterior	-0.02	0.01	0.00	0.00	0.03	0.00	0.00	0.00	-0.02
3D_Rot Tensor Fascia Lata	-0.03	-0.01	0.00	-0.02	0.01	-0.06	0.00	-0.03	-0.03
3D_Rot Piriformis	0.02	-0.02	0.00	0.02	-0.03	0.01	-0.02	-0.02	-0.02
3D_Rot Obturator Internus	0.06	0.02	0.00	-0.03	-0.01	0.00	0.02	0.05	0.04
3D_Rot Gemellus Superior	-0.01	-0.05	0.00	-0.04	-0.07	0.03	-0.05	-0.01	0.02
3D_Rot Gemellus Inferior	-0.06	-0.01	0.00	0.00	-0.03	0.02	0.00	-0.03	-0.02
3D_Rot Quadratus Femoris	-0.01	-0.05	0.00	0.04	-0.02	-0.01	-0.05	-0.05	-0.03
3D_Rot Obturator Externus	0.04	0.03	0.00	0.06	0.02	0.06	0.01	0.02	-0.01
3D_Rot Biceps Femoris (Long Head)	-0.10	-0.01	0.00	0.00	-0.06	0.01	-0.01	0.02	0.00
3D_Rot Semitendinosus	0.02	0.04	0.00	-0.02	0.09	-0.01	0.04	0.01	0.00
3D_Rot Semimembranosus	-0.05	-0.02	0.00	0.03	0.02	-0.05	-0.02	-0.05	-0.02

Spearman Rank Correlations	Percentage Of Dislocation	Sum Forces tot	FP Perc Along Femur	Sum Forces FP x	Sum Forces FP y	Sum Forces FP z	Sum Forces FP tot	Projected F over Path	% of total force in pat direction
M_L_Ratio Iliopsoas	0.03	0.00	0.00	-0.06	0.05	-0.02	0.00	0.01	0.01
M_L_Ratio Pectineus	0.01	-0.01	0.00	-0.01	-0.01	-0.03	-0.01	0.04	0.03
M_L_Ratio Sartorius	0.00	0.05	0.00	0.08	0.03	-0.02	0.04	0.04	0.02
M_L_Ratio Rectus Femoris	0.01	0.06	0.00	-0.05	-0.02	-0.02	0.05	0.02	0.02
M_L_Ratio Adductor Longus	-0.04	0.04	0.00	0.02	0.02	0.09	0.04	0.00	-0.01
M_L_Ratio Adductor Brevis	-0.12	-0.03	0.00	0.00	-0.07	-0.02	-0.03	-0.04	-0.01
M_L_Ratio Adductor Magnus Minimus	-0.02	-0.05	0.00	-0.03	0.02	0.01	-0.05	-0.06	-0.02
M_L_Ratio Adductor Magnus Middle	0.02	0.05	0.00	-0.02	-0.02	0.00	0.05	0.01	0.01
M_L_Ratio Adductor Magnus Posterior	0.00	-0.02	0.00	-0.06	-0.02	-0.05	-0.02	-0.03	-0.02
M_L_Ratio Gracilis	0.03	0.07	0.00	0.08	0.05	0.03	0.06	0.01	-0.01
M_L_Ratio Gluteus Max	-0.02	0.05	0.00	0.01	0.04	0.01	0.05	-0.02	-0.03
M_L_Ratio Gluteus Medius Anterior	0.05	-0.04	0.00	0.03	0.00	0.02	-0.04	-0.04	-0.04
M_L_Ratio Gluteus Medius Middle	-0.01	0.01	0.00	0.02	-0.03	-0.02	0.01	0.01	0.03
M_L_Ratio Gluteus Medius Posterior	0.01	0.05	0.00	0.04	-0.06	0.03	0.05	0.01	0.00
M_L_Ratio Gluteus Minimus Anterior	-0.06	-0.01	0.00	0.03	-0.04	-0.04	-0.01	0.07	0.08
M_L_Ratio Gluteus Minimus Middle	-0.03	0.04	0.00	-0.02	-0.01	0.05	0.04	0.04	0.04
M_L_Ratio Gluteus Minimus Posterior	-0.01	0.01	0.00	-0.04	-0.07	-0.02	0.01	0.02	0.02
M_L_Ratio Tensor Fascia Lata	0.10	-0.04	0.00	-0.06	0.05	-0.03	-0.03	-0.04	-0.03
M_L_Ratio Piriformis	0.00	-0.08	0.00	-0.04	0.00	0.00	-0.08	-0.02	-0.03
M_L_Ratio Obturator Internus	0.00	0.02	0.00	-0.02	0.03	-0.03	0.02	-0.02	-0.01
M_L_Ratio Gemellus Superior	-0.01	0.00	0.00	-0.09	-0.02	0.01	-0.01	0.00	0.01
M_L_Ratio Gemellus Inferior	0.02	-0.10	0.00	0.04	-0.02	-0.01	-0.09	-0.07	-0.04
M_L_Ratio Quadratus Femoris	-0.05	-0.01	0.00	0.04	-0.06	-0.01	0.01	-0.04	-0.04
M_L_Ratio Obturator Externus	-0.04	0.05	0.00	0.02	-0.01	-0.01	0.06	0.02	-0.01
M_L_Ratio Biceps Femoris (Long Head)	-0.03	-0.01	0.00	0.04	0.03	0.03	-0.01	-0.01	0.01
M_L_Ratio Semitendinosus	-0.05	0.04	0.00	-0.04	0.08	0.03	0.04	0.00	-0.03
M_L_Ratio Semimembranosus	0.04	0.04	0.00	-0.01	-0.06	0.07	0.03	0.08	0.04

Spearman Rank Correlations	Percentage Of Dislocation	Sum Forces tot	FP Perc Along Femur	Sum Forces FP x	Sum Forces FP y	Sum Forces FP z	Sum Forces FP tot	Projected F over Path	% of total force in pat direction
Flexion_i	-0.03	-0.13	0.00	-0.45	-0.19	0.01	-0.15	-0.13	-0.14
Abduction_i	0.04	0.05	0.00	-0.39	-0.01	-0.14	0.05	0.00	0.02
E_Rotation_i	-0.01	-0.04	0.00	-0.07	-0.15	0.03	-0.03	-0.02	0.00
BWeight	0.05	0.05	0.00	-0.09	-0.03	0.03	0.05	0.00	0.00
Leg_Perc_Weight	-0.02	0.11	0.00	0.01	-0.09	0.12	0.11	0.04	-0.01
PreStretch	0.03	-0.16	0.00	-0.09	-0.20	0.00	-0.16	-0.08	-0.04
Hip Muscle Ins X Iliopsoas	0.02	0.44	0.00	-0.08	0.24	0.47	0.40	0.16	-0.01
Rel_Flex	0.02	0.04	0.00	0.01	-0.02	0.00	0.03	-0.02	-0.03
Rel_Abd	0.07	-0.02	0.00	0.03	-0.01	-0.03	-0.01	-0.04	-0.01
Rel_Rot	0.01	0.04	0.00	-0.02	0.08	-0.08	0.05	-0.04	-0.05
Flexion_e	0.01	0.00	0.00	0.05	0.00	-0.04	0.00	-0.02	0.00
Abduction_e	0.04	-0.01	0.00	0.00	0.02	0.01	-0.03	-0.07	-0.08
E_Rotation_e	0.01	-0.01	0.00	0.10	-0.04	0.05	0.00	0.00	-0.02
Percentage_Of_Dislocation	1.00	0.04	0.00	0.00	0.07	-0.02	0.04	0.00	0.00
Leg Centroid x		0.04	0.00	-0.10	-0.01	-0.19	0.03	0.05	0.09
Leg Centroid y		0.04	0.00	-0.10	-0.01	-0.20	0.03	0.05	0.09
Leg Centroid z		0.04	0.00	-0.10	-0.01	-0.20	0.03	0.05	0.09
Sum_Forces x		0.04	0.00	0.94	0.07	0.24	0.07	0.05	0.00
Sum_Forces y		0.22	-0.01	0.09	1.00	0.14	0.21	-0.05	-0.13
Sum_Forces z		0.49	0.00	0.18	0.14	0.99	0.45	0.23	0.01
Sum_Forces tot		1.00	-0.01	0.01	0.21	0.49	0.94	0.45	0.19
Sum_Moments x			-0.01	0.06	0.93	-0.06	0.10	-0.07	-0.13
Sum_Moments y			0.00	-0.83	-0.14	0.00	0.03	0.01	-0.03
Sum_Moments z			0.00	0.43	-0.37	0.13	0.28	0.29	0.29
FP_Perc_Along_Femur			1.00	-0.02	0.00	0.01	-0.08	0.00	0.01
Sum_ForcesFP x				1.00	0.08	0.18	0.04	0.06	0.03
Sum_ForcesFP y					1.00	0.14	0.21	-0.04	-0.13
Sum_ForcesFP z						1.00	0.46	0.24	0.01
Sum_ForcesFP tot							1.00	0.42	0.14
ProjectedFoverPath								1.00	0.84
Sum_MomentsFP x									-0.13
Sum_MomentsFP y									0.00
Sum_MomentsFP z									0.34
% of total force in pat direction									1.00

Table 24: Spearman Rank Correlation Matrix for Graf type IV direct path

Spearman Rank Correlations	Percentage Of Dislocation	Sum Forces tot	FP Perc Along Femur	Sum Forces FP x	Sum Forces FP y	Sum Forces FP z	Sum Forces FP tot	Projected F over Path	% of total force in pat direction
Area Iliopsoas	-0.05	-0.13	0.00	0.00	-0.12	0.06	-0.14	-0.01	0.01
Area Pectineus	-0.06	-0.10	0.00	-0.08	-0.01	0.03	-0.10	-0.10	-0.11
Area Sartorius	-0.04	-0.11	0.00	0.05	-0.06	-0.01	-0.11	0.02	0.05
Area Rectus Femoris	-0.08	-0.10	0.00	-0.05	-0.10	0.05	-0.11	0.04	0.04
Area Adductor Longus	-0.02	-0.04	0.00	0.07	-0.03	-0.01	-0.05	0.09	0.09
Area Adductor Brevis	-0.02	0.05	0.00	-0.12	0.08	0.03	0.04	-0.11	-0.06
Area Adductor Magnus Minimus	0.04	-0.08	0.00	0.04	-0.06	-0.02	-0.10	0.07	0.05
Area Adductor Magnus Middle	-0.01	-0.09	0.00	-0.01	-0.07	-0.06	-0.09	0.06	0.10
Area Adductor Magnus Posterior	-0.01	-0.13	0.00	0.04	0.05	-0.08	-0.13	-0.03	-0.03
Area Gracilis	-0.07	-0.12	0.00	0.04	-0.06	0.09	-0.13	-0.01	-0.01
Area Gluteus Max	0.02	-0.14	0.00	0.02	-0.01	-0.04	-0.14	-0.01	-0.01
Area Gluteus Medius Anterior	-0.01	-0.12	0.00	0.05	-0.02	-0.02	-0.11	-0.01	-0.04
Area Gluteus Medius Middle	-0.13	0.02	0.00	0.02	0.02	0.07	0.01	-0.01	0.00
Area Gluteus Medius Posterior	0.02	-0.06	0.00	-0.06	0.02	0.00	-0.07	-0.05	-0.04
Area Gluteus Minimus Anterior	-0.02	-0.02	0.00	0.01	-0.09	0.11	-0.03	0.03	0.02
Area Gluteus Minimus Middle	-0.02	-0.04	0.00	-0.01	-0.04	0.04	-0.05	-0.01	-0.01
Area Gluteus Minimus Posterior	-0.04	-0.13	0.00	-0.01	-0.04	0.04	-0.14	-0.07	-0.06
Area Tensor Fascia Lata	-0.08	-0.15	0.00	0.00	-0.03	0.04	-0.15	0.00	0.00
Area Piriformis	-0.04	-0.11	0.00	-0.05	-0.02	0.02	-0.13	-0.08	-0.02
Area Obturator Internus	0.08	-0.12	0.00	-0.02	-0.09	0.06	-0.12	-0.09	-0.09
Area Gemellus Superior	-0.01	-0.06	0.00	-0.05	0.02	-0.19	-0.06	-0.01	0.02
Area Gemellus Inferior	-0.03	-0.17	0.00	0.01	-0.06	0.03	-0.18	-0.03	-0.01
Area Quadratus Femoris	0.03	-0.01	0.00	-0.11	-0.07	0.14	-0.02	-0.07	-0.04
Area Obturator Externus	0.06	-0.03	0.00	-0.14	-0.05	-0.04	-0.04	-0.07	-0.09
Area Biceps Femoris (Long Head)	-0.02	-0.09	0.00	0.01	-0.02	-0.02	-0.10	-0.04	-0.05
Area Semitendinosus	0.00	-0.09	0.00	0.05	-0.03	-0.08	-0.09	0.00	0.02
Area Semimembranosus	0.01	-0.13	0.00	0.02	-0.02	-0.04	-0.14	-0.01	0.03

Spearman Rank Correlations	Percentage Of Dislocation	Sum Forces tot	FP Perc Along Femur	Sum Forces FP x	Sum Forces FP y	Sum Forces FP z	Sum Forces FP tot	Projected F over Path	% of total force in pat direction
Femur.Length	0.02	0.04	0.00	-0.01	-0.07	0.08	0.04	-0.02	0.00
Femur.L_Trochanteric	0.00	-0.08	0.00	0.00	0.06	-0.02	-0.07	-0.08	-0.10
Femur.Shaft_Width	-0.02	0.02	0.00	0.04	0.03	-0.02	0.02	0.06	0.08
Femur.Deviation_Angle	0.01	0.04	-0.01	-0.02	-0.02	0.05	0.04	0.00	0.07
Femur.Sagittal_Bowing_Ang	-0.08	-0.02	0.00	0.00	-0.14	0.01	-0.01	0.09	0.08
Femur.Coronal_Bowing_Ang	-0.10	0.03	0.00	-0.04	-0.03	0.07	0.02	-0.05	-0.06
Femur.Head_Diam	-0.08	0.12	0.00	-0.06	0.09	0.00	0.11	-0.01	-0.02
Femur.Anteversion_Angle	0.05	0.01	0.00	0.10	-0.20	0.38	0.03	0.06	0.02
Femur.Incline_Angle	-0.01	0.05	0.00	-0.15	-0.05	0.02	0.03	0.02	0.07
Femur.Condyle_Diameter	-0.04	-0.01	0.00	-0.01	0.05	-0.04	-0.03	-0.03	-0.06
Femur.Condyle_Spacing	0.00	0.08	0.00	0.00	-0.02	0.08	0.07	0.04	0.04
Femur.Epicondyle_Dist	-0.02	0.05	0.00	-0.04	-0.08	-0.02	0.04	0.02	0.01
Femur.Head_Module_E	0.04	-0.06	0.00	0.02	0.09	-0.03	-0.04	-0.05	-0.04
Femur.Head_Module_v	0.03	0.01	0.00	-0.05	-0.05	0.00	0.01	0.04	0.05
Hip.Acetabulum_Diam	-0.02	0.05	0.00	0.01	-0.05	0.14	0.04	-0.01	-0.04
Hip.Acetabulum_Module_E	-0.04	-0.04	0.00	0.00	0.06	-0.04	-0.02	-0.01	-0.01
Hip.Acetabulum_Module_v	-0.05	0.04	0.00	0.11	0.06	-0.05	0.04	-0.01	-0.01

Spearman Rank Correlations	Percentage Of Dislocation	Sum Forces tot	FP Perc Along Femur	Sum Forces FP x	Sum Forces FP y	Sum Forces FP z	Sum Forces FP tot	Projected F over Path	% of total force in pat direction
3D_Rat Iliopsoas	0.03	-0.01	0.00	0.08	-0.04	0.03	-0.01	0.01	0.04
3D_Rat Pectineus	0.10	-0.03	0.00	0.01	0.08	-0.04	-0.02	-0.07	-0.08
3D_Rat Sartorius	0.01	-0.02	0.00	-0.07	0.04	0.01	-0.02	-0.10	-0.09
3D_Rat Rectus Femoris	-0.07	-0.13	0.00	0.06	-0.08	0.02	-0.12	0.06	0.06
3D_Rat Adductor Longus	-0.07	0.01	0.00	-0.09	0.04	-0.02	0.01	-0.08	-0.07
3D_Rat Adductor Brevis	-0.06	0.04	0.00	-0.11	0.05	0.05	0.04	-0.11	-0.08
3D_Rat Adductor Magnus Minimus	0.06	0.02	0.00	-0.02	0.04	0.09	0.02	-0.04	-0.07
3D_Rat Adductor Magnus Middle	-0.04	-0.03	0.00	0.02	0.02	0.01	-0.03	-0.03	-0.05
3D_Rat Adductor Magnus Posterior	0.11	0.00	0.00	-0.03	-0.02	0.06	0.00	-0.05	-0.02
3D_Rat Gracilis	0.06	-0.06	0.00	-0.01	0.05	-0.05	-0.06	-0.03	0.00
3D_Rat Gluteus Max	-0.01	0.05	0.00	0.07	-0.01	0.10	0.05	0.03	0.05
3D_Rat Gluteus Medius Anterior	0.05	-0.03	0.00	-0.13	0.00	0.00	-0.03	-0.05	-0.04
3D_Rat Gluteus Medius Middle	0.01	-0.02	0.00	-0.11	0.02	0.07	-0.02	-0.10	-0.07
3D_Rat Gluteus Medius Posterior	-0.05	-0.03	0.00	0.01	-0.03	0.01	-0.03	0.04	0.01
3D_Rat Gluteus Minimus Anterior	0.06	0.05	0.00	0.06	0.00	0.14	0.05	0.01	-0.03
3D_Rat Gluteus Minimus Middle	-0.06	-0.03	0.00	0.08	0.10	-0.01	-0.02	0.01	0.05
3D_Rat Gluteus Minimus Posterior	-0.02	0.04	0.00	-0.03	-0.03	0.00	0.05	0.04	0.08
3D_Rat Tensor Fascia Lata	-0.02	-0.01	0.00	-0.02	-0.04	0.14	-0.01	-0.04	-0.01
3D_Rat Piriformis	0.02	0.04	0.00	0.07	-0.09	0.09	0.04	0.01	0.00
3D_Rat Obturator Internus	-0.02	0.07	0.00	-0.05	0.10	-0.03	0.06	-0.06	-0.07
3D_Rat Gemellus Superior	-0.01	-0.10	-0.01	-0.01	0.06	-0.06	-0.11	-0.01	-0.02
3D_Rat Gemellus Inferior	-0.07	-0.05	0.00	-0.02	0.07	0.01	-0.06	-0.09	-0.08
3D_Rat Quadratus Femoris	0.04	0.03	0.00	-0.06	-0.07	0.04	0.04	0.03	0.03
3D_Rat Obturator Externus	-0.14	0.02	0.00	-0.06	-0.01	0.06	0.03	-0.04	-0.03
3D_Rat Biceps Femoris (Long Head)	-0.01	0.00	0.00	-0.06	-0.01	0.01	0.00	0.00	0.00
3D_Rat Semitendinosus	0.00	0.05	0.00	-0.05	-0.06	0.11	0.05	-0.03	-0.03
3D_Rat Semimembranosus	0.01	0.02	0.00	-0.05	0.01	-0.07	0.02	0.03	0.00

Spearman Rank Correlations	Percentage Of Dislocation	Sum Forces tot	FP Perc Along Femur	Sum Forces FP x	Sum Forces FP y	Sum Forces FP z	Sum Forces FP tot	Projected F over Path	% of total force in pat direction
3D_Rot Iliopsoas	0.01	0.06	0.00	-0.08	0.02	-0.01	0.06	-0.06	-0.03
3D_Rot Pectineus	-0.02	-0.01	0.00	-0.02	-0.04	0.07	-0.01	-0.04	-0.02
3D_Rot Sartorius	0.10	-0.05	0.00	0.12	0.08	-0.08	-0.05	0.00	0.01
3D_Rot Rectus Femoris	-0.01	0.00	0.00	-0.03	0.06	-0.04	-0.01	-0.04	-0.02
3D_Rot Adductor Longus	-0.02	0.02	0.00	0.00	-0.01	0.00	0.04	-0.03	0.00
3D_Rot Adductor Brevis	-0.03	0.02	0.00	0.01	0.03	0.07	0.02	-0.01	-0.02
3D_Rot Adductor Magnus Minimus	-0.04	-0.10	0.00	0.04	0.02	0.00	-0.08	-0.04	-0.02
3D_Rot Adductor Magnus Middle	0.01	-0.02	0.00	-0.09	-0.08	0.13	-0.03	-0.08	-0.06
3D_Rot Adductor Magnus Posterior	0.10	0.00	0.00	-0.01	0.02	-0.01	0.01	-0.04	-0.05
3D_Rot Gracilis	0.02	0.10	0.00	0.03	-0.06	0.01	0.12	0.06	0.10
3D_Rot Gluteus Max	-0.03	-0.04	0.00	0.00	-0.05	0.00	-0.04	-0.02	-0.03
3D_Rot Gluteus Medius Anterior	0.00	0.02	0.00	-0.07	0.02	0.04	0.00	0.02	0.01
3D_Rot Gluteus Medius Middle	0.00	0.02	0.01	0.06	0.05	0.08	0.03	-0.03	-0.02
3D_Rot Gluteus Medius Posterior	0.07	-0.05	0.00	0.04	0.02	-0.01	-0.05	0.01	-0.01
3D_Rot Gluteus Minimus Anterior	0.04	-0.05	0.00	0.07	0.00	0.01	-0.05	0.04	0.03
3D_Rot Gluteus Minimus Middle	0.05	0.11	0.00	0.05	0.00	-0.06	0.11	0.11	0.11
3D_Rot Gluteus Minimus Posterior	0.14	-0.02	0.00	-0.06	0.05	0.01	-0.01	-0.08	-0.02
3D_Rot Tensor Fascia Lata	-0.03	0.05	0.00	0.09	-0.07	0.10	0.05	0.14	0.11
3D_Rot Piriformis	-0.04	-0.01	0.00	0.00	-0.07	0.04	0.01	0.00	-0.02
3D_Rot Obturator Internus	-0.03	0.04	0.00	-0.02	-0.04	0.01	0.04	0.09	0.08
3D_Rot Gemellus Superior	0.06	-0.16	0.00	0.06	-0.01	0.04	-0.15	-0.01	0.00
3D_Rot Gemellus Inferior	-0.01	0.04	0.00	-0.02	-0.04	0.18	0.04	-0.01	0.01
3D_Rot Quadratus Femoris	-0.06	-0.01	0.00	-0.05	0.06	0.01	-0.02	-0.08	-0.05
3D_Rot Obturator Externus	0.01	-0.02	0.00	0.12	0.00	-0.03	-0.02	0.06	0.04
3D_Rot Biceps Femoris (Long Head)	0.01	-0.05	0.00	0.04	-0.04	0.05	-0.04	0.06	0.08
3D_Rot Semitendinosus	-0.02	0.03	0.00	-0.05	0.09	-0.01	0.01	-0.09	-0.05
3D_Rot Semimembranosus	-0.04	0.05	0.00	-0.01	-0.08	0.13	0.04	-0.01	0.03

Spearman Rank Correlations	Percentage Of Dislocation	Sum Forces tot	FP Perc Along Femur	Sum Forces FP x	Sum Forces FP y	Sum Forces FP z	Sum Forces FP tot	Projected F over Path	% of total force in pat direction
M_L_Ratio Iliopsoas	-0.01	-0.12	0.00	0.04	0.01	-0.09	-0.12	-0.01	-0.01
M_L_Ratio Pectineus	0.03	0.00	0.00	-0.06	0.01	0.02	-0.01	0.00	-0.05
M_L_Ratio Sartorius	-0.05	0.01	0.00	-0.03	0.00	-0.03	-0.03	0.08	0.08
M_L_Ratio Rectus Femoris	0.01	0.02	0.00	0.03	0.03	-0.03	0.02	-0.04	-0.01
M_L_Ratio Adductor Longus	-0.02	0.02	0.00	0.09	-0.05	0.05	0.02	-0.01	0.01
M_L_Ratio Adductor Brevis	0.05	-0.02	0.00	0.07	0.00	-0.03	-0.01	0.04	0.03
M_L_Ratio Adductor Magnus Minimus	-0.09	0.04	0.00	0.01	-0.15	0.10	0.04	0.04	0.06
M_L_Ratio Adductor Magnus Middle	-0.08	-0.04	0.00	-0.07	0.05	0.00	-0.04	-0.08	-0.05
M_L_Ratio Adductor Magnus Posterior	0.02	-0.01	0.00	-0.03	0.02	0.08	-0.02	-0.02	-0.01
M_L_Ratio Gracilis	0.04	0.03	0.00	0.01	-0.04	0.05	0.04	0.09	0.03
M_L_Ratio Gluteus Max	0.04	-0.04	0.00	0.03	0.04	-0.07	-0.02	-0.02	-0.08
M_L_Ratio Gluteus Medius Anterior	0.01	-0.03	0.00	-0.07	0.09	-0.07	-0.04	-0.08	-0.09
M_L_Ratio Gluteus Medius Middle	0.08	0.03	0.00	-0.07	0.00	0.01	0.02	-0.02	0.03
M_L_Ratio Gluteus Medius Posterior	0.07	-0.08	0.00	0.03	-0.03	0.05	-0.07	-0.01	-0.06
M_L_Ratio Gluteus Minimus Anterior	0.07	-0.04	0.00	-0.03	-0.05	-0.10	-0.03	0.04	0.05
M_L_Ratio Gluteus Minimus Middle	-0.08	-0.02	0.00	0.02	-0.07	0.06	-0.02	0.06	0.06
M_L_Ratio Gluteus Minimus Posterior	-0.04	0.05	0.00	-0.06	-0.01	-0.01	0.04	0.02	0.01
M_L_Ratio Tensor Fascia Lata	0.03	0.06	0.00	0.04	-0.05	-0.01	0.06	0.05	0.12
M_L_Ratio Piriformis	-0.05	0.01	0.00	0.01	0.03	-0.02	0.01	0.00	0.00
M_L_Ratio Obturator Internus	0.04	-0.05	0.00	0.10	-0.05	-0.03	-0.05	0.10	0.11
M_L_Ratio Gemellus Superior	-0.07	-0.06	0.00	-0.09	-0.07	-0.05	-0.07	0.09	0.09
M_L_Ratio Gemellus Inferior	0.01	0.10	0.00	0.00	0.03	0.01	0.11	-0.03	-0.01
M_L_Ratio Quadratus Femoris	-0.13	0.12	0.00	0.07	0.00	0.10	0.12	0.07	0.04
M_L_Ratio Obturator Externus	-0.11	0.04	0.00	0.01	-0.06	0.03	0.03	0.06	-0.01
M_L_Ratio Biceps Femoris (Long Head)	0.08	-0.07	0.00	0.03	-0.02	0.09	-0.07	-0.01	-0.06
M_L_Ratio Semitendinosus	0.04	0.03	0.00	0.04	0.05	-0.01	0.03	-0.01	0.05
M_L_Ratio Semimembranosus	-0.02	0.00	0.00	0.07	-0.09	-0.07	0.01	0.08	0.13

Spearman Rank Correlations	Percentage Of Dislocation	Sum Forces tot	FP Perc Along Femur	Sum Forces FP x	Sum Forces FP y	Sum Forces FP z	Sum Forces FP tot	Projected F over Path	% of total force in pat direction
Flexion_i	0.04	0.05	0.00	-0.47	-0.23	0.28	0.00	-0.19	-0.15
Abduction_i	0.02	0.24	0.00	-0.46	-0.05	-0.08	0.21	-0.17	-0.11
E_Rotation_i	-0.04	-0.02	0.00	-0.10	-0.16	0.10	-0.03	-0.03	-0.04
BWeight	-0.05	0.07	0.00	-0.06	-0.02	0.00	0.09	0.05	0.06
Leg_Perc_Weight	0.10	-0.03	0.00	-0.03	0.07	-0.05	-0.03	-0.04	-0.05
PreStretch	0.09	-0.12	-0.01	0.05	-0.19	0.04	-0.11	0.10	0.09
Hip Muscle Ins X Iliopsoas	0.04	0.32	-0.01	-0.03	0.22	0.26	0.31	-0.17	-0.15
Rel_Flex	-0.04	0.02	0.00	0.01	0.01	0.06	0.02	-0.06	-0.06
Rel_Abd	-0.02	0.02	0.00	-0.01	0.04	0.00	0.03	-0.07	-0.06
Rel_Rot	-0.05	0.03	0.00	-0.10	0.19	-0.08	0.01	-0.10	-0.06
Flexion_e	0.03	0.03	0.00	-0.02	0.05	-0.05	0.02	0.00	-0.01
Abduction_e	0.05	-0.11	0.00	0.07	0.05	0.02	-0.11	0.02	0.03
E_Rotation_e	-0.01	0.00	0.00	0.04	-0.01	-0.03	0.00	-0.03	0.05
Percentage_Of_Dislocation	1.00	-0.06	0.00	0.05	0.06	-0.05	-0.06	-0.02	-0.01
Leg Centroid x		0.05	0.00	-0.02	0.01	-0.21	0.05	-0.03	0.01
Leg Centroid y		0.06	0.00	-0.02	0.01	-0.23	0.05	-0.02	0.02
Leg Centroid z		0.06	0.00	-0.02	0.01	-0.23	0.05	-0.02	0.02
Sum_Forces x		-0.16	0.00	0.98	0.08	-0.11	-0.10	0.49	0.38
Sum_Forces y		-0.06	0.00	0.11	1.00	-0.38	-0.05	-0.43	-0.41
Sum_Forces z		0.14	-0.01	-0.15	-0.38	1.00	0.11	-0.05	-0.09
Sum_Forces tot		1.00	-0.02	-0.17	-0.06	0.14	0.97	0.18	0.23
Sum_Moments x			0.00	0.21	0.84	-0.64	-0.15	-0.24	-0.26
Sum_Moments y			0.00	-0.91	-0.23	0.29	0.16	-0.36	-0.29
Sum_Moments z			-0.01	0.57	-0.06	-0.05	0.37	0.62	0.61
FP_Perc_Along_Femur			1.00	-0.02	0.00	-0.01	-0.09	-0.03	-0.05
Sum_ForcesFP x				1.00	0.11	-0.15	-0.11	0.47	0.37
Sum_ForcesFP y					1.00	-0.38	-0.05	-0.43	-0.41
Sum_ForcesFP z						1.00	0.11	-0.05	-0.09
Sum_ForcesFP tot							1.00	0.19	0.24
ProjectedFoverPath								1.00	0.85
Sum_MomentsFP x									-0.26
Sum_MomentsFP y									-0.03
Sum_MomentsFP z									0.63
% of total force in pat direction									1.00

APPENDIX C: PUBLICATIONS AND PRESENTATIONS

Journal papers:

1. Huayamave, V., Lozinski, B., Rose, C., Ali, A., Divo, E. Moslehy, F., Kassab, A., and Price, C., "Biomechanical Evaluation of Femoral Anteversion in Developmental Dysplasia of the Hip and Potential Implications for Closed Reduction" Journal of Clinical Biomechanics, 2020, Vol 72, pp. 175-182.
2. M. Zwawi, F. Moslehy, C. Rose, V. Huayamave, A. Kassab, E. Divo, B. J. Jones, and C. T. Price, "Developmental dysplasia of the hip: A computational biomechanical model of the path of least energy for closed reduction" J. Orthop. Res., vol. 35, no. 8, pp. 1799–1805, Aug. 2017.
3. V. Huayamave, C. Rose, S. Serra, B. Jones, E. Divo, F. Moslehy, A. J. Kassab, and C. T. Price, "A patient-specific model of the biomechanics of hip reduction for neonatal developmental dysplasia of the hip: Investigation of strategies for low to severe grades of DDH" J. Biomech., Vol. 48, no. 10, pp. 1–8, Jul. 2015.

Conference Papers:

1. Huayamave, V., Rose, C., Divo. E., Moslehy, F., Kassab, A.J., and Price, C.T., "Mechanics ofHip Dysplasia Reduction in Infants with Pavlik Harness Using Patient Specific Geometry",Proc. of the 2014 International Congress and Exposition ASME Paper IMECE 2014- 3660ßNovember 14-20, Montreal, Canada (3rd place Track3-13: biomedical and biotechnology PhD Paper Competition).

Poster Presentations:

1. B. Lozinski, H. Ali, V. Huayamave, C. Rose, B. Jones, E. Divo, A. Kassab, and C. Price, "Biomechanical Investigation of the Influence of Increased Femoral Anteversion on the Success of Reduction of Severe Grades of Developmental

Dysplasia of the Hip with the Pavlik Harness" Annual Meeting of the Biomedical Engineering Society BMES 2017, 11-14 October 2017, Phoenix, Arizona (Abstract and Poster).

2. B. Lozinski, H. Ali, V. Huayamave, C. Rose, B. Jones, E. Divo, A. Kassab, and C. Price, "Increased Femoral Anteversion and Knee External Rotation Influence on Reduction of Severe Grades of Developmental Dysplasia of the Hip", International Mechanical EngineeringCongress & ExpositionIMECE 2017, 3-9 November 2017, Tampa, Florida (Abstract and Poster).
3. Huayamave, V., Rose, C., Divo, E., Moslehy, F., Kassab, A. J., and Price, C.T., " Femoral Anteversion Angle Influence on Severe Grades of Developmental Dysplasia of the Hip using the Pavlik Harness", Annual Meeting of the Biomedical Engineering Society BMES 2015, 7–10 October 2015, Tampa, Florida (Extended abstract and poster presentation)
4. Huayamave, V., Rose, C., Divo. E., Moslehy, F., Kassab, A.J., and Price, C.T., "Mechanics ofHip Dysplasia Reduction with the Pavlik Harness: recent developements for IHDI Grade 4Dislocations", 12th international symposium on Computer Methods in Biomechanics andBiomedical Engineering, Amsterdam, Netherlands October 13 - 15, 2014 (Abstract and Poster)
5. Huayamave, V., Rose, C., Divo. E., Moslehy, F., Kassab, A.J., and Price, C.T., "Mechanics ofhip dysplasia reduction in infants using the Pavlik harness on patient-specific geometry", Proc. of7th World Congress on Biomechanics, Humphrey, J. and Kamm, R. (eds.), Boston July 6-11,2014 (Abstract and poster session).

Invited Talks:

1. Huayamave, V., and Rose, C., “Mechanics of Hip Dysplasia Reduction in Infants with the Pavlik Harness using Patient Specific Geometry”,Pediatric Orthopedic Society of North America POSNA 2014, Hollywood, CA, April 30- May 3, 2014.

Other publications:

1. C. Rose, J. Mcconnell, and S.-E. Song, “Application of a Single Actuator Multiple Manipulation (SAMM) Mechanism”, Florida Conference on Recent Advances in Robotics 2018, 10-11 May 2018, Orlando, Florida (Paper and Presentation)
2. M. Basingab, C. Rose, L. Rabelo, K. Nagadi, E. Gutiérrez, and W. Il Jung, “Business Model Analysis using Agent-Based Simulation for the Internet of Things and Predictive Maintenance”, IX Simposio Internacional de Ingeniería Industrial 9siii 2016, Brasil, 19-21 October, 2016.(Symposium)
3. “IHDI Team Researches Anatomical Severity of Dislocated Hips | International Hip Dysplasia Institute”, 2015. [Online]. Available: https://hipdysplasia.org/news/ihdi-team-researches-anatomical-severity-of-dislocated-hips/. [Accessed: 11-Apr-2019].(Article)
4. C. Rose Petrilli, “Diseño estructural de un semitráiler”,FIMCP ESPOL 2012, Guayaquil, Ecuador.(Bachelor’s Thesis)

LIST OF REFERENCES

[1] E. Peled, M. Eidelman, A. Katzman, and V. Bialik, "Neonatal incidence of hip dysplasia: Ten years of experience," *Clin. Orthop. Relat. Res.*, vol. 466, no. 4, pp. 771–775, Apr. 2008, doi: 10.1007/s11999-008-0132-8.

[2] P. J. Klisic, "Congenital dislocation of the hip--a misleading term: brief report.," *J. Bone Joint Surg. Br.*, vol. 71, no. 1, p. 136, Jan. 1989, doi: 10.1302/0301-620X.71B1.2914985.

[3] S. Godward and C. Dezateux, "Surgery for congenital dislocation of the hip in the UK as a measure of outcome of screening. MRC Working Party on Congenital Dislocation of the Hip. Medical Research Council.," *Lancet (London, England)*, vol. 351, no. 9110, pp. 1149–52, Apr. 1998, Accessed: Apr. 08, 2019. [Online]. Available: http://www.ncbi.nlm.nih.gov/pubmed/9643684.

[4] S. Tibrewal, V. Gulati, and M. Ramachandran, "The Pavlik method," *J. Pediatr. Orthop. B*, vol. 22, no. 6, pp. 516–520, Nov. 2013, doi: 10.1097/BPB.0b013e328365760e.

[5] R. T. Loder and E. N. Skopelja, "The Epidemiology and Demographics of Hip Dysplasia," *ISRN Orthop.*, vol. 2011, pp. 1–46, 2011, doi: 10.5402/2011/238607.

[6] R. Graf, *Hip Sonography: Diagnosis and Management of Infant Hip Dysplasia - R. Graf.* .

[7] N. J. Murphy, J. P. Eyles, and D. J. Hunter, "Hip Osteoarthritis: Etiopathogenesis and Implications for Management," *Advances in Therapy*, vol. 33, no. 11. Springer Healthcare, pp. 1921–1946, Nov. 01, 2016, doi: 10.1007/s12325-016-0409-3.

[8] D. A. Michaeli, S. B. Murphy, and J. A. Hipp, “Comparison of predicted and measured contact pressures in normal and dysplastic hips,” *Med. Eng. Phys.*, vol. 19, no. 2, pp. 180–186, Mar. 1997, doi: 10.1016/S1350-4533(96)00051-3.

[9] Z. Fu, J.-P. Yang, P. Zeng, and Z.-L. Zhang, “Surgical implications for residual subluxation after closed reduction for developmental dislocation of the hip: A long-term follow-up,” 2014, doi: 10.1111/os.12113.

[10] M. Webster, Joseph B., MD; Murphy, Douglas P., *Atlas of Orthoses and Assistive Devices- ClinicalKey*, Fifth. Philadelphia, 2019.

[11] V. Huayamave *et al.*, “A patient-specific model of the biomechanics of hip reduction for neonatal developmental dysplasia of the hip: Investigation of strategies for low to severe grades of DDH,” *J. Biomech.*, vol. 48, no. 10, pp. 1–8, Jul. 2015, doi: 10.1016/j.jbiomech.2015.03.031.

[12] B. Lozinski *et al.*, “Biomechanical Investigation of the Influence of Increased Femoral Anteversion on the Success of Reduction of Severe Grades of Developmental Dysplasia of the Hip with the Pavlik Harness,” 2017, Accessed: Apr. 11, 2019. [Online]. Available: www.bmes.org.

[13] B. Lozinski *et al.*, “Increased Femoral Anteversion and Knee External Rotation Influence on Reduction of Severe Grades of Developmental Dysplasia of the Hip,” 2017, Accessed: Apr. 11, 2019. [Online]. Available: https://www.asme.org/events/imece2017/program#/track/detail/721.

[14] M. Zwawi *et al.*, “Developmental dysplasia of the hip: A computational biomechanical model of the path of least energy for closed reduction,” *J. Orthop. Res.*, vol. 35, no. 8, pp. 1799–1805, Aug. 2017, doi: 10.1002/jor.23461.

[15] M. Benson, J. Fixsen, M. Macnicol, and K. Parsch, *Children's orthopaedics and fractures: Third Edition*. Springer London, 2010.

[16] S. L. Delp *et al.*, "OpenSim: Open-source software to create and analyze dynamic simulations of movement," *IEEE Trans. Biomed. Eng.*, vol. 54, no. 11, pp. 1940–1950, Nov. 2007, doi: 10.1109/TBME.2007.901024.

[17] R. Graf, "Fundamentals of sonographic diagnosis of infant hip dysplasia," *J. Pediatr. Orthop.*, vol. 4, no. 6, pp. 735–40, Nov. 1984, Accessed: Apr. 10, 2019. [Online]. Available: http://www.ncbi.nlm.nih.gov/pubmed/6392336.

[18] R. Graf, K. Lercher, S. Scott, T. S. Copyright®, and S. Stolzalpe, "Essentials of infant hip sonography according to GRAF."

[19] I. H. D. I. IHDI, "Hip Health in Baby Carriers, Baby Seats, and Other Equipment | International Hip Dysplasia Institute." http://hipdysplasia.org/developmental-dysplasia-of-the-hip/prevention/baby-carriers-seats-and-other-equipment/ (accessed Jun. 16, 2015).

[20] U. Narayanan, K. Mulpuri, W. N. Sankar, N. M. P. Clarke, H. Hosalkar, and C. T. Price, "Reliability of a New Radiographic Classification for Developmental Dysplasia of the Hip.," *J. Pediatr. Orthop.*, vol. 00, no. 00, Sep. 2014, doi: 10.1097/BPO.0000000000000318.

[21] M. Ortolani, "Congenital hip dysplasia in the light of early and very early diagnosis.," *Clin. Orthop. Relat. Res.*, no. 119, pp. 6–10, Sep. 1976, Accessed: Apr. 12, 2019. [Online]. Available: http://www.ncbi.nlm.nih.gov/pubmed/954324.

[22] S. F. Olsen, H. C. Blom, and K. Rosendahl, "Introducing universal ultrasound screening for developmental dysplasia of the hip doubled the treatment rate," *Acta*

Paediatr., vol. 107, no. 2, pp. 255–261, Feb. 2018, doi: 10.1111/apa.14057.

[23] D. Tönnis, *Congenital Dysplasia and Dislocation of the Hip in Children and Adults*. Berlin, Heidelberg: Springer Berlin Heidelberg, 1987.

[24] H. Atalar, H. Dogruel, H. Selek, B. A. Tasbas, A. Bicimoglu, and C. Gunay, "A comparison of ultrasonography and radiography in the management of infants with suspected developmental dysplasia of the hip.," *Acta Orthop. Belg.*, vol. 79, no. 5, pp. 524–9, Oct. 2013, Accessed: Apr. 12, 2019. [Online]. Available: http://www.ncbi.nlm.nih.gov/pubmed/24350513.

[25] N. M. Clarke, H. T. Harcke, P. McHugh, M. S. Lee, P. F. Borns, and G. D. MacEwen, "Real-time ultrasound in the diagnosis of congenital dislocation and dysplasia of the hip.," *J. Bone Joint Surg. Br.*, vol. 67, no. 3, pp. 406–12, May 1985, Accessed: Apr. 12, 2019. [Online]. Available: http://www.ncbi.nlm.nih.gov/pubmed/3889008.

[26] H. Atalar, U. Sayli, O. Y. Yavuz, I. Uraş, and H. Dogruel, "Indicators of successful use of the Pavlik harness in infants with developmental dysplasia of the hip.," *Int. Orthop.*, vol. 31, no. 2, pp. 145–50, Apr. 2007, doi: 10.1007/s00264-006-0097-8.

[27] R. Graf and M. Synder, "Hip sonography worldwide-experience, results, problems Ultrasonografia stawu biodrowego na świecie-doświadczenia, wyniki problemy," *Chir. Narzadow Ruchu Ortop. Pol*, vol. 85, no. 4, pp. 29–34, 2020, doi: 10.31139/chnriop.2020.85.3-4.1.

[28] A. H. Crawford, C. T. Mehlman, and R. W. Slovek, "The fate of untreated developmental dislocation of the hip: long-term follow-up of eleven patients.," *J. Pediatr. Orthop.*, vol. 19, no. 5, pp. 641–4, Accessed: Apr. 12, 2019. [Online].

Available: http://www.ncbi.nlm.nih.gov/pubmed/10488867.

[29] N. G. Papadimitriou, A. Papadimitriou, J. E. Christophorides, T. A. Beslikas, and P. K. Panagopoulos, “Late-presenting developmental dysplasia of the hip treated with the modified Hoffmann-Daimler functional method.,” *J. Bone Joint Surg. Am.*, vol. 89, no. 6, pp. 1258–68, Jun. 2007, doi: 10.2106/JBJS.E.01414.

[30] K. Iwasaki, “Treatment of congenital dislocation of the hip by the Pavlik harness. Mechanism of reduction and usage.,” *J. Bone Joint Surg. Am.*, vol. 65, no. 6, pp. 760–7, Jul. 1983, Accessed: May 27, 2015. [Online]. Available: http://jbjs.org/content/65/6/760.abstract.

[31] S. Suzuki, “Reduction of CDH by the Pavlik harness. Spontaneous reduction observed by ultrasound.,” *J. Bone Joint Surg. Br.*, vol. 76, no. 3, pp. 460–2, May 1994, Accessed: May 29, 2015. [Online]. Available: http://www.ncbi.nlm.nih.gov/pubmed/8175854.

[32] P. L. Ramsey, S. Lasser, and G. D. MacEwen, “Congenital dislocation of the hip. Use of the Pavlik harness in the child during the first six months of life.,” *J. Bone Joint Surg. Am.*, vol. 58, no. 7, pp. 1000–4, Oct. 1976, Accessed: May 29, 2015. [Online]. Available: http://www.ncbi.nlm.nih.gov/pubmed/977608.

[33] S. Mubarak, S. Garfin, R. Vance, B. McKinnon, and D. Sutherland, “Pitfalls in the use of the Pavlik harness for treatment of congenital dysplasia, subluxation, and dislocation of the hip.,” *J. Bone Joint Surg. Am.*, vol. 63, no. 8, pp. 1239–48, Oct. 1981, Accessed: May 28, 2015. [Online]. Available: http://www.ncbi.nlm.nih.gov/pubmed/7287794.

[34] H. Atalar, C. Gunay, and M. Komurcu, “Functional Treatment of Developmental

Hip Dysplasia with the Tübingen Hip Flexion Splint," *HIP Int.*, vol. 24, no. 3, pp. 295–301, May 2014, doi: 10.5301/hipint.5000128.

[35] E. Heikkilä, "Comparison of the Frejka pillow and the von Rosen splint in treatment of congenital dislocation of the hip.," *J. Pediatr. Orthop.*, vol. 8, no. 1, pp. 20–1, 1988, Accessed: Apr. 12, 2019. [Online]. Available: http://www.ncbi.nlm.nih.gov/pubmed/3335616.

[36] D. Wenger, H. Samuelsson, H. Düppe, and C. J. Tiderius, "Early treatment with the von Rosen splint for neonatal instability of the hip is safe regarding avascular necrosis of the femoral head: 229 consecutive children observed for 6.5 years.," *Acta Orthop.*, vol. 87, no. 2, pp. 169–75, 2016, doi: 10.3109/17453674.2015.1126158.

[37] B. J. Burger, J. D. Burger, C. F. A. Bos, J. Hermans, P. M. Rozing, and J. P. Vandenbroucke, "Frejka pillow and Becker device for congenital dislocation of the hip: Prospective 6-year study of 104 late-diagnosed cases," *Acta Orthop. Scand.*, vol. 64, no. 3, pp. 305–311, Jan. 1993, doi: 10.3109/17453679308993632.

[38] A. Tegnander, K. J. Holen, S. Anda, and T. Terjesen, "Good results after treatment with the Frejka pillow for hip dysplasia in newborns: a 3-year to 6-year follow-up study.," *J. Pediatr. Orthop. B*, vol. 10, no. 3, pp. 173–9, Jul. 2001, Accessed: Apr. 12, 2019. [Online]. Available: http://www.ncbi.nlm.nih.gov/pubmed/11497357.

[39] P. Lafforgue, "Pathophysiology and natural history of avascular necrosis of bone," *Joint Bone Spine*, vol. 73, no. 5. Joint Bone Spine, pp. 500–507, Oct. 2006, doi: 10.1016/j.jbspin.2006.01.025.

[40] J. P. Sharma and R. Salhotra, "Tourniquets in orthopedic surgery.," *Indian J. Orthop.*, vol. 46, no. 4, pp. 377–83, Jul. 2012, doi: 10.4103/0019-5413.98824.

[41] R. M. Martin, A. McCarthy, G. D. Smith, D. P. Davies, and Y. Ben-Shlomo, "Infant nutrition and blood pressure in early adulthood: The Barry Caerphilly Growth study," *Am. J. Clin. Nutr.*, vol. 77, no. 6, pp. 1489–1497, Jun. 2003, doi: 10.1093/ajcn/77.6.1489.

[42] Betts J. Gordon *et al.*, "Blood Flow, Blood Pressure, and Resistance," in *Anatomy and Physiology | OpenStax*, 2013.

[43] M. A. Waxman, "Using physics to investigate blood flow in arteries: A case study for premed students," *Am. J. Phys.*, vol. 78, no. 9, pp. 970–973, Sep. 2010, doi: 10.1119/1.3379292.

[44] T. Malinin and E. A. Ouellette, "Articular cartilage nutrition is mediated by subchondral bone: A long-term autograft study in baboons," *Osteoarthr. Cartil.*, vol. 8, no. 6, pp. 483–491, Nov. 2000, doi: 10.1053/joca.1999.0324.

[45] J. Y. Rho, L. Kuhn-Spearing, and P. Zioupos, "Mechanical properties and the hierarchical structure of bone," *Med. Eng. Phys.*, vol. 20, no. 2, pp. 92–102, Mar. 1998, doi: 10.1016/S1350-4533(98)00007-1.

[46] K. Snethen, "A computed tomography-based model of the infant hip anatomy for dynamic finite element analysis of hip dysplasia biomechanics 2013," 2018.

[47] W. F. Dostal and J. G. Andrews, "A three-dimensional biomechanical model of hip musculature.," *J. Biomech.*, vol. 14, no. 11, pp. 803–12, Jan. 1981, Accessed: May 22, 2015. [Online]. Available: http://www.ncbi.nlm.nih.gov/pubmed/7334040.

[48] S. L. Delp *et al.*, "OpenSim: open-source software to create and analyze dynamic simulations of movement.," *IEEE Trans. Biomed. Eng.*, vol. 54, no. 11, pp. 1940–50, Nov. 2007, doi: 10.1109/TBME.2007.901024.

[49] E. M. Arnold, S. R. Ward, R. L. Lieber, and S. L. Delp, “A model of the lower limb for analysis of human movement,” *Ann. Biomed. Eng.*, vol. 38, no. 2, pp. 269–279, Feb. 2010, doi: 10.1007/s10439-009-9852-5.

[50] L. Li, D. Bryant, T. van Heugten, and P. J. Bos, “Physical limitations and fundamental factors affecting performance of liquid crystal tunable lenses with concentric electrode rings.,” *Appl. Opt.*, vol. 52, no. 9, pp. 1978–86, Mar. 2013, Accessed: Sep. 13, 2018. [Online]. Available: http://www.ncbi.nlm.nih.gov/pubmed/23518745.

[51] E. Marieb, *Human anatomy & physiology*, 4th ed. Menlo Park Calif. ;;Harlow: Benjamin Cummings, 1998.

[52] D. Shier, J. Butler, and R. Lewis, *Hole’s essentials of human anatomy & physiology*, 10th ed. McGraw-Hill, 2009.

[53] A. Magid and D. J. Law, “Myofibrils bear most of the resting tension in frog skeletal muscle.,” *Science*, vol. 230, no. 4731, pp. 1280–2, Dec. 1985, Accessed: Apr. 09, 2019. [Online]. Available: http://www.ncbi.nlm.nih.gov/pubmed/4071053.

[54] A. V. Hill, “The Series Elastic Component of Muscle,” *Proceedings of the Royal Society of London. Series B, Biological Sciences*, vol. 137. Royal Society, pp. 273–280, doi: 10.2307/82551.

[55] Y.-C. Fung, “Mathematical representation of the mechanical properties of the heart muscle,” *J. Biomech.*, vol. 3, no. 4, pp. 381–404, Jul. 1970, doi: 10.1016/0021-9290(70)90012-6.

[56] C. Stecco *et al.*, “Histological characteristics of the deep fascia of the upper limb.,” *Ital. J. Anat. Embryol.*, vol. 111, no. 2, pp. 105–10, Accessed: Apr. 12, 2019.

[Online]. Available: http://www.ncbi.nlm.nih.gov/pubmed/16981399.

[57] T. L. Wickiewicz, R. R. Roy, P. L. Powell, and V. R. Edgerton, "Muscle architecture of the human lower limb.," *Clin. Orthop. Relat. Res.*, no. 179, pp. 275–83, Oct. 1983, Accessed: Apr. 09, 2019. [Online]. Available: http://www.ncbi.nlm.nih.gov/pubmed/6617027.

[58] Y. Gao and M. Leineweber, "Mechanical Properties of Aging Skeletal Muscle," Springer, Cham, 2015, pp. 75–93.

[59] J. A. C. Martins, E. B. Pires, R. Salvado, and P. B. Dinis, "A numerical model of passive and active behavior of skeletal muscles," *Comput. Methods Appl. Mech. Eng.*, vol. 151, no. 3–4, pp. 419–433, Jan. 1998, doi: 10.1016/S0045-7825(97)00162-X.

[60] J. M. Winters and S. L. Y. Woo, *Multiple Muscle Systems -- Biomechanics and Movement Organizations.* New York: Springer-Verlag, 1990.

[61] A. V. Hill, *First and Last Experiments in Muscle Mechanics: A. V. Hill: 9780521076647: Amazon.com: Books*. Cambridge University Press, 1970.

[62] Y. C. Fung, "Structure and Stress-Strain Relationship of Soft Tissues," *American Zoologist*, vol. 24. Oxford University Press, pp. 13–22, 1984, doi: 10.2307/3882748.

[63] O. J. Ardila, E. a. Divo, F. a. Moslehy, G. T. Rab, A. J. Kassab, and C. T. Price, "Mechanics of hip dysplasia reductions in infants using the Pavlik harness: A physics-based computational model," *J. Biomech.*, vol. 46, no. 9, pp. 1501–1507, 2013, doi: 10.1016/j.jbiomech.2013.03.031.

[64] D. G. Thelen, "Adjustment of muscle mechanics model parameters to simulate dynamic contractions in older adults.," *J. Biomech. Eng.*, vol. 125, no. 1, pp. 70–7,

Mar. 2003, Accessed: May 29, 2015. [Online]. Available: http://www.ncbi.nlm.nih.gov/pubmed/12661198.

[65] S. L. Delp, “Surgery simulation: a computer graphics system to analyze and design musculoskeletal reconstructions of the lower limb,” Stanford, 1990.

[66] R. H. Jensen and D. T. Davy, “An investigation of muscle lines of action about the hip: A centroid line approach vs the straight line approach,” *J. Biomech.*, vol. 8, no. 2, pp. 103–110, Mar. 1975, doi: 10.1016/0021-9290(75)90090-1.

[67] H. Gray and C. D Clemente, *Anatomy of the human body* . Philadelphia: Lea & Febiger, 1985.

[68] S. Goostray and C. Toldt, “Atlas of Human Anatomy,” *Am. J. Nurs.*, vol. 27, no. 3, p. 240, 1927, doi: 10.2307/3409752.

[69] + 1 Leibowitz, W. ; Schmidt, M. ; Kester, S. ; Logan, and Schinski, “The Anterior Bow of the Femur and its Influence on Femoral Placement.”

[70] A. H. K. Abdelaal *et al.*, “Radiological assessment of the femoral bowing in Japanese population,” *SICOT-J*, vol. 2, p. 2, 2016, doi: 10.1051/sicotj/2015037.

[71] Z. Bao *et al.*, “The assessment of femoral shaft morphology in the sagittal plane in Chinese patients with osteoarthritis-a radiographic analysis,” *J. Orthop. Surg. Res.*, vol. 12, no. 1, p. 127, Aug. 2017, doi: 10.1186/s13018-017-0626-8.

[72] S. C. Carlson, “Catenary,” *Encyclopædia Britannica*. Encyclopædia Britannica, Feb. 03, 2017, Accessed: Nov. 16, 2020. [Online]. Available: https://www.britannica.com/science/catenary.

[73] R. Drillis, R. Contini, and M. Bluestein, “Body Segment Parameters - A Survey of Measurement Techniques.”

[74] H. Yin, L. Zhang, D. Li, L. Xiao, and M. Cheng, “The gray matter volume of the right insula mediates the relationship between symptoms of depression/anxiety and sleep quality among college students,” *Journal of Health Psychology*, 2019. https://doi.org/10.1177/1359105319869977 (accessed Nov. 16, 2020).

[75] A. Baharev, S. Kemény, and P. Student, “On the computation of the noncentral F and noncentral beta distribution,” *Stat. Comput.*, vol. 18, no. 3, pp. 333–340, 2008, doi: 10.1007/s11222-008-9061-3.

[76] G. Trenkler, “Continuous univariate distributions,” *Comput. Stat. Data Anal.*, vol. 21, no. 1, p. 119, Jan. 1996, doi: 10.1016/0167-9473(96)90015-8.

[77] J. R. Van Dorp and S. Kotz, “A novel extension of the triangular distribution and its parameter estimation,” *J. R. Stat. Soc. Ser. D Stat.*, vol. 51, no. 1, pp. 63–79, 2002, doi: 10.1111/1467-9884.00299.

[78] S. Umeyama, “Least-Squares Estimation of Transformation Parameters Between Two Point Patterns,” *IEEE Trans. Pattern Anal. Mach. Intell.*, vol. 13, no. 4, pp. 376–380, 1991, doi: 10.1109/34.88573.

[79] “The National Library of Medicines Visible Human Project.” http://www.nlm.nih.gov/research/visible/visible_human.html (accessed May 29, 2015).

[80] A. Eriksson, “Muscle mechanics and,” *Pharmacology*, p. 219, 2006, Accessed: Apr. 11, 2019. [Online]. Available: https://search-ebscohost-com.ezproxy.net.ucf.edu/login.aspx?direct=true&db=nlebk&AN=28696.

[81] J. A. Friederich and R. A. Brand, “Muscle fiber architecture in the human lower limb,” *J. Biomech.*, vol. 23, no. 1, pp. 91–95, Jan. 1990, doi: 10.1016/0021-

9290(90)90373-B.

[82] L. Cui, H. Maas, E. J. Perreault, and T. G. Sandercock, “In situ estimation of tendon material properties: Differences between muscles of the feline hindlimb,” *J. Biomech.*, vol. 42, no. 6, pp. 679–685, Apr. 2009, doi: 10.1016/j.jbiomech.2009.01.022.

[83] S. L. Delp *et al.*, “OpenSim: Open-source software to create and analyze dynamic simulations of movement,” *IEEE Trans. Biomed. Eng.*, vol. 54, no. 11, pp. 1940–1950, Nov. 2007, doi: 10.1109/TBME.2007.901024.

[84] S. R. Ward, C. M. Eng, L. H. Smallwood, and R. L. Lieber, “Are current measurements of lower extremity muscle architecture accurate?,” *Clin. Orthop. Relat. Res.*, vol. 467, no. 4, pp. 1074–1082, 2009, doi: 10.1007/s11999-008-0594-8.

[85] R. . Hensinger, *Standards in Pediatric Orthopedics. Tables, Charts and Graphs Illustrating Growth*, no. 1. New York: Raven Press Books, 1986.